Assessing the Value of Stable Water Isotopes in Hydrologic Modeling:
A Dual-Isotope Approach

By

Tegan Linnea Holmes

A Thesis submitted to the Faculty of Graduate Studies of

The University of Manitoba

In partial fulfilment of the requirements of the degree of

MASTER OF SCIENCE

Department of Civil Engineering

University of Manitoba

Winnipeg, Manitoba

Abstract

This thesis presents the development of a dual-isotope simulation in a hydrological model, and its application to the lower Nelson River basin. The purpose of this study is to find if the simulation of stable water isotopes aids in hydrological simulation, and if a dual-isotope simulation is an improvement over a single-isotope simulation.

The isoWATFLOOD model was enhanced to include δ^2H and improve physical representativeness. The model was calibrated using various isotope and flow simulation error functions. Internal hydrologic storages and fluxes were verified by comparing simulated isotope values to observed isotope data.

Adding isotope error to the calibration resulted in small but consistent improvements to the physical basis of calibrated parameter values. Isotope simulation error was found to be the best predictor of streamflow simulation performance beyond the calibration period. The dual-isotope simulation identified a number of model limitations and potential improvements from the verification of internal hydrologic storages.

Acknowledgments

Firstly, I would like to thank my advisor, Dr. Trish Stadnyk, for her support and guidance throughout my time here at the University of Manitoba. Thank you as well to Dr. Chani Welch, who was always there to provide sound advice and more questions.

This research was funded by the Natural Sciences and Engineering Research Council of Canada, the University of Manitoba and Manitoba Hydro. Manitoba Hydro also provided substantial funding for the collection of data used in this study, including the contribution of their hydrometric staff for sample collection and equipment maintenance. Water Survey of Canada personnel were also of assistance in sample collection. Thank you as well to the Environmental Isotope Laboratory, run by Alberta Innovates Technology Futures, for conducting stable water isotope analysis of the collected samples, particularly Dr. John J. Gibson and Mr. Paul Eby. I am also grateful for the assistance of Dr. Nicholas Kouwen in integrating my tracer model into the WATFLOOD hydrological model.

Thank you to my fellow students in Water Resources, you made studying here immeasurably better. For their assistance with this research, a few deserve special acknowledgment: Carly Delavau, for her work on the original LNRB model and assistance with isotopic precipitation inputs; Brittany Toews, for completing the original LNRB model; Kevin Sagan, for advice and assistance in updating the LNRB WATFLOOD model; and Aaron Smith, for information on the LNRB itself.

Finally, a heartfelt thank you to my parents, for their unstinting love and support.

Contents

List of Tables

List of Figures

1 Introduction

Water is an essential part of the economy in Canada, from agriculture to drinking water to hydroelectric generation; and accurate prediction of future water supply is of importance for planning and development of infrastructure. Hydrologic modeling provides essential information for water management at all scales, and improving the reliability of model simulations leads to improved design and management decisions. Modeling streamflow accurately is a significant challenge in many regions of Canada as data availability are a significant limitation, where streamflow and weather station observations can be rare, and with limited record lengths (Coulibaly, et al., 2013). Data scarcity is particularly acute in northern Canada, where the region's remoteness and limited accessibility limits the expansion of data networks. The limited data available increases the difficulty of, but also the need for, hydrologic modeling in this region in order to increase our knowledge of changes in streamflow and hydrologic regimes. In order to predict flows in ungauged locations, or with different climatic conditions than the present or recent past, hydrologic models must accurately represent the physical processes generating streamflow. Information on individual hydrologic processes, however, is even less common than weather or hydrometric data, and is even more costly to obtain across large, remote regions.

A potential part of the solution to the issue of data scarcity is the collection of stable water isotope samples. These naturally occurring, non-reactive tracers can provide additional information on water sources and hydrological processes (Birks & Gibson, 2009). Models that can simulate both flow and isotopic composition simultaneously can be compared to observed isotope data (more easily obtained via grab samples), adding new information to the calibration, validation and verification of the model, and helping to identify if the model is providing the right answer for the right reasons (Kirchner, 2006).

Depending on the sample source, stable water isotopes can inform the modeling of large catchments, headwaters or specific flow sources such as groundwater or snowmelt (Birks & Gibson, 2009).

An isotopic and hydrologic model developed for use in mesoscale Canadian watersheds already exists: the isoWATFLOOD model (Stadnyk, et al., 2013). The isoWATFLOOD model simulates the value of $\delta^{18}O$, a stable water isotope, in all storages and fluxes in the WATFLOOD hydrologic model, producing a continuous simulation of the isotope in streamflow (Stadnyk-Falcone, 2008). The model has been shown to successfully simulate isotopic variation in streamflow, runoff components and evaporation in boreal watersheds, both seasonally and continuously (Stadnyk, et al., 2013).

1.1 Objectives

In order to learn more about the potential of stable water isotopes to improve hydrologic simulations, this research will:

1. Expand isoWATFLOOD to include $\delta^{2}H$, and produce isotope frameworks;
2. Enhance the isoWATFLOOD model to improve physical representativeness and model function in large and/or regulated watersheds;
3. Introduce isotopes to the current DDS optimization objective function for WATFLOOD and compare calibrations using isotopes and flow to a calibration using exclusively flow; and
4. Perform model verification for internal WATFLOOD hydrologic storages and fluxes by comparing simulated isotope values to relevant observed isotope data.

The main objective of this research is to answer the following questions:

- What is the effect of including isotope simulation error in the calibration?
- Does the hydrological simulation benefit from the simulation of stable water isotopes?
- Is the additional simulation of $\delta^{2}H$ an improvement over simulating only $\delta^{18}O$?

2 A Review: Hydrological and Stable Water Isotope Modeling

This chapter reviews the general principles of hydrologic modeling, the known behaviour of stable water isotopes, both in the atmosphere and in a watershed, and the simulation of stable water isotopes within the environment. Prior work using stable water isotope simulations in conjunction with a hydrologic model is also discussed.

2.1 Hydrological Modeling

Hydrologic models simulate the movement of water using mathematical equations to predict streamflow. Hydrological modeling may also simulate the movement and distribution of water in a watershed. Hydrologic models can be used to investigate flow generation processes, predict future streamflow discharge, or estimate the basin water balance. Many different hydrologic models, varying in structure and complexity, have been developed to simulate global, continental, regional, and more localized hydrologic cycles.

Hydrologic models can be classified along a continuum, ranging from a conceptual model to a fully physically-based model. A physically-based model simulates streamflow and hydrologic processes within the watershed using equations based on the physical properties of the area. A physically-based model simulates both water and energy balances in detail, and allows for the verification of internal processes such as evaporation or groundwater flows. The more fully physically-based a model is, the more input data is required to setup and run the model, and also generally increases the computational demand required to run the model. Physically-based models are best suited to simulating flows in small and intensively studied basins, where all hydrologic storages and fluxes can be accurately defined and simulated (Singh & Frevert, 2006).

Conceptual models do not use physics to simulate flows, and parameters have no direct (i.e., measurable) physical meaning; the accuracy of the model depends on parameter calibration using observed flows at the point of interest. Conceptual models can be extremely simple and require minimal input data; but because parameter values depend on previously observed flows, conceptual models are less reliable when conditions differ significantly from the original development period, or period of calibration (e.g., land use change or differing climatic conditions) (Kirchner, 2006). Conceptual models can be applied to any watershed, provided there is an adequate flow record.

Hydrologic models are also sub-classified along a continuum between lumped and distributed modeling systems, depending on the degree to which the watershed response is aggregated. A fully lumped model aggregates the entire watershed into a single response unit with averaged parameters, while a distributed model produces a hydrologic response from each piece of a fine divided area to find the total response of the watershed (Singh & Frevert, 2006). Many models are classified as semi-distributed, with the watershed area divided into sub-basins based on topography, hydrologic response units based on land cover or grouped response units based on a combination of topography and land cover. Increasing the degree to which a model is distributed increases the model complexity, and the data and computational power required to run the model; but can also allow model parameters to be transferred between watersheds because they have a more physical basis. Transferability is desirable for ungauged watersheds or modeling in remote regions where input and observed data are scarce.

Regardless of the type or complexity of the hydrological model, there will always be uncertainty in the simulated flow produced by the model. Errors arise in the input data for the model, from measurement or distribution, which will be processed through a model structure with its own assumptions, and parameters that either have measurement uncertainty or were calibrated to uncertain measurements (Beven, et al., 2008; Beven & Binley, 1992). The combined effect of measurement and structural error

on model output is highly complex, and the resulting uncertainty in the model output can be difficult to assess (Beven, et al., 2008; Beven, 2008). Model parameters can be calibrated to produce an optimal match between modeled and observed flows, but due to the uncertainty in both the simulated and observed values, it cannot be determined if the optimal parameter set will produce the most accurate flow simulation as the true flow is unknown due to observational uncertainty (Beven, 2008). Other parameter sets result in simulated flows that agree nearly as well with the observed flow, and these parameter sets may be superior to the optimal set in simulating flows during a validation period, or in matching the true, rather than the observed, uncertain flow (Beven, 2006). As the flows produced by the final results of these different models are equivalent, given the information available to compare them, the unidentifiability of a best parameter set is termed equifinality (Beven, 2006).

Although the best parameter set for a particular model structure and simulation period may not be identifiable, this is not equivalent to it not existing (Hamilton, 2007). A wide range of parameter sets may produce equivalent flow simulations in the calibration period, but their performance in periods with changing hydrologic conditions may diverge widely as some parameters may have produced a good simulated flow for the wrong reasons (Kirchner, 2006). For example, a parameter set may simulate total flow accurately, but with an unrealistically low evaporation rate and gradually increasing groundwater storage. When using hydrologic models for predicting flows for changing conditions, equifinality increases the uncertainty in simulated flows (Ehret, et al., 2014). The addition of new types of data, beyond flow measurements have been found to reduce equifinality, as there are fewer parameter sets that will produce an equivalent result (Her & Chaubey, 2015; Kirchner, 2006; Bergstrom, et al., 2002). Stable water isotope data have been used in the calibration of hydrologic models, as isotopes can be simulated with the same model structure as streamflow (Bergstrom, et al., 2002).

2.2 Stable Water Isotope Hydrology

Water molecules occur in a number of stable isotopes, of which the most common are $^{1}H_2{}^{16}O$, $^{1}H_2{}^{18}O$ and $^{2}H^{1}H\,^{16}O$. By far the most abundant is $^{1}H_2{}^{16}O$, while $^{1}H_2{}^{18}O$, generally called either oxygen-18 or ^{18}O, represents 0.205% of all water molecules, and $^{2}H^{1}H\,^{16}O$, called deuterium, ^{2}H or D, represents about 0.031% (Gat, 1996). While there are other stable isotopes of water, they are not typically measured as they are even less common than deuterium or ^{18}O. The quantity of a stable water isotope in a water sample is typically expressed as a relative abundance, sometimes as an atom ratio, or *R*, of D/H or $^{18}O/^{16}O$, but typically relative to ocean water isotope abundance. The δ value is defined as:

$$\delta‰ = (R/R_{std} - 1) \times 10^{3} \qquad (2.1)$$

where R_{std} comes from the world standard (Vienna Standard Mean Ocean Water, VSMOW2, or previously VSMOW) (Gat, 1996). The VSMOW is a water standard used to define the isotopic composition of fresh water and is intended to represent average ocean water, that is, the majority of water on earth. The VSMOW2 standard was created to replace the original VSMOW water (supplies of which were being exhausted) where the composition of VSMOW2 was calibrated to be as similar as possible to VSMOW.

2.2.1 Isotopes in Precipitation

Stable water isotopes would be of little interest were it not for the fact that the small difference in molecular mass results in variation of isotopic abundance in natural waters. Isotopes have different equilibrium vapor pressures, and differing rates of molecular diffusion in the gas phase; these differences have their most significant effect during phase change in the water cycle, primarily in the change from liquid to vapor (i.e., during evaporation) (Gibson & Edwards, 2002). The greater mass of the rare stable water isotope causes evaporation at a slower rate, which produces predictable variations in the molecular composition of water. Water evaporated from the ocean, and therefore precipitation, has

a lower (depleted) δ than its source, and the δ of an evaporating water body will gradually increase (enrich) as lighter isotopes are preferentially removed.

Precipitation is formed from condensed atmospheric vapor, the isotopic composition of which can be described using the Rayleigh distillation equation when the vapor is in a state of thermodynamic equilibrium (Gat, 1996):

$$R = R_0 f^{(\alpha-1)} \qquad (2.2)$$

Where R_0 is the original molar ratio of the vapor, f is the fraction of the material remaining and α is the fractionation factor. The fractionation factor is temperature dependent and therefore cannot be assumed to be constant through the condensation process (Dansgaard, 1964). Fractionation factors for ^{18}O and D are not identical, but both are determined by the vapor temperature, resulting in a strong correlation between the concentrations of the two isotopes in precipitation, even with variations in source water δ-values. The relationship between the two isotopes found from water samples from around the world is termed the global meteoric water line (GMWL) (Craig, 1961):

$$\delta D = 8\delta^{18}O + 10 \qquad (2.3)$$

The isotopic composition of precipitation in a specific local area can differ significantly from the GMWL, such that a flux-weighted average of local precipitation produces a distinct local meteoric water line (LMWL). Stable water isotopes in precipitation vary seasonally for inland regions, and at higher latitudes (Vachon, et al., 2010; Liu, et al., 2010). These seasonal changes are caused by differences in air temperature and by variations in atmospheric circulation patterns importing water vapor from various sources (Birks & Edwards, 2009). The original composition of precipitated moisture may change due to the oceanic source of the vapor, temperature, or due to the presence of locally evaporated water vapor from lakes or the land surface (Liu, et al., 2010). The isotopic composition of atmospheric water vapor changes as vapor is removed as precipitation, with heavier isotopic species being preferentially removed

and resulting in more depleted precipitation towards continental interiors and to the leeward side of mountain ranges (Vachon, et al., 2010). In North America, measurement of isotopes in precipitation is not ubiquitous, with precipitation samples being analysed for individual research projects, and at select locations as part of the Canadian Network for Isotopes in Precipitation (CNIP; 107 stations), the United States Network for Isotopes in Precipitation (USNIP; 109 stations), and with both contributing to the Global Network for Isotopes in Precipitation (GNIP) in North America (Birks & Gibson, 2009; Welker, 2000; Aggarwal, et al., 2011; Delavau, et al., 2015). Due to the scarcity of measured isotope compositions for precipitation, methods have been developed to estimate compositions that can capture seasonal variability in Canadian precipitation (Delavau, et al., 2011; Delavau, et al., 2015).

2.2.2 Isotope Fractionation

The isotopic composition of water undergoing evaporation changes over time: lighter isotopes are preferentially removed, and the remaining water enriches in the rarer, heavy isotopes. The effect of evaporation on isotopic composition is visible when D is plotted against ^{18}O in a δ-δ plot; evaporating waters separate from meteoric waters on what is termed a local evaporation line (LEL), the slope of which is determined by local conditions (Gibson, et al., 2008). There are two significant components to fractionation: equilibrium and kinetic separation (Gibson, et al., 2008). Equilibrium isotopic fractionation is temperature dependent, with the equilibrium isotopic separation between liquid and water, ε^*, calculated as (Gibson, et al., 2008):

$$\varepsilon^* = \alpha^* - 1 \qquad (2.4)$$

The equilibrium fractionation factor for the liquid to vapor transition, α^*, is calculated using the empirically derived equations from Horita and Wesolowski (1994):

$$\alpha^*_{18O} = e^{\left(-7.685+6.7123*(10^3/\mathrm{T})-1.6664*(10^6/\mathrm{T}^2)+0.35041*(10^9/T^3)\right)/1000} \qquad (2.5)$$

$$\alpha_{2H}^{*} = e^{(1158.8*(T^3/10^9)-1620.1*(\mathrm{T}^2/10^6)+794.84*(\mathrm{T}/10^3)-161.04+2.9992*(10^9/T^3))/1000} \quad (2.6)$$

where α is in decimal format, and T is temperature in degrees kelvin. The kinetic separation of isotope species is dependent on both surface properties and relative humidity, with kinetic isotopic separation, ε_k, defined as (Gat, 1996):

$$\varepsilon_k = C_D n\theta(1-h) \quad (2.7)$$

Where C_D is 28.55‰ for ^{18}O and 25.115‰ for D, h is the relative humidity, n is a turbulence parameter, ranging from 0.5 for turbulent open-water bodies to 1 for static soil water, and θ is a transport resistance factor reduced from unity for large open water bodies (Gibson, et al., 2008).

The isotopic composition of the evaporated water vapor, δ_E, was first modeled by Craig & Gordon (1965) for oceanic waters. A simplified version of the Craig-Gordon equation described the composition of the water vapor as a function of the composition of the evaporating water body, δ_L (Gonfiantini, 1986):

$$\delta_E = \frac{\frac{(\delta_L - \varepsilon^*)}{\alpha^*} - h\delta_a - \varepsilon_k}{1 - h + \varepsilon_k} \quad (2.8)$$

Where δ_a is the isotopic composition of the ambient atmospheric moisture; h, ε and δ are in decimal notation. Isotopes in atmospheric moisture are often assumed to be in equilibrium with those in precipitation, although if evaporated water constitutes a significant fraction of the vapor, this assumption may not be valid (Gibson, et al., 2008). With the assumed relationship between the isotopic composition of atmospheric moisture and the isotopic composition of precipitation, δ_P, which depends on there being no recirculated moisture, δ_a can be calculated as (Gibson, et al., 2016):

$$\delta_A = \frac{\delta_P - \varepsilon^*}{1 + \varepsilon^*} \quad (2.9)$$

with ε^* and δ in decimal notation.

Enrichment is limited by atmospheric conditions, such that a desiccating water body has a limiting isotopic composition, δ^*, reached as the water volume approaches zero (Gibson, et al., 2016):

$$\delta^* = \frac{h\delta_a + \varepsilon_k + \varepsilon^*/\alpha^*}{h - \varepsilon_k - \varepsilon^*/\alpha^*} \quad (2.10)$$

Both the isotopic composition of evaporated moisture and the limiting isotopic composition fall on the LEL. In nature, most water bodies are a mixture of recently precipitated water and fractionated water. When D is plotted against ^{18}O in a δ-δ plot river or lake water falls between the LMWL and the LEL on what is termed the local mixing line (LML). The relative dominance of precipitation or evaporation determines whether the LML will fall closer to the LMWL or the LEL.

2.2.3 Isotope Behavior within a Watershed

Soil and groundwater both have variable isotopic composition over time and with depth, with deeper soil water or ground water exhibiting a more consistent composition over the course of a year; and shallower hydrologically active zones changing rapidly when new water is added (Peralta-Tapia, et al., 2015). When riparian wetlands are present, the water entering a stream will be more stable in composition, as wetlands accumulate water from all soil layers as well as direct runoff and allow for more complete mixing than soil storage (Tetzlaff, et al., 2014).

Evaporation alters the isotopic composition of water in a basin, for any type of storage. Open water, such as wetlands, stream channels or lakes, enriches measurably in summer, while soil water enriches less as the terrestrial transpiration component of evapotranspiration is non-fractionating (Gibson & Reid, 2010). For low relief catchments, riparian zone or wetland water enriches to a greater degree, due to the longer residence time in the catchment, and soil enrichment is likewise increased (Klaus, et al., 2015). Near surface soil water in a boreal catchment has also been observed to enrich, with gradual mixing of enriched water with deeper soil water (Peralta-Tapia, et al., 2015). Evaporative enrichment of water in-stream depends on the relation between the channel flow rate and the evaporative flux; in

small headwater streams the isotope composition vary diurnally with the evaporation rate during low flow periods (Birkel, et al., 2012). The evaporative enrichment in larger channels and lakes is determined by the throughflow rate and evaporation: higher throughflow reduces enrichment (Gibson, et al., 1996; Gibson, et al., 2016). Evaporative enrichment in open water bodies also depends on the atmospheric moisture composition, which can affect larger water bodies such as the Laurentian Great Lakes where evaporate is a significant fraction of the water vapor over the lake (Jasechko, et al., 2014). Enrichment in wetlands is complex, as wetlands possess properties of both soil storage and channels. Vegetation limits enrichment by decreasing the relative contribution of evaporation in evapotranspiration for wetlands unconnected with the channel, while connected wetlands vary between the stream isotope composition and the soil water composition depending on the water level in the stream channel (Hayashi, et al., 2004; Klaus, et al., 2015).

In basins where a snowpack accumulates, snow melt produces a distinct decrease in the isotopic composition of streamflow. The spring freshet in boreal streams is a mix of depleted meltwater and stored water, with snowmelt also adding to wetland and lake storages (St Amour, et al., 2005; Hayashi, et al., 2004). The relative contribution of snowmelt is dependent on the land cover and topography in the basin, with connected wetlands increasing water mixing and reducing the peak snowmelt contribution (St Amour, et al., 2005). Frozen soils have a reduced infiltration capacity, but meltwater does produce depleted soil water near the surface (Peralta-Tapia, et al., 2015).

2.3 Stable Water Isotope Modeling

Stable water isotopes have been modeled in many ways and for many purposes; this section will focus on the modeling of stable water isotopes as a tracer, particularly hydrological models with a process-based representation of flow generation, as suggested by Kirchner (2006).

2.3.1 History

Modeling stable water isotopes in terrestrial water originated in two separate scientific developments in the 1960's. The first was the study of stable water isotopes in global meteoric and oceanic waters, and their temporal and spatial variation (Craig, 1961; Dansgaard, 1964; Craig & Gordon, 1965). The second was the development of hydrograph separation techniques using tracers, including bomb-produced tritium (Eriksson, 1963) and ions (Pinder & Jones, 1969). With knowledge of the isotopic composition of rain and snow, as well as streamflow, flow separations could be performed using oxygen-18 as a tracer to identify groundwater or snowmelt contributions (Dinçer, et al., 1970; Sklash & Fritz, 1976). Groundwater was found to be a main contributor to peak flows, rather than direct rainfall or surface runoff (Sklash & Fritz, 1976). With the development of more complex numerical models for analysis of tracer responses, such as the work by Niemi (1978), isotopic data was used to determine not only the contribution of groundwater to streamflow, but also the mean transit time of sub-surface flows and groundwater storage volumes (Małoszewski & Zuber, 1982; Maloszewski, et al., 1983; Kennedy, et al., 1986).

A key finding of the early work with isotope tracers is the predominance of old or pre-event water in the peak streamflow of storm events, separate from water originating from the precipitation event itself (Martinec, 1975; Kennedy, et al., 1986). Rainfall causes the rapid mobilization of water already stored in the watershed, resulting not only in a prompt streamflow (or stormflow) response to rainfall, but an isotopic response which is generally damped (Kirchner, 2003). The difference in response is generally attributed to the difference between the velocity of water, or the rate of movement of water molecules, which determines the response of the isotopic composition and the celerity of the pressure wave produced by the addition of rain water, thereby determining the streamflow response (McDonnell & Beven, 2014).

Natural isotopic tracers have also been used to assess the contributions of multiple storages within a watershed to streamflow (Turner, et al., 1987). Once hydrograph separations had expanded further to include multiple isotopic storage models and complex tracer mixing, tracers were used to explore the differences between hydrologic storages (Harris, et al., 1995). Isotopes continue to be useful in hydrograph separations when a three component approach is used (Klaus & McDonnell, 2013). These insights from isotopic tracers into the processes generating streamflow (i.e. groundwater flows) have then been used to improve the modeling of the process itself (Mehlhorn, et al., 1999). Furthermore, tracers have been used as an additional measure for the performance of a hydrological model (Bergstrom, et al., 2002).

2.3.2 Strategies

Incorporating tracers in general and stable water isotopes in particular, with hydrological simulation requires additional modeling decisions for the mathematical conceptualization of tracer movement through the watershed. The most commonly used strategy is to add state variables to quantify either tracer concentrations within the hydrological storages or tracer volumes corresponding to water volumes, and have tracer movement between storages or into streamflow controlled by flux equations matching those used to control the flow of water. The number of storages and the connections between them vary based on the structure of the hydrologic model and the tracer simulation being added. The ^{18}O simulation added to the HBV model by Bergstrom et al. (2002) included the same surface, soil, upper saturated zone and lower saturated zone storages in each lumped sub-basin as the hydrologic model, with tracer concentrations for each storage added and used to define tracer fluxes out of each compartment. The work in Dunn et al. (2008) used a similar lumped iso-hydrologic model with multiple ground storages, though total tracer volumes for each storage unit were used, and tracer fluxes were calculated based on the relative tracer and water volumes (Dunn, et al., 2007). Birkel et al. (2010) modeled the tracer flux in per mille, and the deuterium response in the stream using a weighted

average of tracer and water outputs from the upper and lower storages in the model. Storages may also be defined based on land cover, as well as soil depth and saturation, with isotope and water hydrologic response units (Smith, et al., 2016). In isoWATFLOOD, a distributed model, every water storage compartment in all grid cells and grouped response units has an associated isotope volume, with isotope fluxes determined by the isotope volumetric concentration of the originating compartment (Stadnyk, et al., 2013).

Tracer simulations generally assume that storage units are completely mixed over the modeling time interval, with uniform tracer concentrations throughout the compartment. The time interval over which complete mixing is assumed varies between models, with Birkel et al. (2010) and Smith et al. (2016) using a daily time step in lumped models, while the distributed isoWATFLOOD model uses hourly time steps (Stadnyk, et al., 2013). A partial mixing model for tracers has been shown to produce different and less identifiable residence times for water than a model assuming complete mixing (Fenicia, et al., 2010). While partial mixing is believed to be more physically representative, using partial mixing (rather than complete mixing) adds to the model complexity. If an additional, separate storage is needed for tracer mixing, either as passive storage or for partial mixing, additional model parameters are required -adding additional uncertainty to the model (Birkel, et al., 2010; Fenicia, et al., 2010).

An additional modeling choice that must be made for the simulation of stable water isotopes in particular is whether or not to include fractionation in the model. The enrichment of water due to evaporative fractionation has been well described in theoretical terms and can be simulated using the equations derived from laboratory experiments (Section 2.2.2). Simpler conceptual models, however, such as that described in Birkel et al. (2010) do not include fractionation, despite the inclusion of evapotranspiration as a water flux. When lakes are present in the modeled basin, the addition of fractionation modeling for lake evaporation improves the overall simulation of stable isotopes (Birkel, et

al., 2011). For more physically-based models, fractionation due to evaporation may be added to account for evapotranspiration from wetlands and soil water (Smith, et al., 2016; Stadnyk, et al., 2013). Including fractionation in the isotope simulation is necessary to reproduce the isotope balance in areas with a high prevalence of wetlands and lakes, and where slopes are low (Birkel, et al., 2011; Klaus, et al., 2015).

There have been alternative approaches than state variable simulations developed for the modeling of tracers. Birkel et al. (2012) used Markov switching autoregressive models, a complex stochastic model, to reproduce the temporal dynamics and statistical characteristics of both deuterium and oxygen-18 time series. Weiler et al. (2003) modeled isotopes in streamflow using mechanistic transfer functions to perform event-scale hydrograph separation. Using tritium, a radioactive isotope of water, Davies et al. (2011) validated a subsurface model with preferential flow pathways using random particle tracking to reproduce tracer behavior. McMillan et al. (2012) modeled tracer concentration in streamflow by storing the water age distribution for each storage compartment, calculating the streamflow age distribution from the sum of the distributions of the component fluxes and producing the tracer concentration from the convolution of the outflow age distribution with the precipitation concentrations. These alternative methods provide useful information on isotope behavior but are not well suited to integration into conceptual or semi-physically based hydrological models, as they are either too computationally intensive, or simulate isotopes independently of the flow.

2.3.3 Limitations

As with any type of modeling, there are limitations in the simulation of stable water isotopes in the hydrologic cycle. The most significant issue, and the most limiting in terms of future studies, is the limited amount of isotope observed data available to the modeller (Birkel & Soulsby, 2015). Isotope sampling is often both infrequent and sporadic; depending on field season timing, seasonality, and staff availability. Ideally, isotope concentrations would be available in high-resolution, continuous data series

in order to capture all catchment processes and isotopic (hydrologic) variability. With sub-daily sampling of streamflow, the daily evaporation cycle can be observed in the streamflow of small catchments, as shown by Birkel et al. (2011), and frequent samples also provide information on the finer details of snowmelt contributions to streamflow (Ohlanders, et al., 2013). While streamflow sampling may provide new insights into hydrologic processes in the watershed, improving the measurement of isotopes in precipitation would improve simulations more. Pangle et al. (2013) found that occasional precipitation samples do not capture the true variability of precipitation composition. Without accurate model inputs, simulation results will be of limited utility in the diagnosis of uncertainty and reduce the effectiveness of isotope simulations as a means to improve hydrological models.

The limited number of catchments with isotope data, and the limited distribution of sampling sites within those catchments is another issue for stable isotope simulations. Validation of isotope simulations for catchments or sub-catchments cannot be performed without measured data to compare results to, limiting confidence in the overall simulation (Soulsby, et al., 2015). The lack of widespread sampling also prevents the verification of the simulation in terms of progressive contribution to streamflow and downstream mixing of headwater stream contributions (Tetzlaff, et al., 2014).

Stable water isotopes can be useful when verifying the modeling of flow generating storages contributing to streamflow, as shown by Birkel et al. (2014). However, in order to use stable isotopes to verify internal state variables in hydrologic models, there needs to be relevant isotopic observations. Sporadic sampling of source waters is relatively common for stable isotope studies, but more frequent sampling is needed in order to validate internal flow path sources. Jasechko et al. (2016) used $\delta^{18}O$ to identify the percentage of streamflow from recent precipitation using streamflow sampling instead, finding a relationship between water age and the topographic gradient. In addition to validating internal water storage, such as groundwater or wetlands, stable water isotopes can also provide

information on evaporation and transpiration flux from soil water, as the two processes have different effects of isotopic composition (Jasechko, et al., 2013).

Finally, the simultaneous simulation of stable water isotopes with streamflow can increase the number of parameters required by the model, due to the increased number of simplifying assumptions required. The addition of parameters into a model decreases the identifiability of parameters, and decreases confidence that the model result is produced for the right reasons, particularly if those parameters need to be calibrated (Kirchner, 2006). The uncertainty introduced by additional parameters required for isotope simulation may, however, be compensated for by the added value of more data (i.e., observations) incorporated into the model (Birkel & Soulsby, 2015).

2.4 Stable Water Isotopes in Hydrologic Modeling

Stable water isotope data has been put to diverse uses in hydrologic modeling beyond traditional hydrograph separations. Isotopic compositions have provided new and useful information with respect to model structure and conceptualization, water mixing and storage, and streamflow sources.

Modeling the isotopic composition of streamflow and groundwater can provide an estimate of water storage within a catchment. Birkel et al. (2011) found that the groundwater storage volume required to simulate isotopes in streamflow was significantly larger than that required to simulate the streamflow response; this additional passive storage leads to a damped isotope response in stream water. However, without a strong understanding of the mixing relationships between storage units in the catchment, water residence times are difficult to determine from isotope data, as residence time and isotope composition are not necessarily sensitive to the same parameters (Dunn, et al., 2008). With a coupled isotope tracer and runoff model, Birkel et al. (2015) found that modest storage fluctuations determine flow variability in general; with the difference between high and low flow storage small relative to the

total amount of retained groundwater in the watershed. Isotope data has also provided further evidence for the reduction in water storage in urbanizing areas (Soulsby, et al., 2015).

Conceptualizations of flow pathways from storage compartments to the stream can be improved using stable isotope data and simulation. Bergstrom et al. (2002) found that including by-pass flow from infiltrated water into the upper saturated zone led to significant improvements in isotope simulation; this improvement also produced shorter residence times at high flows when soils were saturated. Fluctuations in the isotopic composition of streamflow in small catchments have been related to near-surface soil water and runoff, which is generally less well-mixed than the groundwater which contributes the majority of streamflow in most areas (Dunn, et al., 2008). In areas with saturated riparian zones or wetlands connected to the main channel, Birkel et al. (2011) found that adding flow from both the upper soil and lower groundwater storages to a saturated riparian zone before entering the channel improved isotope simulations. Iorgulescu et al. (2007) used oxygen-18 as a tracer to evaluate a set of hypotheses regarding the model structure for rainfall input processes, finding that subsurface pathways are significant for the recent precipitation component of stream flow.

As with flow pathways, stable isotopes can be used to identify flow sources within a catchment. Capell et al. (2012) used simulated tracers in model development to identify storages, which resulted in different model structures for upland and lowland areas. More recently, Smith et al. (2016) identified the relative contributions of soil water, ground water and wetland storage to streamflow using a lumped iso-hydrological model for two catchments in northern Canada, finding source variability was most related to late summer precipitation quantities. Similarly, Soulsby et al. (2015) found hillslope and peatland storages to be the primary contributors to stormflow peak flows from their tracer-aided model. Regardless of their differences, it seems that simultaneous isotope-flow models may also be better able to quantify the uncertainty in flow source contributions (Smith, et al., 2016).

Stable isotope tracers can also improve the identifiability of mixing within the watershed which, while less significant to water quantity simulation, is significant to water quality and contaminant modeling. Isotope tracer simulations can aid in distinguishing the degree of groundwater mixing in different catchments (Dunn, et al., 2008). Birkel et al. (2011) found evidence from isotope modeling that even small upstream lakes significantly reduce downstream variability in isotopic composition. Even more important than lakes are connected wetlands or saturated riparian zones, which act as mixing zones for flows generated in the catchment area (Birkel, et al., 2015). Untereiner et al. (2015) found that the isotopic composition of streamflow in a prairie watershed was a good predictor of basin mixing and storage, as well as a predictor of water quality.

If isotopic composition data is collected from water other than streamflow, such as groundwater, soil water or wetlands, isotope simulation can also be used to verify the simulation of internal storages. Birkel et al. (2014) successfully used soil water isotope observations to improve parameter identifiability and improve both streamflow and isotope simulations. With expanded source water sampling, isotope simulations could be used to verify, validate or calibrate internal model processes.

As streamflow stable water isotope data contains useful information about internal processes, such as flow paths and storages it therefore has been incorporated into model calibration in several ways. With sufficient isotopic composition data, a Nash-Sutcliffe efficiency can be calculated for isotopes as well as flow and used as an objective function with Monte-Carlo sampling (Birkel, et al., 2011). Alternatively, Bergstrom et al. (2002) included isotope error in a weighted multi-variable calibration along with flow, snowpack and groundwater errors. Iorgulescu et al. (2007) used the root mean squared error rather than the Nash-Sutcliffe efficiency for the isotope simulation, defining a maximum isotope error for the model to be considered behavioral in the GLUE methodology. Due to infrequent and irregular isotope sampling, Stadnyk et al. (2013) used a combination of Nash-Sutcliffe error and visual inspection of the

isographs to calibrate the model following an automated calibration using exclusively flow error. Isotope data can also be used indirectly in calibration, by using tracers to identify flow component limits, and using these limits as a constraint in calibration (Dunn, et al., 2008). With evidence of improved parameter identifiability, isotope simulation is a promising tool for hydrologic model calibration (Birkel, et al., 2014).

There remain gaps in the work done so far with isotope simulations in hydrological models, particularly for meso- and macro-scale simulations. Auto-calibration with isotopes, dual-isotope simulations and model sub-component verification have not yet been attempted at the operational scale – where perhaps they are most needed due to an increasing number of model assumptions. This study will begin to fill these gaps, with the development of a dual-isotope simulation for the WATFLOOD hydrological model, and the application of this model to the lower Nelson River basin to explore the utility of isotope-enabled auto-calibration and model verification at a large scale.

3 The isoWATFLOOD Model

The isoWATFLOOD model was originally developed to continuously simulate isotopic variation through the hydrologic cycle and to provide a way of verifying the internal streamflow components of the WATFLOOD hydrologic model (Stadnyk-Falcone, 2008). The original isoWATFLOOD model simulated $\delta^{18}O$, which was selected over $\delta^{2}H$ in the model design because its behavior in the environment is somewhat better understood and due to the generally lower measurement error associated with $\delta^{18}O$ (Stadnyk-Falcone, 2008). However, the addition of $\delta^{2}H$ in the model was always intended, and would add a third constraint on the simulated streamflow, reducing uncertainty and allowing the partition and validation of evaporation within basins. This additional information is of particular importance for simulation in sparsely gauged and high-latitude basins, and for the projection of streamflow under climate change.

In this research, the isoWATFLOOD model has been expanded to allow for the simulation of $\delta^{2}H$ in addition to the original $\delta^{18}O$ tracer, which enables the full simulation, continuous over time, of isotopic frameworks in $\delta^{2}H$- $\delta^{18}O$ space and deuterium excess (d-excess). The production of isotopic frameworks has been added as an automated part of a dual-isotope simulation. The addition of another isotope tracer requires the simulation of deuterium compositions in all fluxes and storages included in the WATFLOOD model, independently of the original oxygen-18 simulation. The isotope model has also been restructured to improve efficiency by replacing all iterated mass balance equations with direct solutions, in both the $\delta^{2}H$ and $\delta^{18}O$ simulations, allowing for the use of the dual tracer isotope simulation in a wider variety of basin models; simulation times have been reduced by 30 to 50%. Both isotope simulations were also improved by adding snowpack composition evolution and transpiration as an explicit flux to the two models. The new version of isoWATFLOOD has expanded options for isotope specific forcing data, and can be used in the auto-calibration module for WATFLOOD. The following

chapter will describe the isoWATFLOOD model and how the stable water isotopes $\delta^{18}O$ and $\delta^{2}H$ are transferred between hydrological storage compartments. The WATFLOOD model structure, which is used by the isotope simulation, will be discussed, followed by a description of the isotope model's modules.

3.1 WATFLOOD

The WATFLOOD hydrological model is a partially-physically based, distributed model designed for use on large scales (Kouwen, 2014). WATFLOOD can use remotely-sensed data and has been used to reproduce flows in a variety of watersheds, including the 1 700 00 km^2 Mackenzie basin (Pietroniro, et al., 2006; Toth, et al., 2006).

3.1.1 Model Structure

The watershed area within the WATFLOOD model is divided in two different ways. The first is a spatial division using a grid, with the size and orientation of the grid cells set by the user. Each grid cell has an area, a slope, and a grid type derived automatically from a digital elevation model (DEM). The grid type allows for the variation of channel and baseflow parameters in different parts of the watershed. Grid cells have a single outflow to a downstream grid cell, with the flow direction determined by the relative elevations of the grid cells. The second division of the watershed area is into regions with hydrologically significant land cover types; the land cover types are user specified, based on the vegetation and soil types in the region based on remotely sensed land cover imagery. Each significant land cover type, or land class, has a parameter set for the surface and upper zone of the soil. Most land classes, whether crops or coniferous forest, have separate surface and upper soil zone storage compartments; the impervious land class has a surface storage, but no soil storage. The water and, if present, connected wetland, land classes have no surface or soil storage, but do have a surface area and snowpack.

The spatial and land class divisions of the watershed area are combined such that each grid cell is divided into sections based on the land cover present in the area. All of the area with a specific land cover in the grid cell is grouped into a single grouped response unit, or GRU; not all grid cells contain every land cover so the number of GRU varies between grid cells. Any flow generated within the GRU is added to the channel within the grid cell. GRU and grid cells are illustrated in Figure 3.1.

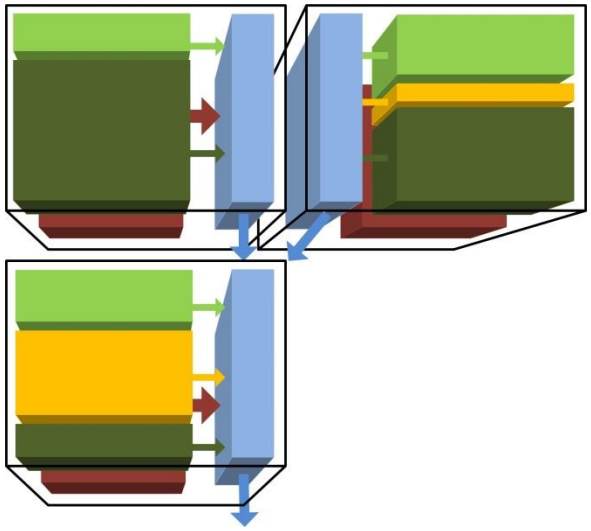

Figure 3.1 GRU (green and yellow blocks) and grid cells (black lines) in WATFLOOD; lower zone and channels are shown in brown and blue respectively.

Each grid cell contains numerous storage compartments, the total number of which is dependent on the number of GRUs. A GRU includes a snow pack, a surface and an upper zone compartment. A grid cell has a single lower zone storage compartment, which is recharged by all GRUs in the cell. If connected wetlands are included in the model, there will be a separate wetland storage compartment between the land and the channel, with outflows from the GRUs and lower zone passing through the wetland rather than to the channel directly. The channel storage receives the flow generated in the grid cell, and is connected to the grid cells upstream and downstream in the channel network. The connected wetland and channel storage also have distinct snow packs. Storage compartments and fluxes in WATFLOOD are illustrated in Figure 3.2.

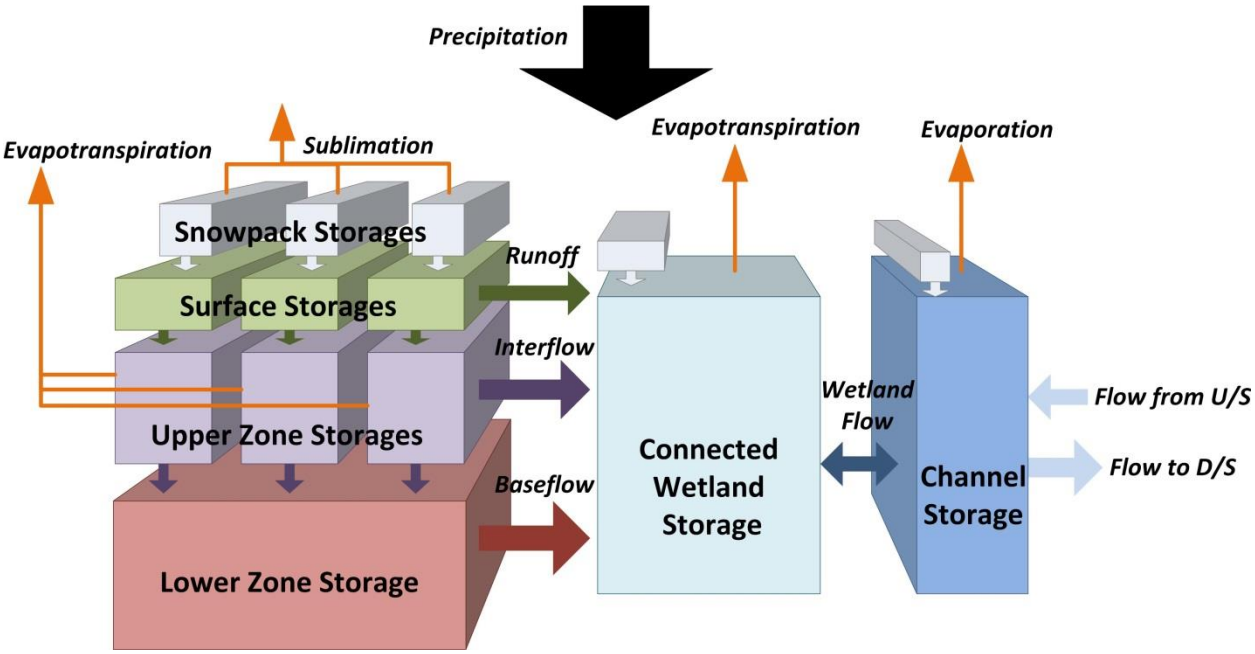

Figure 3.2 Conceptual representation of WATFLOOD hydrology within a grid cell, with this illustration including three land cover groups with soil storage and a connected wetland contributing to grid runoff.

3.1.2 Evaporation and Transpiration Partition

The WATFLOOD model calculates evapotranspiration from soil and wetlands as a single value, but evaporation and transpiration must be considered as distinct processes when modeling stable water isotopes. Therefore, an empirical estimate of the evaporation and transpiration separation was developed (Stadnyk-Falcone, 2008).

The split between evaporation and transpiration depends on the water held in the upper zone of the soil, quantified by the upper zone storage indicator, *UZSI*, which is a function of the soil moisture. Evapotranspiration in WATFLOOD ranges from the potential rate when the soil is saturated, to zero when water content reaches the permanent wilting point, *PWP* (Kouwen, 2014). The upper zone indicator is computed as (Neff, 1996):

$$UZSI = \left(\frac{UZS - PWP}{SAT - PWP}\right)^{1/2} \quad (3.1)$$

where *UZS* is the upper zone storage and *SAT* is the saturated soil storage.

As the soil dries, the transpiration fraction of evapotranspiration increases and the evaporation fraction decreases. The proportion of evaporation, *E*, to evapotranspiration, *ET*, is estimated using a power function (Stadnyk-Falcone, 2008):

$$\frac{E}{ET} = a \cdot UZSI^{b} \qquad (3.2)$$

Where *a* is the maximum evaporation to evapotranspiration fraction for the land class, and *b* is the rate at which the evaporative component of evapotranspiration increases with soil water content. The values of *a* and *b* for each land class are specified by the user in a separate parameter file (Appendix A). The evapotranspiration split had been added to the WATFLOOD model by Stadnyk-Falcone (2008), but the resulting division was not utilized by the isoWATFLOOD model; this ommission is now corrected and evaporation and transpiration are simulated differently in the new isoWATFLOOD model.

3.2 isoWATFLOOD

The isoWATFLOOD model is an isotope simulation for either a single isotope, $\delta^{18}O$ or dual isotopes, $\delta^{18}O$ and $\delta^{2}H$, which can be run coupled to the WATFLOOD hydrological model. isoWATFLOOD simulates isotope volumes in the compartments of the hydrologic model, using the flux between, and storage within, compartments calculated by WATFLOOD. The isotope simulation occurs subsequent to the hydrologic simulation at each time interval. The main module of isoWATFLOOD (isotopes.f) calls a series of subroutines; the subroutines for $\delta^{2}H$ are optional in the simulation. The isoWATFLOOD subroutines in order of computation are shown in Figure 3.3. All ^{2}H modules were developed for the present study, while the ^{18}O modules created by Stadnyk-Falcone (2008) have been restructured to improve efficieny by eliminating iterated solutions and now include snowpack composition evolution and transpiration.

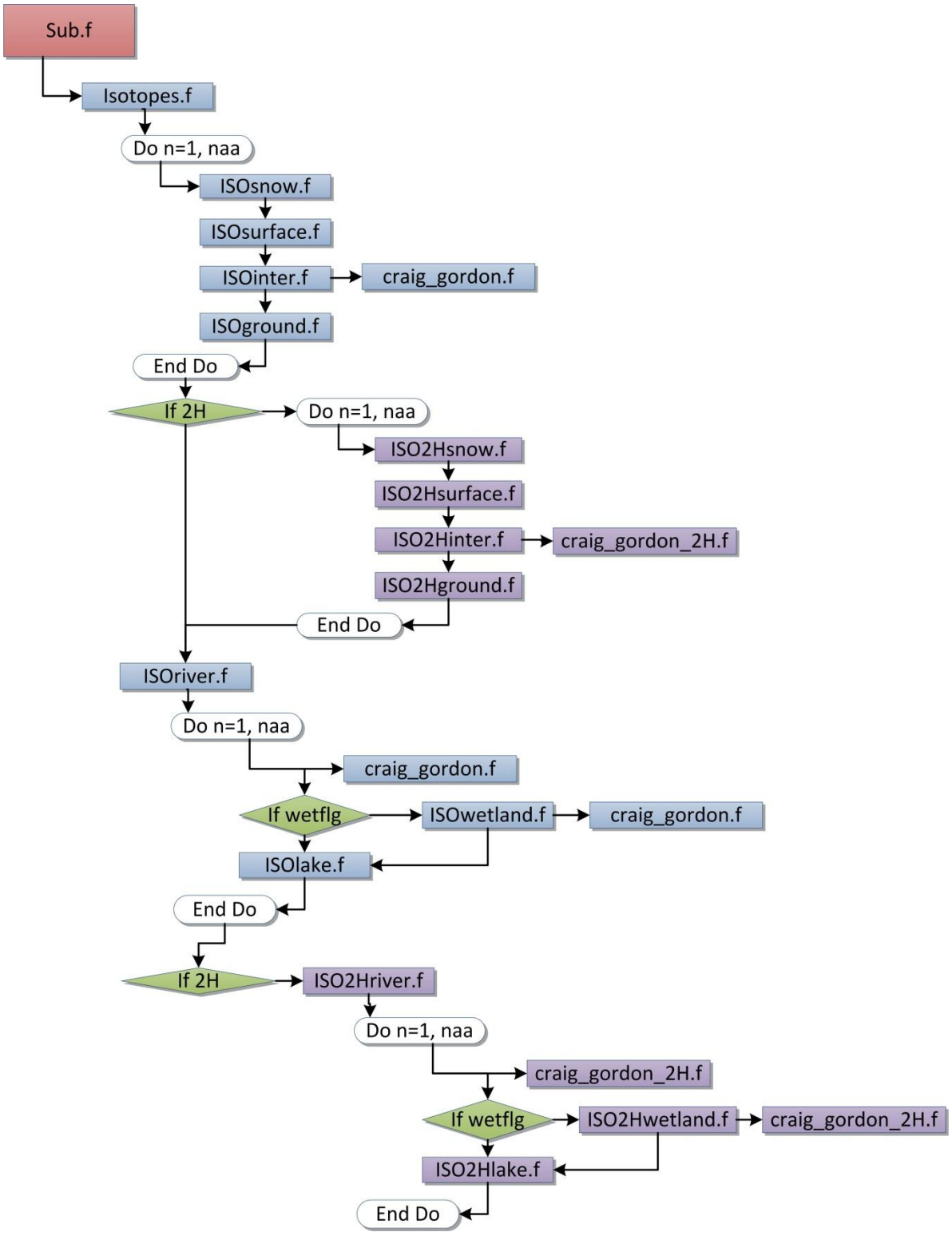

Figure 3.3 Schematic of isoWATFLOOD subroutines where n=1,naa represents the grids in a given watershed model, in order of drainage (high to low elevation).

The isoWATFLOOD model requires the isotopic composition of precipitation and relative humidity as atmospheric forcing in addition to the inputs required for WATFLOOD. The initial isotope concentration of all hydrologic compartments is specified in an input file 'isotope.init'; this initial concentration becomes insignificant as new inflows are added to the compartment and stored water is removed. The spin-up period where the initialization values affect the isotopic composition varies in length as a function of the residence time of the compartment, from less than a day to multiple months.

The isotope volume in each storage compartment is computed each time interval based on the stored volume at the beginning of the time interval, and the inflow and outflow over the time interval. Volumes within WATFLOOD and isoWATFLOOD are measured in cubic meters, while isotope concentrations are unitless. The types of inflows and outflows differ between compartments based on the hydrological behaviors simulated for the storage compartment in WATFLOOD, shown previously in Figure 3.2.

3.2.1 Forcing data

The isoWATFLOOD model requires forcing data beyond the temperature and precipitation data required by the WATFLOOD hydrological model. Firstly, relative humidity is needed to model the behavior of stable water isotopes in evaporating water. Ideally measured relative humidity data should be used as forcing, as it is not easily derived from other atmospheric variables. A new option to read in and use humidity data has therefore been added to the isoWATFLOOD model in order to improve the physical basis of the simulations in this study. Like the temperature data, point measurements of relative humidity are distributed spatially using the distance squared method if there are multiple data locations within the basin, providing a relative humidity value for each grid cell (Kouwen, 2014). The distributed relative humidity data will have the same frequency as the observed data. If no measured data is available, the original method from Stadnyk-Falcone (2008) is used, where relative humidity is estimated using the air temperature.

The model also requires an isotopic composition for precipitation, which, when combined with precipitation data, produces the isotope volume input. There are two options for the precipitation composition forcing: uniform average annual compositions and distributed compositions. The uniform average annual concentration method is both simpler and less representative of daily and seasonal variability in isotopes in precipitation. In the model initialization file, two isotope compositions can be specified for each year, an average composition of rain, and an average composition of snow, both based on long-term observations for the basin. These compositions are then used as the composition of all rainfall and all snowfall across the entire basin for the specified year. While this method does allow for the variation of isotopes in precipitation between years and between winter and summer found in measured compositions, it cannot capture the variation in composition found at finer temporal or spatial scales. Alternatively, the distributed isotope composition read-in, recently developed from the work of Delavau, et al. (2015), can be used. The new gridded composition input files allow for variations in composition across the basin area and the composition time interval can be set by the user should higher-resolution observations be available.

Typically water is only added to the basin area via precipitation; however, flows can be added to the WATFLOOD hydrological model from outside of the watershed area, to account for upstream areas not included in the model, and artificial diversions between watersheds. These flows should not be assumed to have the same concentration as precipitation, so a distinct isotope concentration is needed. The isoWATFLOOD model has therefore been expanded to use observed data as forcing for flows from outside of the modeled area; the isotope concentration of the diverted water is the most temporally proximate observed concentration in the observed time series.

3.2.2 Evaporation fractionation

Stable water isotopes have different physical properties; these differences mean that the isotopes do not change state at the same rate, which alters the isotope concentration of water undergoing phase change in a predictable manner. The most significant process that changes isotope concentrations, or fractionates isotopes in water, is evaporation. To model fractionation due to evaporation the concentration of stable water isotopes in the evaporated water vapor, C_E^{iso}, is needed; this concentration is dependent on both atmospheric conditions and the concentration of the evaporating water body. Isotope concentrations in evaporated water are calculated in craig_gordon.f and craig_gordon_2H.f for $\delta^{18}O$ and $\delta^{2}H$ respectively, as the two isotopes fractionate differently. The isotope composition of evaporating water in delta format, δ_E and the limiting isotopic composition, δ^*, are calculated using the equations presented in Section 2.2.2. The evaporating water composition is dependent on the composition of the water source undergoing evaporation, which can be different for each storage compartment in the model. The simulation uses the composition from the previous time interval in calculating δ_E for any storage undergoing evaporative fractionation, including soil storages, connected wetlands and lakes. The simulated evaporative fractionation assumes that the evaporation source is well mixed, and that the source water composition and all atmospheric conditions remain constant through the simulation time interval which is one hour, or potentially less for wetlands and lakes.

3.2.3 Snowpack

The snowpack stores precipitation before releasing it as melt water, and in WATFLOOD each land class has a snowpack. Precipitation is defined as snow or rain based on the air temperature; when snow falls, the area is covered by the snowpack. The volume stored in the snowpack increases with each snowfall, and loses water to sublimation. During the ripening phase, the snowpack can contain both frozen and liquid water; liquid water can either come from rain falling on snow or from snowmelt. Snowmelt is

modeled based on the air temperature, when the air temperature is greater than the user specified melting temperature for the land class, frozen water is melted and the snowpack area can decrease. If the amount of liquid water in the snowpack exceeds the liquid storage capacity of the snowpack, the excess is transferred either to the surface storage compartment for land classes with soil storages, or directly to the channel or connected wetland for snowpack on the water, connected wetland or impervious land classes. The snowpack mass balance in WATFLOOD is illustrated in Figure 3.4.

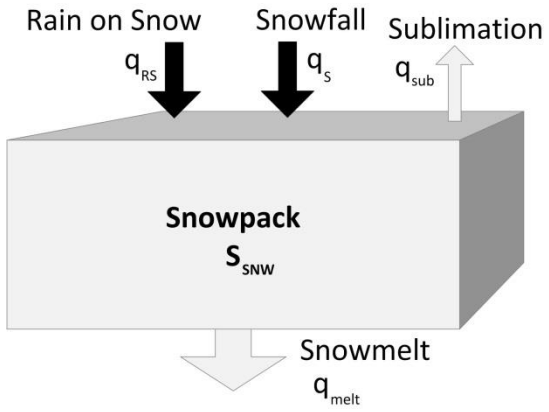

Figure 3.4 Snowpack mass balance in WATFLOOD.

The isotope mass balance of the snowpack is calculated in ISOsnow.f and ISO2Hsnow.f for $\delta^{18}O$ and $\delta^{2}H$, respectively. Each land class within a grid has its own snowpack, the composition of which can now change over time. The isotope volume added to the snowpack, I_{SNW}^{iso}, is a function of the precipitation over the time interval:

$$I_{SNW}^{iso} = \left(C_{RS}^{iso} q_{RS} + C_{S}^{iso} q_{S}\right)\Delta t \qquad (3.3)$$

Where C_S^{iso} and C_{RS}^{iso} are the isotopic concentrations of snow and rain and q_S and q_{RS} are the inflows from snow and rain on the snowpack. The water volume removed from the snowpack, Q_{SNW}, includes snowmelt, q_{melt}, and sublimation, q_{sub}:

$$Q_{SNW} = (q_{melt} + q_{sub})\Delta t \qquad (3.4)$$

The volume of water stored in the snowpack at the end of the time interval, $S_{SNW,2}$, is known because WATFLOOD`s calculations for the time interval are completed prior to the isotope module is run. The volume of isotopes in the snowpack at the end of the time interval, $S^{iso}_{SNW,2}$, can therefore be directly computed as:

$$S^{iso}_{SNW,2} = \frac{S^{iso}_{SNW,1} + I^{iso}_{SNW}}{1 + Q_{SNW}/S_{SNW,2}} \quad (3.5)$$

Where $S^{iso}_{SNW,1}$ is the volume of isotopes in the snowpack at the beginning of the time interval. The concentration of isotopes in the snowpack, C^{iso}_{SNW}, is calculated using the storage volumes at the end of the time interval:

$$C^{iso}_{SNW} = \frac{S^{iso}_{SNW,2}}{S_{SNW,2}} \quad (3.6)$$

This concentration is also the concentration assigned to the snowmelt and sublimation fluxes removed from the snowpack based on the assumption that fractionation from melt and sublimation is negligible. The snowpack composition is constant through the pack depth, and through the time interval, based on an assumption of instant and complete mixing of the snowpack through its depth. While this is not physically possible, as the pack is solid water and does not readily mix, the implication of this assumption is that melt and sublimation occur evenly through the entire snowpack depth.

3.2.4 Surface Storage

The surface storage in the WATFLOOD model represents water stored on the ground surface in small depression storages. Surface storage for each land class is divided into two parts: snow covered area and bare area. The snow covered area is defined by the area of the snowpack, which is reduced as the pack melts; the snow covered area can have different soil properties than the bare area. Meltwater from the snowpack is added to surface storage, as is glacial melt if any glaciers are included in the model. Rain over the bare area of the surface is also added; the rainfall inflow can be reduced by interception (on

vegetation) depending on the land class. Infiltration from the surface to the upper zone of soil is calculated based on the soil properties and the depth of ponded water. The volume of water in the surface compartment cannot exceed the depression storage for the land class; excess water becomes direct runoff. Evaporation from surface storage is assumed to be negligible and is therefore not included in the model, since surface storage is highly transient. A surface water storage compartment with all possible fluxes is illustrated in Figure 3.5.

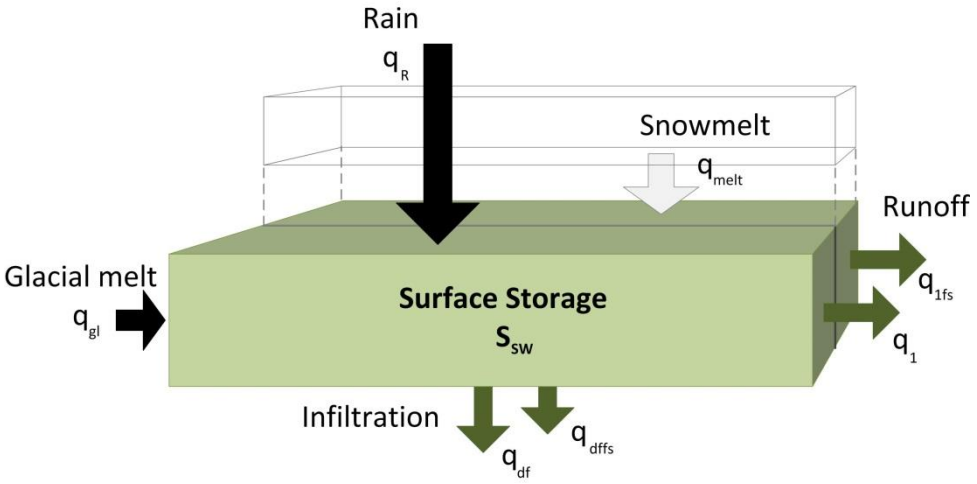

Figure 3.5 Surface storage mass balance in WATFLOOD.

The surface isotope mass balance is calculated in ISOsurface.f and ISO2Hsurface.f for $\delta^{18}O$ and $\delta^{2}H$, respectively, with separate surface compartments for each land class within a grid. The isotope volume added to the surface compartment, I_{SW}^{iso}, includes rain on bare ground, q_R, snowmelt, q_{melt}, and glacial melt, q_{gl}:

$$I_{SW}^{iso} = \left(C_R^{iso} q_R + C_{SNW}^{iso} q_{melt} + C_{gl}^{iso} q_{gl}\right)\Delta t \qquad (3.7)$$

Where C_R^{iso} is the isotope concentration of rain, C_{SNW}^{iso} is the isotope concentration of snowmelt (from ISOsnow.f or ISO2Hsnow.f) and C_{gl}^{iso} is the isotope concentration of glacial melt. The volume of water removed from surface storage, Q_{SW}, includes infiltration from bare and frozen soil, q_1 and q_{1fs}, and lateral runoff into the channel or wetlands from bare and frozen soil, q_{df} and q_{dffs} :

$$Q_{SW} = \left(q_1 + q_{1fs} + q_{df} + q_{dffs}\right)\Delta t \quad (3.8)$$

The volume of water in the surface compartment at the end of the time interval, $S_{SW,2}$, is known from the calculations completed in WATFLOOD before the isotope module is run. Two separate cases exist for the surface isotope mass balance, depending on the water volume retained in the surface compartment. If the water volume is greater than zero, the isotope volume in the surface compartment at the end of the time interval, $S_{SW,2}^{iso}$, is calculated using the isotope volume in the surface compartment at the beginning of the time interval, $S_{SW,1}^{iso}$:

$$S_{SW,2}^{iso} = \frac{S_{SW,1}^{iso} + I_{SW}^{iso}}{1 + Q_{SW}/S_{SW,2}} \quad (3.9)$$

The concentration of the outflow from surface storage, C_{SW}^{iso}, is then:

$$C_{SW}^{iso} = \frac{S_{SW,2}^{iso}}{S_{SW,2}} \quad (3.10)$$

In the case where there is no water volume remaining at the end of the time interval (i.e., outflow exceeds storage), $S_{SW,2}$ will be equal to zero and the isotope volume will be:

$$S_{SW,2}^{iso} = 0 \quad (3.11)$$

However, the outflow from the surface compartment may still be positive, either from the infiltration of old storage, new inflows, or some combination of the two. The concentration of the outflow from surface storage is then:

$$C_{SW}^{iso} = \frac{S_{SW,1}^{iso} + I_{SW}^{iso}}{S_{SW,1} + I_{SW}} \quad (3.12)$$

Where $S_{SW,1}$ is the water volume in the surface compartment at the beginning of the time interval, and I_{SW} is the volume of water added over the time interval:

$$I_{SW} = \left(q_R + q_{melt} + q_{gl}\right)\Delta t \quad (3.13)$$

The surface water isotope model assumes instant and complete mixing of the surface water and constant isotopic composition within the hourly time interval. These assumptions are reasonable, as the surface water storage volume is small and very shallow, such that any new inputs (which would be of constant composition across the GRU area) would be mixed throughout the surface water depth immediately.

3.2.5 Upper Zone Storage

The WATFLOOD model has two subsurface compartments: upper zone and lower zone storage. The upper zone is immediately below the surface, and can be saturated or unsaturated. Like surface storage, the upper zone for each land class is divided into snow covered area and bare area; the snow covered area is defined by the area of the snowpack and this frozen soil can have different properties than the bare area (defined by WATFLOOD parameters). Water enters the upper zone compartment through infiltration from the associated surface compartment. Evapotranspiration occurs only from the upper zone for land classes with surface and upper zone storages; the evapotranspiration loss depends on the amount of water stored in the upper soil storage. If there is sufficient water stored in the upper zone, vertical drainage to the lower zone and lateral interflow will both occur. An upper zone storage compartment with all possible fluxes is illustrated in Figure 3.6.

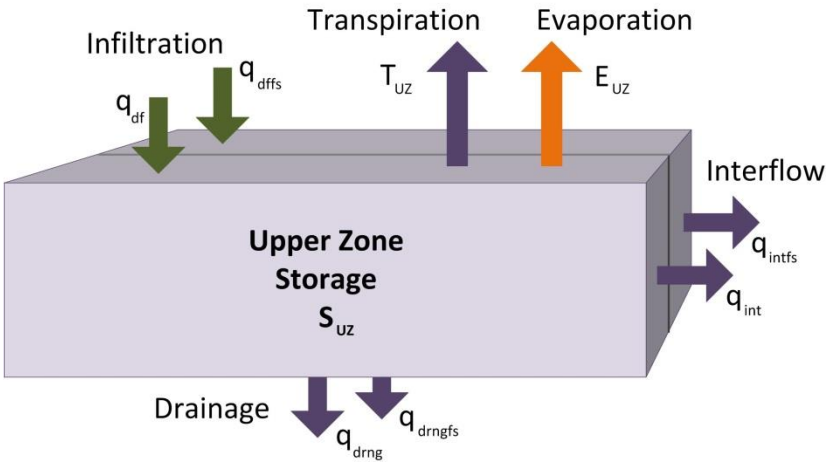

Figure 3.6 Upper zone storage mass balance in WATFLOOD.

The upper zone isotope mass balance is calculated in ISOinter.f and ISO2Hinter.f for $\delta^{18}O$ and $\delta^{2}H$, respectively, with separate surface compartments for each land class within a grid. The upper zone storage model for isotopes has been modified extensively in the course of this study from the original work by Stadnyk-Falcone (2008), with the introduction of a transpiration flux being the most notable addition. The isotope volume entering the upper zone, I_{UZ}^{iso}, includes both infiltration from bare soil, q_{df}, and from frozen soil, q_{affs}:

$$I_{UZ}^{iso} = C_{SW}^{iso}(q_{df} + q_{affs})\Delta t \qquad (3.14)$$

The isotopic concentration of the inflow, C_{SW}^{iso}, is the concentration of the surface storage, calculated previously in ISOsurface.f or ISO2Hsurface.f. The volume of water moved from the upper zone to other compartments, Q_{UZ}, is the summation of vertical drainage and lateral interflow:

$$Q_{UZ} = (q_{int} + q_{intfs} + q_{drng} + q_{drngfs})\Delta t \qquad (3.15)$$

Where q_{int} and q_{intfs} are interflow from bare and frozen soil, and q_{drng} and q_{drngfs} are drainage from bare and frozen soil. The volume of water both transpired, T_{UZ}, and evaporated, E_{UZ}, from the upper zone over the time interval are also removed, separated as described in Section 3.1.2. Transpiration is assumed to be non-fractionating in isoWATFLOOD, with transpired water having the same isotopic

concentration as the upper zone storage. Evaporated water is given the isotopic concentration $C_{UZ,E}^{iso}$, calculated in craig_gordon.f or craig_gordon_2H.f (Section 3.2.2). The volume of isotopes in the upper zone at the end of the time interval, $S_{UZ,2}^{iso}$, can be calculated directly, since all other variables; including $S_{UZ,1}^{iso}$, the volume of isotopes in the upper zone at the beginning of the time interval and $S_{UZ,2}$, the water volume in the upper zone at the end of the time interval; are known:

$$S_{UZ,2}^{iso} = \frac{S_{UZ,1}^{iso} + I_{UZ}^{iso} - C_{UZ,E}^{iso} E_{UZ}}{1 + (Q_{UZ} + T_{UZ})/S_{UZ,2}} \quad (3.16)$$

The isotopic concentration of the drainage and interflow depends on the concentration of the upper zone storage:

$$C_{UZ}^{iso} = \frac{S_{UZ,2}^{iso}}{S_{UZ,2}} \quad (3.17)$$

The upper zone isotope model assumes instant and complete mixing through the upper zone depth, such that the source water for the evaporated water isotope composition is fully mixed; this assumption will not be realistic when new water is added to the storage, since the rate of movement through the soil will be less than needed for complete mixing even over the simulation time interval. The isotopic composition of the upper zone storage and fluxes are assumed to be constant through the one hour simulation time interval, and meteorological conditions affecting evaporative fractionation are also assumed to be constant through this period. The isotopic composition of the lower zone storage is assumed to have no effect on the upper zone composition.

3.2.6 Lower Zone Storage

The lower zone soil water storage compartment represents the saturated zone not affected by surface conditions. The lower zone storage is not divided by land cover or snow cover; all upper zone storage compartments (from each land cover class) in a grid drain into the one lower zone storage in the grid. The lower zone has a single outflow, baseflow: the magnitude of which depends on the volume stored in

the lower zone. Deep groundwater flows are not currently included in the WATFLOOD model. A lower zone storage compartment with all possible fluxes is illustrated in Figure 3.7.

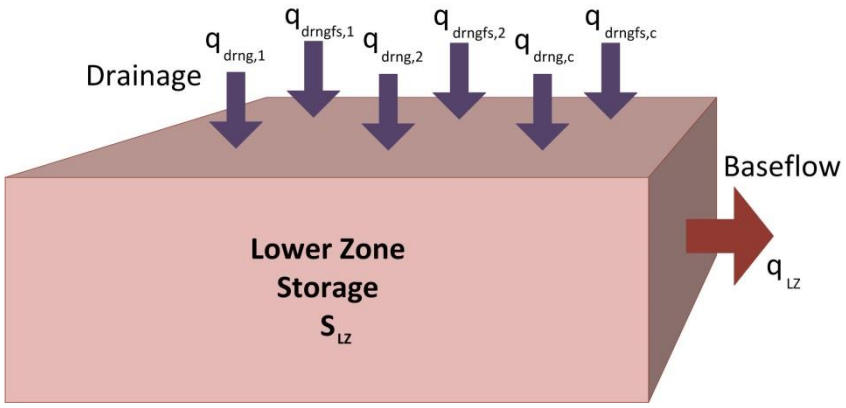

Figure 3.7 Lower zone storage mass balance in WATFLOOD, with drainage from the upper zone storages.

The lower zone isotope mass balance is calculated in ISOground.f and ISO2Hground.f for $\delta^{18}O$ and $\delta^{2}H$, respectively. All drainages originating in upper zone storages, including bare soil drainage, q_{drng}, and frozen soil drainage, q_{drngfs}, are included in the isotope volume added to the lower zone, I_{LZ}^{iso}:

$$I_{LZ}^{iso} = \sum_{i=1}^{c} C_{UZ,i}^{iso}\left(q_{drng,i} + q_{drngfs,i}\right)\Delta t \qquad (3.18)$$

Where *c* is the number of land classes with upper zone storages and C_{UZ}^{iso} is the isotopic concentration of the upper zone, calculated in ISOinter.f or ISO2Hinter.f. The only outflow from the lower zone is the baseflow, q_{lz}, so the volume of water removed from the lower zone storage, Q_{LZ}, is:

$$Q_{LZ} = q_{lz}\Delta t \qquad (3.19)$$

The volume of isotopes in the lower zone at the beginning of the time interval, $S_{LZ,1}^{iso}$, and the volume of water in the lower zone at the end of the time interval, $S_{LZ,2}$, are known from WATFLOOD, so the volume of isotopes in the lower zone storage can be calculated directly:

$$S_{LZ,2}^{iso} = \frac{S_{LZ,1}^{iso} + I_{LZ}^{iso}}{1 + Q_{LZ}/S_{LZ,2}} \quad (3.20)$$

The baseflow concentration, C_{LZ}^{iso}, depends on the lower zone storage at the end of the time interval:

$$C_{LZ}^{iso} = \frac{S_{LZ,2}^{iso}}{S_{LZ,2}} \quad (3.21)$$

The lower zone storage is assumed to be instantly and completely mixed regardless of the storage volume, and the isotopic composition of the lower zone storage and outflow are assumed to be unvarying through the one hour simulation time interval. The instant and completing mixing assumption for the lower zone will not be accurate when new inflows are added to the stored volume, as the groundwater volume can be very large.

3.2.7 Connected Wetland

The WATFLOOD hydrological model has optional connected wetlands; the connected wetland model represents wetlands directly connected to the river or stream. There is the potential for water to flow from the wetland to the stream, and for water to flow from the stream into the wetland (depending on the hydraulic gradient) (Kouwen, 2014). As connected wetlands occur on the edges of channels (i.e., riparian zones), water coming from the land is added to the connected wetland as inflow, with the wetland acting as a buffer. The connected wetlands land class has its own snowpack; the meltwater from this snowpack is added directly to the wetland. Rain falling over the connected wetland area is also added directly to the connected wetland storage compartment. Both evaporation and transpiration are removed from the connected wetland. The connection between the wetland and the channel can transfer water in either direction; if the hydraulic head in the wetland is greater than the head in the channel water will flow from the wetland into the channel, otherwise the flow will reverse direction and the channel will lose flow to the wetland. A connected wetland storage compartment with fluxes is

illustrated in Figure 3.8; the number of runoff and interflow influxes depends on the number of GRU present in the grid cell.

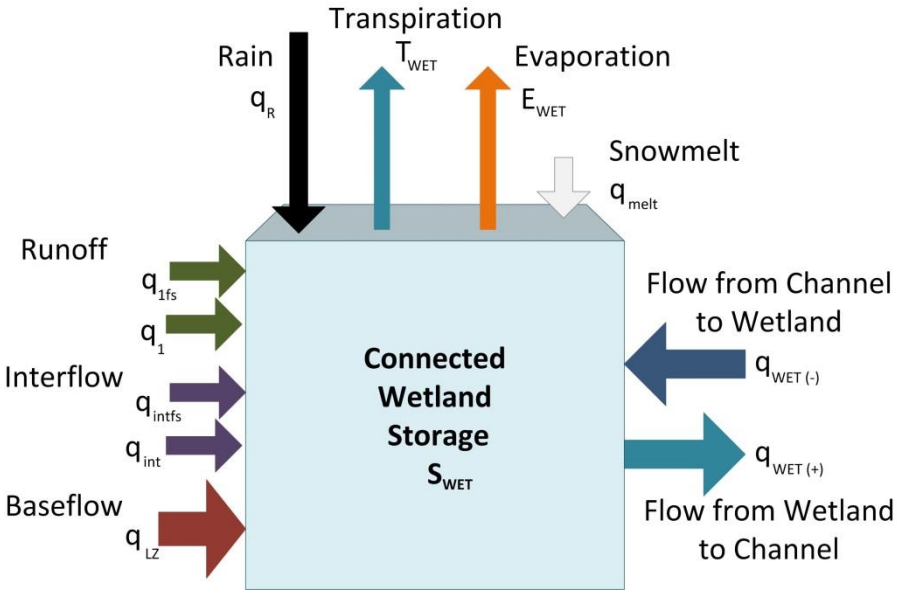

Figure 3.8 Connected wetland mass balance in WATFLOOD.

If connected wetlands are used by the WATFLOOD model, the connected wetlands isotope mass balance is calculated in ISOwetland.f and ISO2Hwetland.f for $\delta^{18}O$ and $\delta^{2}H$, respectively. Evaporation, a fractionating process, occurs in connected wetlands. The fractionation is modeled using the equations for the volume-dependent model lakes presented in Gibson (2002). The first step is to find the isotopic concentration of the wetland without evaporative enrichment. The inflow and outflow from the wetland depends on the direction of flow between the wetland and the channel. If the flow, q_{WET}, is positive, water is moving from the wetland to the channel. The volume of isotopes added to the wetland storage over the current time interval, $I^{iso}_{WET,2}$, includes isotopes from direct rainfall, q_R, snowmelt from the wetland snowpack, q_{melt}, interflow from bare and frozen soil, q_{int} and q_{intfs}, direct runoff from bare and frozen soil, q_1 and q_{1fs}, and baseflow, q_{lz}:

$$I^{iso}_{WET,2} = \left(C^{iso}_R q_R + C^{iso}_{SNW} q_{melt}\right)\Delta t + \sum_{i=1}^{c}\left(C^{iso}_{UZ,i}\left(q_{int,i} + q_{intfs,i}\right) + C^{iso}_{SW,i}\left(q_{1,i} + q_{1fs,i}\right)\right)\Delta t \quad (3.22)$$

$$+ C^{iso}_{LZ} q_{lz}\Delta t - C^{iso}_{WET,1}(E_{WET} + T_{WET})\Delta t$$

Where *c* is the number of terrestrial land classes, C^{iso}_R is the isotopic concentration of rainfall, C^{iso}_{SNW} is the isotopic concentration of snowmelt (from ISOsnow.f or ISO2Hsnow.f), C^{iso}_{UZ} is the isotopic concentration of the upper zone (from ISOinter.f or ISO2Hinter.f), C^{iso}_{SW} is the isotopic concentration of surface water (from ISOsurface.f or ISO2Hsurface.f), and C^{iso}_{LZ} is the isotopic concentration of the lower zone (from ISOground.f or ISO2Hground.f). Evaporation, E_{WET}, and transpiration, T_{WET}, from the wetland are removed from the inflow; both are assumed to have the isotope concentration of the wetland storage at the beginning of the time interval, $C^{iso}_{WET,1}$ in the initial mass balance. Because evapotranspiration is removed from the inflow, the volume of water removed from the wetland storage over the current time interval, $Q_{WET,2}$, depends only on the flow into the channel:

$$Q_{WET,2} = q_{WET}\Delta t \quad (3.23)$$

WATFLOOD calculates the storage in connected wetlands using the inflow and outflow from the current and the previous time interval. The isotope storage calculation must match the method used for water, but because the water mass balance has already been calculated for the time interval, the storage of isotopes in the wetland at the end of the time interval, $S^{iso}_{WET,2}$, can be calculated directly, without iteration:

$$S^{iso}_{WET,2} = \frac{S^{iso}_{WET,1} + \left(I^{iso}_{WET,1} + I^{iso}_{WET,2} - Q^{iso}_{WET,1}\right)/2}{1 + Q_{WET,2}/2S_{WET,2}} \quad (3.24)$$

where $S^{iso}_{WET,1}$ is the storage of isotopes in the wetland at the beginning of the time interval, $I^{iso}_{WET,1}$ is the volume of isotopes added to the wetland in the previous time interval, $Q^{iso}_{WET,1}$ is the volume of isotopes removed from the wetland in the previous time interval, and $S_{WET,2}$ is the storage of water in the wetland at the end of the time interval.

If the flow, q_{WET}, is negative, water is moving from the channel into the wetland. In this case, the volume added to the wetland also includes the wetland flow, which is subtracted since it is negative:

$$I_{WET,2}^{iso} = \left(C_R^{iso} q_R + C_{SNW}^{iso} q_{melt}\right)\Delta t + \sum_{i=1}^{c} \left(C_{UZ,i}^{iso}\left(q_{int,i} + q_{intfs,i}\right) + C_{SW,i}^{iso}\left(q_{1,i} + q_{1fs,i}\right)\right)\Delta t \\ + C_{LZ}^{iso} q_{lz}\Delta t - C_{WET,1}^{iso}(E_{WET} + T_{WET})\Delta t - C_{STR,1}^{iso} q_{WET}\Delta t \quad (3.25)$$

The flow from the channel is assumed to have the same concentration as the streamflow in the previous time interval, $C_{STR,1}^{iso}$. Both evapotranspiration and the wetland-channel flow are included in $I_{WET,2}^{iso}$, therefore:

$$Q_{WET,2} = 0 \quad (3.26)$$

The equation for $S_{WET,2}^{iso}$ is then simplified to:

$$S_{WET,2}^{iso} = S_{WET,1}^{iso} + \left(I_{WET,1}^{iso} + I_{WET,2}^{iso} - Q_{WET,1}^{iso}\right)/2 \quad (3.27)$$

For either case the current isotopic concentration of the connected wetland storage, $C_{WET,2}^{iso}$, is:

$$C_{WET,2}^{iso} = \frac{S_{WET,2}^{iso}}{S_{WET,2}} \quad (3.28)$$

The second step, which is only needed if there is evaporation occurring over the time interval, is to calculate the enrichment of the wetland due to evaporation. From the equations in Gibson (2002), the isotopic concentration in delta format of an evaporating water body is calculated using the isotopic concentration of the connected wetland in delta format, $\delta_{WET,2}$:

$$\delta_{WET,E} = \delta_S - \left(\delta_S - \delta_{WET,2}\right)\left(\frac{S_{WET,2}}{S_{WET,1}}\right)^{-\left(1+m\frac{E}{I}\right)/\left(1-\frac{E}{I}-\frac{Q}{I}\right)} \quad (3.29)$$

Where *E* is the volume of water evaporated over the time interval, *I* is the volume of water added to the wetland over the time interval from land outflows, precipitation, snowmelt and flow from the channel and *Q* is the volume of water removed from the wetland either into the stream channel or through

transpiration. $S_{WET,2}$ is the volume of water at the end of the time interval, and $S_{WET,1}$ is the water volume at the beginning of the time interval. The value *m* is defined by Welhan and Fritz (1977) as:

$$m = \frac{h - \varepsilon^*/\alpha^* - \varepsilon_k}{1 - h - \varepsilon_k} \quad (3.30)$$

Where *h* is the fractional relative humidity, and ε^*, α^* and ε_k are calculated as described in Section 3.2.2. δ_S is the steady state isotopic concentration of the evaporating water body:

$$\delta_S = \frac{\delta_I + m\frac{E}{I}\delta^*}{1 + m\frac{E}{I}} \quad (3.31)$$

Where δ_I is the isotopic concentration of *I* in delta format, and δ^* is calculated as described in Section 3.2.2.

The enriched isotopic concentration is then used to update the isotope volume in storage, and the isotope concentration of the storage:

$$S^{iso}_{WET,2} = C^{iso}_{WET,E} S_{WET,2} \quad (3.32)$$

$$C^{iso}_{WET,2} = C^{iso}_{WET,E} \quad (3.33)$$

Regardless of whether the wetland was enriched, the isotope outflow volume $Q^{iso}_{WET,2}$ is calculated for the mass balance calculation in the subsequent time interval:

$$Q^{iso}_{WET,2} = C^{iso}_{WET,2} Q_{WET,2} \quad (3.34)$$

The connected wetland isotope model assumes that all inflows, whether precipitation or groundwater, are instantly and completely mixed into the wetland storage. Meteorological conditions affecting evaporative fractionation and the isotopic composition of the wetland outflow are assumed to be constant over the simulation time interval, which may be hourly or sub-hourly depending on the routing time interval.

3.2.8 River Routing

The WATFLOOD hydrologic model routes flow through a channel network within a defined drainage network (with drainage order determined by elevation from the DEM). Each grid contains one section of the network channel storage, which can receive water from multiple upstream grids. Rain and snowmelt over the channel area are added to the grid channel storage, as is the flow generated in the grid land area if connected wetlands are not present, and evaporation is removed. If connected wetlands are included, flow from the wetland to the channel is added to the storage, or removed if the flow reverses directions. The outflow from the channel storage to the downstream receiving grid is calculated using hydrologic storage routing, based on the continuity equation, and using the Manning equation to relate flow and discharge. A channel storage compartment with fluxes is illustrated in Figure 3.9; there can be multiple flows from upstream grids, depending on the drainage network.

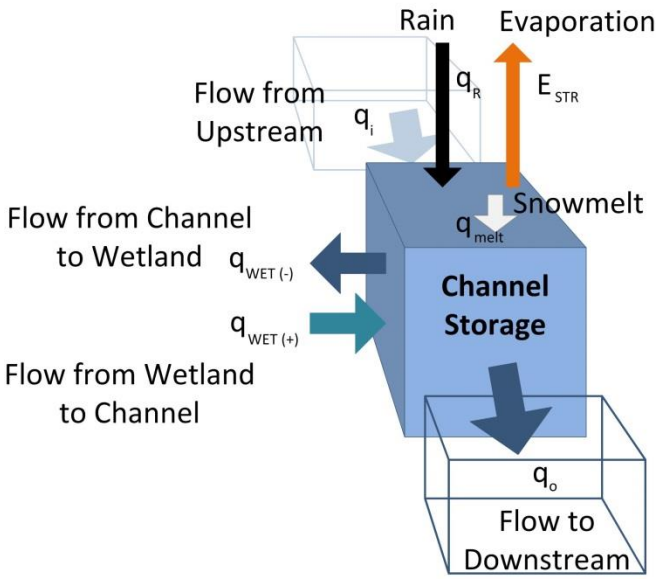

Figure 3.9 Channel mass balance in WATFLOOD.

Routing isotopes in the channel is done in ISOriver.f and ISO2Hriver, for $\delta^{18}O$ and $\delta^{2}H$, respectively. The flow of isotopes matches that of water, with the change in storage dependent on the inflow and outflow at the beginning and end of the time interval. There are three possible cases for the calculation of the

incoming volume of isotopes for the current time interval, $I^{iso}_{STR,2}$. In the most common case, $I^{iso}_{STR,2}$ includes all isotopes coming from upstream grids, $Q^{iso}_{STR,2,U/S}$, and inflows from the connected wetland, rainfall and snowmelt, with evaporation removed:

$$I^{iso}_{STR,2} = \sum Q^{iso}_{STR,2,U/S} + \left(C^{iso}_{WET,2} q_{WET} + C^{iso}_{R} q_R + C^{iso}_{SNW} q_{melt} - C^{iso}_{STR,1} E_{STR}\right)\Delta t \quad (3.35)$$

Where $C^{iso}_{WET,2}$ is the isotopic concentration of the wetland at the end of the time interval (from ISOwetland.f or ISO2Hwetland.f), q_{WET} is the flow between the channel and wetland, C^{iso}_{R} is the isotopic concentration of rainfall, q_R is the rainfall over the channel, C^{iso}_{SNW} is the isotopic concentration of snowmelt (from ISOsnow.f or ISO2Hsnow.f), q_{melt} is the snowmelt from the channel snowpack, $C^{iso}_{STR,1}$ is the isotopic concentration of the channel at the beginning of the time interval and E_{STR} is the volume of water evaporated from the channel over the time interval. Although evaporation is a fractionating process, enrichment due to evaporation is not currently included in the isoWATFLOOD model, as evaporation directly from the stream channel is not a significant part of the mass balance, and the combination of turbulent flow and short residence time in the channel are assumed to prevent fractionation in streams on the scale typically simulated in WATFLOOD. The flow from the connected wetland can also be negative, such that channel water is transferred to the connected wetland, with the wetland flow having the concentration of the channel at the beginning of the time interval:

$$I^{iso}_{STR,2} = \sum Q^{iso}_{STR,2,U/S} + \left(C^{iso}_{STR,1} q_{WET} + C^{iso}_{R} q_R + C^{iso}_{SNW} q_{melt} - C^{iso}_{STR,1} E_{STR}\right)\Delta t \quad (3.36)$$

Finally, if connected wetlands are not used in the WATFLOOD model, water from the land area is added to the channel directly:

$$I^{iso}_{STR,2} = \sum Q^{iso}_{STR,2,U/S} + \sum_{i=1}^{c} \left(C^{iso}_{UZ,i}\left(q_{int,i} + q_{intfs,i}\right) + C^{iso}_{SW,i}\left(q_{1,i} + q_{1fs,i}\right)\right)\Delta t + C^{iso}_{LZ} q_{lz}\Delta t + \left(C^{iso}_{R} q_R + C^{iso}_{SNW} q_{melt} - C^{iso}_{STR,1} E_{STR}\right)\Delta t \quad (3.37)$$

Where *c* is the number of terrestrial land classes, q_{int} and q_{intfs} are interflow from bare and frozen soil, C_{UZ}^{iso} is the isotopic concentration of the upper zone (from ISOinter.f or ISO2Hinter.f), C_{SW}^{iso} is the isotopic concentration of surface water (from ISOsurface.f or ISO2Hsurface.f), q_1 and q_{1fs} are direct runoff from bare and frozen soil, C_{LZ}^{iso} is the isotopic concentration of the lower zone (from ISOground.f or ISO2Hground.f) and q_{lz} is baseflow. Only the outflow to the downstream grid, q_o, is included in the outflow volume in the current time interval, $Q_{STR,2}$:

$$Q_{STR,2} = q_o \Delta t \qquad (3.38)$$

The isotope storage in the channel at the end of the time interval, $S_{STR,2}^{iso}$, is calculated from the isotope storage at the beginning of the time interval, $S_{STR,1}^{iso}$; the isotope volume added in the current and previous time intervals, $I_{STR,1}^{iso}$ and $I_{STR,2}^{iso}$; the isotope volume removed in the previous time interval, $Q_{STR,1}^{iso}$; and the water stored in the channel at the end of the time interval, $S_{STR,2}$:

$$S_{STR,2}^{iso} = \frac{S_{STR,1}^{iso} + \left(I_{STR,1}^{iso} + I_{STR,2}^{iso} - Q_{STR,1}^{iso}\right)/2}{1 + Q_{STR,2}/2S_{STR,2}} \qquad (3.39)$$

The concentration of isotopes in the channel storage and outflow is:

$$C_{STR,2}^{iso} = \frac{S_{STR,2}^{iso}}{S_{STR,2}} \qquad (3.40)$$

The volume of isotopes removed in the current time interval is also calculated for the mass balance in the subsequent interval:

$$Q_{STR,2}^{iso} = C_{STR,2}^{iso} Q_{STR,2} \qquad (3.41)$$

All channel storage in a grid cell is assumed to be instantly and completely mixed, and the outflow composition is assumed to be constant for the simulation time interval, which may be hourly or sub-hourly depending on the routing time interval.

3.2.9 Reservoir Routing

Natural lakes and regulated reservoirs can be included in WATFLOOD by designating grid cells as part of a reservoir. In these grid cells, the water land class is lake area, rather than channel area as it is in standard grids. Lakes can be made up of a single or multiple grid cells, with the water area from each grid being part of the same lake storage compartment. Connected wetlands are not present in lake grid cells; if any flow is generated in the land area, it is added directly to the lake, along with flow from all upstream grid cells and all wetland area is included in the land area. As with channel storage, rainfall and snowmelt from the water area are added directly to the lake, and evaporation is removed. There is a single discharge to the downstream receiving grid cell, with the flow rate typically determined from a user-specified storage-discharge relationship (Kouwen, 2014). A lake storage compartment with fluxes is illustrated in Figure 3.10; the number of runoff and interflow influxes depends on the number of GRU present in reservoir grid cells, and the total number of grid cells included in the reservoir.

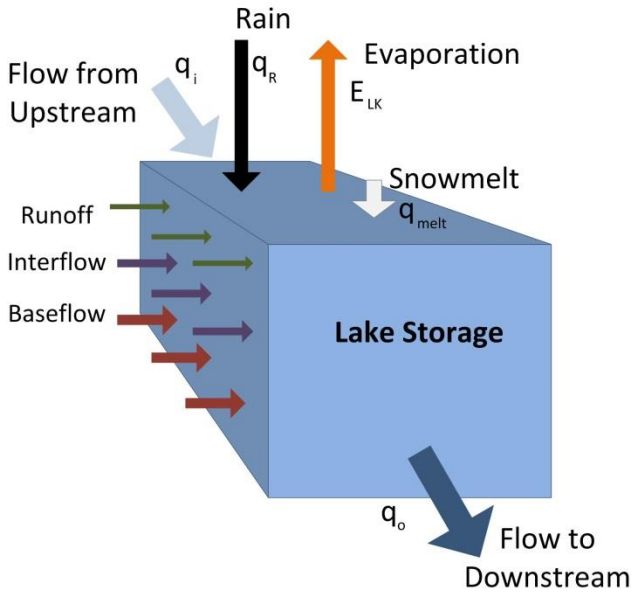

Figure 3.10 Lake mass balance in WATFLOOD.

Routing isotopes in lakes is performed in ISOlake.f and ISO2Hlake.f for $\delta^{18}O$ and $\delta^{2}H$, respectively. Evaporative fractionation is modeled using the equations for the time-dependent model lakes presented

in Gibson (2002). Firstly, the isotopic concentration of the lake prior to evaporative enrichment is calculated from the mass balance in the lake. The isotope volume added into the lake in the current time interval, $I_{LK,2}^{iso}$; including upstream flows, $Q_{STR,2,U/S}^{iso}$; and flows generated from land in the lake grids, snowmelt, and rainfall:

$$I_{LK,2}^{iso} = \sum Q_{STR,2,U/S}^{iso} + \sum_{r=1}^{n}\left(\sum_{i=1}^{c}\left(C_{UZ,i,r}^{iso}\left(q_{int,i,r} + q_{intfs,i,r}\right) + C_{SW,i,r}^{iso}\left(q_{1,i,r} + q_{1fs,i,r}\right)\right)\Delta t + C_{LZ,r}^{iso} q_{lz,r}\Delta t\right) + \left(C_R^{iso} q_R + C_{SNW}^{iso} q_{melt} - C_{LK,1}^{iso} E_{LK}\right)\Delta t \quad (3.42)$$

Where *c* is the number of terrestrial land classes, *n* is the number of grids in the lake, q_{int} and q_{intfs} are interflow from bare and frozen soil, C_{UZ}^{iso} is the isotopic concentration of the upper zone (from ISOinter.f or ISO2Hinter.f), C_{SW}^{iso} is the isotopic concentration of surface water (from ISOsurface.f or ISO2Hsurface.f), q_1 and q_{1fs} are direct runoff from bare and frozen soil, C_{LZ}^{iso} is the isotopic concentration of the lower zone (from ISOground.f or ISO2Hground.f) and q_{lz} is baseflow, C_R^{iso} is the isotopic concentration of rainfall, q_R is the rainfall over the lake, C_{SNW}^{iso} is the isotopic concentration of snowmelt (from ISOsnow.f or ISO2Hsnow.f) and q_{melt} is the snowmelt from the lake snowpack. Evaporation over the time interval, E_{LK}, is assigned the concentration of the lake at the beginning of the time interval, $C_{LK,1}^{iso}$, in the initial mass balance. Only the outflow from the lake to the downstream receiving grid, q_o, is included in $Q_{LK,2}$, the volume of water removed from the lake storage over the current time interval:

$$Q_{LK,2} = q_o \Delta t \quad (3.43)$$

The isotope storage in the lake at the end of the time interval, $S_{LK,2}^{iso}$ is first calculated from the isotope storage at the beginning of the time interval, $S_{LK,1}^{iso}$, the isotope volume added in the current and

previous time interval, $I_{LK,1}^{iso}$ and $I_{LK,2}^{iso}$, the isotope volume removed in the previous time interval, $Q_{LK,1}^{iso}$, and the water stored in the lake at the end of the time interval, $S_{LK,2}$:

$$S_{LK,2}^{iso} = \frac{S_{LK,1}^{iso} + \left(I_{LK,1}^{iso} + I_{LK,2}^{iso} - Q_{LK,1}^{iso}\right)/2}{1 + Q_{LK,2}/2S_{LK,2}} \quad (3.44)$$

The isotope concentration of the lake without evaporative enrichment is then calculated as:

$$C_{LK,2}^{iso} = \frac{S_{LK,2}^{iso}}{S_{LK,2}} \quad (3.45)$$

If any evaporation occurs over the time interval, a new enriched isotope concentration in delta notation, $\delta_{LK,E}$, is calculated using the equations from Gibson (2002):

$$\delta_{LK,E} = \delta_S - \left(\delta_S - \delta_{LK,2}\right)e^{-\left(1+m\frac{E}{I}\right)\frac{It}{V}} \quad (3.46)$$

Where *E* is the volume of water evaporated over the time interval, *I* is the volume of water added to the lake over the time interval from land outflows, precipitation, snowmelt and flow from upstream and *V* is the volume of water in the lake at the beginning of the time interval. This equation assumes that the lake volume is constant over the simulation time interval. $\delta_{LK,2}$ is the isotope concentration of the lake without evaporative enrichment in delta notation. The value *m* is defined by Welhan and Fritz (1977) (see equation 3.30). The enriched isotopic concentration is then used to update the isotope volume in storage, and the isotope concentration of the storage:

$$S_{LK,2}^{iso} = C_{LK,E}^{iso} S_{LK,2} \quad (3.47)$$

$$C_{LK,2}^{iso} = C_{LK,E}^{iso} \quad (3.48)$$

Regardless of whether the lake was enriched, the isotope volume removed in the current time interval, $Q_{LK,2}^{iso}$ is calculated for the mass balance calculation in the subsequent time interval:

$$Q_{LK,2}^{iso} = C_{LK,E}^{iso} Q_{LK,2} \quad (3.49)$$

The lake isotope simulation assumes instant and complete mixing of the lake, and constant isotopic compositions for the lake storage and outflow over the simulation time interval, which may be hourly or sub-hourly depending on the routing time interval. The meteorological conditions affecting evaporative fractionation are assumed to be constant over the simulation time interval, and evaporation is assumed to have no effect on the isotopic composition of atmospheric moisture.

3.3 Summary of Enhancements to isoWATFLOOD

The isoWATFLOOD model has been both expanded and enhanced during the course of this research, in order to improve the utility of the model. Changes to the stable water isotope model include:

- The independent simulation of a second stable water isotope, δ^2H;
- Automated production of isotopic frameworks in δ^2H- $\delta^{18}O$ space;
- The calculation of *d*-excess in dual-isotope simulations;
- Temporally evolving snowpack isotopic compositions;
- Transpiration as a distinct simulated flux;
- Sub-hourly isotope simulations for wetlands, rivers and lakes;
- The option to use observed relative humidity data during simulation;
- Forcing data inputs for diverted flows from outside the modeled area;
- Automated error calculation for isotope simulations;
- The option to use isotope error in WATFLOOD auto-calibration; and
- The replacement of all iterated with direct solutions within the isotope simulation, to improve simulation efficiency.

These changes have not only added a new isotope simulation (δ^2H), but have improved the physical representativeness of the model, decreased simulation run-times by 30 to 50% and rendered isotope simulations in large and regulated watersheds feasible.

4 Study Region

In order to meet the objectives of this study, a study site with extensive isotopic data was needed. The lower Nelson River basin (LNRB) was selected, as numerous sites within the basin have been sampled since 2010, when a stable water isotope monitoring network (SWIMN) was initiated (Smith, et al., 2015). The LNRB is also the type of basin stable isotope modeling is expected to be most useful for: remote, sparsely gauged and with a short period of record (Tetzlaff, et al., 2015). The watershed is large (>90,000 km^2), located in the mid-latitude Canadian boreal forest ecoregion, and wetland and surface water dominated; so the WATFLOOD model is appropriate to use for this study (Kouwen, 2014). Furthermore, a WATFLOOD model of the basin was developed prior to this study, and was available for use in this research.

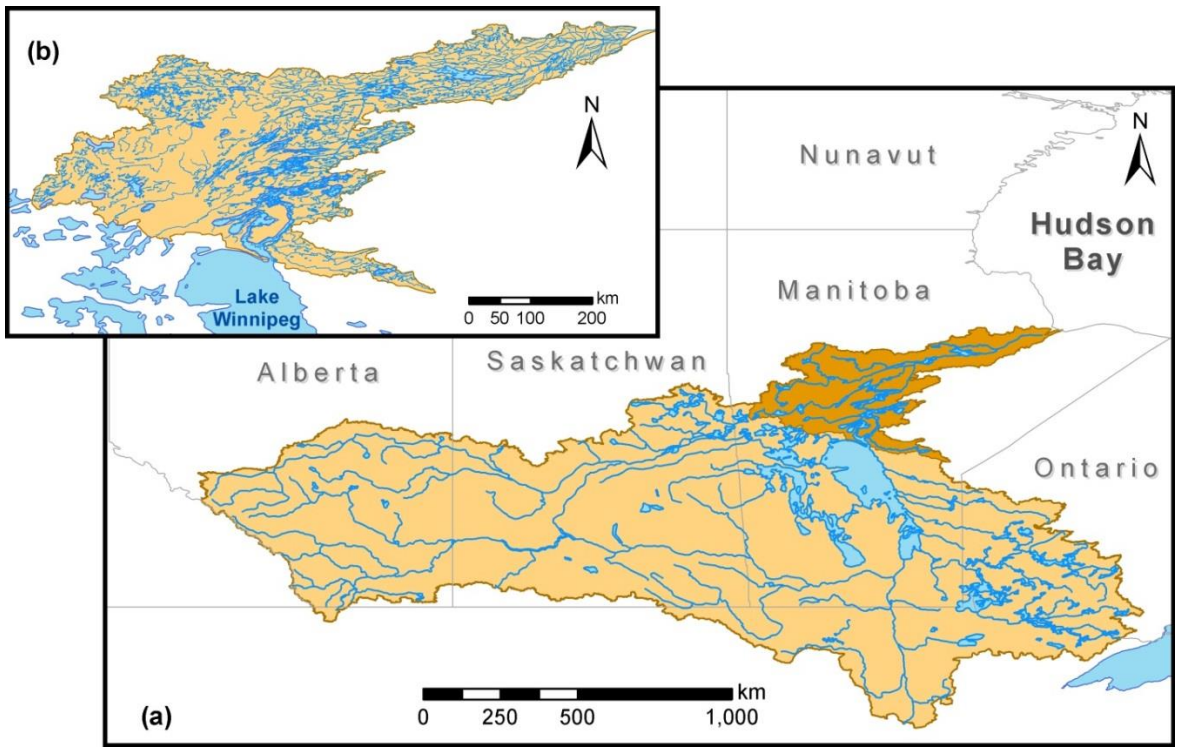

Figure 4.1 (a) The Nelson River basin showing the portion that is considered the lower Nelson River basin (LNRB) and (b) The lower Nelson River basin, from Lake Winnipeg to the Nelson River outlet to Hudson Bay.

The Nelson River basin (NRB) is one of the largest river basins in Canada (1,100,000km^2), draining southern Alberta, Saskatchewan and Manitoba, part of north-western Ontario and a portion of the northern United States (Figure 4.1). The basin includes the Saskatchewan River, the Winnipeg River and the Red and Assiniboine rivers, all of which flow into Lake Winnipeg. The LNRB (90,500km^2) is the downstream sub-basin in the NRB, collecting all water from the NRB before it drains into Hudson Bay through the Nelson River itself.

The following sections describe the LNRB's climate, geology, ecology and hydrology, followed by a description of the hydrometric, isotopic and meteorological data used in this study.

4.1 Climate

The LNRB has a sub-arctic continental climate, characterized by cool summers, cold winters and moderate precipitation and humidity. The snow-free season is short, generally beginning in May and ending in October, with a daily average temperature in summer of 11.5°C over the 1981-2010 climate normal period (Environment Canada, 2016). Winter is drier and cold, where the average daily temperature for the season being around -18°C; January is the coldest month, with an average daily temperature of -23.9°C. Due to the mid- to high latitude of the basin, there are significantly more sunlight hours in summer than winter. Climate normal data is shown in Table 4.1.

Table 4.1 Climate normal data from the Class A meteorological station at Thompson Airport (climate ID: 506922) (Environment Canada, 2016)

Thompson Airport Climate ID: 5062922	
Daily Average (°C)	-2.9
Rainfall (mm)	340.2
Snowfall (cm)	187
Precipitation (mm)	509.2

Precipitation is highest in July, the warmest month of the year in the region, with an average daily temperature of 16.2°C. The majority of precipitation falls in the summer months as rain; approximately 65% of annual precipitation is rainfall. Snow contributes the remaining 35% of annual precipitation in the longer winter season. Given that annual precipitation is only 500mm, evapotranspiration in the region is high, with a loss of approximately 300mm to 350mm per year; and evaporation from open water being even higher at around 450mm per year (Smith, et al., 2015; Environment Canada, 2016). The LNRB is sub-humid, with a mean average relative humidity of 79%- 0600LST and 58%- 1500LST (Environment Canada, 2016).

4.2 Geology

The LNRB lies in large part on the Canadian Shield, a recently glaciated area dominated by shallow or exposed bedrock. The region has extremely low relief, with a maximum elevation of 335 m.a.s.l., and the outlet to Hudson Bay at sea level the average basin slope is 0.037%; elevations for the LNRB are shown in Figure 4.2. Due to the low gradient in the region, surface water bodies such as small lakes and wetlands are prevalent, and the main rivers have numerous channelized lakes.

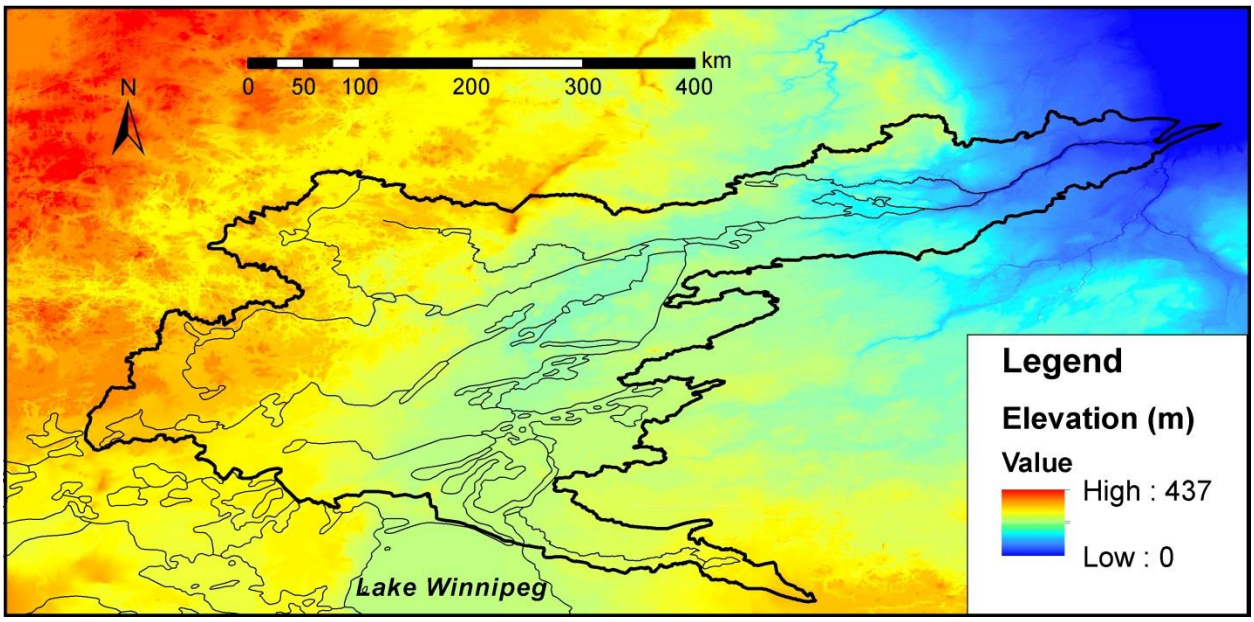

Figure 4.2 Digital elevation map of the LNRB region (Natural Resources Canada, 2011).

The soil in the LNRB is shallow, leaving the Precambrian igneous and metamorphic rocks of the Canadian Shield near the surface or exposed (Agriculture Canada, 2016). In addition to being shallow, due to erosion from glaciers, soils in the LNRB are generally low in organic content, dominated by clays and poorly draining. The majority of the LNRB is underlain by sporadic discontinuous permafrost (between 10 to 50% permafrost), while the downstream Northeastern portion is up to 90% permafrost (Smith, et al., 2015).

4.3 Ecology

The LNRB is located in the boreal forest ecoregion and is largely undeveloped; population is sparse and there are very few roads in the region. Based on satellite land cover imagery obtained from GeoBase® (Natural Resources Canada, 2011) the most common land cover is coniferous forest: 35% of the watershed is covered by coniferous forest of varying densities. Various types of wetlands are the next most prevalent cover in the area; with bogs, fens (wetlands connected to the stream channel) and wetlands covering 26% of the region. Shrub areas and open water are also common, covering 16% and

14% of the basin area respectively. Deciduous and mixed forests are present in the basin, but rare. The land cover for the LNRB is illustrated in Figure 4.3.

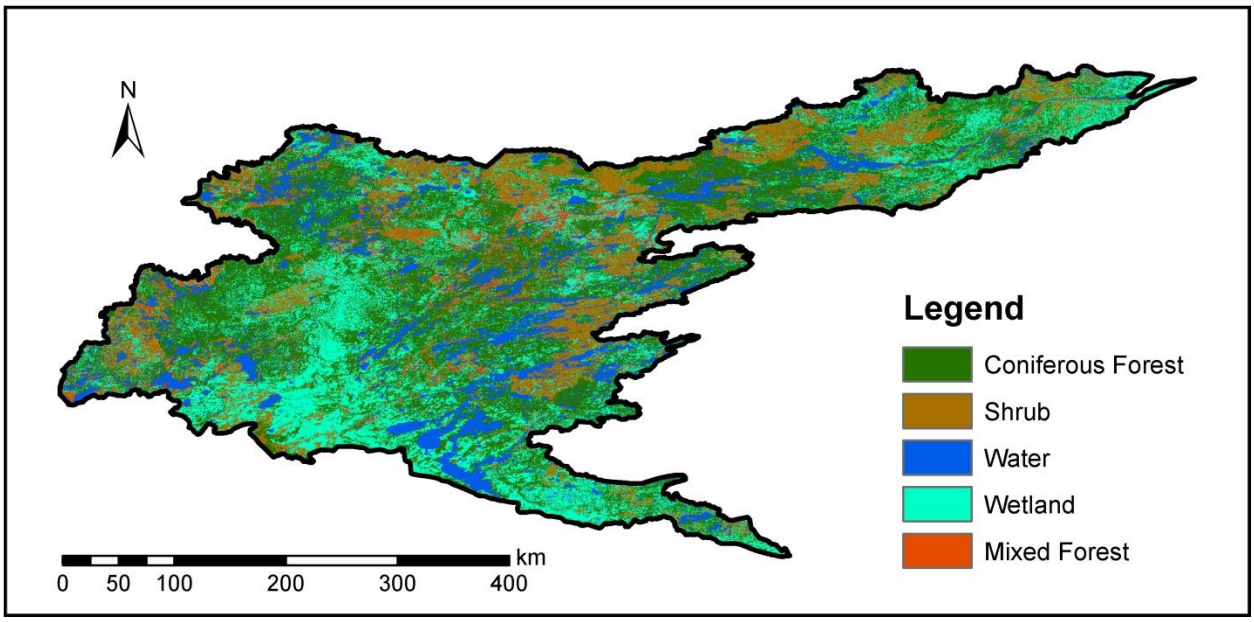

Figure 4.3 Land cover in the LNRB (Natural Resources Canada, 2011).

4.4 Hydrology

The largest river in the LNRB is the Nelson River, which conveys water from Lake Winnipeg to Hudson Bay. There are a number of other significant rivers within the 90,500 km^2 area of the LNRB, including the Burntwood River (26,000 km^2), the Grass River (16,000 km^2), the Odei River (6,300 km^2), the Rat River (6,600 km^2), the Minago River (4,700 km^2) and the Gunisao River (5,100 km^2). Although the area is remote, flows in the LNRB are not exclusively natural: Manitoba Hydro currently has 6 operational hydroelectric generating stations within the watershed, one currently under construction (i.e., Keeyask), and one proposed future development (i.e., Conawapa); generating stations are shown in Figure 4.4. Furthermore, significant flows from outside the basin enter via the Churchill River Diversion (CRD), which has a license maximum of 850 cms but flows up to 990 cms may be diverted under current regulations; inflows from the CRD are regulated with the Notigi Control Structure (Manitoba Sustainable

Development, 2016). The CRD connects the Churchill River at South Indian Lake to the Rat River in the northwest of the LNRB, which is a tributary of the Burntwood River. The majority of the flow in the lower Burntwood River therefore comes from the CRD. The majority of the flow in the Nelson River itself comes from Lake Winnipeg; on average 2200 cms enters the LNRB from the lake, nearly two thirds of the total flow at the river outlet (Water Survey of Canada, 2016).

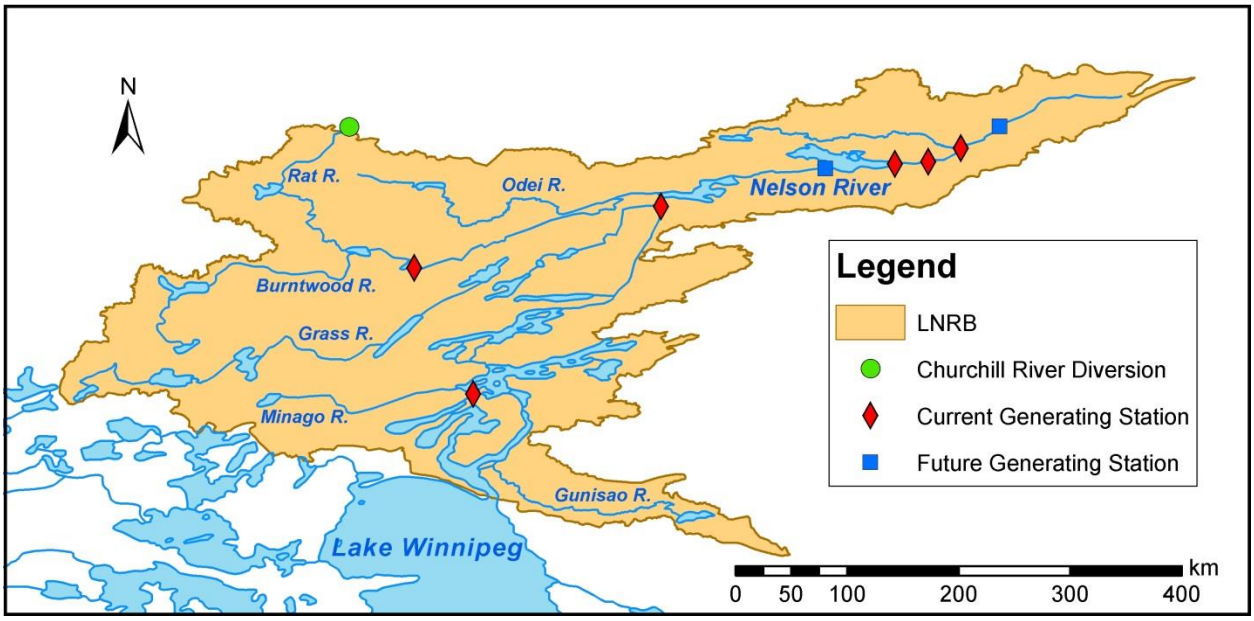

Figure 4.4 Manitoba Hydro generating stations in the LNRB. The proposed Conawapa development (furthest downstream) and Keeyask development currently under construction are also shown.

The main stem rivers in the LNRB (i.e., the Nelson and its largest local tributary, the Burntwood, which also carries CRD flows) have low seasonal flow variability due to regulation and large drainage areas. Smaller rivers and headwater streams in the region have highly variable flow rates throughout the year, with peak flows generally coming from the spring freshet and occasionally late summer storm events. The LNRB has very low slopes in most areas, with the common channelized lakes moderating flow variability. Wetlands cover large areas of the basin, storing significant volumes of water, which also moderate streamflow response to rainfall and snowmelt events; however, extremely shallow soil limits groundwater storage and groundwater flows.

4.5 Hydrometric Data

The LNRB is sparsely gauged, with 17 active hydrometric gauges, listed in Table 4.2, within its 90,500 km^2 area, or 1 gauge per 5,300 km^2. The length of the continuous flow records varies among these stations and is also somewhat limited, with the earliest continuous record beginning in the 1950's, and the average continuous record length being 40 years (Water Survey of Canada, 2016).

Table 4.2 Active hydrometric gauges measuring flow within the LNRB (Water Survey of Canada, 2016).

	Gauge ID	Drainage area (km^2)	Start Year	Mean annual discharge (cms)
BURNTWOOD RIVER ABOVE LEAF RAPIDS	05TE002	5 810	1985	22.9
FOOTPRINT RIVER ABOVE FOOTPRINT LAKE	05TF002	643	1977	3.21
SAPOCHI RIVER NEAR NELSON HOUSE	05TG006	391	1992	2.15
ODEI RIVER NEAR THOMPSON	05TG003	6 110	1979	34.3
BURNTWOOD RIVER NEAR THOMPSON	05TG001	18 500	1957	621
TAYLOR RIVER NEAR THOMPSON	05TG002	886	1970	5.07
GRASS RIVER ABOVE STANDING STONE FALLS	05TD001	15 400	1959	64.6
NELSON RIVER (WEST CHANNEL) AT JENPEG	05UB009	974 500	1976	1 880
NELSON RIVER (EAST CHANNEL) BELOW SEA RIVER FALLS	05UB008	976 000	1978	361
GUNISAO RIVER AT JAM RAPIDS	05UA003	4 610	1976	18
NELSON RIVER AT KELSEY GENERATING STATION	05UE005	1 050 000	1960	2 300
KETTLE RIVER NEAR GILLAM	05UF004	1 090	1969	13.2
WEIR RIVER ABOVE THE MOUTH	05UH002	2 190	1977	15.6
NELSON RIVER AT KETTLE GENERATING STATION	05UF006	1 100 000	1988	3 420
NELSON RIVER AT LONG SPRUCE GENERATING STATION	05UF007	1 100 000	1988	3 430
LIMESTONE RIVER NEAR BIRD	05UG001	3 270	1976	21.5
ANGLING RIVER NEAR BIRD	05UH001	1 560	1979	11.6

The majority of flow gauges in the LNRB are run by the Water Survey of Canada, which currently measures water level, which, in conjunction with a manually determined rating curve for the channel,

can be used to determine flow rate. Flows are periodically measured and channels surveyed to maintain up-to-date rating curves for the gauge location. There are large numbers of hydrometric gauges recording water level only in the LNRB, most of which are monitored by Manitoba Hydro hydrometrics. There are also four generating stations on the Nelson River for which the operator, Manitoba Hydro, shares observed flows: Jenpeg, Kelsey, Kettle, and Long Spruce. As flows from generating stations are regulated, these gauged points are much less useful for modeling purposes. The active hydrometric gauges measuring flow in the LNRB area are shown in Figure 4.5.

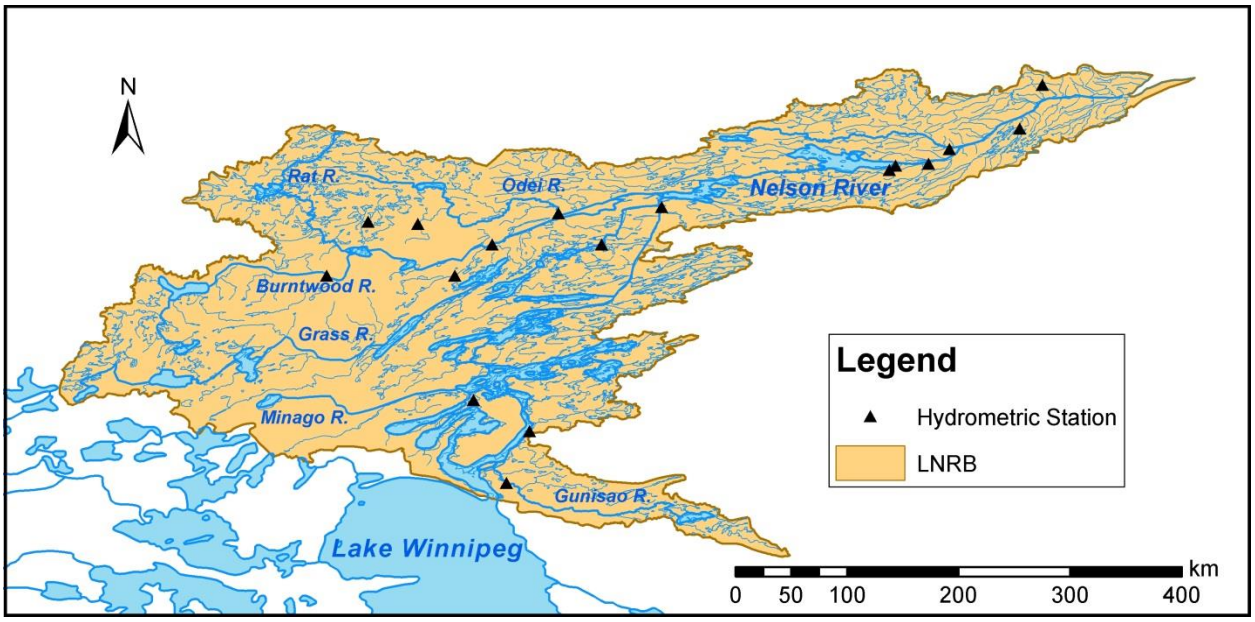

Figure 4.5 Active hydrometric stations measuring flow in the LNRB (Water Survey of Canada, 2016).

Hydrometric gauging stations are not equally distributed throughout the basin. Station density is higher in the North and Northeast of the basin, while the Southwest currently has no active gauges, and a single discontinues flow gauge on the upper Grass River (ID 05TB002).

4.6 Isotope Data

Starting in March 2010, water samples for isotope measurement have been collected in the LNRB as part of the Stable Water Isotope Monitoring Network (SWIMN) (Smith, et al., 2015). The majority of

samples are taken from surface waters in rivers and lakes, with three locations where precipitation samples are taken, three shallow groundwater sample sites, and one Class “A” evaporation pan. Winter sampling of ground water is not possible due to freezing, and composite snow samples are taken in place of precipitation collection during this season. Isotope sampling occurs at the majority of hydrometric stations where flow is measured in the LNRB, and also at other sites in the central LNRB based on accessibility and hydrological significance. Surface water sampling locations are generally sampled once or twice a month during the open water season, and occasionally during ice-on; amounting to 5-6 samples per year on average. Additionally, a basin-wide synoptic survey is performed each year in early summer at regular and additional sampling sites (2011-2016); a fall synoptic survey has recently been added to the monitoring program and has been conducted once so far in 2015, with a second fall survey planned for 2016. Sites sampled as part of the regular program are illustrated in Figure 4.6; sites sampled as part of the synoptic survey only are not included as this data was not used in this study.

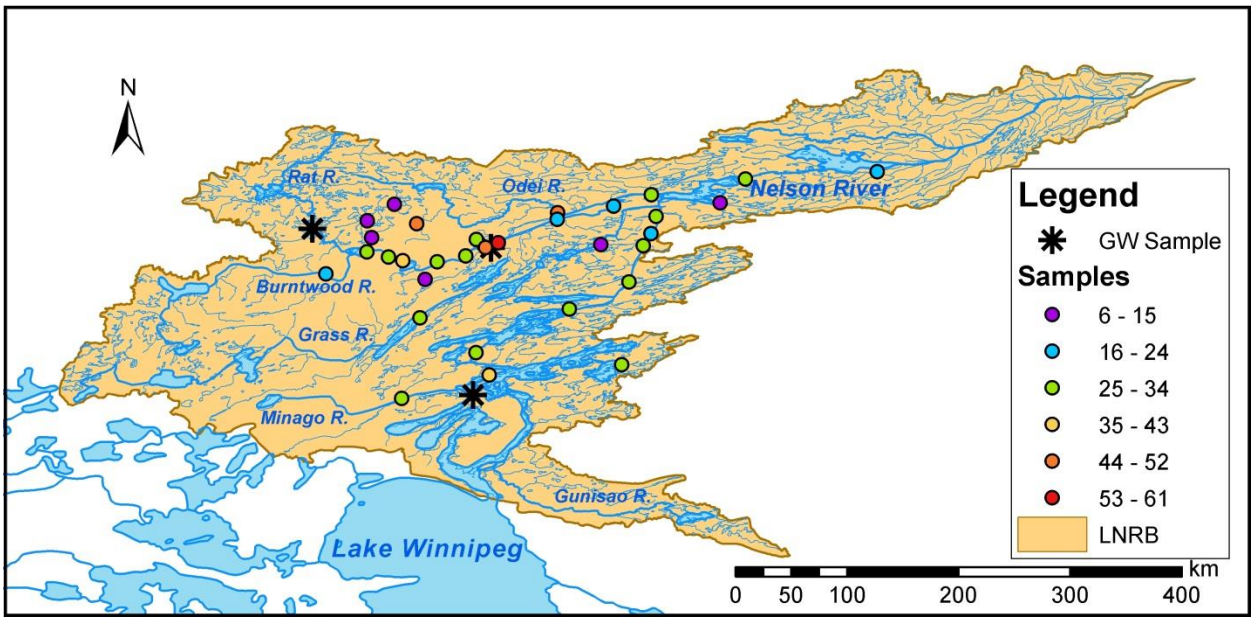

Figure 4.6 Stable water isotope sampling locations within the modeled area of the LNRB for 2010-2014. Surface water sites are indicated by colored circles. Groundwater and precipitation sites are indicated by an asterix. The evaporation pan is located at the groundwater sample site on the Rat River.

Surface water samples are taken from the section of the river experiencing turbulent flow using a 500-mL sampling bottle attached to an extendable pole. Two 30-mL water samples were taken from the larger bottle in high-density polyethylene Nalgene® bottles, capped and sealed with electrical tape at the neck of the bottle to minimize evaporation. During ice-on, water samples are collected by auguring through the ice cover and collecting water using a plastic bailer. Samples are analyzed for deuterium and oxygen-18 at the University of Victoria Environmental Isotope Laboratory managed by Alberta Innovates Technology Futures. The isotope compositions are analyzed using a Delta V Advantage stable isotope mass spectrometer; a Gasbench II peripheral was used for oxygen-18, and an HDevice peripheral for deuterium. Results are standardized by comparing the in-house standard with Vienna Standard Mean Ocean Water (VSMOW2), isotopic compositions being reported relative to VSMOW2 as delta values (‰). The uncertainty in the reported values is ±0.2‰ for oxygen-18 and ±1‰ for deuterium (Smith, et al., 2015).

The variability of stable water isotopes in the LNRB region is dependent on basin area, flow regime and geography (Smith, et al., 2015). Smaller rivers have significantly more variability in isotopic composition than larger rivers, due to their shorter residence times and flow paths. The more northerly basins in the LNRB have lower isotope values, with the water from the Churchill River diversion, from north of the LNRB having the most depleted composition. Headwater basins have high observed variability, both inter-annually and across flow regimes, with temporal isotopic variation generally differing between basins. This difference in variation patterns suggests that headwater basins have different dominating end-members, likely due to the land cover and connectivity within the basin (Smith, et al., 2015).

4.7 Forcing Data

In order to run the isoWATFLOOD model, multiple types of forcing data are required. Firstly, weather data are needed to run the hydrological model. Precipitation records from 13 Environment Canada (EC) weather stations in the LNRB and surrounding area were used as input data (Environment Canada, 2016); the point values were distributed across the basin using distance squared weighting (Kouwen, 2014). Temperature data, used by the model for evapotranspiration and snowmelt modeling, came from the same EC stations and was likewise distributed over the basin area using distance squared weighting. Relative humidity input data were added to the model for the purposes of this research, specifically for the simulation of isotopes. Relative humidity is not recorded at all EC sites; however it is generally measured at airport weather stations: six stations had RH observations in the LNRB region during the isotope simulation period. These point observations were distributed in the same manner as air temperature data. All EC stations used as data sources for the simulation are shown in Figure 4.7.

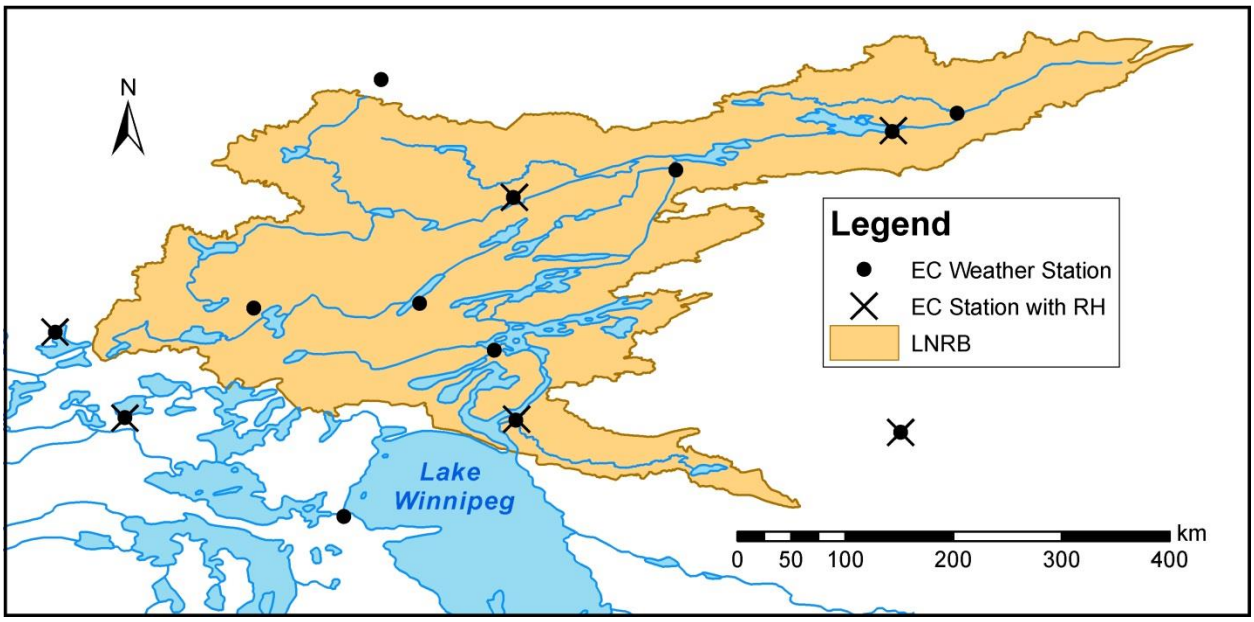

Figure 4.7 Environment Canada meteorological stations in the LNRB region with data for the modeled study period (1981-2014) (Environment Canada, 2016).

The model does not cover the entire extents of the Nelson River basin, therefore flows from upstream areas not directly simulated, and so these flows are also required as forcing data. The previously completed WATFLOOD model of the LNRB begins after Playgreen Lake, at the Jenpeg generating station, so data from the hydrometric stations on the Nelson River at Jenpeg (05UB009) and below Sea River Falls (05UB008) are used as forcing. Flows from the Churchill River Diversion (CRD) were included in the simulation by forcing simulated flows at the Notigi Control Structure on the Rat River, downstream of the CRD, to match the observed flows provided by Manitoba Hydro (who operate the control structure).

As described in Section 3.2.1, the isotope simulation requires the isotopic composition of precipitation as isoWATFLOOD forcing data. For the LNRB model, a new distributed precipitation method was used, with precipitation composition varying both spatially and temporally on a monthly time-step. The composition values come from the empirical model developed by Delavau, et al. (2015), which uses geographic and climatic indicators in a geospatial interpolation using multiple linear regression.

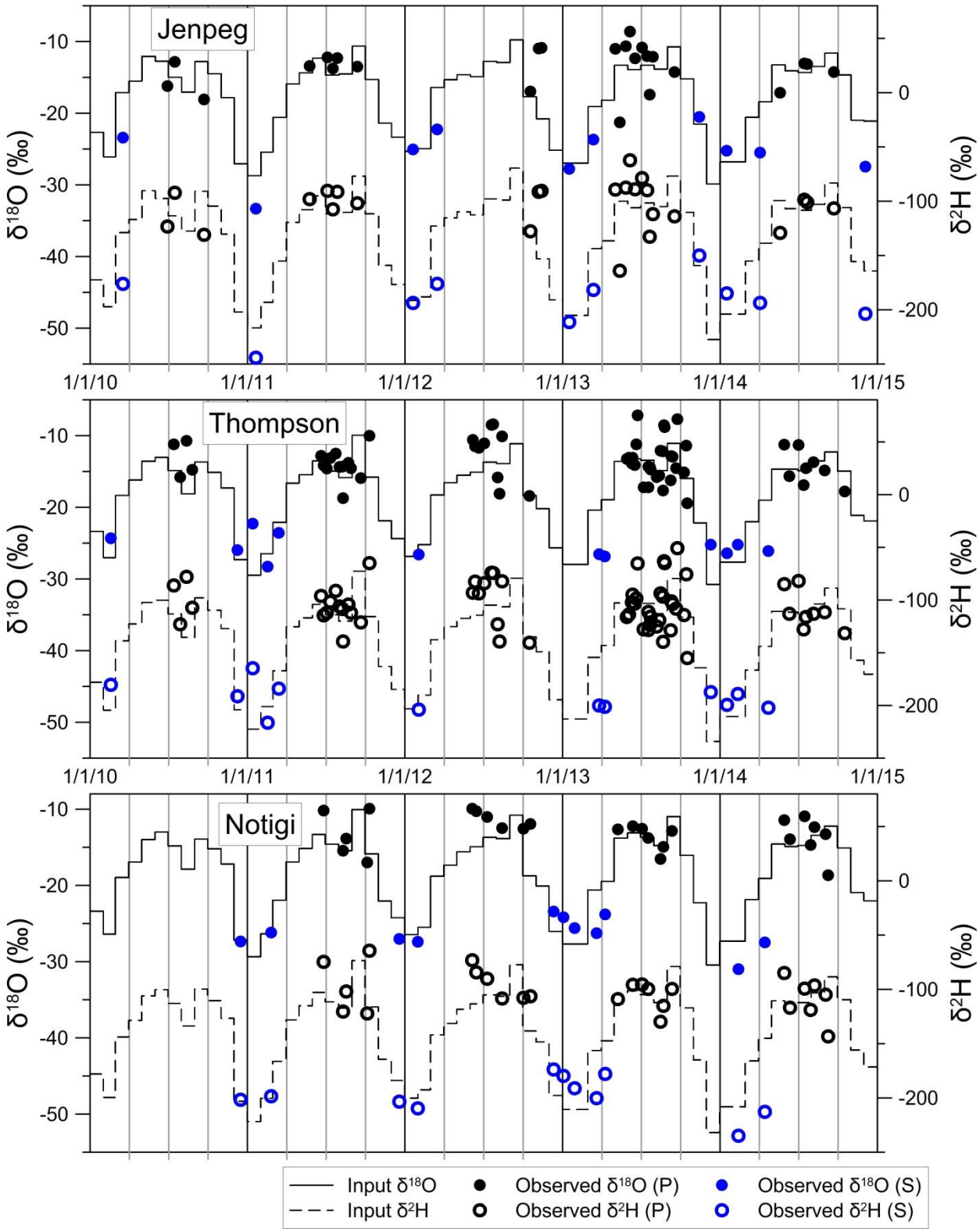

Figure 4.8 Comparison of isotopes in precipitation forcing (Delavau, et al., 2015) to observed data.

The isotopic compositions generated by the isotopic composition of precipitation model, using latitude and precipitable water content among other variables with Köppen regionalization, provide continuous isotopes in precipitation input to isoWATFLOOD (Delavau, et al., 2015). When compared to the observed precipitation compositions at the most frequently sampled sites (Figure 4.8), the empirical model appears to capture the seasonal variability well, and some of the inter-annual variability in the study period. As the most intensively sampled site, however, Thompson shows the model has difficulties reproducing the true variation in precipitation given its monthly resolution. For larger basins, monthly values may be sufficient as rainfall inputs will be well mixed; but error may be significant for smaller streams with shorter times of concentration.

Inflows added to the model from upstream areas also require isotopic compositions as forcing. Isotope sampling occurred at all three forcing locations: Jenpeg, Notigi and the Nelson River east channel. Observed and forced isotope values for the most variable of these locations, the Nelson River east channel, are shown in Figure 4.9.

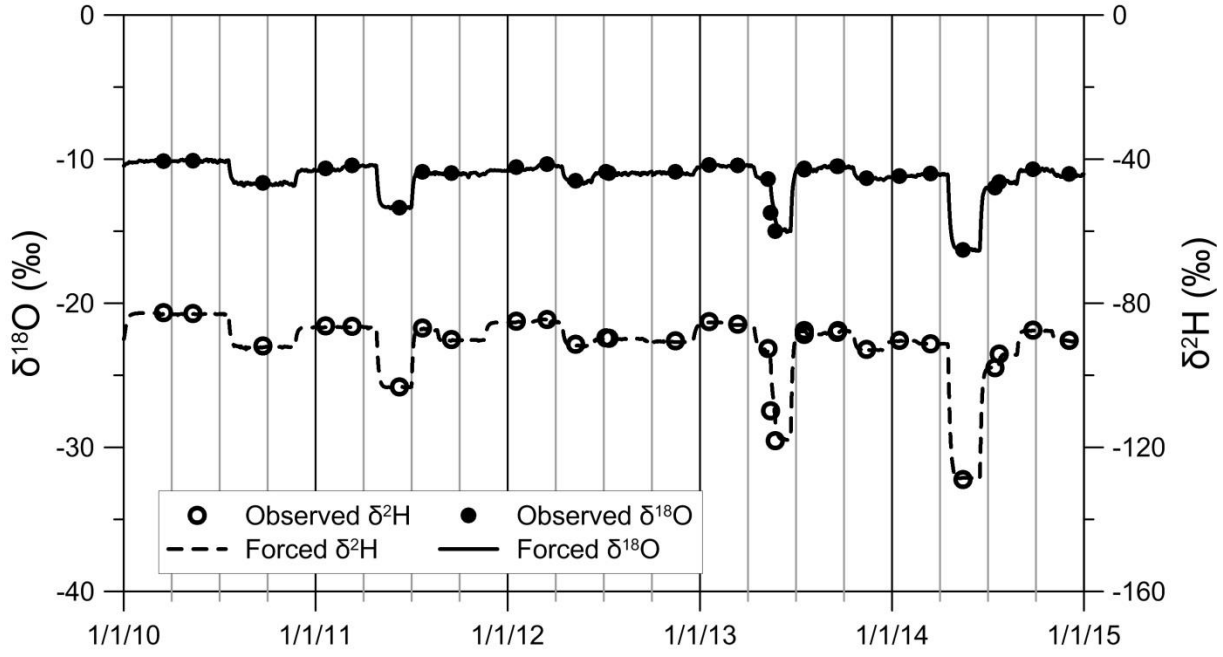

Figure 4.9 Observed and forced inflow isotope values for the Nelson River east channel.

Inflows to the model area were assigned the most temporally proximate observed isotopic composition; this produces an irregular step-function for the composition of Lake Winnipeg and Churchill River flows.

Forcing data required for the isotope simulation, namely relative humidity data and precipitation and forced inflow compositions, were only acquired for the portion of the study period (1981-2014) with observed isotope data (2010-2014) as there is little benefit to simulating isotopes without observations available as a comparison. The isotope simulation, both calibration and validation, are therefore constrained to the 5-year period beginning in 2010, while the hydrologic simulation can include the earlier period as well.

5 Testing a Dual-Isotope Approach: Model Calibration and Validation

A WATFLOOD model of the LNRB was completed prior to this study; this model was used as the starting point for modeling the LNRB using isoWATFLOOD. The initial model was re-calibrated using the current WATFLOOD auto-calibration method, with isotope error included in the error function. Three separate calibration trials were run: (1) using only flow error in calibration, (2) flow and oxygen-18 error, and (3) flow, oxygen-18 and deuterium error.

This chapter will describe the initial WATFLOOD model and the calibration method used for this study, along with the calibration results. Performance during model validation will be presented and discussed, and the effect of including isotope simulation error in the calibration will be analyzed.

5.1 Initial Model Setup & Prior Calibration

The previously completed WATFLOOD model includes the majority of the LNRB, covering an area of 80,000 km^2. The modeled area begins at the flow gauges on the Nelson River at Jenpeg and the east channel, and ends at the Nelson River estuary region near Hudson Bay. Most sub-basins in the LNRB are included in the model, but not the Gunisao River or the Playgreen Lake areas. The WATFLOOD model is distributed, so the modeled area is divided into grid cells, with each cell in the model covering approximately 100 km^2, resulting in 797 modeled cells for the LNRB. The grid cells are divided into different river classes depending on streamflow characteristics and location, with 9 distinct river classes included in the model (Figure 5.1). Cells are further subdivided into GRUs; the LNRB model uses 9 GRU types, which depend primarily on land cover for their definition, with soil type also being considered. In addition to the required water, connected and disconnected wetland and impervious area groups, the model also includes coniferous forest, mixed forest, treed rock, shrub and bog classifications. The treed

rock group is defined as coniferous forest over near surface bedrock, from the surficial geology (Fulton, 1995). The bog grouping includes only wetland with short vegetation. Other wetland areas are divided into connected and disconnected wetland using a fractional split, with 65% being disconnected and 35% connected in the LNRB model.

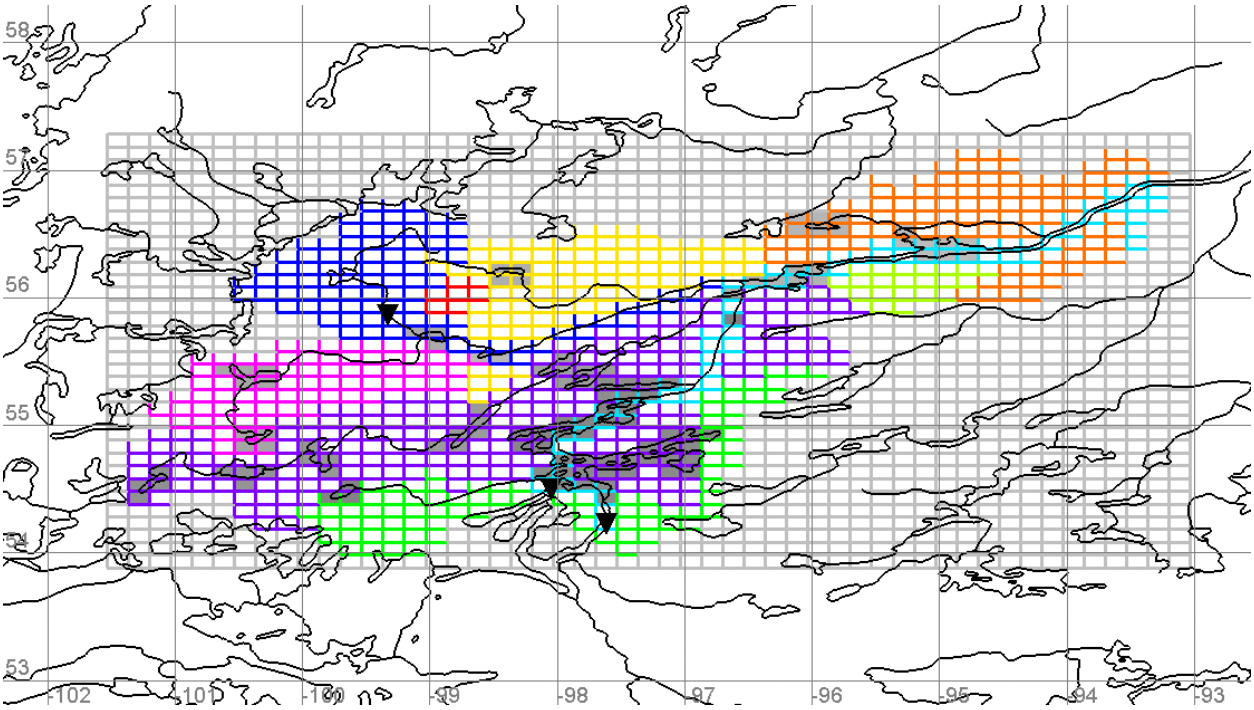

Figure 5.1 Map of WATFLOOD LNRB model setup. Colors of grid borders indicate river classes, with gray grid cells being outside the modeled domain. Forced flows are marked with black triangles. Cells which are part of a modeled lake or reservoir are greyed in.

Nineteen of the largest lakes in the LNRB are modeled as reservoirs in the WATFLOOD model, which means that the water class in cells included in the reservoir are grouped together and treated as a single storage unit (Kouwen, 2014). Flows out of these reservoirs or lakes are defined based on storage-discharge curves; each lake has its own release function, which was calibrated using data provided by Manitoba Hydro. There are two diversions included in the LNRB model, located on the east and west channels of the Nelson River downstream of Playgreen Lake. The CRD is modeled by forcing simulated flows at the Notigi Control Structure to equal the observed flows at that location. The LNRB WATFLOOD

model uses annual input files, which start at the beginning of the calendar year. In order to stabilize forced inflows to the model, several months of simulation are need for model spin-up. Therefore, as the model uses year-long data files, an entire year of simulation is required for model spin-up. This also removed the need for distributed snowpack input data.

The previous model calibration period ran from 2003 to 2011, with 2002 used as a spin-up year. The model was calibrated using the standard dynamically dimensioned search (DDS) algorithm method, as recommended by Kouwen (2014). Parameters to which the flow simulation was most sensitive were grouped based on their likelihood to interact, and the DDS auto-calibration was used to calibrate the groups of parameters sequentially. The error function used in the calibration was the average Nash-Sutcliffe error for all gauges included in the calibration (Nash & Sutcliffe, 1970). The parameter set from this calibration may be found in Appendix A.

The resulting model of the LNRB performs adequately, based on the recommendation for NSE by Moriasi, et al. (2007) in the calibration and validation periods, and was considered an acceptable representation of the LNRB for this study. However, if a WATFLOOD model for the LNRB were to developed in future, different modeling decisions may be made, with the potential to improve the hydrological model (discussed in Section 7.1).

5.2 Calibration Methodology

The calibrations performed in this research are based on the standard auto-calibration methodology for WATFLOOD. An external executable for the dynamically dimensioned search (DDS) algorithm is available that works in conjunction with the WATFLOOD model executable to run DDS as described in Tolson & Shoemaker (2007). The DDS algorithm searches the parameter space to optimize model performance, with the distance moved within the parameter space changing as a function of the parameter limits, the total number of parameter sets evaluated and the number of parameter sets already evaluated (hence

the dynamic descriptor). The DDS method is efficient, which is important for WATFLOOD as the model has a very large number of parameters, and can produce good calibration results, often avoiding local optima (Kouwen, 2014). However the current DDS executable for WATFLOOD saves only the final parameter set, and evaluates parameter set performance using a single error value, therefore no uncertainty assessment can be performed.

5.2.1 Error Function

The error function used by the WATFLOOD DDS executable is user-specified, with the only requirement being that it produces a single error value. The most commonly used error function for WATFLOOD auto-calibration is the Nash-Sutcliffe error, defined as (Nash & Sutcliffe, 1970):

$$NSE = \frac{\sum_{t=1}^{T}(Q_o^t - Q_s^t)^2}{\sum_{t=1}^{T}\left(Q_o^t - \overline{Q_o}\right)^2} \quad (5.1)$$

Where Q_o is the observed discharge and Q_s is the simulated discharge. In cases where there are multiple gauges within the model, NSE values are averaged to produce a single number for auto-calibration. The commonly reported Nash-Sutcliffe efficiency value is related to the Nash-Sutcliffe error by:

$$NS = 1 - NSE \quad (5.2)$$

The Nash-Sutcliffe error was selected for the flow error in this study as it is well understood, frequently used and includes both flow timing error and volume error in the final value. The Nash-Sutcliffe error does, however, have a number of known issues or limitations. The differences between the observed and simulated values are squared, resulting in a bias toward correcting high flow simulation at the expense of simulation in low flow periods (Krause, et al., 2005). Since the simulation error is normalized using the variance in the flow, gauges with low flow variability have inflated Nash-Sutcliffe errors, and high variability gauges have lower Nash-Sutcliffe errors, if the difference between simulation and observation is the same. This renders the comparison of Nash-Sutcliffe errors between flow gauges

difficult, and when Nash-Sutcliffe errors are combined, as done by the WATFLOOD error function, lower variability flow stations will be over-emphasized in the calibration. By decomposing the Nash-Sutcliffe error criterion, Gupta et al. (2009) found that optimizing the Nash-Sutcliffe error results in an under-estimation of variability, such that simulated hydrographs are flattened relative to the observed hydrograph.

The Nash-Sutcliffe error could also be used for quantifying the isotope simulation error as well as the flow error, but it was deemed unsuitable for the isotope observations available in the LNRB. Isotope observations at many sites were taken both rarely and irregularly, although some have reasonably continuous data series. The regularly sampled sites would allow a reliable estimation of composition variability, but this could not be produced for many sites. Since the Nash-Sutcliffe error is normalized using observed variability, applying it at sites with undependably realistic variability introduces weighting problems when averaging errors from multiple sites. Instead, the similar normalized root mean squared error (NRMSE) is used for the isotope simulation in this study, defined as:

$$NRMSE = \frac{\sqrt{\sum_{i=1}^{n}\left(I_o^i - I_s^i\right)^2}}{\left|\overline{I_o}\right|} \qquad (5.3)$$

Where I_o is the observed isotopic composition and I_s is the simulated isotopic composition. Since it is normalized by the mean composition rather than the variability, the NRMSE is much less sensitive to the number of observations than the NSE.

For this study, three distinct error functions were used in calibration, to test the effect of using the different isotope simulations in the calibration. The first is already part of the WATFLOOD executable, as it uses only flow data:

$$E = \overline{NSE} \qquad (5.4)$$

Two new error functions were added, the first of which uses flow and oxygen-18 data:

$$E = \overline{NSE}/5 + \overline{NRMSE}_{O^{18}} \quad (5.5)$$

So that the acceptable flow error value and the acceptable isotope error value would have approximately equal weight in the error function, the Nash-Sutcliffe error is divided by five. The third error function is much the same as the second, but uses the average error of the two isotope simulations (^{18}O and ^{2}H):

$$E = \overline{NSE}/5 + \left(\overline{NRMSE}_{O^{18}} + \overline{NRMSE}_{H^{2}}\right)/2 \quad (5.6)$$

The error functions all give equal weight to any flow gauges or isotope sites that are included in the auto-calibration process.

5.2.2 Calibration Parameter Selection

There are many parameters in the WATFLOOD model, with 24 parameter types set up for calibration. As each river and land class has its own individual parameters, the total number of parameters included in the calibration can be extremely large. In the LNRB model, up to 146 parameters could be calibrated. Fortunately, many parameters can be estimated by other means or have little influence on the flow simulation. When calibrated parameters exceed approximately 10, however, an auto-calibration method is highly unlikely to find the global optimum for a solution within the typical optimization time frame due to the sheer size of the parameter space (Tolson & Shoemaker, 2007). Even using DDS, a method intended for highly parameterized, computationally intensive models, a truly optimal calibration is not expected. Large numbers of calibrated parameters are unavoidable with the current DDS methodology for WATFLOOD, but the number selected should be held to a minimum. The following approach was therefore designed, to restrict the number of calibrated parameters as much as possible without negatively impacting the final model performance.

In order to identify the most important parameters for calibration, a basic parameter sensitivity assessment was performed for the Odei River, a large headwater basin with natural flows in the LNRB. The Odei River was selected as it has both isotope and flow data and has land cover representative of the northern area in the LNRB; however, the assessment is limited as other sub-basins may be hydrologically distinct and may therefore have different parameter sensitivities. The isoWATFLOOD simulation was run for the year 2010, oxygen-18 was the only isotope simulated. Each parameter was varied individually, with coniferous forest representing changes in land class parameters (given it is most prevalent in the area). The parameters included in the sensitivity assessment are those calibrated in the original development of the LNRB model: each parameter used in the sensitivity assessment was set first at the lower bound, then at the upper bound for the parameter value, while all other parameters were held at their original value. The flow and isotope simulations at each of the bounds were then compared to find the maximum difference in the simulation from varying an individual parameter, with the assumption that the relationship between the parameter and the simulation is monotonic. To facilitate comparison, all changes are presented as percent change from the original (previously calibrated LNRB model) value. The significance of change in the simulation is dependent on the type of parameter under consideration: a river class parameter affects the entire sub-basin, while a land class parameter influences only a fraction of the area, and a snow parameter changes a fraction of the area for a single season. Flow and isotope sensitivity are also different, as flows are naturally more variable relative to the annual average than isotopic compositions. Significance levels were predetermined for each parameter type based on these differences, as shown in Table 5.1.

Table 5.1 Parameter significance definitions used in this study.

Parameter Type	Significance	Significance Value	Flow		Isotope	
River	very significant	3	>10%		>5%	
	significant	2	<10%	>5%	<5%	>2.5%
	somewhat significant	1	<5%	>1%	<2.5%	>0.5%
	insignificant	0	<1%		<0.5%	
Land	very significant	3	>5%		>2.5%	
	significant	2	<5%	>2.5%	<2.5%	>1.2%
	somewhat significant	1	<2.5%	>0.5%	<1.2%	>0.2%
	insignificant	0	<0.5%		<0.2%	
Snow	very significant	3	>2.5%		>1.2%	
	significant	2	<2.5%	>1.2%	<1.2%	>0.6%
	somewhat significant	1	<1.2%	>0.2%	<0.6%	>0.1%
	insignificant	0	<0.2%		<0.1%	

Change in mean value, standard deviation (σ), and range were considered in the assessment of isotope and flow simulations in order to test changes in average outputs, variability and extreme values. The results are listed in Table 5.2.

Table 5.2 WATFLOOD parameter sensitivity assessment for the Odei River, with percent change reflecting the change from the original calibrated value for the existing LNRB model.

	Flow			Isotope		
	Change in mean (%)	Change in σ (%)	Change in range (%)	Change in mean (%)	Change in σ (%)	Change in range (%)
River:						
Baseflow coefficient (flz)	16.1	38.7	53.2	-1.6	26.7	9.9
Baseflow power (pwr)	1.7	12.6	30.9	0.0	5.1	2.6
Channel roughness (r2n)	20.8	59.5	98.7	-0.4	29.3	40.2
Wetland porosity (theta)	14.0	29.2	43.2	-3.2	36.3	43.0
Wetland conductivity (kcond)	5.2	22.4	33.7	-1.1	9.9	8.6
Land:						
Interflow coefficient (rec)	0.2	0.8	3.1	-0.1	0.4	0.5
Infiltration coefficient (ak)	0.1	0.7	1.8	-0.1	0.4	0.0
Frozen soil infiltration coefficient (akfs)	0.1	0.1	0.1	-0.2	0.9	4.1
Upper zone retention (retn)	17.9	16.5	19.3	0.0	7.0	1.1
Lower zone recharge coefficient(ak2)	1.0	3.7	13.3	-0.3	1.3	0.8
Frozen soil lower zone recharge coefficient (ak2fs)	0.1	0.2	0.1	-0.1	0.3	0.4
Interception capacity multiplier(fratio)	6.0	6.5	6.8	-0.1	0.2	0.4
Snow:						
Melt factor (fm)	2.8	0.4	2.5	-0.3	1.1	1.8
Melt base temperature (base)	1.5	0.7	2.2	0.0	1.0	2.0
Sublimation rate (sublim_rate)	11.5	2.4	1.8	-0.7	0.2	0.8

The parameter sensitivity assessment was used as the basis for calibration parameter selection in the present study, with each parameter given a significance value from 0 to 3 (see Table 5.1) from an average of the six values presented in Table 5.2. Since parameters for processes that interact with other processes should be calibrated simultaneously, the significance score is multiplied by an interaction factor, ranging from 0 (no major interaction) to 2 (for processes which influence multiple other processes significantly). These significance scores are based on user knowledge of the model and internal code structure: the more connections that exist between the simulated storage (affected by the

parameter) and storages controlled by other parameters, the higher the interaction factor. Finally, parameters which can reasonably be specified based on available data, such as climatic conditions or vegetation, need not be calibrated and therefore their calibration importance score is multiplied by 0. The resulting scores for parameter selection during calibration are shown in Table 5.3.

Table 5.3 Calibration parameter selection matrix with scores reflecting parameter impact on the simulation, and likelihood of parameter interaction.

	Significance rating	**Interaction factor**	**Other means of parameter selection available**	**Calibration importance score**
River:				
Baseflow coefficient (flz)	2.7	1.0	1.0	2.7
Baseflow power (pwr)	2.0	1.0	1.0	2.0
Channel roughness (r2n)	2.5	0.0	1.0	0.0
Wetland porosity (theta)	2.8	2.0	1.0	5.7
Wetland conductivity (kcond)	2.5	2.0	1.0	5.0
Land:				
Interflow coefficient (rec)	0.8	2.0	1.0	1.7
Infiltration coefficient (ak)	0.5	1.0	1.0	0.5
Frozen soil infiltration coefficient (akfs)	0.8	1.0	1.0	0.8
Upper zone retention (retn)	2.2	2.0	1.0	4.3
Lower zone recharge coefficient (ak2)	1.7	2.0	1.0	3.4
Frozen soil lower zone recharge coefficient (ak2fs)	0.3	1.0	1.0	0.3
Interception capacity multiplier (fratio)	1.8	0.0	0.0	0.0
Snow:				
Melt factor (fm)	2.2	1.0	1.0	2.2
Melt base temperature (base)	1.7	1.0	0.0	0.0
Sublimation rate (sublim_rate)	2.0	1.0	0.0	0.0

Eight parameter types with a score over one were therefore included in the general calibration parameter set (Table 5.3), as they are significant to either the flow or isotope simulation, are likely to interact with the other parameters, and cannot be reasonably determined from other data. Calibrating

these parameter types leads to 63 individual parameters being calibrated together (given there are 9 river classes and 9 land classes, 6 of which have soil storages). The channel roughness parameters are also significant, but because they are not expected to change the optimal values of other parameter types significantly, these parameters were calibrated separately from the general set.

5.3 Model Calibration

Three separate model calibrations were completed, each using a different error function for optimization as discussed in Section 5.2.1, which resulted in three distinct parameter sets: the flow calibration (F), the flow and oxygen-18 calibration (O) and the flow, oxygen-18 and deuterium calibration (OH). The number of calibrated parameter sets was limited to three, as the available computational resources did not permit additional simultaneous simulations, and time constraints did not allow sequential calibrations as the dual-isotope simulation model calibration required 4 months to complete.

A five-year calibration period was used, from 2010 to 2014, with 2009 used as a model spin-up year. This period was selected for two reasons: firstly, and most importantly, it is the period of record for stable water isotope observations in the LNRB; second, it contains a range of hydrological conditions, which allows for more robust flow and isotopic calibrations. Weather data for the five years are shown in Table 5.4, along with climate normal for comparison.

Table 5.4 Annual temperature and precipitation data from Thompson Airport Climate ID: 5062922 (2010-2014) (Environment Canada, 2016).

Thompson Airport Climate ID: 5062922	**2010**	**2011**	**2012**	**2013**	**2014**	**Climate Normal (1981-2010)**
Daily Average (°C)	-0.1	-1.9	-1.9	-3.8	-4.2	-2.9
Rainfall (mm)	484.9	465	400.3	310.2	383.6	340.2
Snowfall (cm)	171.8	110.5	198.5	167.4	209.2	187
Precipitation (mm)	624	551.3	552.4	427.4	537.8	509.2

Both 2013 and 2014 were cooler than average conditions, while 2010-2012 was warmer, with 2010 being significantly warmer than normal. In 2010, conditions were also much wetter than normal, with normal snowfall and much more rainfall. The following year, 2011, had a similar amount of rainfall but a below normal snowfall. The year closest to normal conditions was 2012, when snowfall and rainfall were both somewhat above average. The year 2013 was abnormally dry, with low rainfall and a smaller snowpack; much of the snow that fell in 2013 fell in the final months of the year. This, combined with above normal snowfall in 2014, resulted in a very large snowpack in the spring of 2014. Although short, the five year calibration period contains dry conditions, normal conditions, high rainfall years, and a large snowpack, thus covering much of the normal variability in the LNRB.

The three DDS calibrations were run simultaneously, with any parameter set producing a lower error value automatically replacing the previous best parameter set. The initial parameter set for all three calibrations was the parameter set from the original model set-up and calibration. The general parameter set (see Section 5.1.2) was calibrated using sequential 1000 simulation trials until simulation improvement became negligible. The channel roughness parameters were then calibrated similarly. A total of 10,000 simulations were run for each of the three model calibrations (F, O, and OH). The three resultant calibrated parameter sets may be found in Appendix A. The following sections describe the flow simulation calibration, the isotope simulation calibration, with flow and isotope simulation results for all three parameter sets, and the final parameter sets resulting from the calibrations.

5.3.1 Flow Simulation Calibration

There are 14 flow gauges within the modeled area of the LNRB, 10 of which were used in calibration (see Figure 4.5 for all gauges in the LNRB). Two gauges not used in calibration are direct generating station discharges, and are therefore not useful in calibrating natural flows. Two gauges, residing on minor tributaries in the north-east of the basin, were excluded because the distribution of gauges across

the basin is uneven and, as the DDS error function weights all calibrated gauges equally, using all of the gauges in the over-represented north-east would bias the calibration of land cover parameters to this area. The remaining stations include most of the sub-basins in the LNRB and main stem, large sub-basins and smaller, headwater gauges.

All calibrated flow stations show adequate performance statistics during the calibration period, from all three calibrated parameter sets, although performance varies significantly between gauges. Flow simulation performance statistics for the three calibrations (using flow, F, flow and ^{18}O, O, and flow and dual isotopes, OH) are shown below in Table 5.5 (see Table 4.2 for drainage areas).

Table 5.5 Simulation statistics at streamflow gauges in the LNRB and the approaches to model calibration for the period (2010-2014).

Station name	Station ID	Nash-Sutcliffe			R^2			%Dv		
		F	O	OH	F	O	OH	F	O	OH
GRASS RIVER ABOVE STANDING STONE FALLS	05TD001	0.57	0.56	0.55	0.57	0.56	0.55	-0.7	1.1	0.2
BURNTWOOD RIVER ABOVE LEAF RAPIDS	05TE002	0.56	0.54	0.54	0.58	0.55	0.56	13.1	13.5	15.1
FOOTPRINT RIVER ABOVE FOOTPRINT LAKE	05TF002	0.78	0.77	0.77	0.78	0.77	0.78	5.5	5.5	6.1
BURNTWOOD RIVER NEAR THOMPSON	05TG001	0.82	0.79	0.80	0.82	0.79	0.80	-2.3	-2.2	-2.2
TAYLOR RIVER NEAR THOMPSON	05TG002	0.53	0.54	0.54	0.65	0.65	0.65	-41.6	-40.2	-40.2
ODEI RIVER NEAR THOMPSON	05TG003	0.76	0.74	0.75	0.78	0.76	0.76	-12.2	-10.5	-10.1
SAPOCHI RIVER NEAR NELSON HOUSE	05TG006	0.55	0.52	0.50	0.62	0.61	0.60	34.1	36.8	37.6
NELSON RIVER AT KELSEY GS	05UE005	0.91	0.93	0.93	0.92	0.93	0.93	3.2	3.3	3.3
LIMESTONE RIVER NEAR BIRD	05UG001	0.63	0.64	0.63	0.64	0.65	0.64	-10.8	-9.8	-9.6
WEIR RIVER ABOVE THE MOUTH	05UH002	0.60	0.61	0.62	0.63	0.64	0.65	-17.6	-16.7	-16.8
Average:		**0.670**	**0.664**	**0.663**	**0.700**	**0.692**	**0.692**	**-2.92**	**-1.93**	**-1.66**

The gauges with the best simulated flows are those with contributions from forced upstream inflows: namely the Nelson at Kelsey GS and the Burntwood near Thompson. Other flow simulations perform adequately as well; the Odei and Footprint Rivers' simulations are particularly good, with NS values over 0.7 and moderate percent deviations. Simulations in lake-influenced rivers are marginal, with the Grass and the upper Burntwood Rivers reaching NS values between 0.55 and 0.6. The worst performances during flow calibration are from the Sapochi and Taylor Rivers: two of the gauges with the smallest upstream area. These gauges have marginal NS values and high percent deviation for flows, due in part to inaccurate upstream areas as grid cells were not scaled for small sub-basins. A single grid cell is approximately 100 km^2, so the inclusion or absence of one cell in a small sub-basin (e.g., with a true drainage area of 400 km^2) leads to very large percent error in simulated drainage area.

The flow-only (F) calibration generally shows better streamflow performance statistics than the flow and isotope calibrations (O and OH), as was expected for the calibration period as the flow calibration optimized flow exclusively, making no error trade off to optimize isotope simulation. Differences are, however, small and not universal: a few gauges have higher NS values from isotope calibrations, and for many gauges, the percent deviation was lower for isotope calibrations such that average deviation was better when isotope calibrations are performed. Including isotopes in the calibration error function has no significant negative impact on flow simulation performance during the calibration period, as can be seen in Figures 5.2, 5.3 and 5.4, where differences between the flow simulations are minimal.

Considering the simulations as time-series hydrographs, the Burntwood and Odei River simulations still perform well, as illustrated in Figure 5.2.

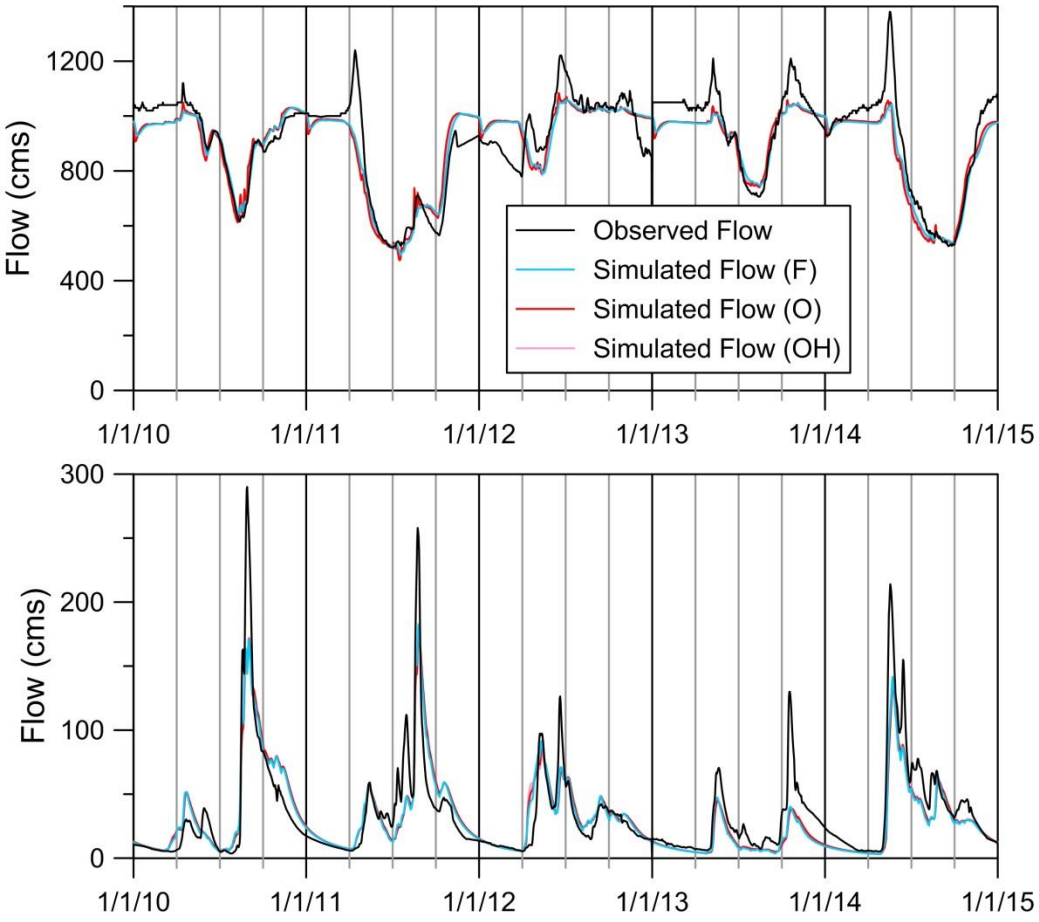

Figure 5.2 Burntwood River near Thompson (top; WSC ID 05TG001, 18 500 km^2) and Odei River (bottom; WSC ID 05TG003, 6 110 km^2) hydrographs during the calibration period for the three calibration methodologies (F, O, and OH).

Streamflow peak and recession timing are well simulated in these larger rivers, for both rainfall and snowmelt events. Flow magnitudes are not as well modeled, with damped flow variability as expected from using NSE in the optimization error function, and extreme peak flows are significantly too low, while low flows are generally too high. All three calibrations produce very similar simulated total streamflow.

Smaller river basins exhibit similar successes and failures for streamflow simulation as the larger river basins discussed above, as can be seen in Figure 5.3.

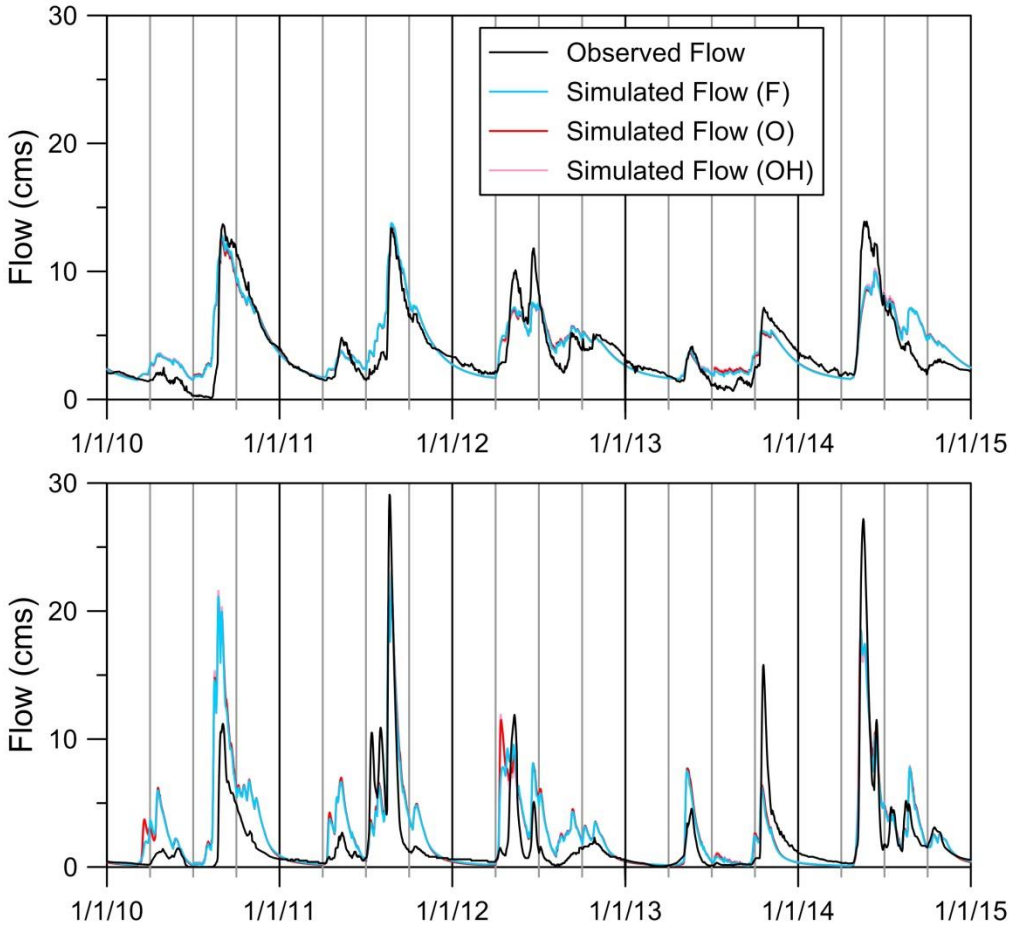

Figure 5.3 Footprint River (top; WSC ID 05TF002, 643 km^2) and Sapochi River (bottom, WSC ID 05TG006, 391 km^2) hydrographs during the calibration period for the three calibration methodologies (F, O, and OH).

The Footprint and the Sapochi Rivers are of similar size and located near each other, but the two streams have dissimilar hydrographs. The Footprint River is much less variable, while the Sapochi River responds rapidly and has highly variable flows. The simulation replicates the flows in the Footprint sub-basin better, but the simulation has even less variability than observed. The Sapochi River simulation performs reasonably well in terms of timing, but flow magnitudes are consistently wrong (flows are generally too high), except during extreme peaks. The simulated upstream area for this gauge is 39% too large, as the WATFLOOD grid is misaligned for this sub-basin. As with larger rivers, all three calibrations result in similar simulated streamflows.

At the gauge on the Grass River, a river with many in-stream lakes and a large drainage area, simulated peak flow timing matches that observed reasonably, but flow magnitudes are generally significantly different, illustrated in Figure 5.4.

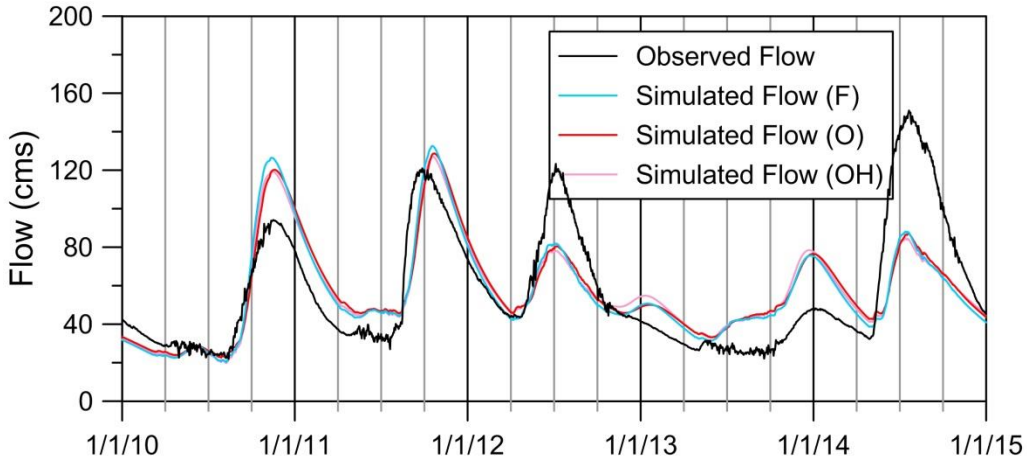

Figure 5.4 Grass River (WSC ID 05TD001, 15 400 km^2) hydrograph during the calibration period for the three calibration methodologies (F, O, and OH).

The most likely reason for the volume errors on the Grass River is the simulation of the six upstream lakes, for which the storage-discharge relationships were not included in the calibration. Too much water is released in dry years and too little in a subsequent wet year. Either the simulation of these lakes should be improved, or they should not be modeled as reservoirs in WATFLOOD. Nevertheless, the flow simulations, at gauges with or without upstream lakes, are acceptable over the calibration period, from 2010 to 2014.

5.3.2 Isotope Simulation Calibration

There are many sample sites available in the LNRB for isotope observations, with data available from 2010, but they are not all of equal quality or utility. A site selected for model calibration or validation requires frequent observations distributed throughout the calibration period, and similarly sites need to be distributed throughout the modeled area. Sites selected for the isotope model calibration were limited to the site with the most observations within each major sub-basin in the LNRB. If two sites in a

sub-basin are of similar quality, the more downstream site was chosen, as the downstream site includes flows from the upstream site, thus allowing calibration of both. Six sites were used in calibrating the isotope model, listed in Table 5.6, having an average of seven observations per year; and only one site has a year without isotope observations (i.e. the Odei River was added to SWIMN a year after the network was initiated, hence observations are only available for 2011-2014).

Table 5.6 Isotope sampling sites used in calibration (2010-2014) with drainage areas and locations.

Basin	Site	Station ID[1]	Samples	Drainage Area (km^2)	Latitude (°)	Longitude (°)
Grass	Setting Lake	R-MH-05TC701	25	11 000	55.15	-98.47
Minago	Minago River below Hill Lake	R-MH-05UC702	28	4 000	54.50	-98.61
Burntwood	Burntwood River below Miles Heart Bridge	R-MH-05TG702	61	18 600	55.75	-97.83
Upper Nelson	Kelsey Generating Station	R-MH-05UE005 R-MH-05UF792	32	1 050 000	56.04	-96.53
Odei	Odei River near Thompson	R-MH-05TG003	44	6 100	56.00	-97.35
Lower Nelson	Nelson River at Clarke Lake	R-MH-05UF766 R-MH-05UF759	26	1 100 000	56.27	-95.84

[1]Internal SWIMN database ID where isotope data are catalogued at the University of Manitoba, also reflecting WSC gauge ID.

The error in the isotope simulation is quantified using RMSE and NRMSE (Section 5.2.1). The average $\delta^{18}O$ NRMSE for the six sites was included in the isotope calibrations (i.e., O and OH), with final error values reported in Table 5.7.

Table 5.7 $\delta^{18}O$ simulation error at the six calibration sites for 2010-2014.

Basin	Site	RMSE (‰)			NRMSE		
		F	O	OH	F	O	OH
Grass	Setting Lake	0.9	0.8	0.8	0.07	0.06	0.07
Minago	Minago River below Hill Lake	1.5	1.2	1.3	0.11	0.09	0.10
Burntwood	Burntwood River below Miles Heart Bridge	0.3	0.2	0.2	0.02	0.02	0.02
Upper Nelson	Kelsey Generating Station	0.5	0.4	0.4	0.05	0.04	0.04
Odei	Odei River near Thompson	1.2	1.0	1.0	0.09	0.07	0.07
Lower Nelson	Nelson River at Clarke Lake	0.4	0.4	0.4	0.03	0.03	0.03
Average:		**0.80**	**0.67**	**0.69**	**0.063**	**0.053**	**0.054**

Including $\delta^{18}O$ error in the model calibration reduces average error, with headwater sub-basins showing more improvement (i.e., reduced error) in the $\delta^{18}O$ simulation. The Burntwood and both Nelson isotope simulations perform very well; just as with the flow simulation, when a large fraction of the simulated streamflow is forced, there is good agreement between observation and simulation.

Only the dual-isotope calibration (OH) included $\delta^{2}H$ error in the calibration, with deuterium simulation performance statistics reported in Table 5.8.

Table 5.8 $\delta^{2}H$ simulation error at the six calibration sites for 2010-2014

Basin	Site	RMSE (‰)			NRMSE		
		F	O	OH	F	O	OH
Grass	Setting Lake	7.7	7.7	6.8	0.07	0.07	0.07
Minago	Minago River below Hill Lake	7.6	10.6	7.0	0.07	0.10	0.07
Burntwood	Burntwood River below Miles Heart Bridge	1.6	1.6	1.6	0.01	0.01	0.01
Upper Nelson	Kelsey Generating Station	3.3	3.3	3.2	0.04	0.04	0.04
Odei	Odei River near Thompson	7.2	6.0	5.5	0.06	0.05	0.05
Lower Nelson	Nelson River at Clarke Lake	2.9	2.8	2.7	0.03	0.03	0.03
Average:		**5.05**	**5.32**	**4.47**	**0.049**	**0.051**	**0.043**

The RMSE values for δ^2H are higher than those for $\delta^{18}O$, as δ^2H is approximately an order of magnitude larger than $\delta^{18}O$, but the NRMSE values are similar between the two isotopes. The model calibration that included deuterium (i.e., OH) results in the lowest simulation error for deuterium (Table 5.8, OH columns). The difference between error at sites with forced flows and error at sites without forced flows is the same for both isotopes, with very low error when forced flows contribute to the flow. Interestingly, the single-isotope calibration (i.e., O) results in a worse average NRMSE for δ^2H than the flow calibration. This indicates that δ^2H error cannot be considered equivalent to the $\delta^{18}O$ error, and that a single-isotope calibration should not be expected to improve the simulation of both stable water isotopes.

Time-series plots of the observed and simulated isotopic compositions, or isographs, reveal more information regarding isotope simulation performance. The Clarke Lake (Figure 5.5) isograph strongly resembles those for the Burntwood River near Thompson and the Nelson River at Kelsey, all of which are dominated by forced inflows (all calibration site isographs provided in Appendix B).

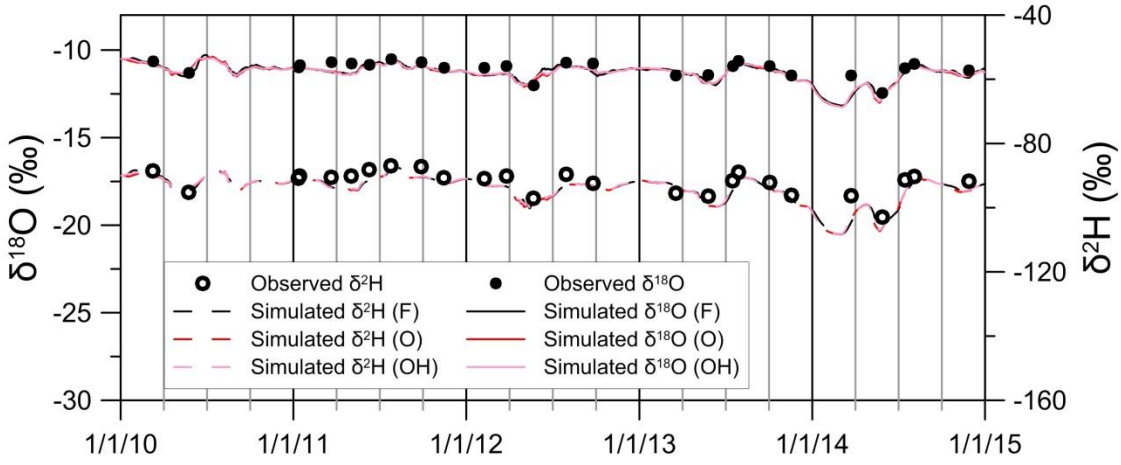

Figure 5.5 Clarke Lake isograph showing simulated and observed δ^2H and $\delta^{18}O$ over the calibration period (2010-2014) for the three calibrated parameter sets (F, O, and OH).

Clarke Lake is the most downstream sub-basin in the LNRB, receiving water from the Burntwood, Odei, Grass and Minago Rivers, as well as the Churchill River diversion and Lake Winnipeg. Due to the amount

of mixing from all these sources, the isotopic composition varies even less than the flow , as was found by Yi, et al. (2010) for the Mackenzie River, a Canadian river basin over 1 000 000 km^2. The isotope simulation matches the observed values very well, showing that the isotopic forcing and isotope-streamflow routing in isoWATFLOOD are performing adequately. However, regardless of whether or not isotopes were included in the error function, the isotopic simulations are all equally as good, with little to no deviations among model calibrations.

For the isoWATFLOOD model to produce results useful for calibration, the stream should not be so large that mixing removes the variability in isotope composition (i.e. basin areas less than 50 000 km^2), but it should be large enough that the mixing assumptions of the model are valid (i.e. should contain at least 3 grid cells such that routing will influence streamflow), which for this WATFLOOD model requires drainage areas of over 300 km^2. Three of the calibrated sites in the LNRB fit both of these criteria: the Minago River (4 000 km^2), Setting Lake on the Grass River (11 000 km^2), and the Odei River (6 100 km^2). Isographs for these sites are presented in Figure 5.6.

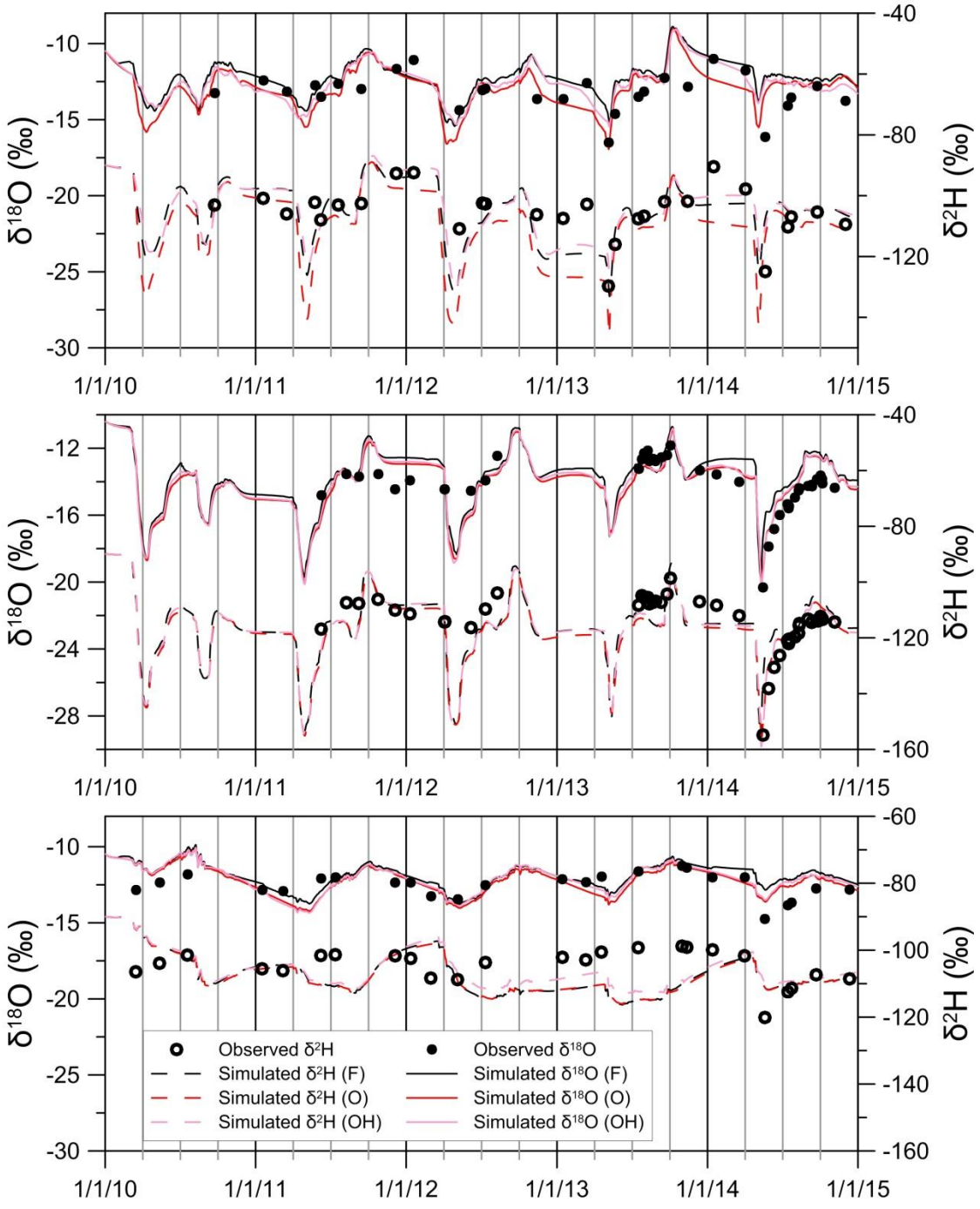

Figure 5.6 Minago River (top), Odei River (middle) and Setting Lake (bottom) isographs showing simulated and observed δ^2H and $\delta^{18}O$ over the calibration period (2010-2014) for the three calibrated parameter sets (F, O, and OH).

The match between observed and simulated isotopes is generally good at all sites, with simulations following observed trends, if not replicating the observed values. The Minago River isograph shows the

largest divergence between the three model calibrations, likely because there is no flow data available to counter-balance the influence of isotopes on calibration at this site. The single isotope calibration (i.e., O) produces the best simulation of oxygen-18, but also produces a worse simulation of deuterium than the flow-only calibration; a further indication that calibrating one isotope will not necessarily result in an improved simulation of a different stable water isotope. The overall simulation of isotopes in the Minago is good, with two exceptions. Firstly, over the winter of 2012-2013, the $\delta^{18}O$ simulations for all three calibrations are similar to the observed values, but the $\delta^{2}H$ simulations are lower than the observed values, indicating streamflow was a combination of late fall precipitation (lower $\delta^{2}H$) and over enriched (i.e. over evaporated) stored water ($\delta^{18}O$) mixed together. Secondly, for the freshet of 2014, following a very large snowpack, the simulated drop in isotope values is much briefer than observed (though maximum depletion was well simulated), indicating meltwater is leaving the basin too quickly. Together, these simulation errors point to insufficient wetland storage in the Minago River basin model, which could cause all of the observed errors in the simulation: too little water stored in fall resulting in over enrichment, late fall precipitation dominating the total stored water volume and insufficient melt water retention. The constant fraction used to define connected wetlands is particularly problematic in the Minago basin, where over half of wetlands are connected to the channel; a more physically based definition of connected wetlands would increase the wetland area, and therefore the wetland storage volume. The Odei River isotope simulation is the best of the three calibrated headwater isotope sites, with agreement during the 2014 freshet and subsequent months being particularly good. The Odei River is the sub-basin best suited to accurate isotope simulation: the WATFLOOD grid scale in the LNRB model is suitable to the size of this sub-basin, and lakes do not have a significant effect on the flow, as there is a single headwater lake simulated in the Odei basin and it lies significantly upstream of the gauge. The Grass River, on the other hand, is dominated by in-stream lakes which significantly attenuate the flow. In the Grass River basin, the $\delta^{18}O$ simulation at Setting Lake matches observed trends well; but the $\delta^{2}H$

simulation is significantly poorer and follows different trends. Given simulated δ^2H often enriches in fall or winter, when it ought to be depleted, the assumptions used in simulating isotopes in reservoirs are likely not reasonable in this sub-basin. The complete mixing assumption is likely violated here given the volume of storage within lakes and the simulation time-scale, and the modeled lake storages in WATFLOOD may also be unrealistic.

5.3.3 Resultant Parameter Values

The flow and isotope simulations the three calibrated parameter sets produce are similar to each other, however, that does not mean that the resultant parameter sets are the same. The same final streamflow can result from very different internal flow paths, with different contributions from groundwater and soil water, as well as water retention in the soils or wetlands. Parameter values resulting from the three calibrations were compared (Table 5.9) as an initial analysis of the effect of including isotope simulation error on the calibration on parameter values.

Table 5.9 Average parameter values and standard deviations relative to potential parameter range for each of the final calibrated parameter sets. River parameters are averaged for all river classes, land parameters averaged for land classes with soil storage, and snow parameters averaged for all land classes.

Parameter type	Average value			Standard Deviation		
Parameter	**F**	**O**	**OH**	**F**	**O**	**OH**
River						
Baseflow coefficient (flz)	0.60	0.61	0.56	0.37	0.31	0.31
Baseflow power (pwr)	0.56	0.68	0.67	0.30	0.26	0.27
Channel roughness (r2n)	0.20	0.24	0.21	0.14	0.17	0.16
Wetland porosity (theta)	0.44	0.34	0.38	0.31	0.40	0.33
Wetland conductivity (kcond)	0.57	0.63	0.65	0.31	0.37	0.35
Land						
Interflow coefficient (rec)	0.49	0.58	0.59	0.26	0.38	0.41
Upper zone retention (retn)	0.39	0.40	0.41	0.35	0.39	0.42
Lower zone recharge coefficient (ak2)	0.59	0.73	0.78	0.33	0.26	0.29
Snow						
Melt factor (fm)	0.41	0.37	0.31	0.37	0.30	0.26

It should firstly be noted that the three calibrations do not provide a sample large enough for the differences between flow and isotope calibrated parameter sets to be statistically significant. The trends in parameter values are still useful, however, in that they can provide direction for further analysis and future studies.

The baseflow power (pwr) parameters are higher for isotope calibrations, resulting in baseflows which are more responsive to new water. Both baseflow parameter (pwr, lzf) types vary less between river classes for the isotope calibrations, which indicates that baseflow for these calibrations may be more physically representative, given that river classes in the model are unrelated to sub-surface properties and therefore should exhibit similar groundwater flow response. Wetland porosity (theta) tends to be lower when isotopes are included in calibration, and the wetland conductivity (kcond) higher: both

these changes increase the wetland outflow response. The interflow coefficient (rec) and the recharge coefficient (ak2) parameter types, both of which control flow rates out of the upper zone (to connected wetlands and the lower zone, respectively) increase, on average, for isotope calibrations; increasing the soil outflow responsiveness and decreasing the residence time of water in the upper (soil) zone. Snow melt rates (fm) decrease, on average, for isotope calibrations, with the variation between the melt rates for different land classes being lower than for the flow-only calibration. As with the groundwater parameters, this may be an indication of increased physical representativeness, as more similar melt rates point to less over-tuning of parameters. Overall, the parameter sets indicates more responsive flows, and less water stored in the upper zone from using isotope error in calibration.

5.4 Model Validation

The flow and isotope simulations from isoWATFLOOD were validated differently: the first using a temporal sample split, and the latter, a spatial sample split. Flow simulations for the three calibrated parameter sets were validated using flow data from 1982 to 2009, with 1981 used as a spin-up year. Isotope data is only available from 2010 to 2014, and a 5-year period was considered too short to separate into two time-series for calibration and validation while preserving adequate hydrological variability in both series. Isotope sites are therefore split into calibration and validation sets instead: seven of the most frequently sampled sites, which were not used to calibrate the model, were used to validate the isotope simulation from 2010 to 2014, with 2009 used for model spin-up.

5.4.1 Isotope Simulation Validation

Isotope sampling sites used during model validation of isotope simulations (see Table 5.10) have fewer observations, with an average of 5 (rather than 7) per year, and are less evenly distributed throughout the modeled area.

Table 5.10 Isotope sampling sites used in validation (2010-2014) with drainage areas and locations.

Basin	Site	Station ID[1]	Samples	Drainage Area (km^2)	Latitude (°)	Longitude (°)
Upper Burntwood	Burntwood above Leaf Rapids	R-MH-05TE703	16	5 800	55.50	-99.22
Odei	Sapochi River	R-MH-05TG006	46	390	55.91	-98.49
Burntwood	Footprint River	R-MH-05TF782	13	640	55.93	-98.89
Upper Nelson	Nelson at Clearwater Lake	R-MH-05UE703 R-MH-05UE713	26	1 050 000	55.34	-96.78
Grass	Grass below Standing Stone Falls	R-MH-05TD001	8	15 400	55.74	-97.00
Burntwood	Burntwood above Split Lake	R-MH-05TG722	29	25 000	56.14	-96.60
Burntwood	Taylor River	R-MH-05TG002	7	890	55.50	-98.19

[1]Internal SWIMN database ID where isotope data are catalogued at the University of Manitoba, also reflecting WSC gauge ID.

The error in the isotope simulation is again quantified using RMSE and NRMSE (Section 5.2.1). The $\delta^{18}O$ simulation error is shown in Table 5.11, for validation sites from 2010 to 2014.

Table 5.11 $\delta^{18}O$ simulation error at validation sites for 2010-2014 for the three model calibrations.

		RMSE (‰)			NRMSE		
Basin	**Site**	**F**	**O**	**OH**	**F**	**O**	**OH**
Upper Burntwood	Burntwood above Leaf Rapids	0.9	1.8	1.8	0.07	0.14	0.14
Odei	Sapochi River	1.7	1.5	1.5	0.12	0.11	0.10
Burntwood	Footprint River	3.8	4.0	4.0	0.30	0.32	0.32
Upper Nelson	Nelson at Clearwater Lake	0.5	0.5	0.5	0.05	0.04	0.04
Grass	Grass below Standing Stone Falls	1.3	1.8	1.6	0.11	0.15	0.13
Burntwood	Burntwood above Split Lake	0.5	0.4	0.3	0.04	0.03	0.03
Burntwood	Taylor River	1.3	2.0	2.0	0.09	0.15	0.14
	Average	**1.43**	**1.72**	**1.66**	**0.111**	**0.134**	**0.130**

Errors are greater at validation sites than at sites used in model calibration (Table 5.11 versus 5.7), as is expected. Unlike the average errors for calibration sites, the average isotope simulation errors for the validation sites are higher for the isotope calibrations than the flow calibration. Sites that strongly resemble calibration sites and are on the same river (i.e. Nelson at Clearwater Lake and Burntwood above Split Lake) have low error, and the errors for the isotope calibrations (O and OH) were lower than those for the flow (F) calibration. The Sapochi River, a headwater stream of the Odei River (a calibration site) with similar land cover has moderate error and better performance from the isotope calibrated simulations. The Taylor River, Grass River and Burntwood River above Leaf Rapids also have moderate error, but worse isotope simulations from parameter sets calibrated using isotope error in the objective function. The Grass River validation site is significantly downstream of the site Grass sub-basin calibration site, with additional in-stream lakes. The Taylor River is a small tributary of the Burntwood River which is calibrated at a site dominated by Churchill River diversion flow, reducing the importance of local inflows such as the Taylor River in the calibration. The Burntwood River above Leaf Rapids gauge resides in a separate river class from the lower Burntwood in the model, and this river class contains no isotope sites used in model calibration. The Footprint River has high isotope simulation error and it is also in a river class which has no isotope sites in calibration. Such circumstances help explain the inability of isotope calibration to improve isotope ($\delta^{18}O$ or $\delta^{2}H$) simulations.

The $\delta^{2}H$ simulation error values from 2010 to 2014 at all validation sites are in provided in Table 5.12.

Table 5.12 δ^2H simulation error at validation sites for 2010-2014 from the three model calibrations.

		RMSE (‰)			NRMSE		
Basin	**Site**	**F**	**O**	**OH**	**F**	**O**	**OH**
Upper Burntwood	Burntwood above Leaf Rapids	8.8	11.9	11.6	0.08	0.11	0.11
Odei	Sapochi River	14.4	12.9	13.3	0.12	0.11	0.12
Burntwood	Footprint River	14.4	14.7	14.5	0.14	0.14	0.14
Upper Nelson	Nelson at Clearwater Lake	3.8	3.7	3.7	0.04	0.04	0.04
Grass	Grass below Standing Stone Falls	11.4	11.6	9.6	0.11	0.11	0.09
Burntwood	Burntwood above Split Lake	2.3	2.3	2.1	0.02	0.02	0.02
Burntwood	Taylor River	7.1	7.4	7.3	0.06	0.07	0.07
	Average	**8.89**	**9.22**	**8.89**	**0.083**	**0.086**	**0.083**

As with the $\delta^{18}O$ simulations, δ^2H simulations have higher error at validation sites than at calibration sites (Table 5.12 versus 5.8). Differences in the δ^2H simulation error between calibrations is smaller than for $\delta^{18}O$, but on average, the dual-isotope calibration (OH) performs best on average when simulating deuterium, even if it performs slightly worse at some sites. The errors are all acceptable, although simulations for the Footprint River are again the worst, and are only marginally acceptable based on criteria outlined in Moriasi, et al. (2007).

Time-series plots of the observed and simulated isotopic compositions for the Footprint River and the Sapochi River (validations) are shown below in Figure 5.7 (all validation site isographs provided in Appendix C).

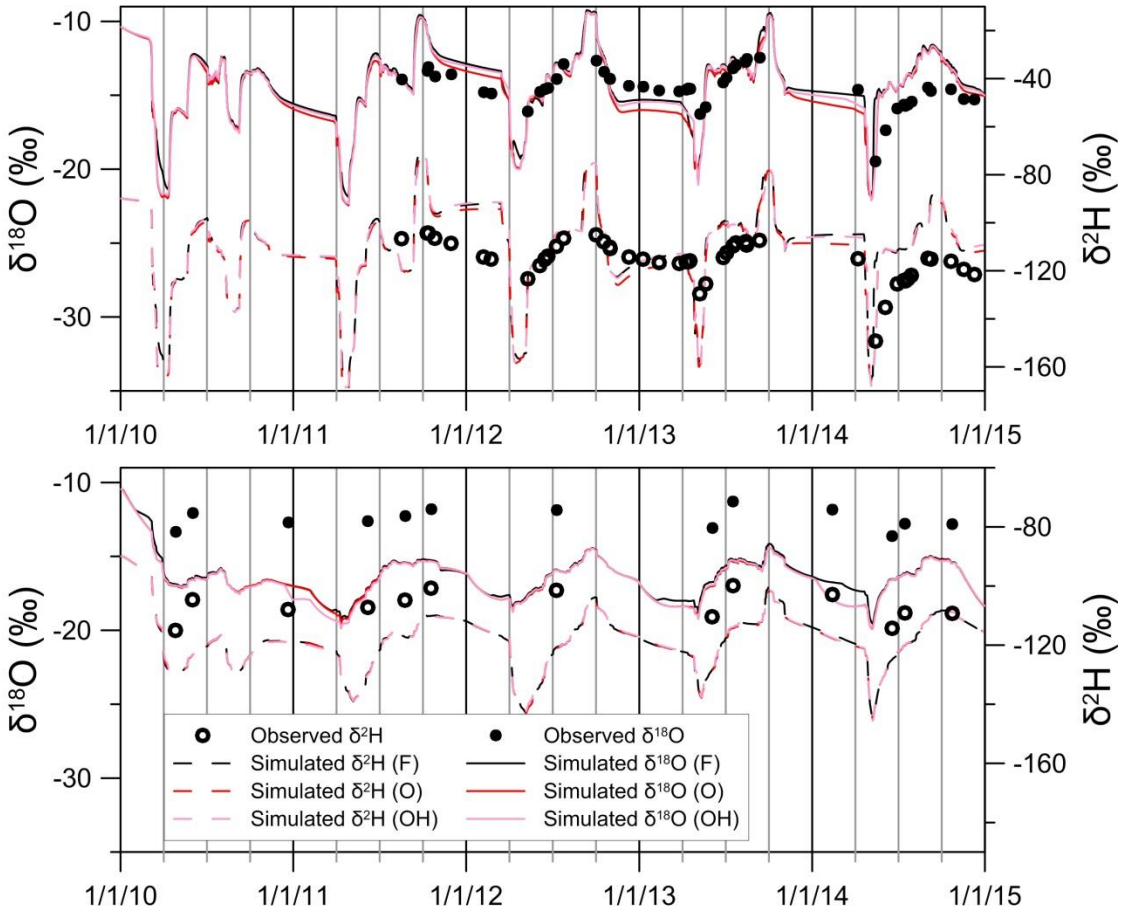

Figure 5.7 Sapochi River (top) and Footprint River isographs with δ^2H and $\delta^{18}O$ simulated and observed (2010-2014) for the three parameter sets (F, O, and OH).

The Sapochi River simulations generally follow the same trends as the observed data, and most of the simulation produces values that match closely to the observed data. The simulation does not always match low flow observations (i.e., in winter), and simulations consistently do not retain enough snowmelt, as seen from the too rapid recovery of the simulated values following the 2013 and 2014 freshets. The simulation of the Footprint River, in contrast, is a consistently poor match to observed isotope data, although the trends are in agreement. The calibrations for the Footprint River, which is in a distinct river class with no isotope data used in its calibration, produce groundwater parameters that retain water in the lower zone, and wetland parameters that prevent substantial water retention in connected wetlands. Surface water inflows to the stream maintain some variability in the isotopic

simulation, but the dominance of highly mixed and old groundwater (due to the very large lower zone storage and the assumptions of the isotope model) produce a very damped, too depleted, and inaccurate isograph. The Burntwood River above Leaf Rapids site is also in a river class calibrated without isotope data; the isograph for the site is shown in Figure 5.8.

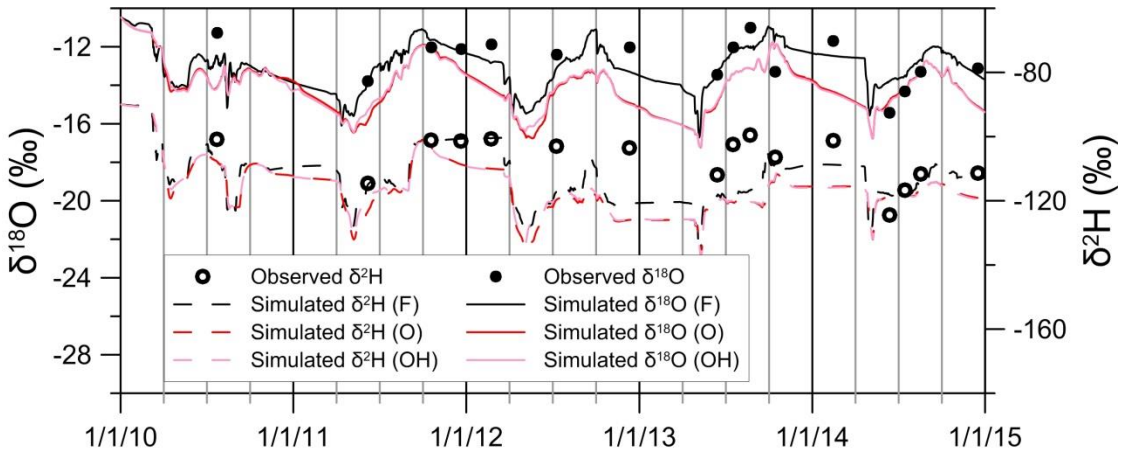

Figure 5.8 Burntwood River above Leaf Rapids isograph with simulated and observed δ^2H and $\delta^{18}O$ (2010-2014) for the three parameter sets (F, O, and OH).

Although a better simulation than the Footprint River, the isotopic simulation for the Burntwood River above Leaf Rapids site still has significant error. The δ^2H and $\delta^{18}O$ simulations also follow different trends, when the observed values do not, indicating excess evaporation, likely due to the headwater lakes in the upper Burntwood area. From the validation of the isotope model, it can be concluded that the isotopic simulation can perform reasonably at sites it was not calibrated for, but reasonable performance is dependent on having parameters calibrated to isotope observations. River classes calibrated without any isotopic observations (i.e. the upper Burntwood and Footprint Rivers) do not perform well in validation.

5.4.2 Flow Simulation Validation

The flow simulations were validated using data from 1982 to 2009, with 1981 used as a spin-up year for the model. In general, the flow simulations perform well in the validation period; flow simulation statistics are shown in Table 5.13.

Table 5.13 Flow simulation statistics for the validation period (1982-2009).

Station name	Station ID	Nash-Sutcliffe			R^2			%Dv		
		F	O	OH	F	O	OH	F	O	OH
Grass River	05TD001	0.61	0.61	0.59	0.96	0.96	0.95	-26.4	-24.8	-24.6
Burntwood above Leaf Rapids	05TE002	0.63	0.59	0.61	0.93	0.91	0.92	-19.6	-19.2	-17.8
Footprint River	05TF002	0.44	0.40	0.40	0.92	0.91	0.92	39.3	42.9	43.6
Burntwood near Thompson	05TG001	0.79	0.78	0.78	0.98	0.98	0.98	-5.8	-5.7	-5.7
Taylor River	05TG002	0.59	0.61	0.61	0.95	0.96	0.96	-42.2	-40.9	-41.0
Odei River	05TG003	0.70	0.69	0.70	0.98	0.97	0.98	-16.6	-14.8	-14.5
Sapochi River	05TG006	0.65	0.64	0.63	0.95	0.94	0.94	16.0	18.4	19.0
Nelson at Kelsey GS	05UE005	0.87	0.88	0.88	0.99	0.99	0.99	3.4	3.5	3.5
Limestone River	05UG001	0.50	0.51	0.52	0.93	0.92	0.92	-15.5	-14.1	-14.0
Weir River	05UH002	0.50	0.49	0.50	0.96	0.96	0.96	-18.8	-17.5	-17.5
Average:		**0.629**	**0.619**	**0.622**	**0.955**	**0.950**	**0.952**	**-8.63**	**-7.23**	**-6.91**

The average NS values for streamflow simulations are lower in the validation period than calibration, as is typical; and the calibrations using isotopes again have somewhat worse NS values than the flow-only calibration. The percent deviations in flow are significantly higher during validation than calibration, with simulated flow more likely to be lower than observed flows. Simulated flows from the two isotope calibrations are generally higher than from the flow calibration, resulting in less flow volume error from the isotope calibrations, on average. The Taylor and Sapochi Rivers have significant volume error in validation as they did in the calibration period, again caused largely by errors in the modelled drainage area (i.e., 20% too low and 39% too high, respectively). These errors are caused by a mismatch between

the rectilinear WATFLOOD grid and the natural drainage area; in both cases the grid boundary is located on the wrong side of a flow gauge, with most of a grid cell being either erroneously added or removed from the gauge drainage area. The Footprint River also has a very large overestimate in flow volume; however, it also has a poor NS score. The Footprint River is the only gauge with a consistently low NS value (i.e. below 0.5), but the Limestone and Weir Rivers are also marginal. All three of these gauges perform worse in validation than in the calibration period; this is evidence the parameters for these basins are not accurately simulating flows in average conditions, or over the long-term. The Nelson, Odei and Burntwood (near Thompson) Rivers have slightly better simulation statistics during the calibration period; but the Grass, upper Burntwood, Sapochi and Taylor Rivers actually perform better during the validation, barring the increased average volume error. These rivers perform better in average flow years, and average flow years are more common in the validation period than the calibration period.

The hydrographs over the validation period provide further insight on overall model performance: due to the lengthy validation period, average annual hydrographs are shown, beginning with the Burntwood and Odei Rivers (Figure 5.9).

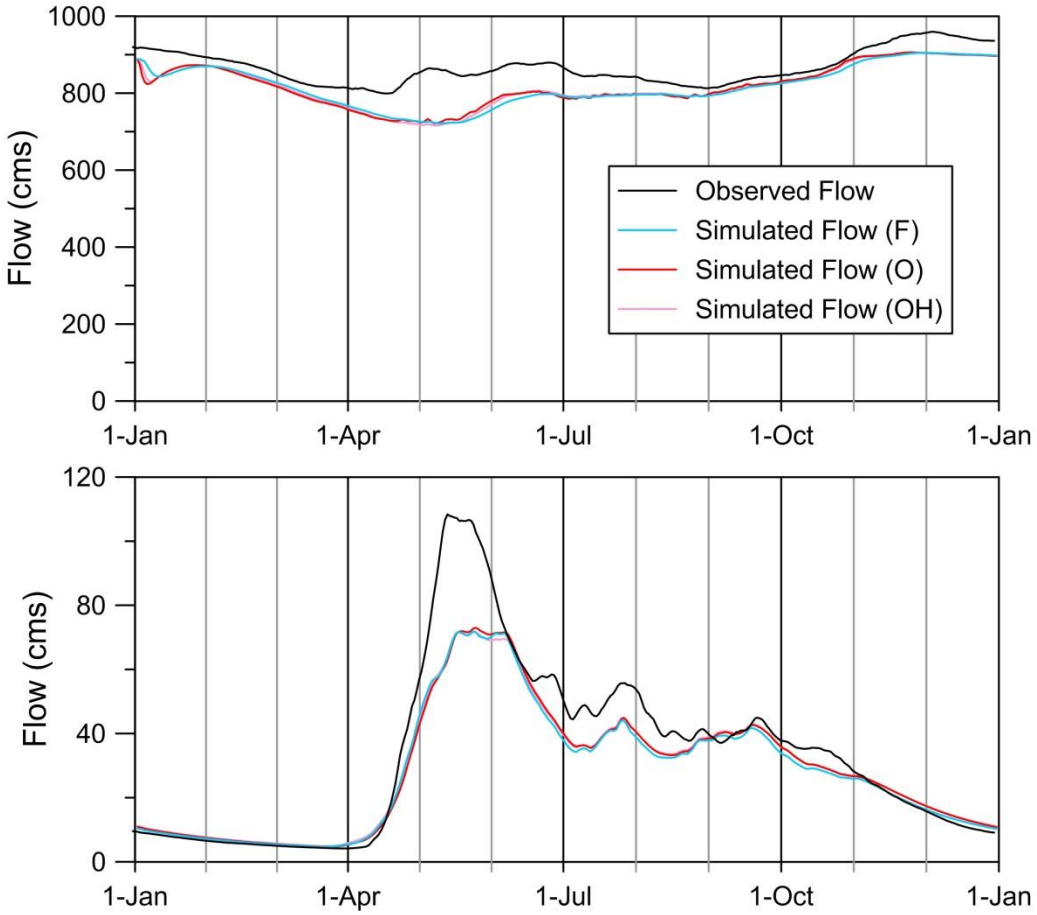

Figure 5.9 Burntwood River near Thompson (top; WSC ID 05TG001, 18 500 km^2) and Odei River (bottom, WSC ID 05TG003, 6 110 km^2) average annual hydrographs for the validation period (1982-2009) for the three model calibrations (F, O, and OH).

The simulations for the gauge on the Burntwood River near Thompson are a good match to observed flow, but this is expected given the dominance of the Churchill River diversion on flows for the lower Burntwood River. Flow rates during the freshet period, however, are too low. The Odei River, a large tributary of the Burntwood River with natural flows, has good low flow simulations and good timing of snowmelt and rainfall peak flows; but flows are much too low for the freshet, and too low in the summer as well. The Grass River (Figure 5.10) is similar: the high and low flow timing is good, but simulated peak flows are not high enough.

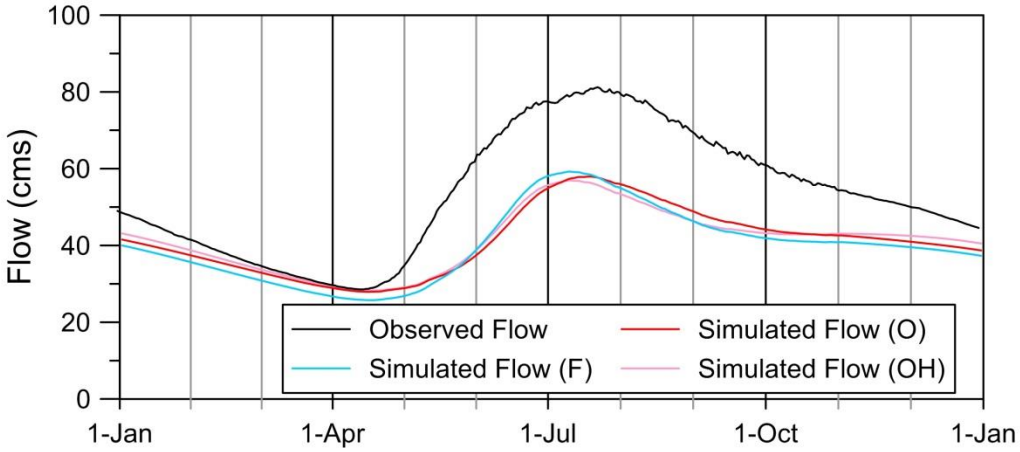

Figure 5.10 Grass River (WSC ID 05TD001, 15 400 km^2) average annual hydrograph for the validation period (1982-2009) for the three model calibrations (F, O and OH).

Average simulated water losses from the LNRB are clearly too high; it is less obvious why simulated losses are too great. The greatest divergence between observed and simulated flows is during the spring freshet, but this could be due to excess sublimation producing too little simulated snowpack, or due to insufficient storage of water in the wetlands and soil over the winter. The larger divergence of simulated relative to observed streamflow for the Grass River, with its many lakes, rather than the Odei River points to simulated open water or lake evaporation rates exceeding the true values.

Both the Sapochi and the Footprint Rivers have excess simulated flow and similar annual average flows, but are otherwise quite different (see Figure 5.11).

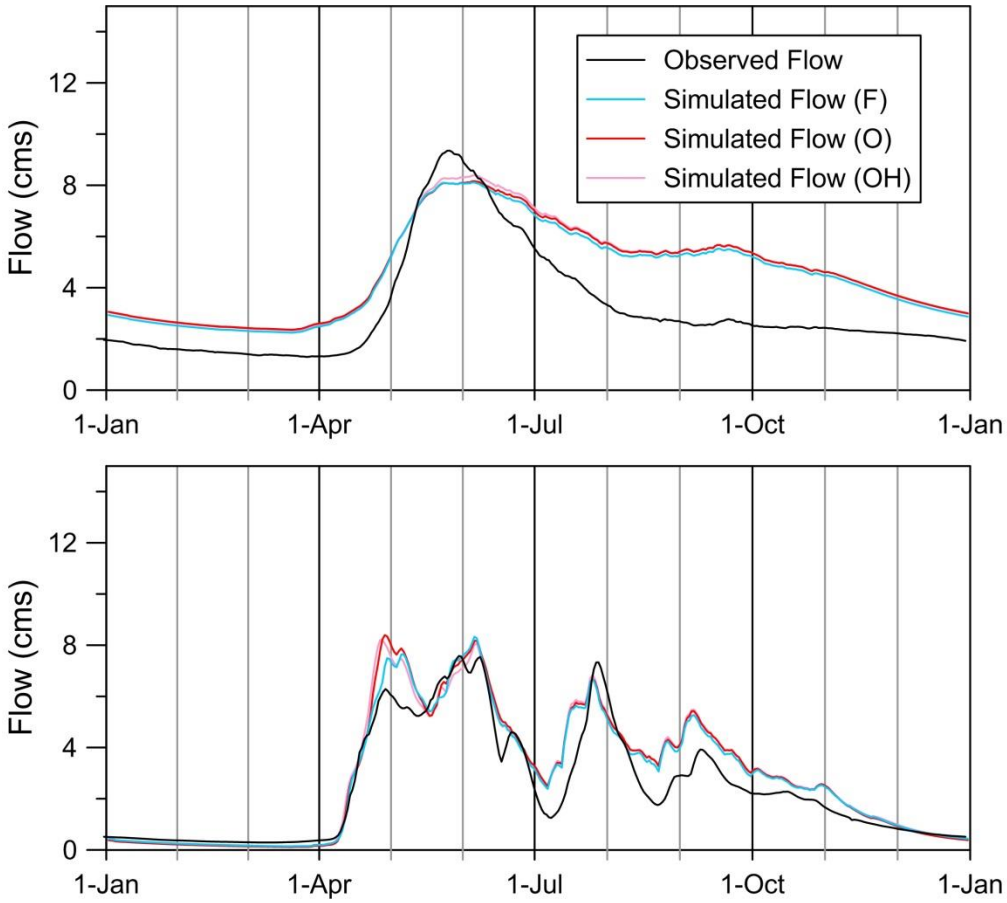

Figure 5.11 Footprint River (top; WSC ID 05TF002, 643 km^2) and Sapochi River (bottom, WSC ID 05TG006, 391 km^2) average annual hydrographs for the validation period (1982-2009) for the three model calibrations (F, O, and OH).

The Footprint River simulation is generally poor, with simulated low flows being too high and simulated high flows being too low; although snow melt timing is, on average, correct. The Footprint River has very good flow statistics during the calibration period, but results are significantly worse during validation. The Sapochi River, on the other hand, has better statistics for validation than calibration; the parameters continue to produce acceptable simulations in the longer validation period and as the validation has relatively fewer extreme flow years than the calibration period, the simulation statistics improve. The Footprint River is simulated well for the anomalously high and low flow years in the calibration with high groundwater storage and flows and low wetland storage, but in the long term, with average

precipitation, this combination of high groundwater flows and low wetland storage results in a mediocre simulation with too little variation in flows and poor flow simulation performance statistics.

5.4.3 Prediction of Simulation Performance

The case of the Sapochi and Footprint Rivers demonstrates that Nash-Sutcliffe efficiency scores in the calibration period are not necessarily good predictors of simulation performance outside of that period: the Footprint has an average NS value of 0.77 in calibration, but only 0.41 in validation; while the Sapochi increases its NS value from 0.52 in calibration to 0.64 in validation. This is a non-trivial problem; one of the primary uses of hydrologic models is to simulate flows outside of periods with observed flows, and it would therefore be useful be able to predict simulation performance beyond the calibration period from within the period. The simulation of Footprint River shows that performance prediction using calibration NS values alone is unreliable; when all gauges are considered, the NS statistic alone continues to be a poor predictor of performance during validation (Figure 5.12(a)). While calibration NS values are related to validation NS values, used here as a single value simulation performance indicator, the relationship is weak, with an R^2 of only 0.25. Other flow simulation statistics prove even less reliable at predicting validation flow simulation performance.

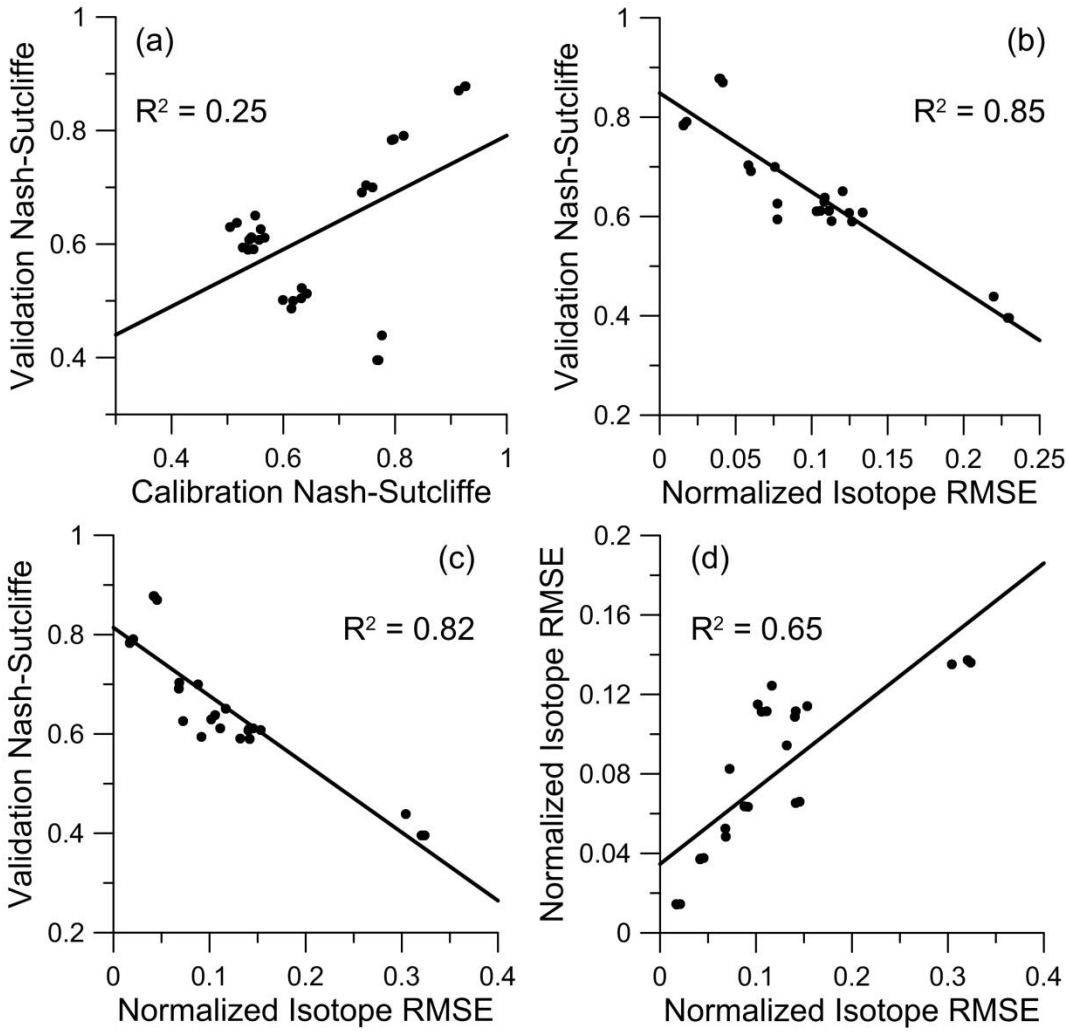

Figure 5.12 Scatter plots of calibration and validation period statistics. (a) validation NS vs calibration NS (b) validation NS vs average NRMSE (c) validation NS vs $\delta^{18}O$ NRMSE (d) $\delta^{2}H$ NRMSE vs $\delta^{18}O$ NRMSE. All three calibrations are included in scatter plots.

The isotope simulation error in the five-year calibration period, on the other hand, reliably predicts the flow NS value in the validation period, with an R^2 value of 0.85 when comparing average isotope NRMSE from 2010-2014 to the NS value from 1981-2009 (Figure 5.12(b)). The poor simulation of isotopes in the Footprint River proves to be a good indicator of the poor flow simulation outside of calibration, as the moderately accurate isotope simulations in the Grass and upper Burntwood Rivers predict adequate flow simulations in those rivers in the validation period. Using a single isotope error, from the $\delta^{18}O$ simulation, is nearly as good as using both isotopes, with only a small decrease in predictive capability

from an R^2 value of 0.85 to 0.82 (Figure 5.12(c)). The two isotope errors are not interchangeable however, as shown in Figure 5.12(d); although the majority of predictive information from isotopic simulation is gained by one isotope, including a deuterium simulation does add additional predictive information.

Although isotope-flow calibrations do not perform better than the flow-only calibrations in the validation period (slightly better volume deviations, but slightly worse NS values from the isotope-assisted calibrations), the predictive capability of isotope simulation error demonstrates that isotope simulation has the potential to improve calibration. How best to utilize this potential cannot be determined from the results of this research as there are multiple possibilities:

1. Isotope error could be used much as it was in this study, but with a larger weight given to isotope NRMSE in the error function and with a more complete set of isotope sites in calibration such that isotope error is used in the calibration of all parameters;
2. Isotope simulation might instead be used as one part of a multi-objective calibration; or
3. Isotope simulation error may best be used as a separate test for unrepresentative parameter sets outside of auto-calibration.

5.5 Effect of Isotope Error on Flow Simulation

The overall effect on total streamflow of including isotope error in the objective function is small, yielding slightly more flow for isotope calibrations than the flow-only calibration. However, based on the analysis of changes in parameter values (Section 5.3.3), flow sources are affected by isotope-enabled calibration and these should be examined in addition to the total streamflow. Wetland, upper zone and lower zone flow parameters have consistent differences between the calibration methodologies and these compartments show increases in outflow from isotope-enabled calibrations. This conclusion is also consistent with that reached by considering the hydrologic variables that stable water isotopes

most affected: evaporation and water retention. Evapotranspiration rates in the model are determined by storage in the upper zone, while the lower zone and connected wetland storages are the two main storages for retaining and mixing flows. To determine the overall effect parameter variations between calibrations have on flows, headwater grid cell responses (i.e. cells with no contributions from upstream grid cells, that is, grid cells along the watershed boundary) in all river classes were recorded from WATFLOOD simulations for the three calibrated parameter sets during the validation period. Headwater grid cells were used in this initial analysis to reduce the effects of streamflow routing and variable downstream channel roughness. The average annual hydrograph of mean outflows from headwater grid cells in all river classes (all classes having equal weight) is shown in Figure 5.13.

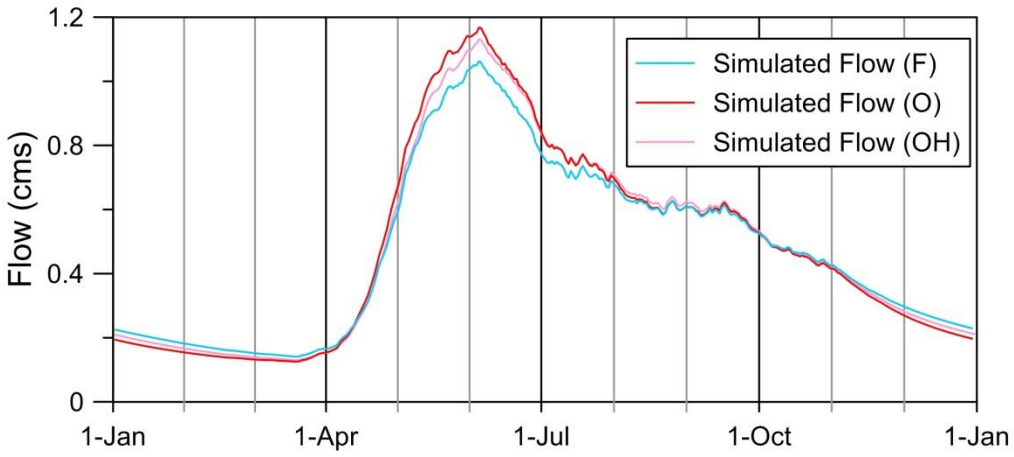

Figure 5.13 Average annual hydrograph of headwater grid cells. Grid cells with no upstream contributions from each of the river classes are averaged (all river classes having equal weight) to illustrate the differences between the calibration methodologies (F, O, and OH).

Outflows from headwater grids show marked differences between calibrated parameter sets - more obvious than at downstream flow gauge locations - though both have small increases in total annual flow for isotope calibrations. In the winter low flow period, the flow-only calibration yields slightly higher flows, but in the spring freshet flows are appreciably higher for both isotope calibrations. The isotope calibrations are more responsive to precipitation or snowmelt inputs, while the flow-only calibration yields a more damped flow response overall. The same averaged headwater grid cell

outflows shown in the time-series plot (Figure 5.13) are also compared in Figure 5.14. As there is no observed flow data for headwater grid cells, the different calibration methodologies are plotted against each other (i.e. the flow-only calibration is compared to the single isotope calibration, and so on) to display the differences between them. A 1:1 line is included as reference only; the closer the simulation comparison plots to the 1:1 line, the more similar two calibrations are to each other. Plotting below the 1:1 line indicates that the dependent calibration produces lower flows than the independent calibration for that comparison line, and plotting above the 1:1 line indicates the reverse. The three linear best fits are shown on the figure: flow-only vs single isotope calibrations (blue), flow-only vs dual isotope calibrations (green) and single isotope vs dual isotope calibrations (red). The dependent calibration is listed first in the description of the lines.

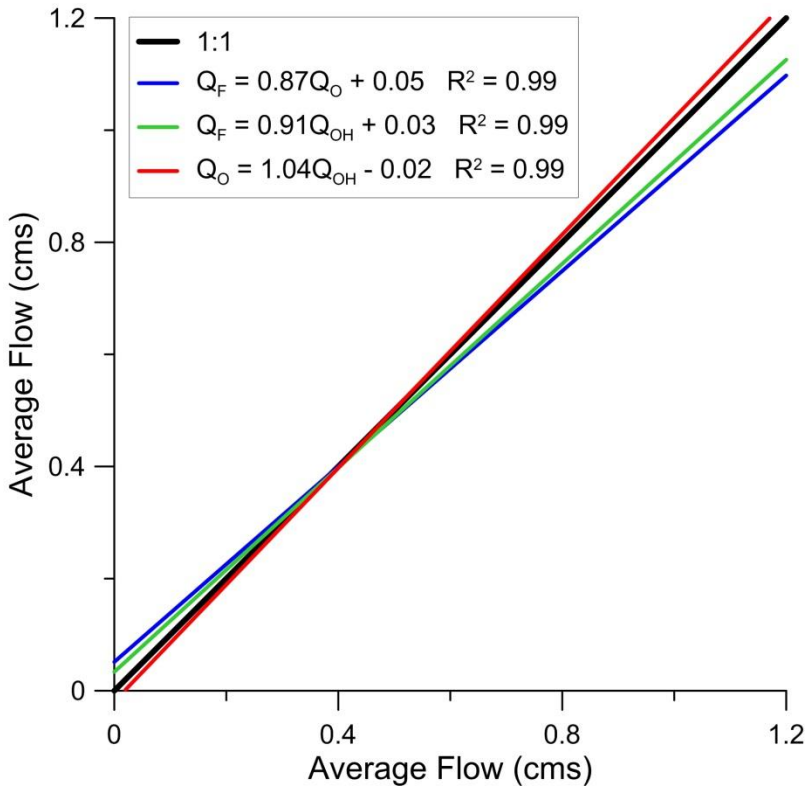

Figure 5.14 Calibration methodologies (F, O, and OH) for average headwater grid outflows compared against each other and their linear best-fits for flow-only vs single isotope (blue), flow-only vs dual isotope (green) and single isotope vs dual isotope (red) calibrations.

When compared to each other, the two isotope calibrations (red line) are near equivalents, plotting near the 1:1 line. Both are similar relative to the flow-only calibration (blue and green lines), showing only small decreases in low flows and larger increases in high flows. The single-isotope calibration (blue line) diverges more from the flow-only calibration than the dual-isotope calibration (green line); the difference between the two lines is small and may be due to the different importance of evaporation in the deuterium simulation (OH) than the oxygen-18 (O) simulation. In order to find why headwater grid outflows vary between calibrations, streamflow needs to be decomposed into its source components: lower zone outflows are compared (Figure 5.15); as with Figure 5.14, the different calibration methodologies are plotted against each other to display the differences between them.

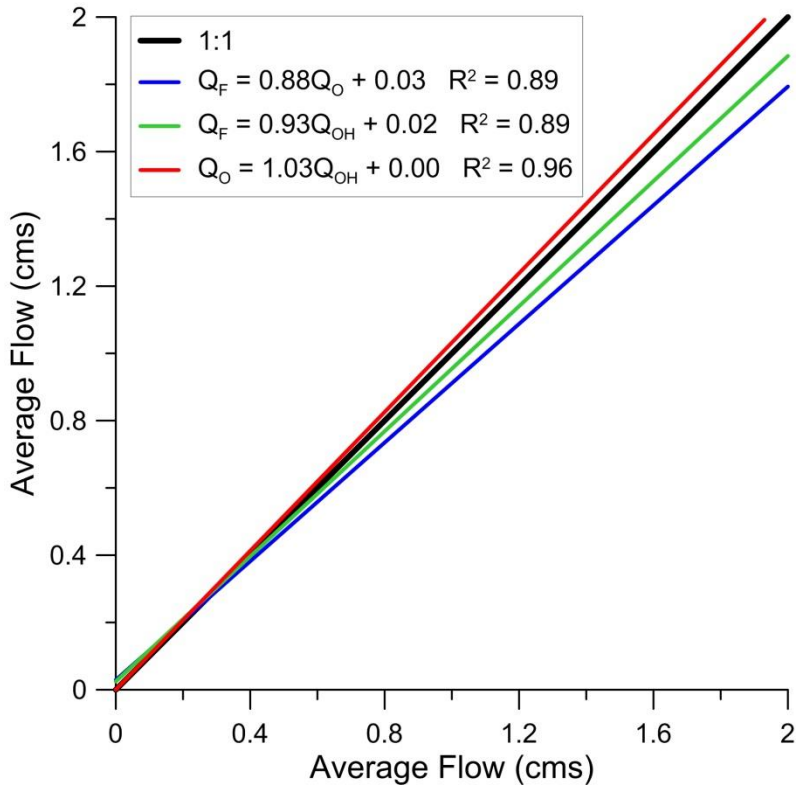

Figure 5.15 Calibration methodologies (F, O, and OH) average lower zone outflows compared and the linear best-fits for flow-only vs single isotope (blue), flow-only vs dual isotope (green) and single isotope vs dual isotope (red) calibrations.

Lower zone or groundwater outflows diverge more between calibrations than total streamflow, with the dual-isotope calibration (green line) slightly increasing peak groundwater outflow (i.e. plots below the 1:1 line), while the single-isotope calibration (blue line) produces more extreme peaks. The calibrations are approximately consistent for low-flows. The lower zone is more responsive to new inputs (i.e. flow out of the lower zone increases to a higher rate in less time when water is added to the lower zone storage) for the isotope-calibrated parameter sets: less water is being retained in the lower storage zone when isotope error is included in the calibration. This finding is consistent with the geology of the LNRB where soils are very shallow and bedrock is near-surface, which limits the amount of water that can be stored in (and released from) the sub-surface. Along with the lower zone, connected wetlands act to moderate and mix flows; wetland outflows from headwater grids are compared in Figure 5.16; like Figure 5.14 and Figure 5.15, the different calibration methodologies plotted against each other to display the differences between them.

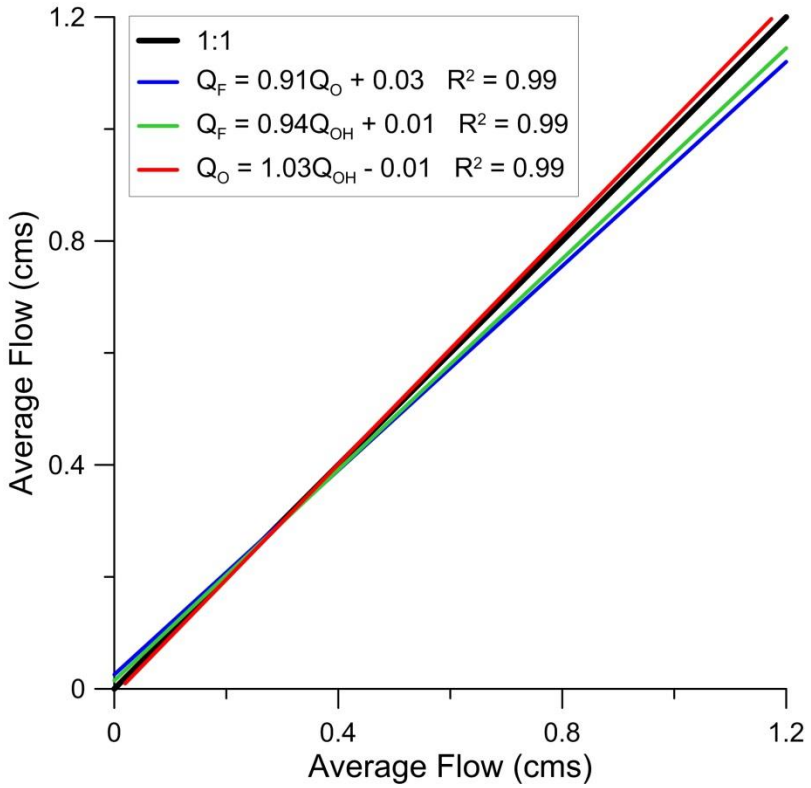

Figure 5.16 Calibration methodologies (F, O, and OH) average connected wetland outflows compared and the linear best-fits for flow-only vs single isotope (blue), flow-only vs dual isotope (green) and single isotope vs dual isotope (red) calibrations.

Wetland outflows from all calibrations are in closer agreement than groundwater outflows from headwater grids, although the isotope-enabled calibrations again have somewhat higher peak flows than the flow-only calibration. The relationships between the calibrations for wetland outflow are similar to the relationships for total headwater outflow (Figure 5.16 and Figure 5.14): this is entirely expected as wetland outflow is the primary contributor to headwater streamflow in the LNRB. Wetland outflow becomes more interesting when it is compared with the groundwater flows. If wetland outflows remain similar, and groundwater peak flow increases, the amount of water stored in the wetland is increasing. This conclusion applies to both isotope calibrations, as both have larger increases in groundwater peak flow than increases in wetland peak outflow. Therefore the isotope-enabled calibrations have shifted water storage from groundwater to the wetlands. This is reasonable for the

LNRB area, as it is dominated by near-surface bedrock and has large areas covered by surficial wetland complexes. This shift is much more pronounced for the single-isotope calibration, which has a much larger difference between the increase in groundwater relative to the increase in wetland outflow; comparing the blue line to the green, the difference in larger for groundwater (Figure 5.15) than for wetland outflow (Figure 5.16). The difference between the two isotope-enabled calibrations is explained by the relative importance of evaporation in the dual isotope simulation (that includes deuterium) relative to the single isotope (oxygen-18) simulation: evaporative enrichment affects the oxygen-18 simulation more. The error in the dual-isotope simulation is less affected by evaporation than single isotope simulation, and evaporation occurs in wetlands - but not from the groundwater storage. It is therefore to be expected that the dual isotope calibration produce different ratios of groundwater to wetland storage.

At the sub-basin scale, cumulative contributions from single grid cells to streamflow should produce similar changes in streamflow source components at gauge locations as is found for headwater grid cells. This is indeed seen in the percent contributions from the three types of internal WATFLOOD storage (Table 5.14), with values coming from the virtual tracer module in WATFLOOD (Kouwen, 2014).

Table 5.14 Contributions from WATFLOOD internal storage averaged for all simulated LNRB gauge locations with natural (unregulated) flows (1982-2009).

Flow source component	Abbrev.	F	O	OH
Surface runoff (%)	**SW**	2.5	2.6	2.6
Upper zone lateral flow (%)	**IF**	31.2	26.7	29.2
Lower zone outflow (%)	**GW**	66.3	70.8	68.2

Lower zone outflows contribute a larger percentage of water to total streamflow using the isotope-enabled calibrated parameter sets; and as with headwater grid cells, the increase is greatest for the single-isotope calibration. Contributions from upper zone storage directly to connected wetlands are

reduced for isotope-enabled calibrations: again with a larger change in the single-isotope calibration. Direct surface runoff remains consistent between calibrations, which is expected as surface water is not a significant contributor to total streamflow, and parameters relating to surface storages were not calibrated in this study. The difference between the isotope calibrations for upper and lower zone contributions is likely also driven by evaporation (similar to wetland-groundwater storage difference): the upper zone loses water to evapotranspiration, while the lower zone does not. The effect of evaporation on the isotope simulation error depends on the isotope simulations included in the calculation (i.e. ^{18}O or both ^{18}O and ^{2}H). It is therefore to be expected that the different isotope calibrations will produce somewhat different ratios of upper zone flow to lower zone flow.

Variations also exist between sub-basins. At the flow gauge location with the largest area unaffected by regulated or diverted flows (i.e., the Grass River), flows are highly attenuated and the difference between the two isotope-enabled calibrations is relatively small (Figure 5.17).

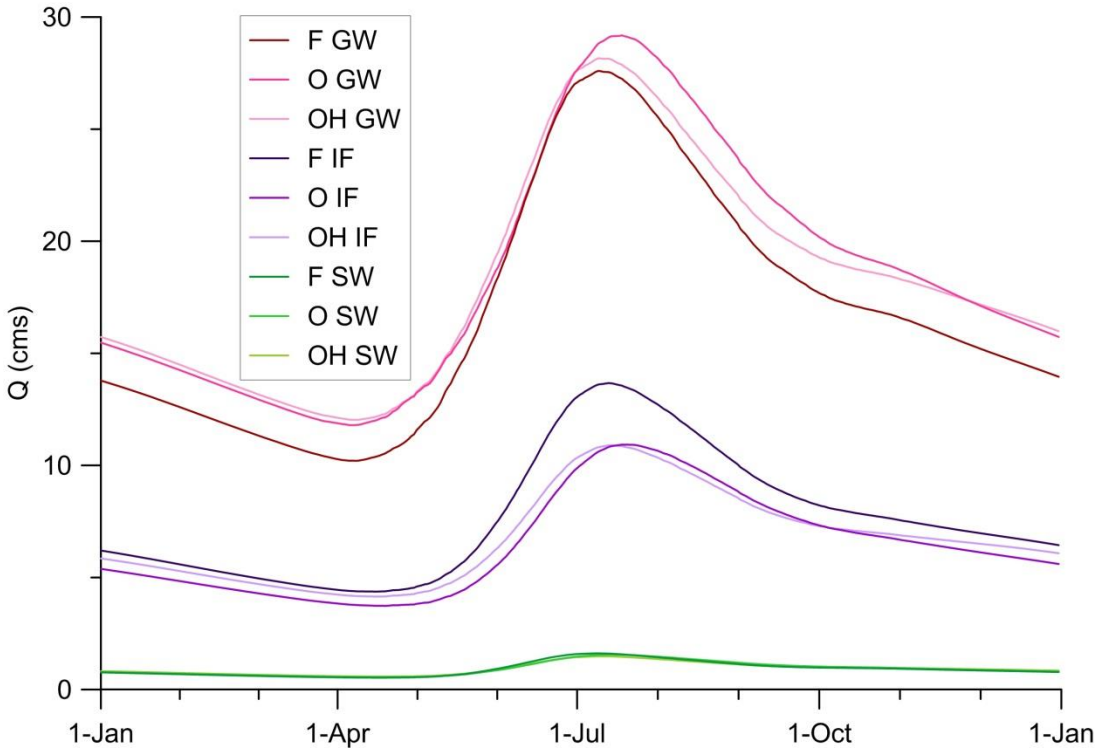

Figure 5.17 Average annual hydrograph of virtual tracers at the Grass River gauge (WSC ID 05TD001) for 1982-2009. Flow component contributions from surface water (SW), upper zone (IF) and lower zone (GW) storage are shown for each calibration methodology (F, O, and OH).

Flows in the Grass River (Figure 5.10) show low variability due to the many in-stream lakes in the basin, and because of the high percentage of basin area covered by wetlands. Upper zone contributions to total streamflow from both isotope calibrations are very similar and lower than that from the flow-only calibration; lower zone contributions are somewhat similar, and are higher than that from the flow-only calibration. The total flow in all three calibrations is therefore largely similar (Figures 5.4 and 5.10). Total flows are also similar for all three calibrations at the flow gauge with the smallest drainage area in this study: the Sapochi River (Figure 5.18).

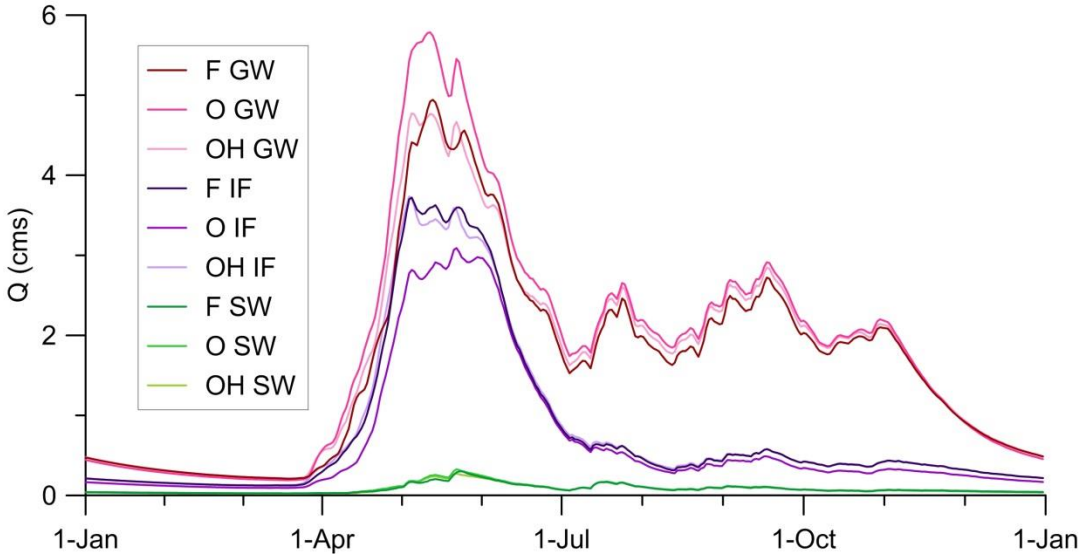

Figure 5.18 Average annual hydrograph of virtual tracers at the Sapochi River gauge (WSC ID 05TG006) for 1982-2009. Flow component contributions from surface water (SW), upper zone (IF) and lower zone (GW) storages are shown for each calibration methodology (F, O, and OH).

Flows in the Sapochi River are highly variable due to its small drainage area (analogous to headwater grid outflows) and the relatively high proportion of the basin covered by forest, rather than wetland. Also unlike the Grass River, the Sapochi's dual-isotope and flow-only calibrations are the most similar, rather than the two isotope calibrations. The single-isotope calibration results in lower contributions from the upper zone, and higher contributions from the lower zone relative to the other two model calibrations. The difference between the two basins may be related to how water is primarily evaporated from WATFLOOD. In the Grass River, surface water in lakes and wetlands is the primary source of evaporation, while in the Sapochi basin, soil evapotranspiration is of greater significance owing to differences in the land cover distributions, with 76% of the Sapochi basin covered by forest and shrub, while only 54% of the Grass basin is forest or shrub. The redistribution of water between the upper and lower zones therefore has a larger effect on the total evaporation volume in the Sapochi, and the two isotope calibrations are more likely to differ in terms of interflow contribution within this basin, as they do in this study (i.e., 26% of flow comes from the upper zone in the single-isotope calibration, and 31% in the dual-isotope calibration).

Therefore, the use of isotopes in the calibration objective function does significantly influence the resultant optimized parameter set. The streamflow simulations produced from isotope calibration are largely similar to the simulation produced using the flow-only error function in calibration, with only small increases in flow volume. Contributing sources to total streamflow (i.e., internal water storage) in the LNRB model change more noticeably among the different model calibrations. Flow contributions shift from the upper soil zone to the lower zone when isotope error is included in the calibration, and lower zone outflows to the connected wetland tend to respond more rapidly to new inflows. Less water is stored in the lower zone overall with isotope calibration, and more water is in stored in wetlands that are connected to the channel. These changes are reasonable given knowledge of the geology, ecology and hydrology of the LNRB area, however, since groundwater and wetland storages are not observed directly the accuracy of modeled storages and water fluxes cannot be verified.

6 Model Verification with Isotope Data

The isoWATFLOOD model simulates stable water isotope compositions of streamflow, and also for all internal storages and fluxes in the WATFLOOD model. One advantage of simulating internal compositions is that they can be compared to observed isotopic compositions of significant hydrologic storages, such as groundwater or wetland surface water, to verify the simulation. Such verification is theoretically possible using observed water volumes and flows, but in practice (particularly in remote, mid- to high-latitude basins), obtaining these observations is either prohibitively expensive (e.g., measuring groundwater), or technically infeasible (e.g., measuring volumes and flows in large wetlands with numerous inflow and outflow channels). Stable water isotope sampling is simpler, less laborious and time consuming; although groundwater sampling still requires drilling, only occasional monitoring is needed. Adequate isotope data is cheaper to acquire and measure given periodic grab samples suffice to provide information on longer-term processes.

Isotope sampling in the LNRB included more than stream and lake sampling: samples were also taken from shallow groundwater, wetlands, snow packs and an evaporation pan. As with streamflow sampling, source water sampling in the LNRB was both sparse and irregular. This chapter will analyze the ability of the model to simulate a broad range of hydrologic storages, however, due to the intermittent nature of the available observed data, analyses will remain qualitative and cannot be quantified with statistical certainty.

6.1 Snowpack

Snowpack samples were occasionally taken at three sites across the LNRB: Thompson, Jenpeg and the Notigi Control Structure (see Figure 4.6 for locations). For larger snowpacks, multiple samples were taken through snowpack depth, and measured isotopic compositions averaged to produce a single

composite measurement. Simulated snowpack compositions are compared relative to observed (composite) values for all three sites, yielding similar results at all locations. Simulated and observed values for the Notigi snowpack are shown on Figure 6.1, while results for the other sites may be found in Appendix D.

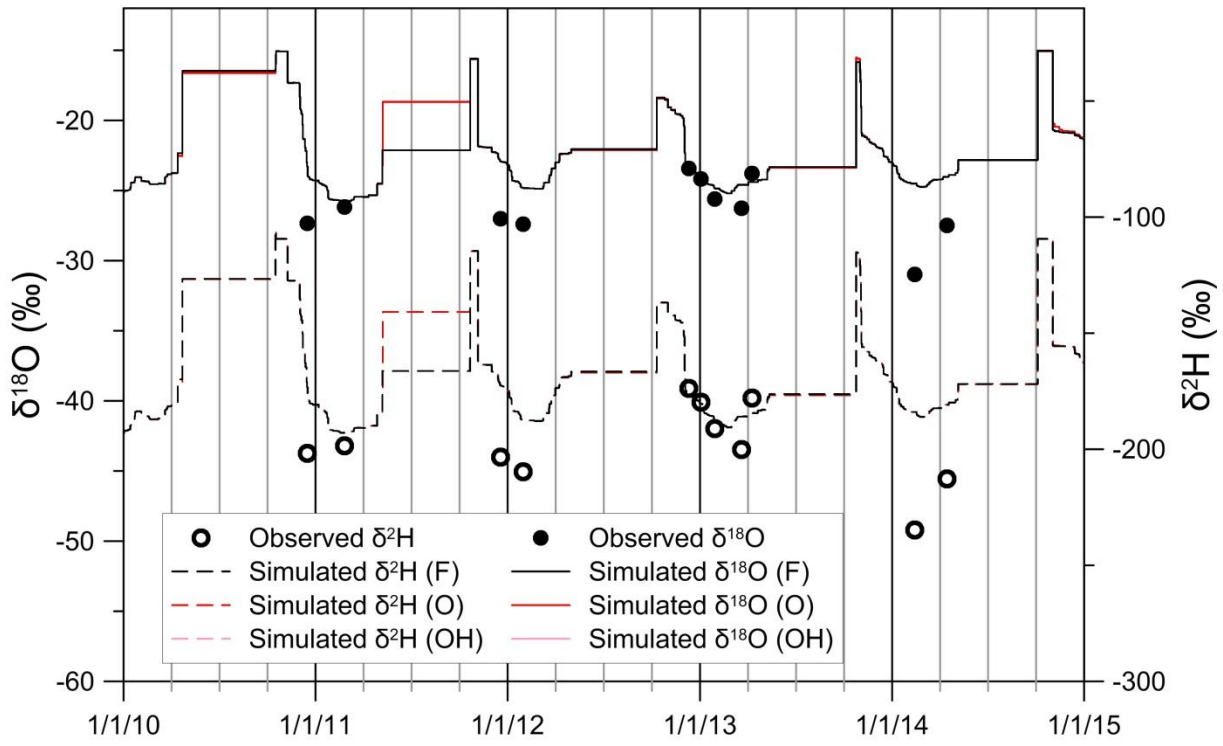

Figure 6.1 Simulated and observed isotopic composition of the snowpack at the Notigi Control Structure.

The agreement between observed and simulated values varies from year to year; the match is good for the 2010-2011 and 2012-2013 winter periods, however simulated values are too high (enriched) for the 2013-2014 and 2011-2012 winter periods. Success of the simulation is highly dependent on the amount of snow accumulated during late fall: early snowfall was very high in 2013 and high in 2011, while in 2010 and 2013, little snow accumulated in October and November. No precipitation samples were taken during early fall periods (see Section 4.7 for the input data comparison to observed values), so no definitive conclusions are possible but it is likely that the monthly isotope in precipitation forcing data are not an adequate representation of the complex mixed-precipitation events occurring in late fall in

this region. Isotopic composition of precipitation is known to be affected by the precipitation phase (i.e. solid or liquid), and the isotope simulation may benefit from an explicit differentiation between rain and snow compositions when distributed isotopic precipitation forcing is used.

6.2 Evaporation

Evaporation is one of the hydrologic processes most clearly identifiable from stable water isotope data, whether observed or simulated. As discussed in Section 2.2.2, evaporation preferentially removes lighter isotopic species, leading to enrichment of heavier isotope species in the remaining water volume. Furthermore, the two commonly measured stable water isotopes ($\delta^{18}O$ and $\delta^{2}H$) enrich at differential rates, such that when they are plotted against each other, evaporation causes a change, or offset, in slope.

The *d*-excess value is calculated from the difference between $\delta^{2}H$ and $\delta^{18}O$, where the *d*-excess value is altered by phase change. The *d*-excess value can be used to identify when (and a relative measure of how much) evaporation is occurring, leaving water with a more negative *d*-excess value. To a lesser degree, snowmelt will tend to exhibit more positive *d*-excess values (Gat, 1996). Because *d*-excess combines both isotopes into a single representative value, it enables tracking evaporation in a time-series plot, at any site, relative to observed *d-excess* values from isotopic sampling. The *d*-excess values are used to verify evaporation from simulated internal storages.

6.2.1 Evaporation Pan

Water samples from a Class A evaporation pan at the Notigi Control Structure were analyzed for their stable water isotope composition. The evaporation pan isotopic observations are compared to the simulated isoWATFLOOD local evaporation line (LEL) derived at the Notigi Control Structure (CS) site using an isotopic framework (Figure 6.2).

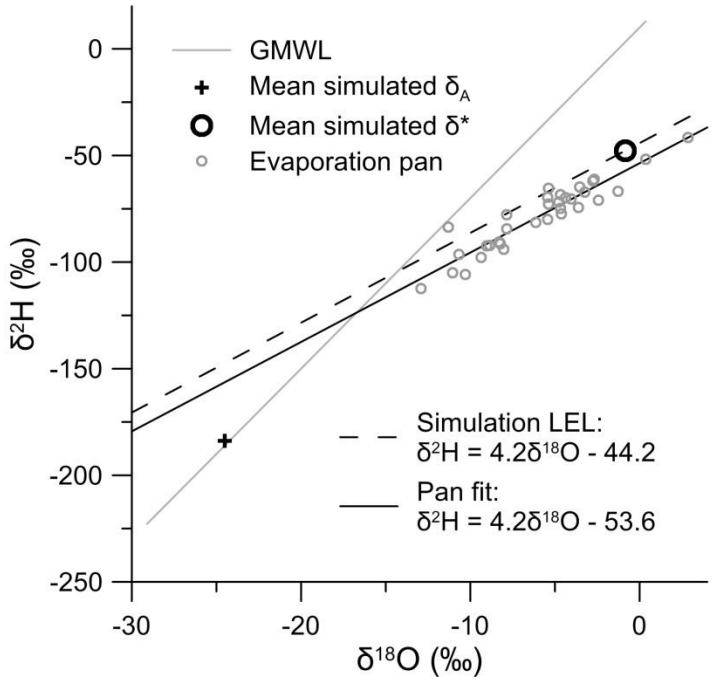

Figure 6.2 Simulated isotope framework derived at Notigi CS for 2010-2014 comparing the simulated LEL to observed evaporation pan data.

There is very strong agreement between observed and simulated evaporation signals, with observed data following the same slope as derived from the simulated LEL for the area. The small offset (in intercept, not slope) seen in the simulated evaporation line is expected as the simulated line includes source water from across the region, while the evaporation pan is limited to a single starting composition prior to evaporative enrichment occurring. The fact that the two lines share the same slope indicates that evaporation is occurring at the same rate (observed and simulated), resulting in the same amount of isotopic enrichment. The evaporative enrichment module in isoWATFLOOD is able to successfully replicate evaporative fractionation in the LNRB.

6.2.2 Soil Evapotranspiration

The *d*-excess results for the sub-surface (soil and groundwater zones) simulated and observed compositions at Thompson are shown in Figure 6.3; *d*-excess results for Notigi and Jenpeg may be seen in Appendix D.

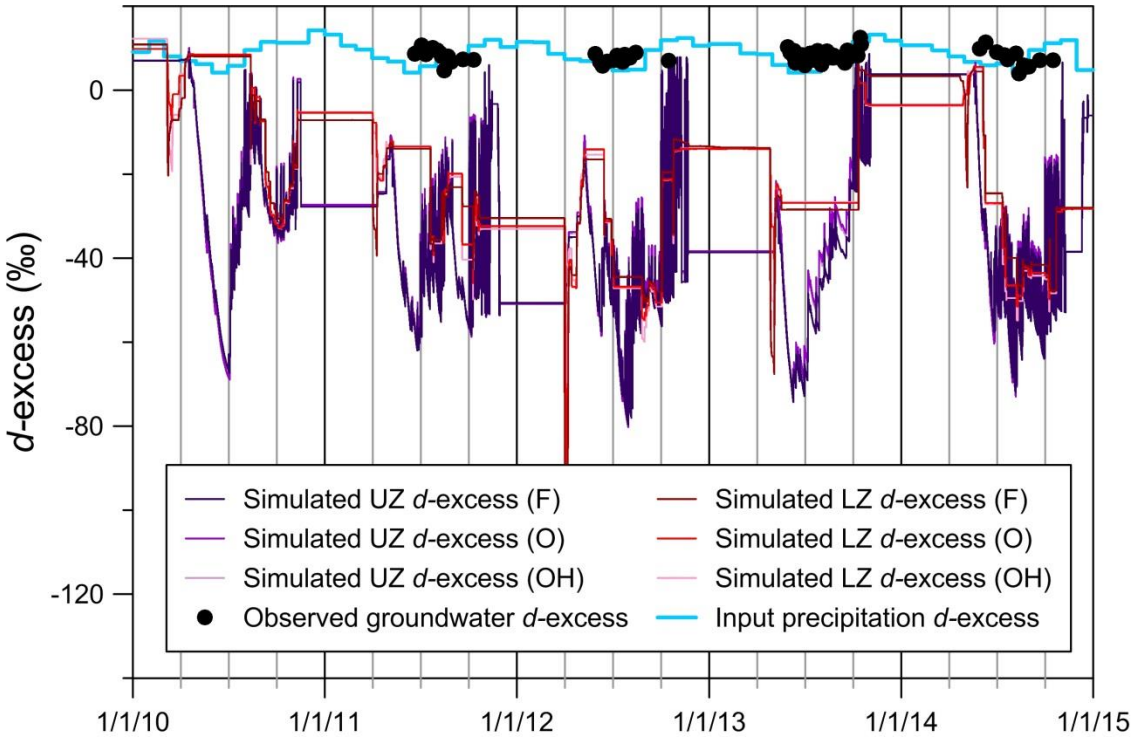

Figure 6.3 Observed groundwater d-excess at Thompson and simulated upper and lower zone d-excess.

Although groundwater samples were taken at three sites across the LNRB, only Thompson is shown here given it has the highest sampling resolution, and all groundwater sites show similar results. Observed *d*-excess values for groundwater track the input precipitation most closely, showing a similar range in and composition of the input precipitation. Observed groundwater *d*-excess values lag behind the precipitation values temporally, indicating groundwater storage and mixing have some effect on observed *d*-excess. Evaporation has little to no effect on groundwater samples, since observed *d*-excess remains generally positive. Simulated soil water (UZ) and subsequently groundwater (LZ), on the other hand, are highly evaporated based on the large negative values of simulated *d*-excess, particularly during summer. There is clearly too much simulated evaporation occurring from the upper zone storage in the model, influencing (through vertical infiltration) the lower zone isotopic composition. Basic statistics for the *d*-excess values for groundwater samples are shown in Table 6.1.

Table 6.1 d-excess statistics for groundwater samples and simulated upper and lower zone compositions.

	Samples	Average (‰)	σ (‰)	Maximum (‰)	Minimum (‰)
observed	107	7.0	2.9	12.6	-9.0
simulated		-22.9	20.9	14.1	-124.2

The average simulated *d*-excess values are much lower than observed, and the simulation is far more variable than the observed values, further supporting the conclusion that too much evaporation is simulated in the soil. The observed results indicate the majority of soil evapotranspiration is transpiration (i.e., non-fractionating), with evaporation being a smaller fraction of total evapotranspiration, agreeing with the recent findings of Jasechko, et al. (2013). These results show a clear need to improve the physical basis of the evapotranspiration split used in WATFLOOD, as the current seasonally unvarying power function is not providing an adequate representation of the soil water system. In revisiting transpiration from the soil storage, the recent work by Evaristo et al. (2015) found that the assumption of well-mixed water stores from which both evaporation and transpiration are removed is not universally, or even generally, applicable and needs to be reconsidered.

6.2.3 Connected Wetland Evaporation

The upper and lower soil zones drain directly into connected wetland storage in (iso)WATFLOOD. Stable water isotope samples were taken from the fen area at Birchtree Lake, a headwater basin region north of Thompson (fens upstream of Birchtree Lake pictured in Figure 6.4).

Figure 6.4 Birchtree Brook and fens near Birchtree Lake (Photo courtesy of T. Stadnyk, July 18, 2013).

Simulated *d*-excess values for connected wetlands are directly compared to observed values from the samples taken from large channelized fens at Birchtree Lake (R-MH-05TG747) in Figure 6.5. The simulated connected wetland isotopic compositions are from the headwater grid cell which contains the sampling site.

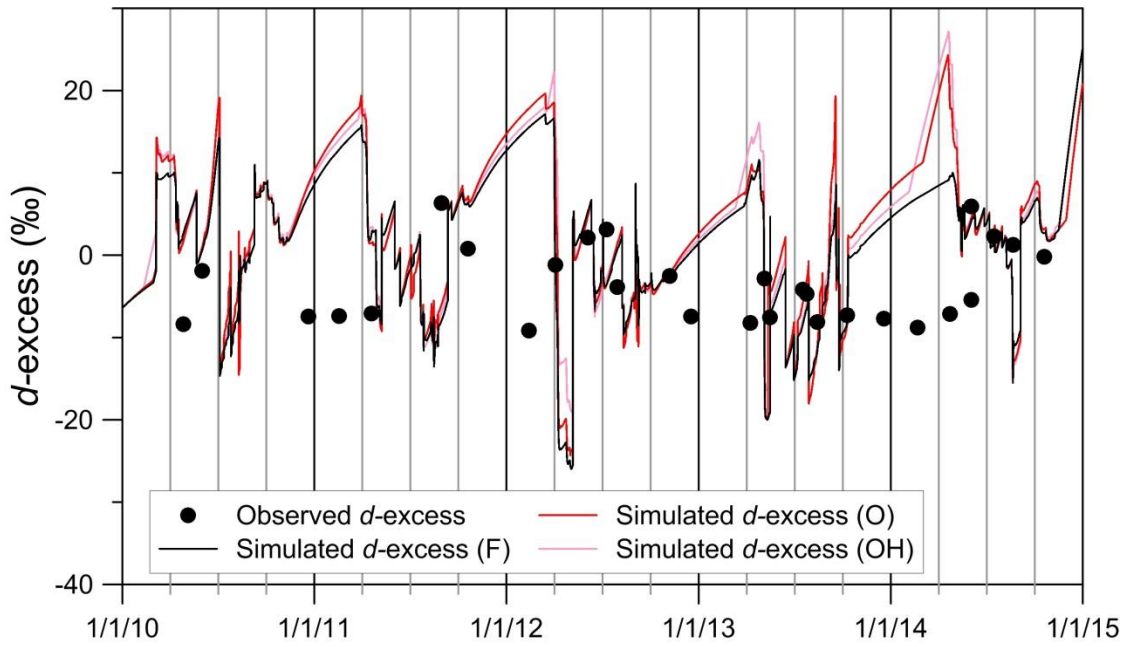

Figure 6.5 Observed wetland d-excess near Birchtree Lake (R-MH-05TG747) and simulated wetland d-excess.

Observed *d*-excess in the wetland varies considerably over the year. The observed *d*-excess is positive during the spring freshet each year, and may remain so for some time if the snowpack was large (e.g., 2014). The observed *d*-excess values decrease gradually over the summer months as evaporation begins to enrich surface waters, with intermittent increases in *d*-excess due to large rain events. Over the winter, observed *d*-excess remains both negative and stable, indicating retention of water from the previous fall. The simulated *d*-excess values replicate only some of these behaviors: the simulation does exhibit an increase in *d*-excess during the freshet, and moderately negative and generally decreasing *d*-excess over summer. In winter, however, simulated *d*-excess is positive and increasing - a significant departure from observed values. The simulation includes small amounts of snowmelt over the course of the winter due to the degree-day melt method used in WATFLOOD, which simulates snowmelt whenever air temperature remains above the specified base melt temperature - which can occur even in mid-winter when the energy balance of the snowpack would normally prevent melting (Kouwen, 2014). As very low volumes of water are retained in the wetland over the winter, snowmelt entering the

wetland dominates the total wetland storage volume in the simulation; which is unrealistic based on the observed isotope data. This issue is confirmed by the statistics for *d*-excess in wetlands, in Table 6.2.

Table 6.2 d-excess statistics for observed and simulated compositions for the wetland near Birchtree Lake

	Samples	Average (‰)	σ (‰)	Maximum (‰)	Minimum (‰)
observed	29	-3.7	4.7	6.3	-9.2
simulated		3.1	8.6	27.2	-26.0

The maximum simulated composition is significantly higher than observed, and the average simulated composition is somewhat higher than observed, confirming the seasonal snowmelt error.

The second issue with the wetland simulation only becomes apparent when wetland and groundwater *d*-excess are considered together. Total evaporation from the wetland surface water in summer is in approximate agreement with the observed data, but the main inflows into the wetland (baseflow and interflow from the upper and lower zones, respectively) have experienced too much evaporation. Therefore, evaporation from the wetland itself is likely too low.

6.2.4 River Channel Evaporation

Smaller streams, such as the Sapochi River (Figure 6.6) also show the same trends in *d*-excess as the connected wetlands, both in observed and simulated values, although with less variability owing to the more damped response in rivers (Table 6.2 vs Table 6.3).

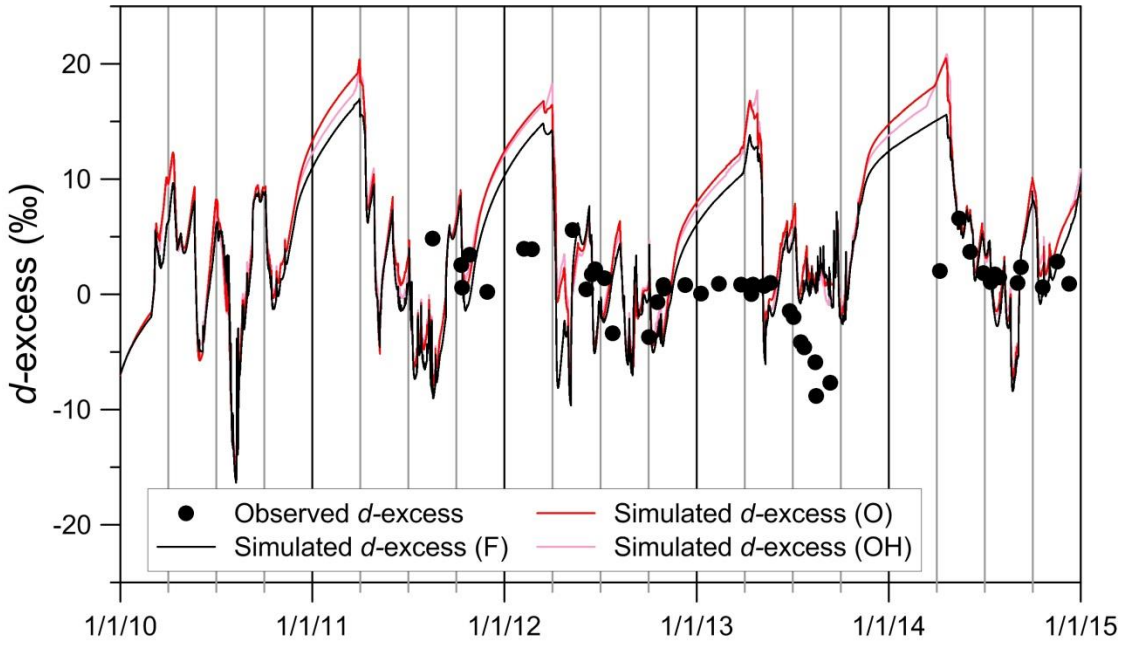

Figure 6.6 Observed streamflow d-excess and simulated streamflow d-excess at Sapochi River gauge (WSC ID 05TG006).

Table 6.3 d-excess statistics for observed and simulated compositions at Sapochi River gauge (WSC ID 05TG006).

	Samples	Average (‰)	σ (‰)	Maximum (‰)	Minimum (‰)
observed	46	0.5	3.1	6.6	-8.8
simulated		5.8	7.0	20.5	-15.0

Like in the wetlands, small amounts of simulated snowmelt feed into streamflow during the ice-on low-flow conditions prevailing in winter. The total simulated evaporative losses experienced by streamflow are generally reasonable in summer, although too much of that evaporation comes directly from soil water. In the driest year, 2013, there is a small under-estimation of evaporation, but in general, good agreement between observed and simulated values is seen in summer, and agreement is poorer during winter (ice-on) conditions.

For larger rivers, such as the Odei River (Figure 6.7), variation in *d*-excess is lower over a year than in smaller streams (Table 6.3 vs Table 6.4), and inter-annual variability is more pronounced.

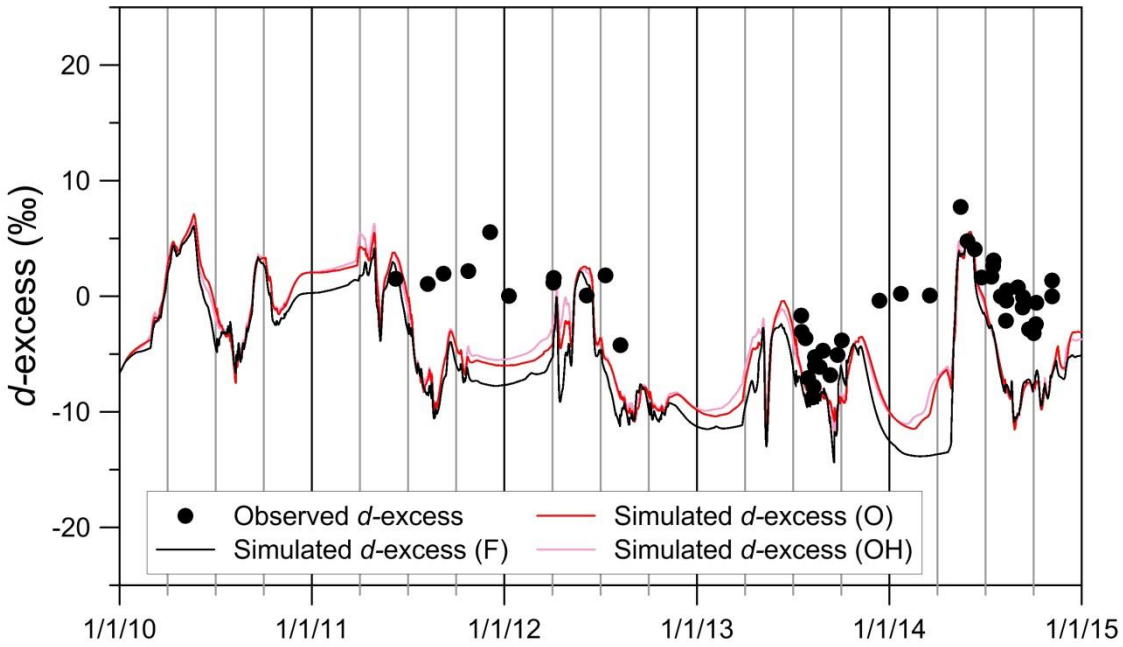

Figure 6.7 Observed streamflow d-excess and simulated streamflow d-excess at Odei River gauge (WSC ID 05TG003).

Table 6.4 d-excess statistics for observed and simulated compositions at Odei River gauge (WSC ID 05TG003).

	Samples	Average (‰)	σ (‰)	Maximum (‰)	Minimum (‰)
observed	48	-0.9	3.6	7.7	-8.7
simulated		-4.2	4.7	7.1	-11.8

Simulated *d*-excess values are generally lower than observed in the Odei River, except during spring freshet when snowmelt inflows dominate the hydrograph. In the Odei River, and in other larger river basins, groundwater inflows dominate simulated low-flows, therefore causing simulated winter *d*-excess values to be too low since simulated soil water evaporation (over the year) is too high. Excess evaporation is also problematic in summer 2014 when higher volumes of snowmelt should have been retained for longer periods than actually occurred in the simulation, based on the positive observed *d*-excess values in June and July, as positive *d*-excess indicates snowmelt.

6.2.5 Lake Evaporation

Observed *d*-excess values for samples taken from lakes show even less variability than those taken from large tributary rivers in the LNRB; however this is not seen in the simulated values for lakes, such as Setting Lake in the Grass River basin, as illustrated on Figure 6.8, and shown by the statistics in Table 6.5.

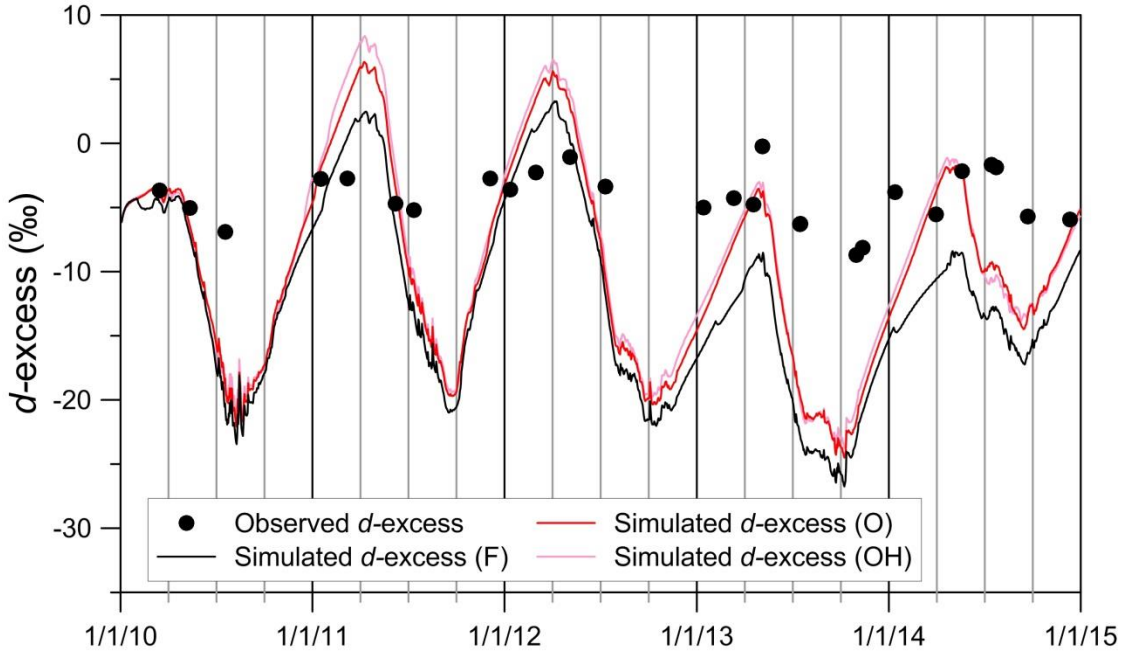

Figure 6.8 Observed streamflow d-excess in Setting Lake (R-MH-05TC701) and d-excess at the outlet of the simulated Setting Lake reservoir.

Table 6.5 d-excess statistics for observed and simulated compositions in Setting Lake (R-MH-05TC701).

	Samples	Average (‰)	σ (‰)	Maximum (‰)	Minimum (‰)
observed	27	-4.2	2.1	-0.2	-8.7
simulated		-10.1	7.7	8.4	-26.8

Simulated *d*-excess values for Setting Lake are far too variable during both the spring freshet and summer evaporative season, and the range of simulated *d*-excess values is too large. Average simulated *d*-excess is also too low, however, so the total evaporative loss is too high in the model. The Hargreaves method used to estimate lake evaporation for the LNRB should be revisited (Kouwen, 2014). A lake

evaporation model for WATFLOOD is being refined, which, if implemented in the LNRB, will improve the lake simulation (Holmes, 2014).

Based on the *d-excess* results overall, the total amount of evaporation in the model appears to be too high. The distribution of evaporation is also problematic, with too much evaporation occurring from soil water and lakes, while not enough is being removed from surface wetlands; this fact would not be known without isotope sampling and a dual-isotope simulation.

6.3 Groundwater

Groundwater samples were taken at three sites in the LNRB: Jenpeg Generating Station, the Notigi Control Structure, and Thompson, from drivepoints or piezometers installed to depths below ground level of 0.5, 1.5 and 0.9 meters, respectively. Lower zone storages in WATFLOOD, however, are not defined by any specific depth, therefore the observed shallow groundwater samples are compared to all three simulated terrestrial storage compartments within the model: surface, upper and lower zones. Results for the Thompson site are shown (Figure 6.9) because it was sampled at the highest resolution; however all three sites show similar behavior (Appendix D).

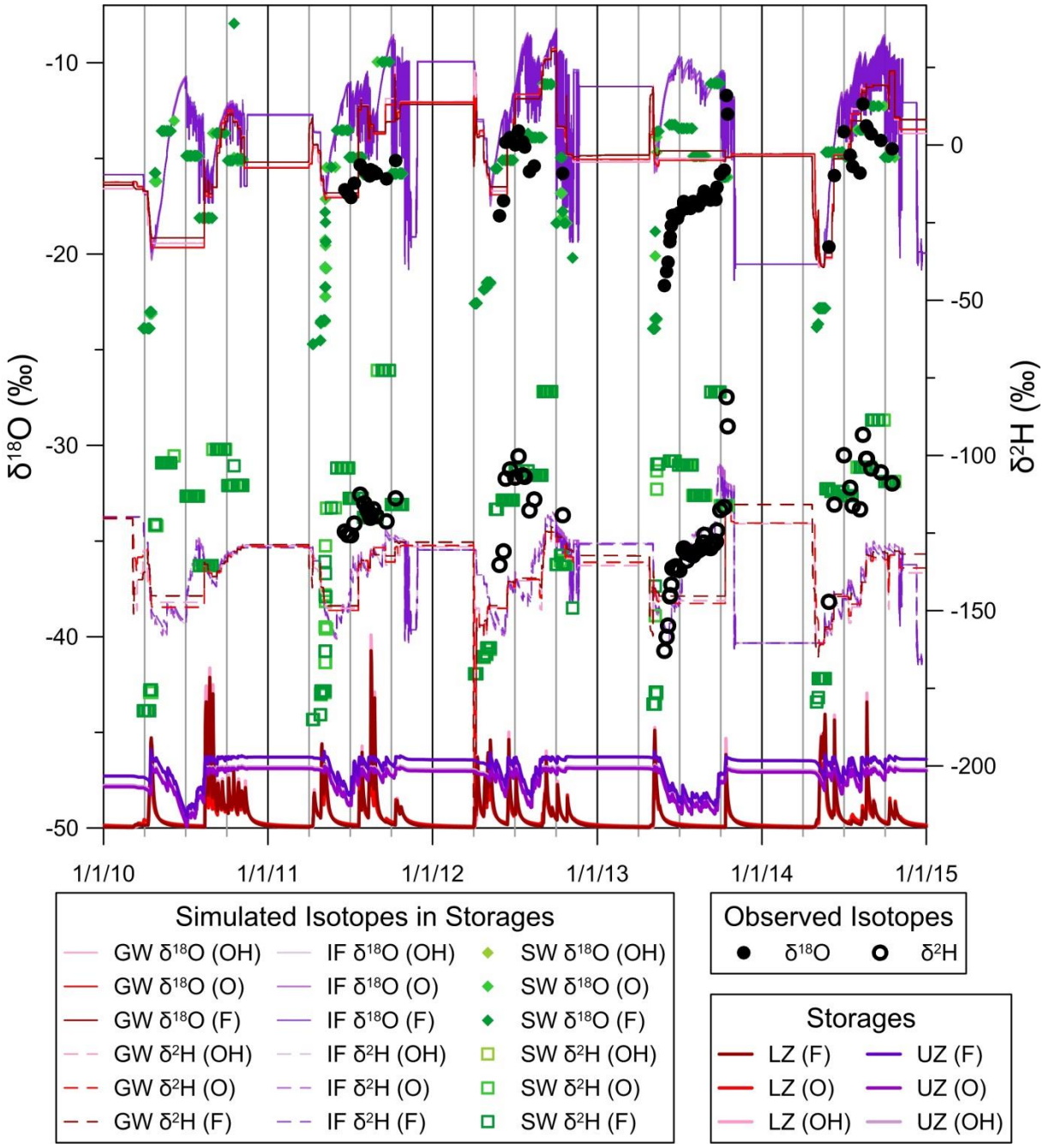

Figure 6.9 Observed and simulated groundwater isotopes with simulated terrestrial storage at Thompson (GW-MH-05TGXXX).

Observed groundwater samples generally follow simulated surface water compositions, with the surface water compartment representing un-infiltrated, non-evaporated water stored directly from rainfall or snowmelt. This agreement indicates that shallow soil water compositions (i.e., the observed data) are

most typically similar to the input composition (i.e., the surface water storage), with little evaporative fractionation or significant mixing occurring in the near-surface soil. Upper zone storages, however, do not generally agree with either the surface water (SW) simulation or the observed values, particularly for $\delta^{18}O$. In summer 2013 (a very dry year), the deuterium simulation for the upper zone (IF) agrees with the observed groundwater values, but the oxygen-18 simulation does not. The divergence between these simulations indicates the amount of evaporation from the upper (soil) zone is too great, agreeing with the findings in Section 6.2.2. The three simulations converge both with each other and with observed values when the upper and lower zone storages, shown as relative values at the bottom of Figure 6.9, increase rapidly from either snowmelt or large rainfall events. This indicates that the recharge of shallow groundwater is simulated reasonably well in the model.

In order to explore the effects of simulated evaporation on groundwater composition further, both isotopes are plotted against each other in the simulated groundwater framework (Figure 6.10). Due to the continuous nature of simulated isotope compositions (i.e., hourly time step over 5 years), individual simulated isotope values are not included in the figure, but are used to find derive the best-fit lines.

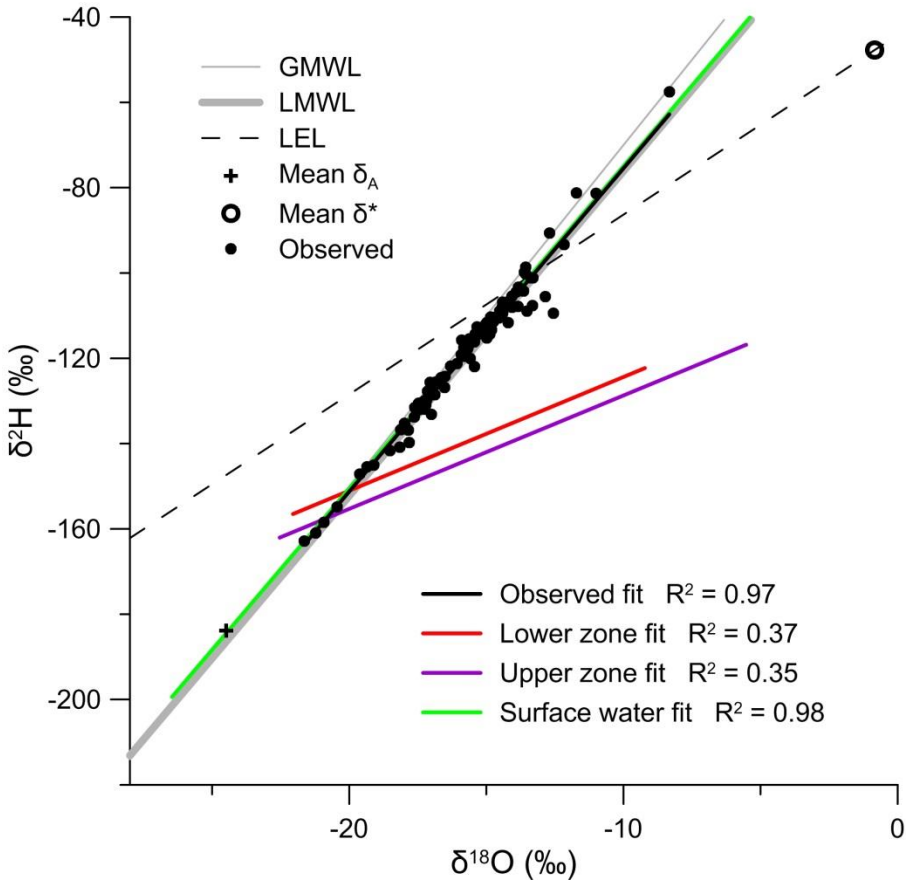

Figure 6.10 Simulated groundwater isotopic framework (2010-2014), showing observed groundwater isotopic compositions. All groundwater samples included in observed values, all three sites and all calibrations included for simulation fits.

Simulated surface water and observed groundwater values both closely follow the meteoric water line (LMWL) for the LNRB. Some groundwater samples diverge from the LMWL and follow the slope of the local evaporation line (LEL), showing that evaporation does occasionally affect shallow groundwater in the LNRB. Upper and lower zone simulations do not exhibit minor evaporative effects; the upper zone shows large and persistent changes in isotopic composition from evaporation (seen from the slope change of the purple linear best fit line), again agreeing with the findings on evaporation in Section 6.2.2. The lower zone receives inflows exclusively from vertical drainage from the upper zone storage, so the evaporative effects from the upper zone are transferred directly to the lower zone, with minor moderation from compartmental mixing. The best fit lines for the upper (purple) and lower (red) zones

have low coefficients of correlation because the simulated values follow not only the LEL slope, but also the LMWL during periods of high infiltration. There is clearly too much water removed from the upper zone via evaporation during model simulation, with only limited and occasional evaporation evident in the observed isotope values from groundwater samples.

The statistics for simulated and observed isotopic composition in groundwater (Table 6.6) provide additional support to these findings.

Table 6.6 Statistics for observed groundwater samples and simulated compositions for upper and lower zone storages, for all three sampling locations.

		Samples	Average (‰)	σ (‰)	Maximum (‰)	Minimum (‰)
$\delta^{18}O$	observed	107	-15.9	2.1	-8.3	-21.6
	simulated upper zone		-13.4	3.4	-5.5	-22.5
	simulated lower zone		-15.0	2.9	-9.2	-22.1
$\delta^{2}H$	observed	107	-119.8	16.4	-57.5	-162.9
	simulated upper zone		-137.7	15.1	-85.6	-190.0
	simulated lower zone		-137.9	12.9	-105.1	-246.9

The statistics for the oxygen-18 simulation are in good agreement with the observation statistics, but those for deuterium diverge significantly, with the simulation being both too low and not variable enough. The divergence in results for the two isotope simulations indicates that evaporation is too large a component of the soil evapotranspiration loss.

Beyond the erroneous simulated soil water evapotranspiration, these results illustrate the need for more robust sampling of ground and soil water. The utility of the groundwater samples is limited by the intermittent nature of the data, with only a single year, 2013, at one sampling location having a continuous sample record for the ice-off period. Furthermore, all samples were taken from similar, relatively shallow depths in the soil column; the fact the samples came from near the surface renders the close agreement between simulated surface water and groundwater samples unsurprising. Water

samples taken from deeper in the soil column would provide a better comparison for the upper and lower zone storages.

6.4 Wetlands

Stable water isotope samples were taken from the connected wetland area at Birchtree Lake (Figure 6.4), a headwater basin region north of Thompson which flows into the Burntwood River. These observed and simulated isotope values for the connected wetland (in the appropriate WATFLOOD grid cell) are shown on Figure 6.11.

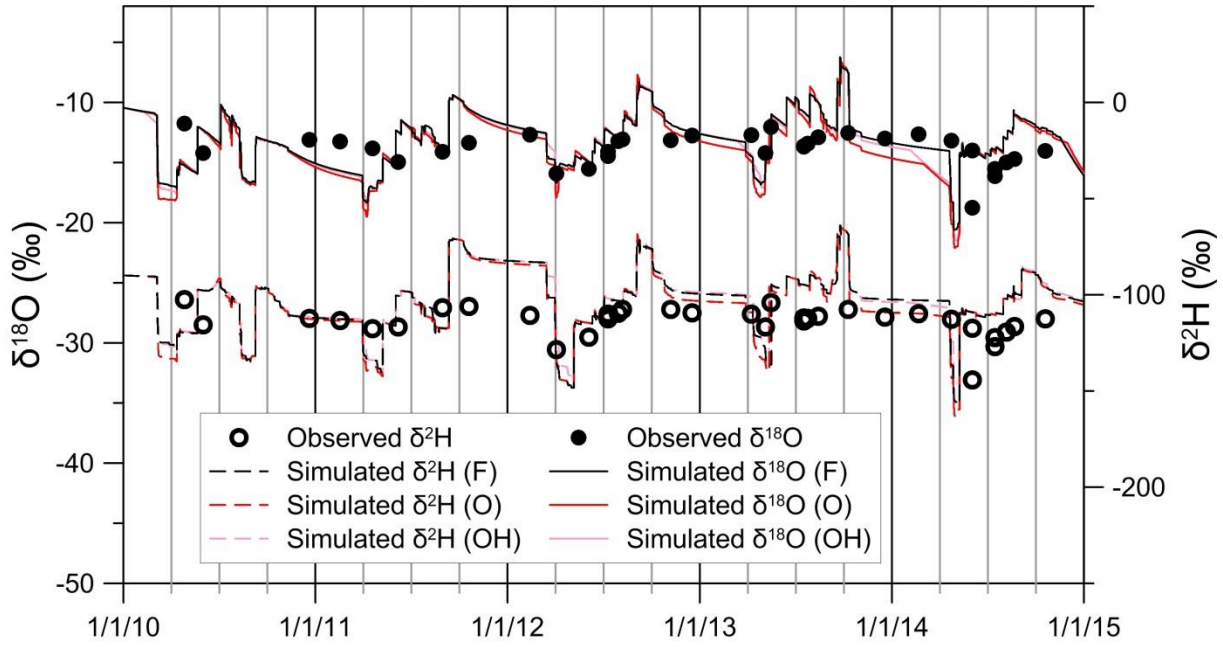

Figure 6.11 Simulated and observed isotopic composition of the connected wetland by Birchtree Lake (R-MH-05TG747).

Agreement between observed and simulated values for the connected wetland is generally fairly good, with approximately the same compositions at roughly the same time. Isotope-enabled calibrations usually produce a better match to the observed data, but the difference (relative to flow-only) is minor in most cases. The wetland composition is too variable over the winter, indicating a combined issue of over-winter snowmelt and insufficient water storage in the wetland. The wetland composition is also

too reactive during periods of large inflow (such as the 2014 snowmelt). In this area, connected wetland simulations would benefit from an increase in wetland storage capacity, which would moderate isotopic responses. Wetland storage capacity might be increased by altering the wetland porosity parameter, but the issue in this case is more likely to be caused by the connected wetland class definition used in the initial model creation, where wetlands were divided into connected and disconnected wetlands using a constant percentage split for all grid cells in the basin. Defining connected wetlands based on actual basin physiography should be the first step towards correcting the wetland storage issue.

Simulated wetland isotopic composition and observations were also plotted in an isotopic framework (Figure 6.12) to further examine wetland evaporation; Table 6.7 shows composition statistics for the wetland.

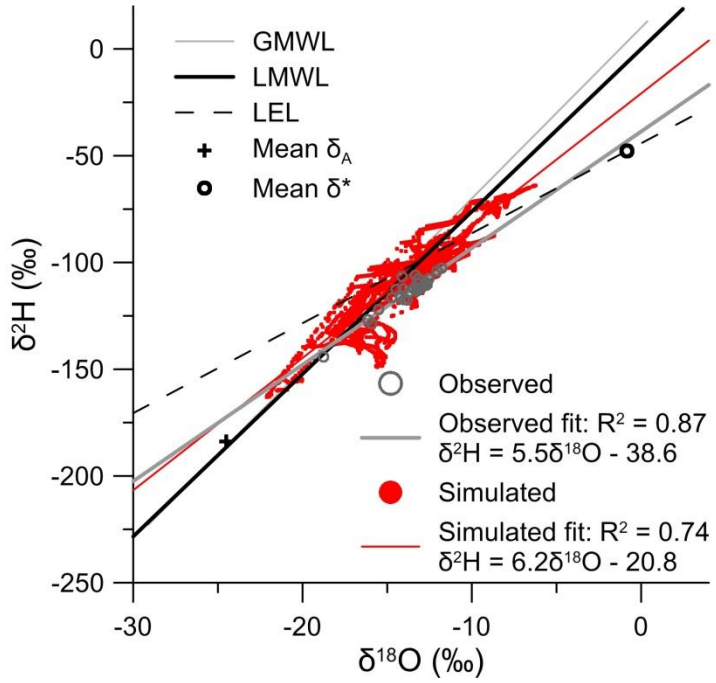

Figure 6.12 Isotope framework (2010-2014) for the connected wetland near Birchtree Lake (R-MH-05TG747) with observed values. All calibration trials included in the simulated values.

Table 6.7 Statistics for observed wetland samples and simulated compositions for the connected wetland near Birchtree Lake (R-MH-05TG747).

		Samples	Average (‰)	σ (‰)	Maximum (‰)	Minimum (‰)
$\delta^{18}O$	observed	29	-13.8	1.4	-11.8	-18.8
	simulated		-13.3	2.2	-6.2	-22.1
$\delta^{2}H$	observed	29	-113.9	8.3	-102.5	-144.2
	simulated		-103.1	15.5	-63.9	-163.1

Observed isotope values plot in the same region of the framework as the majority of the simulated values; however, the range of the simulated values is much larger (unsurprising, given the simulation is continuous, while the observed samples are sporadic). The divergence of the simulated data away from the LMWL and along the slope of the LEL is similar to that seen in the observed data, but to a lesser extent with a simulated slope of only 6.2 (relative to an observed slope of 5.5), with the simulation lying closer to the LMWL slope of 7.6 than the LEL slope of 4.2 (derived in Section 6.2.1). The total amount of evaporation occurring from the water in the wetland is therefore reasonable, but possibly slightly lower than observed. Since the evaporation loss from the wetland's contributing sources is too high (Section 6.3), evaporation from the wetland itself is likely too low.

6.5 Lakes

Multiple lakes in the LNRB were sampled for stable water isotopes; the Grass River basin is selected for this analysis as it has both high sampling frequency and multiple in-stream simulated lakes with no upstream inflow forcing. The isotopic composition results are shown for Setting Lake (R-MH-05TC701), located near the center of the Grass River basin (Figure 6.13).

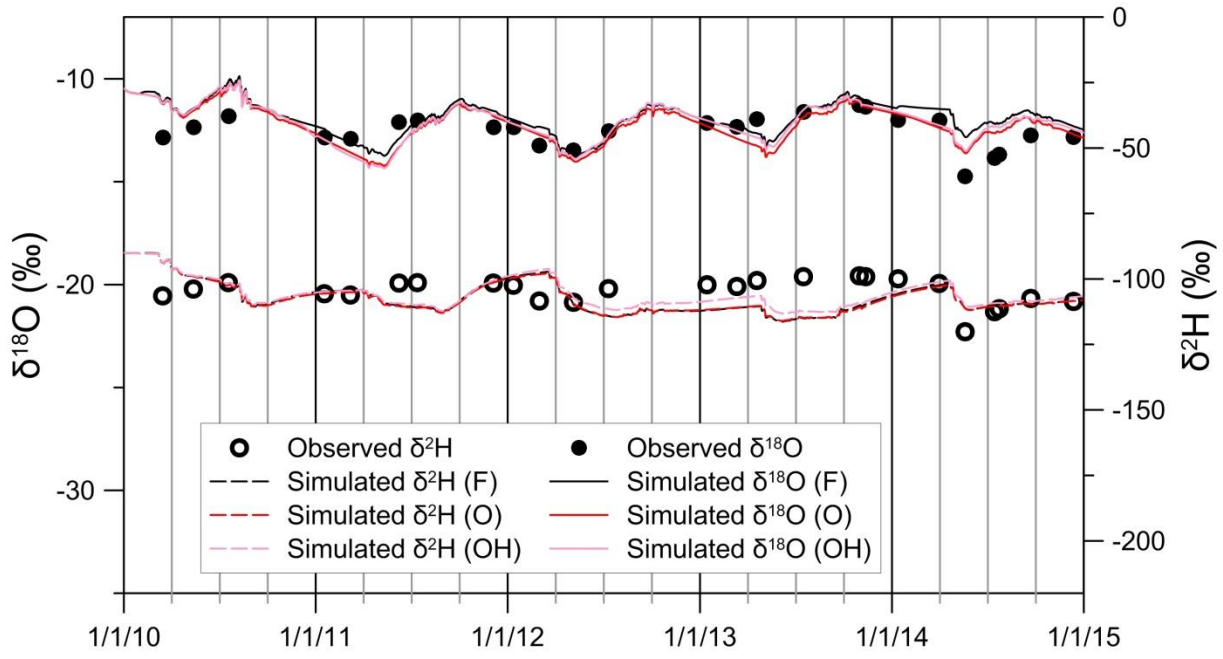

Figure 6.13 Simulated and observed isotopic composition of Setting Lake (R-MH-05TC701), located on the Grass River.

Simulated oxygen-18 values generally match observed data, with simulations typically being slightly more variable than the observations. The deuterium simulation, on the other hand, is slightly less variable than the observations, with simulated and observed values often differing. If only one isotope simulation is considered, the lake model appears to be representing reality fairly well but with a dual-isotope simulation issues become more apparent.

When the isotope simulation further downstream is considered, at the Grass River gauge (05TD001), model deviations from the observed data are magnified (Figure 6.14).

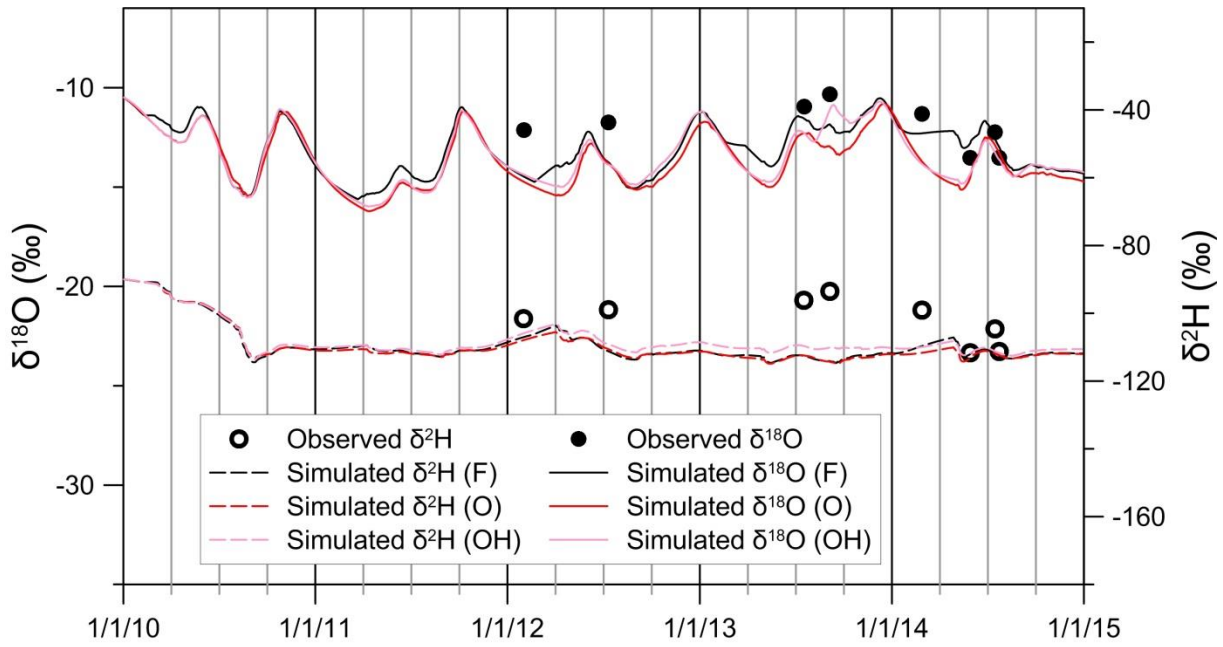

Figure 6.14 Simulated and observed isotopic composition at the Grass River gauge (05TD001) downstream of six simulated lakes, including Setting Lake.

The oxygen-18 simulation is highly variable relative to observed data, whereas the deuterium simulation exhibits very little variation; with minimal relation to the observed data in either simulation. The over-damped deuterium simulation strongly points to excess mixing in lakes; although whether this is caused by excess lake volume or unrepresentative mixing assumptions cannot be determined from these results. If lake volumes are too great, new snowmelt or rainfall inflows to the lake have a minimal effect on the isotopic composition of the water body (as seen here with the deuterium simulation). Alternatively, if the lake has a stratified isotopic composition, even seasonally, the complete mixing assumption used in the lake isotope simulation is invalid and will also remove the isotopic variability of the deuterium simulation. The variation in oxygen-18, particularly relative to that in the deuterium simulation, is indicative of excess evaporation. The isotope framework simulated for Setting Lake supports this conclusion (Figure 6.15), as do the lake composition statistics in Table 6.8.

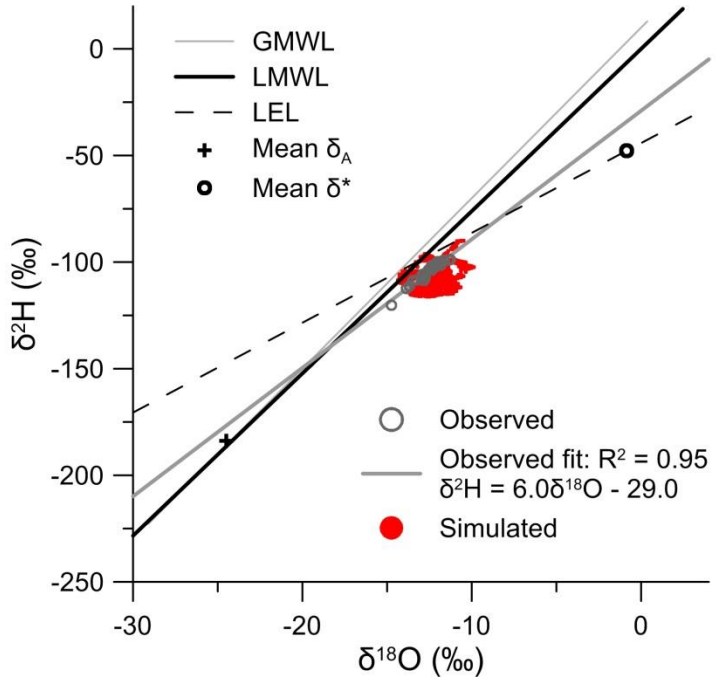

Figure 6.15 Isotope framework (2010-2014) for Setting Lake (R-MH-05TC701), with all calibration trials included in the simulated values.

Table 6.8 Statistics for observed wetland samples and simulated compositions for Setting Lake (R-MH-05TC701).

		Samples	Average (‰)	σ (‰)	Maximum (‰)	Minimum (‰)
$\delta^{18}O$	observed	29	-13.8	1.4	-11.8	-18.8
	simulated		-12.1	0.9	-9.9	-14.4
$\delta^{2}H$	observed	27	-105.3	7.8	-98.8	-141.0
	simulated		-106.8	5.8	-90.0	-116.3

Simulated isotope values are very tightly constrained as a result of less variation, particularly in δ^2H values, than observed, both in the range and standard deviation, when in fact more simulated variability is expected because of the continuous 5-year simulation period. Some simulated values match the observed data, but many diverge from the local mixing line (LML) derived for the lake, following instead the LEL slope. The most likely reason for this divergence is that lakes are seasonally over-evaporated, as *d*-excess values are too low as well (Section 6.2.5). The isotope simulations show that the simulation of

reservoir storage in the WATFLOOD LNRB model are not physically representative of the system, resulting in excessive evaporation and over-mixing.

6.6 River Channels

The final storage compartment, to which all others ultimately contribute in WATFLOOD, is the stream channel. Time-series plots of the observed and simulated isotopic values were presented in Sections 5.3.2 and 5.4.1, with simulated isotope frameworks for the Sapochi and Odei Rivers are shown below on Figure 6.16, for the isotope simulation period (2010-2014) and statistics for the same period in Table 6.9.

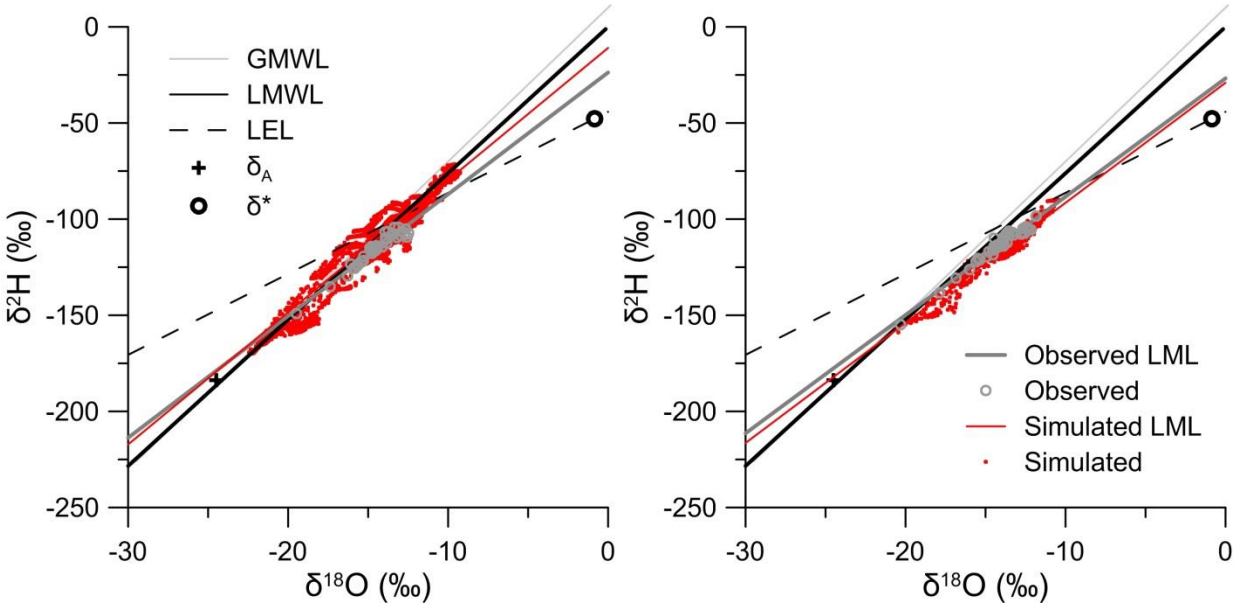

Figure 6.16 Isotope framework (2010-2014) for the Sapochi River (05TG006) (left) and Odei River (05TG003) (right) gauges, with all calibration trials included in the simulated values.

Table 6.9 Statistics for observed wetland samples and simulated compositions for the Sapochi River (05TG006) and Odei River (05TG003).

			Samples	Average (‰)	σ (‰)	Maximum (‰)	Minimum (‰)
$\delta^{18}O$	Sapochi	observed	46	-14.5	1.3	-12.5	-19.5
		simulated		-14.4	2.4	-9.2	-22.5
	Odei	observed	48	-14.1	1.5	-11.8	-20.3
		simulated		-14.0	1.7	-10.4	-20.5
$\delta^{2}H$	Sapochi	observed	46	-115.7	8.6	-104.3	-149.2
		simulated		-110.1	17.5	-71.6	-169.9
	Odei	observed	48	-113.8	9.7	-98.5	-154.8
		simulated		-116.2	11.5	-89.9	-159.3

Streamflow isotope compositions are used in model calibrations including isotope error; therefore it is unsurprising that the observed and simulated values are in agreement, particularly for the Odei River (a calibration site). The Sapochi River simulation performs reasonably well but with more variation in isotope values than is observed. The Sapochi basin is quite small relative to the model scale, however, so it is expected that streamflow is less mixed and more analogous to a headwater grid response. In the Sapochi, the difference between the simulated and observed LML points to input composition (i.e., precipitation) having a greater effect on simulated isotopic composition of streamflow than it should (i.e., less evaporation and water retention in the basin) given the simulated LML is closer to the LMWL than the LEL. The difference in the Sapochi is, however, minor and may also be due to the larger number of simulated than observed values. The Odei River simulated isotopes match the observed extremely well, with a reasonable increase in variability among the simulated values (given the continuous 5-year simulation period), and near identical observed and simulated LML. This result exposes a limitation of examining only total streamflow contribution or composition alone: the good result for the Odei River is the result of error cancellation in soil water and wetland compartments, which would not be diagnosed without source water isotope sampling.

7 Conclusions

This thesis contributes developments to isotope-enabled hydrological modeling, by expanding the functionality of the isoWATFLOOD model, and applies the model in the LNRB. The isoWATFLOOD model, which previously simulated only $\delta^{18}O$, was expanded to simulate $\delta^{2}H$: with two different isotopes, continuously simulated isotope frameworks are now possible, with the automatic production of these added as a feature of isoWATFLOOD. The isotope model was enhanced to improve the physical representativeness: the snow pack storage was improved to allow for an evolving composition over time, transpiration was added as an explicit flux in the model, and observed relative humidity data was added as a possible input to improve the estimation of the isotopic composition of water vapor. In order to run the model in the LNRB, isotopic forcing for diverted flows from outside the modeled area was also introduced. Finally, the entire isotope model was restructured to improve efficiency by solving mass balance equations directly, rather than by iteration; resulting in a 30-50% reduction in simulation time.

Isotope simulation error was also included in a new DDS optimization objective function, and the LNRB model was calibrated in this study using DDS for three separate calibrated parameter sets (1) using only flow error, (2) using flow and $\delta^{18}O$ error, and (3) using flow, $\delta^{18}O$ and $\delta^{2}H$ error. The resulting parameter sets and simulations produced were compared, in terms of both isotope and flow simulation quality. Internal WATFLOOD hydrologic storages and fluxes, such as shallow groundwater and wetlands, were verified using the simulated isotope frameworks and comparison of simulated to observed (where data exist) isotope values.

The effect of adding isotope error to the calibration objective function was minor but consistent, resulting in small differences to calibrated parameter values. Streamflow simulations are similar between all three calibrations, however slightly higher average flows are produced by the isotope

calibrations. Changes in flow source are more substantial than for total streamflow. Sub-surface storage shifts from the upper zone to the lower zone for the isotope-enabled calibrations, effectively reducing evapotranspiration loss. Groundwater outflow becomes more responsive to new inflow, and water storage increases in the connected wetlands. These changes are consistent with the LNRB geology and hydrology given the basin has extensive wetland complexes, and very shallow soils, which suggests the isotope and flow calibrations are more physically based.

Using isotope simulation error in the optimization function did not clearly improve the calibration of the model (as measured by traditional efficacy criteria), but the hydrological simulation benefits from the simulation of stable water isotopes. The isotope simulation error was found to be the best predictor of streamflow simulation performance beyond the calibration period. The isotope simulation can therefore be used to identify physically unrepresentative parameter sets for hydrologic simulations. The isotope simulation also allows for verification of internal hydrologic storage, which identified a number of model limitations and potential improvements. Without isotope-enabled hydrologic modeling, verification of internal storage is not feasible given the lack of observed water balance data; however, with the establishment of the LNRB SWIMN (Smith, et al., 2015), such verification is possible.

The addition of δ^2H simulation error to the calibration had only minor effects on the optimized parameter set. Both isotope calibrations produce similar results to each other and have similar effects on flow sources within the model. When considering the flow simulation outside the calibration period, the majority of the predictive power of the isotope error comes from the simulation of $\delta^{18}O$ error. However, data produced by the δ^2H simulation were a key element in model verification. Adding the δ^2H simulation allows direct verification of evaporation using isotope frameworks, LEL, and *d*-excess. From the dual-isotope simulation verification, it was found that transpiration is too small a component of soil evapotranspiration (i.e., evaporation is too high), wetland evaporation losses are too low, and lake

evaporation losses are too high. These conclusions could not have been drawn from the internal storage verification without the simulation of both stable water isotopes.

7.1 Recommendations

This research has identified some areas for future work, including:

isoWATFLOOD development:

- The snowpack evolution could be further improved by adding fractionation from melt, as melt fractionation may be significant for larger snowpacks. A distinction between the isotopic compositions of solid and liquid precipitation for distributed forcing data, as already exists for annual average forcing compositions, should be investigated.
- Based on the verification results, the mixing assumptions for lakes should be revisited; complete and instant mixing in large lakes appears to be unrealistic. The simulation of isotopes in lakes may be improved by partitioning the lake into active and passive isotope storages, or by dividing the area of larger lakes into distinct isotope compartments.
- Alternative methods to include isotope error in the calibration should be explored, as the method tested in this study had only minor effects on the calibrated parameter set. The isotope error value might be calculated using a different metric, or could be given more weight in the DDS optimization error function. Alternatively, isotope error might be one objective in a multi-objective calibration methodology, or the isotope error might be used as a model constraint (i.e. used to limit the simulation) rather than as an optimization objective. Weighting isotope calibration sites in the isotope simulation objective based on the data quality at the site should be considered as well.
- The potential for stable water isotope simulations to reduce equifinality in hydrological models should be investigated. Whether adding isotope simulation error actually reduces equifinality and (if so) by what degree could be determined by generating a large number of parameter sets with the

Monte Carlo method and comparing the number of behavioral models when only flow error is considered to the number of behavioral models when both flow and isotope error is considered. The isoWATFLOOD model of the LNRB could be used to conduct this analysis.

WATFLOOD development:

- The current WATFLOOD auto-calibration methodology could be greatly improved by introducing multi-objective calibration and by storing all simulation results in calibration to permit more robust analyses of the optimization. The present methodology does not allow for uncertainty assessments, for either parameters or simulated streamflow, in a statistically significant way. The total number of calibrated parameters should also be reduced, potentially by calibrating change factors for parameter groups rather than individual parameter values for each land/river class.
- The WATFLOOD evaporation-transpiration split should be re-examined and made more physically representative: one possible improvement is to allow for seasonal variation in the fraction of water transpired as plant activity varies through the year. A more physically-based evapotranspiration division would allow conclusions to be drawn from the verification results, namely if wetland evaporation is insufficient, and if total soil evapotranspiration losses are in fact being overestimated.
- The land-based potential evapotranspiration method used to calculate the lake evaporation rate should be replaced with a more physically representative evaporation model. While potential evapotranspiration is a reasonable approximation of shallow water bodies, lake evaporation would be better simulated using a more physically-based energy balance approach.

LNRB model:

- The lakes simulated as reservoirs in the WATFLOOD model require further work. The passive lake storage and storage-discharge curves used to simulate lake outflow on unregulated lakes are not currently accurate. The simulated lake volumes should be verified, and corrected if necessary, and

discharge equations should be updated. Removing some of the smaller simulated lakes as WATFLOOD reservoirs should also be explored. Evaporation from lakes is too high for the LNRB; the evaporation rate should be replaced with a more physically representative lake evaporation model (see WATFLOOD recommendations).

- The division of the wetland land cover into connected and disconnected simulated wetlands should have a physical basis, rather than the constant fractional split used previously. The division could instead be based on wetland proximity to open water, other connected wetlands or the channel network, using the variations in the wetland classification derived from satellite data (i.e. vegetation height).
- The total number of river classes in the model should be reduced, as the total number of calibrated parameters is too large, with many river classes having insufficient data to properly calibrate the hydrologic simulation. A more physically-based river classification should be explored, with rivers classes based on channel characteristics and geology rather than sub-basin.
- Some of the simulated gauges on smaller streams, particularly the Sapochi but also the Taylor and Footprint to a lesser degree, have significant drainage area errors, which lead to simulated flow volume errors. The simulated drainage areas should be corrected, either by changing the number of grid cells contributing to a gauge site, or by changing the grid cell areas for very small streams.

Stable water isotope sampling:

- Isotope data and simulation has been shown to be useful for physically-based hydrologic modeling, in model verification particularly, but the utility of isotope simulations could be improved by increasing the amount of observed data, particularly for:
    - Flow sources, such as groundwater and wetlands. Regular and frequent sampling (i.e. multiple samples per month) of shallow and deep groundwater and wetland surface waters

will allow a quantitative verification of these key streamflow sources in hydrological simulation.

- Rivers with natural flows, for which either the streamflow itself is of interest, or the river is representative of an area of interest (i.e. has similar land cover and geomorphology to a larger area). In order to use isotope observation to verify or calibrate a model, sampling should be continuous to capture all hydrological conditions in a year. The importance of frequent sampling is dependent on the variability of the river's isotopic composition, which in turn is dependent on drainage area; large rivers (over 10 000 km^2) might be sampled on a monthly basis or less, while small rivers (under 1000 km^2) are better sampled multiple times per month in the open-water season.

References

Aggarwal, P., Froehlich, K. & Gondfiantini, R., 2011. Contributions of the International Atomic Energy Agency to the development and practice of isotope hydrology. *Hydrogeology Journal,* Volume 19, pp. 5-8.

Agriculture Canada, 2016. *Soils of Canada.* [Online]
Available at: http://www.agr.gc.ca/atlas/
[Accessed 26 June 2016].

Bergstrom, S., Lindstrom, G. & Pettersson, A., 2002. Multi-variable parameter estimation to increase confidence in hydrological modelling. *Hydrological Processes,* 16(1), pp. 413-421.

Beven, K., 2006. A manifesto for the equifinality thesis. *Journal of Hydrology,* 320(1), pp. 18-36.

Beven, K., 2008. On doing better hydrological science. *Hydrological Processes,* 22(1), pp. 3549-3553.

Beven, K. & Binley, A., 1992. The future of distributed models: model calibration and uncertainty prediction. *Hydrological Processes,* 6(1), pp. 279-298.

Beven, K., Smith, P. & Freer, J., 2008. So just why would a modeller choose to be incoherent?. *Journal of Hydrology,* 354(1), pp. 15-32.

Birkel, C., Dunn, S. M., Tetzlaff, D. & Soulsby, C., 2010. Assessing the value of high-resolution isotope tracer data in the stepwise development of a lumped conceptual rainfall–runoff model. *Hydrological Processes,* Volume 24, pp. 2335-2348.

Birkel, C. et al., 2012. A new approach to simulating stream isotope dynamics using Markov switching autoregressive models. *Advances in Water Resources,* Volume 46, pp. 20-30.

Birkel, C. & Soulsby, C., 2015. Advancing tracer-aided rainfall–runoff modelling: a review of progress, problems and unrealised potential. *Hydrological Processes,* 29(1), pp. 5227-5240.

Birkel, C., Soulsby, C. & Tetzlaff, D., 2011. Modelling catchment-scale water storage dynamics: reconciling dynamic storage with tracer-inferred passive storage. *Hydrological Processes,* Volume 25, pp. 3924-3936.

Birkel, C., Soulsby, C. & Tetzlaff, D., 2014. Developing a consistent process-based conceptualization of catchment functioning using measurements of internal state variables. *Water Resources Research,* pp. 3481-3501.

Birkel, C., Soulsby, C. & Tetzlaff, D., 2015. Conceptual modelling to assess how the interplay of hydrological connectivity, catchment storage and tracer dynamics controls nonstationary water age estimates. *Hydrological Processes,* Volume 29, pp. 2956-2969.

Birkel, C. et al., 2012. High-frequency storm event isotope sampling reveals time-variant transit time distributions and influence of diurnal cycles. *Hydrological Processes,* Volume 26, pp. 308-316.

Birkel, C., Tetzlaff, D., Dunn, S. M. & Soulsby, C., 2011. Using lumped conceptual rainfall–runoff models to simulate daily isotope variability with fractionation in a nested mesoscale catchment. *Advances in Water Resources,* Volume 34, pp. 383-394.

Birkel, C., Tetzlaff, D., Dunn, S. M. & Soulsby, C., 2011. Using time domain and geographic source tracers to conceptualize streamflow generation processes in lumped rainfall-runoff models. *Water Resources Research,* Volume 47, p. W02515.

Birks, S. & Edwards, T., 2009. Atmospheric circulation controls on precipitation isotope–climate relations in western Canada. *Tellus,* Volume 61B, pp. 566-576.

Birks, S. & Gibson, J., 2009. Isotope hydrology research in Canada, 2003-2007. *Canadian Water Resources Journal,* 34(2), pp. 163-176.

Capell, R., Tetzlaff, D. & Soulsby, C., 2012. Can time domain and source area tracers reduce uncertainty in rainfall-runoff models in larger heterogeneous catchments?. *Water Resources Research,* Volume 48, p. W09544.

Coulibaly, P., Samuel, J., Pietroniro, A. & Harvey, D., 2013. Evaluation of Canadian National Hydrometric Network density based on WMO 2008 standards. *Canadian Water Resources Journal,* 38(2), pp. 159-167.

Craig, H., 1961. Isotopic variations in meteoric waters. *Science,* Volume 133, pp. 1702-1703.

Craig, H. & Gordon, L. I., 1965. Deuterium and oxygen 18 variations in the ocean and the marine atmosphere. In: E. Tongiorgi, ed. *Stable Isotopes in Oceanographic Studies and Paleotemperatures.* Spoleto: CNRLGN, pp. 9-130.

Dansgaard, W., 1964. Stable isotopes in precipitation. *Tellus,* 16(4), pp. 436-468.

Davies, J., Beven, K., Nyberg, L. & Rodhe, A., 2011. A discrete particle representation of hillslope hydrology: hypothesis testing in reproducing a tracer experiment at Gardsjon, Sweden. *Hydrological Processes,* Volume 25, pp. 3602-3612.

Delavau, C. et al., 2015. North American precipitation isotope (d18O) zones revealed in time series modeling across Canada and northern United States. *Water Resources Research,* Volume 51, pp. 1284-1299.

Delavau, C., Stadnyk, T. & Birks, J., 2011. Model based spatial distribution of oxygen-18 isotopes in precipitation across Canada. *Canadian Water Resources Journal,* 36(4), pp. 313-320.

Dinçer, T. et al., 1970. Snowmelt runoff from measurements of tritium and oxygen-18. *Water Resources Research,* Volume 6, pp. 110-124.

Dunn, S. et al., 2008. Interpretation of homogeneity in δ18O signatures of stream water in a nested sub-catchment system in north-east Scotland. *Hydrological Processes,* Volume 22, pp. 4767-4782.

Dunn, S., McDonnell, J. & Vache, K., 2007. Factors influencing the residence time of catchment waters: a virtual experiment approach. *Water Resources Research,* Volume 43, p. W06408.

Ehret, U. et al., 2014. Advancing catchment hydrology to deal with predictions under change. *Hydrology and Earth System Sciences,* 18(1), pp. 649-671.

Environment Canada, 2016. *Canadian Climate Normals 1981-2010.* [Online]
Available at: http://climate.weather.gc.ca/climate_normals/results_1981_2010_e.html
[Accessed 14 July 2016].

Environment Canada, 2016. *Historical Data.* [Online]
Available at: http://climate.weather.gc.ca/historical_data
[Accessed 22 June 2016].

Eriksson, E., 1963. Atmospheric tritium as a tool for the study of certain hydrologic aspects of river basins. *Tellus,* 15(3), pp. 303-308.

Evaristo, J., Jasechko, S. & McDonnell, J. J., 2015. Global separation of plant transpiration from groundwater and streamflow. *Nature,* Volume 525, pp. 91-94.

Fenicia, F. et al., 2010. Assessing the impact of mixing assumptions on the estimation of streamwater mean residence time. *Hydrological Processes,* Volume 24, pp. 1730-1741.

Fulton, R. J., 1995. *Surficial materials of Canada,* Ottawa: Natural Resources Canada.

Gat, J., 1996. Oxygen and hydrogen isotopes in the hydrologic cycle. *Annual Review Earth Planet Science,* Volume 24, pp. 225-262.

Gibson, J., 2002. Short-term evaporation and water budget comparisons in shallow Arctic lakes using non-steady isotope mass balance. *Journal of Hydrology,* Volume 264, pp. 242-261.

Gibson, J., Birks, S. & Edwards, T., 2008. Global prediction of dA and d2H-d18O evaporation slopes for lakes and soil water accounting for seasonality. *Global Biogeochemical Cycles,* Volume 22, p. GB2031.

Gibson, J., Birks, S. & Yi, Y., 2016. Stable isotope mass balance of lakes: a contemporary perspective. *Quarternary Science Reviews,* Volume 131, pp. 316-328.

Gibson, J. & Edwards, T., 2002. Regional water balance trends and evaporation-transpiration partitioning from a stable isotope survey of lakes in northern Canada. *Global Biogeochemical Cycles,* 16(2), p. 1026.

Gibson, J., Edwards, T. & Prowse, T., 1996. Development and validation of an isotopic method for estimating lake evaporation. *Hydrological Processes,* Volume 10, pp. 1369-1382.

Gibson, J. & Reid, R., 2010. Stable isotope fingerprint of open-water evaporation losses and effective drainage area fluctuations in a subarctic shield watershed. *Journal of Hydrology,* 164(1), pp. 142-150.

Gonfiantini, R., 1986. Environmental isotopes in lake studies. In: P. Fritz & J. Fontes, eds. *Handbook of environmental isotope geochemistry, the terrestrial environment.* New York: Elsevier, pp. 113-168.

Gupta, H. V., Kling, H., Yilmaz, K. K. & Martinez, G. F., 2009. Decomposition of the mean squared error and NSE performance criteria: Implications for improving hydrological modelling. *Journal of Hydrology,* Volume 377, pp. 80-91.

Hamilton, S., 2007. Just say NO to equifinality. *Hydrological Processes,* 21(1), pp. 1979-1980.

Harris, D., McDonnell, J. & Rodhe, A., 1995. Hydrograph separation using continuous open system isotope mixing. *Water Resources Research,* 31(1), pp. 157-171.

Hayashi, M., Quinton, W., Pietroniro, A. & Gibson, J., 2004. Hydrologic functions of wetlands in a discontinuous permafrost basin indicated by isotopic and chemical signatures. *Journal of Hydrology,* Volume 296, pp. 81-97.

Her, Y. & Chaubey, I., 2015. Impact of the numbers of observations and calibration parameters on equifinality, model performance, and output and parameter uncertainty. *Hydrological Processes,* 29(1), pp. 4220-4237.

Holmes, T., 2014. *Development of a Lake Evaporation model for WATFLOOD,* Winnipeg: University of Manitoba.

Horita, J. & Wesolowski, D., 1994. Liquid-vapor fractionation of oxygen and hydrogen isotopes of water from the freezing to the critical temperature. *Geochimica et Cosmochimica Acta,* 58(16), pp. 3425-3437.

Iorgulescu, I., Beven, K. J. & Musy, A., 2007. Flow, mixing, and displacement in using a data-based hydrochemical model to predict conservative tracer data. *Water Resources Research,* Volume 43, p. W03401.

Jasechko, S., Gibson, J. & Edwards, T., 2014. Stable isotope mass balance of the Laurentian Great Lakes. *Journal of Great Lakes Research,* 40(1), pp. 336-346.

Jasechko, S., Kirchner, J. W., M.Welker, J. & McDonnell, J. J., 2016. Substantial proportion of global streamflow less than three months old. *Nature Geoscience,* Volume 9, pp. 126-129.

Jasechko, S. et al., 2013. Terrestrial water fluxes dominated by transpiration. *Nature,* Volume 496, pp. 347-350.

Kennedy, V. et al., 1986. Determination of the components of stormflow using water chemistry and environmental isotopes, Mattole River basin, California. *Journal of Hydrology,* Volume 84, pp. 107-140.

Kirchner, J. W., 2003. A double paradox in catchment hydrology and geochemistry. *Hydrological Processes,* Volume 17, pp. 871-874.

Kirchner, J. W., 2006. Getting the right answers for the right reasons: Linking measurements, analyses, and models to advance the science of hydrology. *Water Resources Research,* 42(1), p. W03S04.

Klaus, J. & McDonnell, J., 2013. Hydrograph separation using stable isotopes: Review and evaluation. *Journal of Hydrology,* Volume 505, pp. 47-64.

Klaus, J. et al., 2015. Where does streamwater come from in low-relief forested watersheds? A dual-isotope approach. *Hydrology and Earth System Sciences,* Volume 19, pp. 125-135.

Kouwen, N., 2014. *WATFLOOD/WATROUTE Hydrological Model Routing & Flood Forecasting System,* s.l.: s.n.

Krause, P., Boyle, D. P. & Base, F., 2005. Comparison of different efficiency criteria for hydrological model assessment. *Advances in Geosciences,* Volume 5, pp. 89-97.

Liu, Z., Bowen, G. & Welker, J., 2010. Atmospheric circulation is reflected in precipitation isotope gradients over the conterminous United States. *Journal of Geophysical Research,* Volume 115, p. D22120.

Maloszewski, P., Rauert, W., Stichler, W. & Hermann, A., 1983. Application of flow models in an Alpine catchment area using tritium and deuterium data. *Journal of Hydrology,* Volume 66, pp. 319-330.

Małoszewski, P. & Zuber, A., 1982. Determining the turnover time of groundwater systems with the aid of environmental tracers: 1. Models and their applicability. *Journal of Hydrology,* Volume 57, pp. 207-231.

Manitoba Sustainable Development, 2016. *Churchill River Diversion.* [Online]
Available at: http://www.gov.mb.ca/waterstewardship/licensing/churchill_river_diversion.html
[Accessed 17 August 2016].

Martinec, J., 1975. Subsurface flow from snowmelt traced by tritium. *Water Resources Research,* 11(3), pp. 496-498.

McDonnell, J. J. & Beven, K., 2014. Debates—The future of hydrological sciences: A (common) path forward? A call to action aimed at understanding velocities, celerities and residence time distributions of the headwater hydrograph. *Water Resource Research,* Volume 50, pp. 5342-5350.

McMillan, H., Tetzlaff, D., Clark, M. & Soulsby, C., 2012. Do time-variable tracers aid the evaluation of hydrological model structure? A multimodel approach. *Water Resources Research,* Volume 48, p. W05501.

Mehlhorn, J., Lindenlaub, M. & Leibundgut, C., 1999. Improving hydrological process modeling by coupling a rainfall-runoff model with tracer techniques. *IAHS Publication,* Volume 254, pp. 157-163.

Moriasi, D. N., Arnold, J. G., Van Liew, M. W. & al, e., 2007. Model evaluation guidelines for systematic quantification of accuracy in watershed simulations. *Transactions of the ASABE,* 50(3), pp. 885-900.

Nash, J. & Sutcliffe, J., 1970. River flow forcasting through conceptual models part 1- a discussion of principles. *Journal of Hydrology,* 10(1), pp. 282-290.

Natural Resources Canada, 2011. *GeoBase.* [Online]
Available at: http://www.geobase.ca/geobase/en/
[Accessed 27 May 2011].

Neff, T. A. M., 1996. *Mesoscale water balance of the boreal forest using operational evapotranspiration approaches in a distributed hydrologic model,* Waterloo: M.A.Sc Thesis, University of Waterloo.

Niemi, A., 1978. Residence time distribution of variable flow processes. *International Journal of Applied Radiation and Isotopes,* Volume 28, pp. 855-860.

Ohlanders, N., Rodriguez, M. & McPhee, J., 2013. Stable water isotope variation in a Central Andean watershed dominated by glacier and snowmelt. *Hydrology and Earth System Sciences,* Volume 17, pp. 1035-1050.

Pangle, L. A. et al., 2013. A new multisource and high-frequency approach to measuring d2H and d18O in hydrological field studies. *Water Resources Research,* Volume 49, pp. 7797-7803.

Peralta-Tapia, A. et al., 2015. Connecting precipitation inputs and soil flow pathways to stream water in contrasting boreal catchments. *Hydrological Processes,* Volume 29, pp. 3546-3555.

Pietroniro, A. et al., 2006. Modelling climate change impacts in the Peace and Athabasca catchment and delta: III—integrated model assessment. *Hydrological Processes,* 20(1), pp. 4231-4245.

Pinder, G. & Jones, J., 1969. Determination of the ground-water component of peak discharge from the chemistry of total runoff. *Water Resources Research,* 5(2), pp. 438-445.

Singh, V. P. & Frevert, D. K., 2006. *Watershed Models.* Boca Raton: CRC Taylor & Francis.

Sklash, M. F. R. & Fritz, P., 1976. A conceptual model of watershed response to rainfall, developed through the use of oxygen-18 as a tracer. *Canadian Journal of Earth Sciences,* Volume 13, pp. 271-283.

Smith, A. A., Delavau, C. J. & Stadnyk, T. A., 2015. Hydrologic Assessment of the Lower Nelson River Basin using Stable Water Isotope Investigations. *Canadian Water Resource Journal,* 20(1), pp. 23-35.

Smith, A., Welch, C. & Stadnyk, T., 2016. Assessment of a lumped coupled flow-isotope model in Boreal catchments. *Hydrological Processes,* p. doi: 10.1002/hyp.10835.

Soulsby, C. et al., 2015. Stream water age distributions controlled by storage dynamics and nonlinear hydrologic connectivity: Modeling with high-resolution isotope data. *Water Resources Research,* Volume 51, pp. 7759-7776.

Soulsby, C., Birkel, C., Geris, J. & Tetzlaff, D., 2015. Spatial aggregation of time-variant stream water ages in urbanizing catchments. *Hydrological Processes,* Volume 29, pp. 3038-3050.

St Amour, N. et al., 2005. Isotopic time-series partitioning of streamflow components in wetland-dominated catchments, lower Liard River basin, Northwest Territories, Canada. *Hydrological Processes,* pp. 3357-3381.

Stadnyk-Falcone, T. A., 2008. *Mesoscale Hydrological Model Validation and Verification using Stable Water Isotopes: The isoWATFLOOD Model,* Waterloo: Ph.D. Thesis, University of Waterloo.

Stadnyk, T. A., Delavau, C., Kouwen, N. & Edwards, T. W. D., 2013. Towards hydrological model calibration and validation: simulation of stable water isotopes using the isoWATFLOOD model. *Hydrological Processes,* Volume 27, pp. 3791-3810.

Tetzlaff, D. et al., 2014. Storage dynamics in hydropedological units control hillslope connectivity, runoff generation, and the evolution of catchment transit time distributions. *Water Resources Research,* Volume 50, pp. 969-985.

Tetzlaff, D. et al., 2015. Tracer-based assessment of flow paths, storage and runoff generation in northern catchments: a review. *Hydrological Processes,* Volume 29, pp. 3475-3490.

Tolson, B. & Shoemaker, C., 2007. Dynamically Dynamically dimensioned search algorithm for computationally efficient watershed model calibration. *Water Resources Research,* 43(1), p. W01413.

Toth, B., Pietroniro, A., Conly, F. M. & Kouwen, N., 2006. Modelling climate change impacts in the Peace and Athabasca catchment and delta: I—hydrological model application. *Hydrological Processes,* 20(1), pp. 4197-4214.

Turner, J., Macpherson, D. & Stokes, R., 1987. The mechanisms of catchment flow processes using natural variations in deuterium and oxygen-18. *Journal of Hydrology,* Volume 94, pp. 143-162.

Untereiner, E., Ali, G. & Stadnyk, T., 2015. Spatiotemporal variability of water quality and stable water isotopes in intensively managed prairie watersheds. *Hydrological Processes,* Volume 29, pp. 4125-4143.

Vachon, R., Welker, J., White, J. & Vaughn, B., 2010. Moisture source temperatures and precipitation d18O-temperature relationships across the United States. *Water Resources Research,* Volume 46, p. W07523.

Vachon, R., Welker, J., White, J. & Vaughn, B., 2010. Monthly precipitation isoscapes (d18O) of the United States: Connections with surface temperatures, moisture source conditions, and air mass trajectories. *Journal of Geophysical Research,* Volume 115, p. D21126.

Water Survey of Canada, 2016. *Wateroffice.* [Online]
Available at: http://wateroffice.ec.gc.ca/
[Accessed 24 June 2016].

Weiler, M., McGlynn, B. L., McGuire, K. J. & McDonnell, J. J., 2003. How does rainfall become runoff? A combined tracer and runoff transfer function approach. *Water Resources Research,* Volume 39, p. 1315.

Welhan, J. & Fritz, P., 1977. Evaporation pan isotopic behavior as an index of isotopic evaporation conditions. *Geochimica et Cosmochimica Acta,* 41(5), pp. 682-686.

Welker, J., 2000. Isotopic (d18O) characteristics of weekly precipitation collected across the USA: an initial analysis with application to water source studies. *Hydrological Processes,* Volume 14, pp. 1449-1464.

Yi, Y. et al., 2008. A coupled isotope tracer method to characterize input water to lakes. *Journal of Hydrology,* 350(1-2), pp. 1-13.

Yi, Y., Gibson, J. J., J.-F. H. & Dick, T. A., 2010. Synoptic and time-series stable isotope surveys of the Mackenzie River from Great Slave Lake to the Arctic Ocean, 2003 to 2006. *Journal of Hydrology,* Volume 383, pp. 223-232.

Appendix A

The initial parameter set with parameter limits, all three calibrated parameter sets, the evapotranspiration split parameters and the initialization values used for the 5-year calibration period are included in this appendix.

Initial Parameter Set (with parameter calibration limits following):

```
:FileType           WatfloodParameter       10.1    # parameter file version number

:CreationDate   18/09/2013 6:46
:GlobalParameters
:iopt   0       # debug level
:itype  0       # channel type - floodplain/no
:itrace 4       # Tracer choice
:a1     -999.999# ice cover weighting factor
:a2     1.5     # Manning`s correction for instream lake
:a3     0.05    # error penalty coefficient
:a4     0.03    # error penalty threshold
:a5     0.985   # API coefficien
:a6     900     # Minimum routing time step in seconds
:a7     0.5     # weighting - old vs. new sca value
:a8     0.1     # min temperature time offset
:a9     0.33    # max heat deficit /swe ratio
:a10    1       # exponent on uz discharce function
:a11    0.01    # bare ground equiv. veg height for ev
:a12    1       # min precip rate for smearing
:fmadjust       0       # snowmelt ripening rate
:fmalow 0       # min melt factor multiplier
:fmahigh        0       # max melt factor multiplier
:gladjust 0     # glacier melt factor multiplier
:rlapse 0       # precip lapse rate mm/m
:tlapse -0.00402874     # temperature lapse rate dC/m
:elvref 0       # reference elevation
:rainsnowtemp   0       # rain/snow temperature
:radiusinflce   241.17  # radius of influence km
:smoothdist     52.752  # smoothing diatance km
:flgevp2        2       # 1=pan;2=Hargreaves;3=Priestley-Taylor
:albe   0.11    # albedo????
:tempa2 50      #
:tempa3 50      #
:tton   50      #
:lat    50      # latitude
:chnl(1)  1     # manning`s n multiplier
:chnl(2)  0.9   # manning`s n multiplier
:chnl(3)  0.8   # manning`s n multiplier
:chnl(4)  0.7   # manning`s n multiplier
:chnl(5)  0.6   # manning`s n multiplier
:EndGlobalParameters
```

#

:RoutingParameters
:RiverClasses 9
:RiverClassName Rat Nelson UBtwd Grass_Split Minago_Cross Kettle Odei Limestone_Mouth Footprint
:flz 3.01E-03 4.03E-03 2.43E-03 1.71E-03 4.72E-03 9.90E-04 2.02E-03 2.22E-03 1.00E-08
:pwr 2.73 2.46 3.34 3.5 3.48 2.75 2.91 1.24 1.34
:r1n 0.4 0.4 0.4 0.4 0.4 0.15 0.4 0.4 0.4
:r2n 3.68E-02 3.20E-03 9.61E-03 1.88E-02 1.29E-02 3.50E-03 1.00E-03 8.97E-03 1.31E-02
:mndr 1 1 1 1 1 1 1 1 1
:aa2 1 1 1 1 1 1 1 1 1
:aa3 4.30E-02 4.30E-02 4.30E-02 4.30E-02 4.30E-02 4.30E-02 4.30E-02 8.60E-02 4.30E-02
:aa4 1 1 1 1 1 1 1 1 1
:theta 0.62 0.865 0.807 0.94 0.807 0.774 0.132 0.188 1.10E-01
:widep 10 30 10 10 10 30 10 30 25
:kcond 0.171 0.168 0.217 0.233 0.183 0.124 0.158 0.223 0.244
:pool 0 0 0 0 0 0 0 0 0
:rlake 1 1 1 1 1 1 1 1 1
:EndRoutingParameters
#
:HydrologicalParameters
:LandCoverClasses 9
:ClassName coniferous mixed_forest treed_rock shrub bogs wetland wetland_con water impervious
:ds 1 10 10 10 0.1 0.1 0.1 0 1
:dsfs 1 10 10 10 0.1 0.1 0.1 0 1
:rec 0.43 0.63 1.45 1.83 0.99 3.32 3.32 0.1 1.00E-11
:ak 14 20 8 5 40 40 40 -1.00E-11 1.00E-11
:akfs 2 3 1 1 30 30 30 -1.00E-11 1.00E-11
:retn 120 70 30 40 300 200 121 139 1.00E-11
:ak2 3.40E-02 5.35E-02 1.43E-03 2.99E-03 0.011 6.24E-03 0.158 9.07E-02 1.00E-11
:ak2fs 2.40E-02 4.35E-02 1.00E-03 2.00E-03 5.00E-03 5.00E-03 6.89E-02 1.00E-03 1.00E-11
:r3 84.8 84.8 84.8 84.8 8.98E-03 8.98E-03 8.98E-03 4 19.7
:r3fs 10 10 10 10 0.1 0.1 0.1 4 10
:r4 10 10 10 1 10 10 10 10 1
:fpet 1 2.08 2.93 1 1 1.98 1.98 0.918 1
:ftall 0.5 0.532 0.558 0.5 0.5 0.581 0.581 0 0.5
:flint 1 1 1 1 1 1 1 1 1
:fcap 0.15 0.15 0.15 0.15 0.15 0.15 0.15 0.15 0.15
:ffcap 0.1 0.1 0.1 0.1 0.1 0.1 0.1 0.1 0.1
:spore 0.3 0.3 0.3 0.3 0.3 0.3 0.3 0.3 0.3
:fratio 0.9 0.9 0.9 0.6 0.9 1.4 1.2 1.5 1
:EndHydrologicalParameters
#
:SnowParameters
:fm 0.077 0.13 0.082 0.179 0.215 0.062 0.062 0.11 0.11
:base 1 0 -1 -1 0 -1 -1 -2 -2
:fmn 0.1 0.1 0.1 0.1 0.1 0.1 0.1 0.1 0.1
:uadj 0 0 0 0 0 0 0 0 0
:tipm 0.1 0.1 0.1 0.1 0.1 0.1 0.1 0.1 0.1
:rho 0.333 0.333 0.333 0.333 0.333 0.333 0.333 0.333 0.333
:whcl 0.035 0.035 0.035 0.035 0.035 0.035 0.035 0.035 0.035
:alb 0.11 0.11 0.11 0.18 0.11 0.11 0.11 0.11 0.11
:sublim_rate 0.1 0.1 0.1 0.2 0.1 0.3 0.3 0.4 0.3

```
:idump   6        8        12       13       17       18       18       20       21
:snocap  6000     6000     -600     -600     -600     -600     -600     -600     -600
:nsdc    2        2        2        2        2        2        2        2        2
:sdcsca  1        1        1        1        1        1        1        1        1
:sdcd    50       50       50       50       50       50       50       100      100
:EndSnowParameters
#
:InterceptionCapacityTable
:IntCap_Jan      1        2.4      0.55     0.1      0.25     3        3        0.11     0.01
:IntCap_Feb      1        2.4      0.55     0.1      0.25     3        3        0.11     0.01
:IntCap_Mar      1        2.4      0.55     0.1      0.25     3        3        0.11     0.01
:IntCap_Apr      1        2.4      0.55     0.1      0.25     3        3        0.11     0.01
:IntCap_May      1        3        0.75     0.25     0.25     3        3        0.11     0.01
:IntCap_Jun      1        4        0.9      0.5      0.25     3        3        0.11     0.01
:IntCap_Jul      1        4        0.9      0.5      0.25     3        3        0.11     0.01
:IntCap_Aug      1        4        0.9      0.5      0.25     3        3        0.11     0.01
:IntCap_Sep      1        4        0.9      0.5      0.25     3        3        0.11     0.01
:IntCap_Oct      1        2.4      0.55     0.1      0.25     3        3        0.11     0.01
:IntCap_Nov      1        2.4      0.55     0.1      0.25     3        3        0.11     0.01
:IntCap_Dec      1        2.4      0.55     0.1      0.25     3        3        0.11     0.01
:EndInterceptionCapacityTable
#

:APILimits
:a5dlt    -0.1
:a5low    0.1
:a5hgh    1
:EndAPILimits
#
:HydrologicalParLimits
:ClassName   coniferous   mixed_forest treed_rock shrub bogs wetland wetland_con water impervious
# infiltration coefficient bare ground
:akdlt    -1       -1       -1       -1       -1       -1       -1       -1       -1
:aklow    1        1        1        1        0.004    0.04     0.04     -2       0.04
:akhgh    20       20       20       20       500      500      500      500      500
# infiltration coefficient snow covered ground
:akfsdlt  -1       -1       -1       -1       -1       -1       -1       -1       -1
:akfslow  1        1        1        1        0.04     0.04     0.04     -2       0.04
:akfshgh  5        5        5        5        500      500      500      500      500
# interflow coefficient
:recdlt   1        1        1        1        1        1        -1       -1       -1
:reclow   5.00E-025.00E-025.00E-025.00E-025.00E-025.00E-025.00E-025.00E-025.00E-02
:rechgh   4        4        4        4        4        4        0.1      0.1      0.1
# overland flow roughness coeff bare ground
:r3dlt    -1       -1       -1       -1       -1       -1       -1       -1       -1
:r3low    1        1        1        1        1        1        1        1        1
:r3hgh    10       10       10       25       25       10       10       10       10
# interception evaporation factor * pet
:fpetdlt  -1       -1       -1       -1       -1       -1       -1       -1       -1
:fpetlow  0.5      0.5      0.5      0.5      0.5      0.5      0.5      0.9      9.00E-02
:fpethgh  5        5        5        5        5        5        5        1.1      1.15
# reduction in PET for tall vegetation
:ftalldlt -1       -1       -1       -1       -1       -1       -1       -1       -1
```

```
:ftalllow 0.5       0.5       0.5       0.5       0.5       0.5       0.5       0.5       0.5
:ftallhgh 1         1         1         1         1         1         1         1         1
# multiplier for interception capacity
:fratiodlt-1        -1        -1        -1        -1        -1        -1        -1        -1
:fratiolow          0.66      0.2       0.66      0.2       0.66      0.66      0.66      0.66      0.66
:fratiohgh          1.5       0.7       1.5       0.7       1.5       1.5       1.5       1.5       1.5
# upper zone retention mm
:retndlt  1         1         1         1         1         1         -1        -1        -1
:retnlow 20         20        10        10        30        30        10        10        10
:retnhgh 150        150       50        50        400       400       150       160       150
# recharge coefficient bare ground
:ak2dlt   1         1         1         1         1         1         -1        -1        -1
:ak2low  1.00E-031.00E-031.00E-031.00E-031.00E-031.00E-031.00E-035.00E-041.00E-03
:ak2hgh  0.2        0.2       0.2       0.2       0.2       0.2       0.2       0.2       0.2
# recharge coefficient snow covered ground
:ak2fsdlt -1        -1        -1        -1        -1        -1        -1        -1        -1
:ak2fslow           -4.32E+08         -4.32E+08         -4.32E+08         -4.32E+08         -4.32E+08         -
4.32E+08            -4.32E+08         -4.32E+08         -4.32E+08
:ak2fshgh           0.2       0.2       0.2       0.2       0.2       0.2       0.2       0.2       0.2
:EndHydrologicalParLimits
#
:GlobalSnowParLimits
# snowmelt ripening rate
:fmadjustdlt        -0.1
:fmadjustlow        0.1
:fmadjusthgh        1
# min melt factor multiplier
:fmalowdlt          -0.1
:fmalowlow          0
:fmalowhgh          1
# max melt factor multiplier
:fmahighdlt         -1
:fmahighlow         0
:fmahighhgh         0
# glacier melt factor multiplier
:gladjustdlt        -1
:gladjustlow        0
:gladjusthgh        0
:EndGlobalSnowParLimits
#
:SnowParLimits
:ClassName   coniferous   mixed_forest treed_rock shrub bogs wetland wetland_con water impervious
# melt factor mm/dC/hour
:fmdlt    1         1         1         1         1         1         1         1         1
:fmlow   5.00E-025.00E-025.00E-025.00E-025.00E-025.00E-025.00E-025.00E-025.00E-02
:fmhgh   0.25       0.25      0.25      0.25      0.25      0.25      0.25      0.25      0.25
# base temperature dC
:basedlt -1         -1        -1        -1        -1        -1        -1        -1        -1
:baselow            -5        -5        -5        -5        -5        -5        -5        -100      -5
:basehgh            5         5         5         5         5         5         5         5         5
# sublimation factor OR ratio
:subdlt   -1        -1        -1        -1        -1        -1        -1        -1        -1
:sublow   -1        0.1       0.1       5.00E-030.1       0.1       0.1       1.00E-030.1
```

```
:subhgh 1.5     0.3     1.5     0.1     1.5     1.5     1.5     1.5     1.5
:EndSnowParLimits
#
:RoutingParLimits
:RiverClassName  Rat Nelson UBtwd Grass_Split Minago_Cross Kettle Odei Limestone_Mouth Footprint
# lower zone oefficient
:flzdlt 1       1       1       1       1       1       1       1       1
:flzlow 1.00E-081.00E-081.00E-081.00E-081.00E-081.00E-081.00E-081.00E-081.00E-09
:flzhgh 5.00E-035.00E-035.00E-035.00E-035.00E-035.00E-035.00E-035.00E-035.00E-03
# lower zone exponent
:pwrdlt 1       1       1       1       1       1       1       1       1
:pwrlow 1       1       1       1       1       1       1       1       1
:pwrhgh 4       4       4       4       4       4       4       4       4
# channel Manning`s n
:r2ndlt -1      -1      -1      -1      -1      -1      -1      -1      -1
:r2nlow 1.00E-041.00E-041.00E-041.00E-041.00E-041.00E-041.00E-041.00E-041.00E-04
:r2nhgh 4.50E-024.50E-024.50E-024.50E-024.50E-024.50E-024.50E-024.50E-024.50E-02
# wetland or bank porosity
:thetadlt1      1       1       1       1       1       1       1       1
:thetalow       1.00E-011.00E-011.00E-011.00E-011.00E-011.00E-011.00E-011.00E-011.00E-01
:thetahgh       0.95    0.95    0.95    0.95    0.95    0.95    0.95    0.95    0.95
# wetland/bank lateral conductivity
:kconddlt       1       1       1       1       1       1       1       1       1
:kcondlow       0.1     0.1     0.1     0.1     0.1     0.1     0.1     0.1     0.1
:kcondhgh       0.25    0.25    0.25    0.25    0.25    0.25    0.25    0.25    0.25
:EndRoutingParLimits
#
```

Flow-only Calibration Parameter Set (F)

```
:FileType           WatfloodParameter       10.1    # parameter file version number

:CreationDate       23/03/2016 6:04
:GlobalParameters
:iopt       0       # debug level
:itype      0       # channel type - floodplain/no
:itrace     4       # Tracer choice
:a1         -999.999# ice cover weighting factor
:a2         1.5     # Correction for instream lake <0=no >0=yes
:a3         0.05    # error penalty coefficient
:a4         0.03    # error penalty threshold
:a5         0.985   # API coefficien
:a6         900     # Minimum routing time step in seconds
:a7         0.5     # weighting - old vs. new sca value
:a8         0.1     # min temperature time offset
:a9         0.33    # max heat deficit /swe ratio
:a10        1       # exponent on uz discharce function
:a11        0.01    # bare ground equiv. veg height for ev
:a12        1       # min precip rate for smearing
:fmadjust           0       # snowmelt ripening rate
:fmalow 0           # min melt factor multiplier
:fmahigh            0       # max melt factor multiplier
```

```
:gladjust 0          # glacier melt factor multiplier
:rlapse   0          # precip lapse rate mm/m
:tlapse   -0.004029          # temperature lapse rate dC/m
:elvref   0          # reference elevation
:rainsnowtemp     0          # rain/snow temperature
:radiusinflce     241.17     # radius of influence km
:smoothdist       52.752     # smoothing diatance km
:flgevp2          2          # 1=pan;2=Hargreaves;3=Priestley-Taylor
:albe     0.11     # albedo????
:tempa2 50         #
:tempa3 50         #
:tton     50       #
:lat      50       # latitude
:chnl(1)  1        # manning`s n multiplier
:chnl(2)  0.9      # manning`s n multiplier
:chnl(3)  0.8      # manning`s n multiplier
:chnl(4)  0.7      # manning`s n multiplier
:chnl(5)  0.6      # manning`s n multiplier
:EndGlobalParameters
#
:RoutingParameters
:RiverClasses      9
:RiverClassName    Rat Nelson UBtwd Grass_Split Minago_Cross Kettle Odei Limestone_Mouth Footprint
:flz      4.48E-03 4.51E-03 4.64E-03 8.20E-04 4.11E-03 1.22E-03 2.52E-03 4.57E-03 1.00E-08
:pwr      1.72     3.04     1.58     3.92     3.15     3.79     3.02     2.05     1.93
:r1n      0.4      0.4      0.4      0.4      0.4      0.15     0.4      0.4      0.4
:r2n      1.86E-02 5.30E-03 3.69E-03 1.24E-02 1.24E-02 2.27E-03 1.10E-03 1.02E-02 1.58E-02
:mndr     1        1        1        1        1        1        1        1        1
:aa2      1        1        1        1        1        1        1        1        1
:aa3      4.30E-02 4.30E-02 4.30E-02 4.30E-02 4.30E-02 4.30E-02 4.30E-02 8.60E-02 4.30E-02
:aa4      1        1        1        1        1        1        1        1        1
:theta    0.424    0.687    0.634    0.908    0.369    0.637    0.404    0.12     0.111
:widep    10       30       10       10       10       30       10       30       25
:kcond    0.217    0.141    0.154    0.199    0.215    0.166    0.242    0.103    0.234
:pool     0        0        0        0        0        0        0        0        0
:rlake    1        1        1        1        1        1        1        1        1
:EndRoutingParameters
#
:HydrologicalParameters
:LandCoverClasses  9
:ClassName   coniferous   mixed_forest treed_rock shrub bogs wetland wetland_con water impervious
:ds       1        10       10       10       0.1      0.1      0.1      0        1
:dsfs     1        10       10       10       0.1      0.1      0.1      0        1
:rec      3.02     2.95     2.1      0.233    1.92     1.7      3.32     0.1      1.00E-11
:ak       14       20       8        5        40       40       40       -1.00E-11          1.00E-11
:akfs     2        3        1        1        30       30       30       -1.00E-11          1.00E-11
:retn     127      126      49.9     12.6     366      291      121      139      1.00E-11
:ak2      0.177    9.07E-02 0.115    0.179    3.39E-03 0.142    0.158    9.07E-02 1.00E-11
:ak2fs    2.40E-02 4.35E-02 1.00E-03 2.00E-03 5.00E-03 5.00E-03 6.89E-02 1.00E-03 1.00E-11
:r3       84.8     84.8     84.8     84.8     8.98E-03 8.98E-03 8.98E-03 4        19.7
:r3fs     10       10       10       10       0.1      0.1      0.1      4        10
:r4       10       10       10       1        10       10       10       10       1
:fpet     1        2.08     2.93     1        1        1.98     1.98     0.918    1
```

```
:ftall  0.5     0.532   0.558   0.5     0.5     0.581   0.581   0       0.5
:flint  1       1       1       1       1       1       1       1       1
:fcap   0.15    0.15    0.15    0.15    0.15    0.15    0.15    0.15    0.15
:ffcap  0.1     0.1     0.1     0.1     0.1     0.1     0.1     0.1     0.1
:spore  0.3     0.3     0.3     0.3     0.3     0.3     0.3     0.3     0.3
:fratio 0.9     0.9     0.9     0.6     0.9     1.4     1.2     1.5     1
:EndHydrologicalParameters
#
:SnowParameters
:fm     0.086   0.064   0.058   0.101   0.241   0.215   0.185   0.051   0.185
:base   1       0       -1      -1      0       -1      -1      -2      -2
:fmn    0.1     0.1     0.1     0.1     0.1     0.1     0.1     0.1     0.1
:uadj   0       0       0       0       0       0       0       0       0
:tipm   0.1     0.1     0.1     0.1     0.1     0.1     0.1     0.1     0.1
:rho    0.333   0.333   0.333   0.333   0.333   0.333   0.333   0.333   0.333
:whcl   0.035   0.035   0.035   0.035   0.035   0.035   0.035   0.035   0.035
:alb    0.11    0.11    0.11    0.18    0.11    0.11    0.11    0.11    0.11
:sublim_rate    0.1     0.1     0.1     0.2     0.1     0.3     0.3     0.4     0.3
:idump  6       8       12      13      17      18      18      20      21
:snocap 6000    6000    -600    -600    -600    -600    -600    -600    -600
:nsdc   2       2       2       2       2       2       2       2       2
:sdcsca 1       1       1       1       1       1       1       1       1
:sdcd   50      50      50      50      50      50      50      100     100
:EndSnowParameters
#
:InterceptionCapacityTable
:IntCap_Jan     1       2.4     0.55    0.1     0.25    3       3       0.01    0.01
:IntCap_Feb     1       2.4     0.55    0.1     0.25    3       3       0.01    0.01
:IntCap_Mar     1       2.4     0.55    0.1     0.25    3       3       0.01    0.01
:IntCap_Apr     1       2.4     0.55    0.1     0.25    3       3       0.01    0.01
:IntCap_May     1       3       0.75    0.25    0.25    3       3       0.01    0.01
:IntCap_Jun     1       4       0.9     0.5     0.25    3       3       0.01    0.01
:IntCap_Jul     1       4       0.9     0.5     0.25    3       3       0.01    0.01
:IntCap_Aug     1       4       0.9     0.5     0.25    3       3       0.01    0.01
:IntCap_Sep     1       4       0.9     0.5     0.25    3       3       0.01    0.01
:IntCap_Oct     1       2.4     0.55    0.1     0.25    3       3       0.01    0.01
:IntCap_Nov     1       2.4     0.55    0.1     0.25    3       3       0.01    0.01
:IntCap_Dec     1       2.4     0.55    0.1     0.25    3       3       0.01    0.01
:EndInterceptionCapacityTable
```

Single-isotope Calibration Parameter Set (O)

```
:FileType           WatfloodParameter       10.1    # parameter file version number

:CreationDate       25/03/2016 5:33
:GlobalParameters
:iopt       0       # debug level
:itype      0       # channel type - floodplain/no
:itrace     4       # Tracer choice
:a1         -999.999# ice cover weighting factor
:a2         1.5     # Correction for instream lake <0=no >0=yes
:a3         0.05    # error penalty coefficient
```

```
:a4	0.03	# error penalty threshold
:a5	0.985	# API coefficien
:a6	900	# Minimum routing time step in seconds
:a7	0.5	# weighting - old vs. new sca value
:a8	0.1	# min temperature time offset
:a9	0.33	# max heat deficit /swe ratio
:a10	1	# exponent on uz discharce function
:a11	0.01	# bare ground equiv. veg height for ev
:a12	1	# min precip rate for smearing
:fmadjust	0	# snowmelt ripening rate
:fmalow	0	# min melt factor multiplier
:fmahigh	0	# max melt factor multiplier
:gladjust	0	# glacier melt factor multiplier
:rlapse	0	# precip lapse rate mm/m
:tlapse	-0.004029	# temperature lapse rate dC/m
:elvref	0	# reference elevation
:rainsnowtemp	0	# rain/snow temperature
:radiusinflce	241.17	# radius of influence km
:smoothdist	52.752	# smoothing diatance km
:flgevp2	2	# 1=pan;2=Hargreaves;3=Priestley-Taylor
:albe	0.11	# albedo????
:tempa2	50	#
:tempa3	50	#
:tton	50	#
:lat	50	# latitude
:chnl(1)	1	# manning`s n multiplier
:chnl(2)	0.9	# manning`s n multiplier
:chnl(3)	0.8	# manning`s n multiplier
:chnl(4)	0.7	# manning`s n multiplier
:chnl(5)	0.6	# manning`s n multiplier
:EndGlobalParameters
#
:RoutingParameters
:RiverClasses	9
:RiverClassName	Rat	Nelson	UBtwd	Grass_Split	Minago_Cross	Kettle	Odei	Limestone_Mouth	Footprint
:flz	4.15E-03	4.96E-03	4.58E-03	2.21E-03	3.94E-03	2.27E-03	2.03E-03	3.28E-03	1.00E-08
:pwr	2.29	1.93	3.28	3.86	3.28	3.21	3.77	3.74	1.89
:r1n	0.4	0.4	0.4	0.4	0.4	0.15	0.4	0.4	0.4
:r2n	1.48E-03	2.03E-03	1.94E-02	1.49E-02	1.98E-02	1.66E-02	2.05E-03	9.75E-03	1.67E-02
:mndr	1	1	1	1	1	1	1	1	1
:aa2	1	1	1	1	1	1	1	1	1
:aa3	4.30E-02	4.30E-02	4.30E-02	4.30E-02	4.30E-02	4.30E-02	4.30E-02	8.60E-02	4.30E-02
:aa4	1	1	1	1	1	1	1	1	1
:theta	0.102	0.162	0.438	0.947	0.133	0.946	0.32	0.374	0.114
:widep	10	30	10	10	10	30	10	30	25
:kcond	0.226	0.106	0.246	0.226	0.2	0.118	0.232	0.146	0.244
:pool	0	0	0	0	0	0	0	0	0
:rlake	1	1	1	1	1	1	1	1	1
:EndRoutingParameters
#
:HydrologicalParameters
:LandCoverClasses	9
:ClassName	coniferous	mixed_forest	treed_rock	shrub	bogs	wetland	wetland_con	water	impervious
```

```
:ds 1 10 10 10 0.1 0.1 0.1 0 1
:dsfs 1 10 10 10 0.1 0.1 0.1 0 1
:rec 2.95 3.98 1.73 7.59E-02 3.69 1.51 3.32 0.1 1.00E-11
:ak 14 20 8 5 40 40 40 -1.00E-11 1.00E-11
:akfs 2 3 1 1 30 30 30 -1.00E-11 1.00E-11
:retn 113 116 49.8 10.7 377 335 121 139 1.00E-11
:ak2 0.194 0.178 5.32E-02 0.182 0.134 0.14 0.158 9.07E-02 1.00E-11
:ak2fs 2.40E-02 4.35E-02 1.00E-03 2.00E-03 5.00E-03 5.00E-03 6.89E-02 1.00E-03 1.00E-11
:r3 84.8 84.8 84.8 84.8 8.98E-03 8.98E-03 8.98E-03 4 19.7
:r3fs 10 10 10 10 0.1 0.1 0.1 4 10
:r4 10 10 10 1 10 10 10 10 1
:fpet 1 2.08 2.93 1 1 1.98 1.98 0.918 1
:ftall 0.5 0.532 0.558 0.5 0.5 0.581 0.581 0 0.5
:flint 1 1 1 1 1 1 1 1 1
:fcap 0.15 0.15 0.15 0.15 0.15 0.15 0.15 0.15 0.15
:ffcap 0.1 0.1 0.1 0.1 0.1 0.1 0.1 0.1 0.1
:spore 0.3 0.3 0.3 0.3 0.3 0.3 0.3 0.3 0.3
:fratio 0.9 0.9 0.9 0.6 0.9 1.4 1.2 1.5 1
:EndHydrologicalParameters
#
:SnowParameters
:fm 0.083 0.067 0.067 0.12 0.165 0.168 0.16 0.054 0.232
:base 1 0 -1 -1 0 -1 -1 -2 -2
:fmn 0.1 0.1 0.1 0.1 0.1 0.1 0.1 0.1 0.1
:uadj 0 0 0 0 0 0 0 0 0
:tipm 0.1 0.1 0.1 0.1 0.1 0.1 0.1 0.1 0.1
:rho 0.333 0.333 0.333 0.333 0.333 0.333 0.333 0.333 0.333
:whcl 0.035 0.035 0.035 0.035 0.035 0.035 0.035 0.035 0.035
:alb 0.11 0.11 0.11 0.18 0.11 0.11 0.11 0.11 0.11
:sublim_rate 0.1 0.1 0.1 0.2 0.1 0.3 0.3 0.4 0.3
:idump 6 8 12 13 17 18 18 20 21
:snocap 6000 6000 -600 -600 -600 -600 -600 -600 -600
:nsdc 2 2 2 2 2 2 2 2 2
:sdcsca 1 1 1 1 1 1 1 1 1
:sdcd 50 50 50 50 50 50 50 100 100
:EndSnowParameters
#
:InterceptionCapacityTable
:IntCap_Jan 1 2.4 0.55 0.1 0.25 3 3 0.01 0.01
:IntCap_Feb 1 2.4 0.55 0.1 0.25 3 3 0.01 0.01
:IntCap_Mar 1 2.4 0.55 0.1 0.25 3 3 0.01 0.01
:IntCap_Apr 1 2.4 0.55 0.1 0.25 3 3 0.01 0.01
:IntCap_May 1 3 0.75 0.25 0.25 3 3 0.01 0.01
:IntCap_Jun 1 4 0.9 0.5 0.25 3 3 0.01 0.01
:IntCap_Jul 1 4 0.9 0.5 0.25 3 3 0.01 0.01
:IntCap_Aug 1 4 0.9 0.5 0.25 3 3 0.01 0.01
:IntCap_Sep 1 4 0.9 0.5 0.25 3 3 0.01 0.01
:IntCap_Oct 1 2.4 0.55 0.1 0.25 3 3 0.01 0.01
:IntCap_Nov 1 2.4 0.55 0.1 0.25 3 3 0.01 0.01
:IntCap_Dec 1 2.4 0.55 0.1 0.25 3 3 0.01 0.01
:EndInterceptionCapacityTable
#
```

Dual-isotope Calibration Parameter Set (OH)

```
:FileType            WatfloodParameter        10.1      # parameter file version number

:CreationDate      26/03/2016 12:39
:GlobalParameters
:iopt      0          # debug level
:itype     0          # channel type - floodplain/no
:itrace    4          # Tracer choice
:a1        -999.999# ice cover weighting factor
:a2        1.5        # Correction for instream lake <0=no >0=yes
:a3        0.05       # error penalty coefficient
:a4        0.03       # error penalty threshold
:a5        0.985      # API coefficien
:a6        900        # Minimum routing time step in seconds
:a7        0.5        # weighting - old vs. new sca value
:a8        0.1        # min temperature time offset
:a9        0.33       # max heat deficit /swe ratio
:a10       1          # exponent on uz discharce function
:a11       0.01       # bare ground equiv. veg height for ev
:a12       1          # min precip rate for smearing
:fmadjust            0          # snowmelt ripening rate
:fmalow 0          # min melt factor multiplier
:fmahigh             0          # max melt factor multiplier
:gladjust 0        # glacier melt factor multiplier
:rlapse    0          # precip lapse rate mm/m
:tlapse    -0.004029          # temperature lapse rate dC/m
:elvref    0          # reference elevation
:rainsnowtemp    0          # rain/snow temperature
:radiusinflce        241.17     # radius of influence km
:smoothdist        52.752     # smoothing diatance km
:flgevp2             2          # 1=pan;2=Hargreaves;3=Priestley-Taylor
:albe      0.11       # albedo????
:tempa2 50         #
:tempa3 50         #
:tton      50         #
:lat       50         # latitude
:chnl(1)   1          # manning`s n multiplier
:chnl(2)   0.9        # manning`s n multiplier
:chnl(3)   0.8        # manning`s n multiplier
:chnl(4)   0.7        # manning`s n multiplier
:chnl(5)   0.6        # manning`s n multiplier
:EndGlobalParameters
#
:RoutingParameters
:RiverClasses        9
:RiverClassName    Rat Nelson UBtwd Grass_Split Minago_Cross Kettle Odei Limestone_Mouth Footprint
:flz       4.66E-033.06E-034.83E-033.39E-032.26E-031.08E-033.13E-032.88E-031.00E-08
:pwr       1.69       3.76       2.73       2.92       3.21       3.18       3.84       3.84       1.89
:r1n       0.4        0.4        0.4        0.4        0.4        0.15       0.4        0.4        0.4
:r2n       4.51E-031.85E-031.97E-021.32E-021.96E-021.52E-021.69E-031.01E-021.67E-02
```

```
:mndr 1 1 1 1 1 1 1 1 1
:aa2 1 1 1 1 1 1 1 1 1
:aa3 4.30E-024.30E-024.30E-024.30E-024.30E-024.30E-024.30E-028.60E-024.30E-02
:aa4 1 1 1 1 1 1 1 1 1
:theta 0.849 0.211 0.392 0.94 0.363 0.259 0.402 0.275 0.118
:widep 10 30 10 10 10 30 10 30 25
:kcond 0.21 0.182 0.228 0.102 0.237 0.219 0.247 0.12 0.238
:pool 0 0 0 0 0 0 0 0 0
:rlake 1 1 1 1 1 1 1 1 1
:EndRoutingParameters
#
:HydrologicalParameters
:LandCoverClasses 9
:ClassName coniferous mixed_forest treed_rock shrub bogs wetland wetland_con water impervious
:ds 1 10 10 10 0.1 0.1 0.1 0 1
:dsfs 1 10 10 10 0.1 0.1 0.1 0 1
:rec 3.07 3.4 3.64 0.262 3.54 0.352 3.32 0.1 1.00E-11
:ak 14 20 8 5 40 40 40 -1.00E-11 1.00E-11
:akfs 2 3 1 1 30 30 30 -1.00E-11 1.00E-11
:retn 115 101 49.7 10.2 383 366 121 139 1.00E-11
:ak2 0.18 0.172 0.173 0.176 0.195 3.87E-020.158 9.07E-021.00E-11
:ak2fs 2.40E-024.35E-021.00E-032.00E-035.00E-035.00E-036.89E-021.00E-031.00E-11
:r3 84.8 84.8 84.8 84.8 8.98E-038.98E-038.98E-034 19.7
:r3fs 10 10 10 10 0.1 0.1 0.1 4 10
:r4 10 10 10 1 10 10 10 10 1
:fpet 1 2.08 2.93 1 1 1.98 1.98 0.918 1
:ftall 0.5 0.532 0.558 0.5 0.5 0.581 0.581 0 0.5
:flint 1 1 1 1 1 1 1 1 1
:fcap 0.15 0.15 0.15 0.15 0.15 0.15 0.15 0.15 0.15
:ffcap 0.1 0.1 0.1 0.1 0.1 0.1 0.1 0.1 0.1
:spore 0.3 0.3 0.3 0.3 0.3 0.3 0.3 0.3 0.3
:fratio 0.9 0.9 0.9 0.6 0.9 1.4 1.2 1.5 1
:EndHydrologicalParameters
#
:SnowParameters
:fm 0.083 0.071 0.054 0.126 0.158 0.145 0.204 0.051 0.119
:base 1 0 -1 -1 0 -1 -1 -2 -2
:fmn 0.1 0.1 0.1 0.1 0.1 0.1 0.1 0.1 0.1
:uadj 0 0 0 0 0 0 0 0 0
:tipm 0.1 0.1 0.1 0.1 0.1 0.1 0.1 0.1 0.1
:rho 0.333 0.333 0.333 0.333 0.333 0.333 0.333 0.333 0.333
:whcl 0.035 0.035 0.035 0.035 0.035 0.035 0.035 0.035 0.035
:alb 0.11 0.11 0.11 0.18 0.11 0.11 0.11 0.11 0.11
:sublim_rate 0.1 0.1 0.1 0.2 0.1 0.3 0.3 0.4 0.3
:idump 6 8 12 13 17 18 18 20 21
:snocap 6000 6000 -600 -600 -600 -600 -600 -600 -600
:nsdc 2 2 2 2 2 2 2 2 2
:sdcsca 1 1 1 1 1 1 1 1 1
:sdcd 50 50 50 50 50 50 50 100 100
:EndSnowParameters
#
:InterceptionCapacityTable
:IntCap_Jan 1 2.4 0.55 0.1 0.25 3 3 0.01 0.01
```

```
:IntCap_Feb     1       2.4     0.55    0.1     0.25    3       3       0.01    0.01
:IntCap_Mar     1       2.4     0.55    0.1     0.25    3       3       0.01    0.01
:IntCap_Apr     1       2.4     0.55    0.1     0.25    3       3       0.01    0.01
:IntCap_May     1       3       0.75    0.25    0.25    3       3       0.01    0.01
:IntCap_Jun     1       4       0.9     0.5     0.25    3       3       0.01    0.01
:IntCap_Jul     1       4       0.9     0.5     0.25    3       3       0.01    0.01
:IntCap_Aug     1       4       0.9     0.5     0.25    3       3       0.01    0.01
:IntCap_Sep     1       4       0.9     0.5     0.25    3       3       0.01    0.01
:IntCap_Oct     1       2.4     0.55    0.1     0.25    3       3       0.01    0.01
:IntCap_Nov     1       2.4     0.55    0.1     0.25    3       3       0.01    0.01
:IntCap_Dec     1       2.4     0.55    0.1     0.25    3       3       0.01    0.01
:EndInterceptionCapacityTable
#
```

Evaporation-Transpiration Split Parameters

```
ii 1 a      0.4
ii 1 b      6.0
ii 2 a      0.2
ii 2 b      8.0
ii 3 a      0.4
ii 3 b      4.0
ii 4 a      0.6
ii 4 b      2.0
ii 5 a      0.6
ii 5 b      2.0
ii 6 a      1.0
ii 6 b      1.0
ii 7 a      1.0
ii 7 b      1.0
```

Isotope Initialization File

```
2                       !2H flag: 1 if running only 18O, 2 if running 18O and 2H
6                       !number of years for isotopes (number of data columns)
delta1      -10.50          !background delta for river water for initilization
delta2      -15.85          !background delta for soil water for initilization
delta3      -15.85          !background delta for groundwater for initilization
delta4      -25.00          !background delta for snow for initilization
isoyear      2009   2010   2011   2012   2013   2014      !year for isotope values (1 column per year)
deltar      -16.52 -16.52 -16.52 -16.52 -16.52 -16.52      !delta value for rain
deltas      -26.79 -25.00 -25.00 -25.00 -25.00 -25.00      !delta value for snow
rfoffset     0.00   0.00   0.00   0.00   0.00   0.00          !per mil depletion for refreezing
smoffset     0.00   0.00   0.00   0.00   0.00   0.00          !per mil enrichment for snow melt
delta2H1     -90.0              !background delta for river water for initilization
delta2H2     -119.8             !background delta for soil water for initilization
delta2H3     -119.8             !background delta for groundwater for initilization
delta2H4     -193.0             !background delta for snow for initilization
deltar2H     -152.0 -152.0 -152.0 -152.0 -152.0 -152.0      !delta 2H value for rain
deltas2H     -228.0 -193.0 -193.0 -193.0 -193.0 -193.0      !delta 2H value for snow
rfoffset2H    5.00   6.00   8.00   8.00   8.00   8.00      !2H per mil depletion for refreezing
smoffset2H    8.00   9.00   9.00   9.00   8.00   8.00      !2H per mil enrichment for snow melt
1           ! This doohickey is to set up the framework calcs: 1: whole basin avg framework, 2: 1 framework per
gauge, 3: multiple frameworks, but with gauges aggregated-> read another file
```

Appendix B

All calibration isographs and hydrographs are in this appendix. For isotope sampling location details, see Table 5.6, and for flow gauge information see Table 4.2.

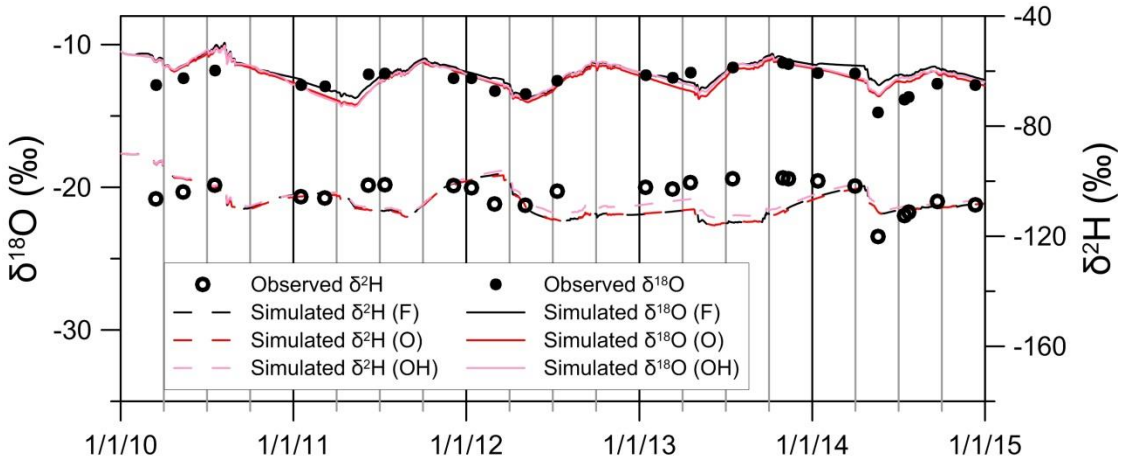

Figure B.1 Setting Lake (R-MH-05TC701) calibrated isograph.

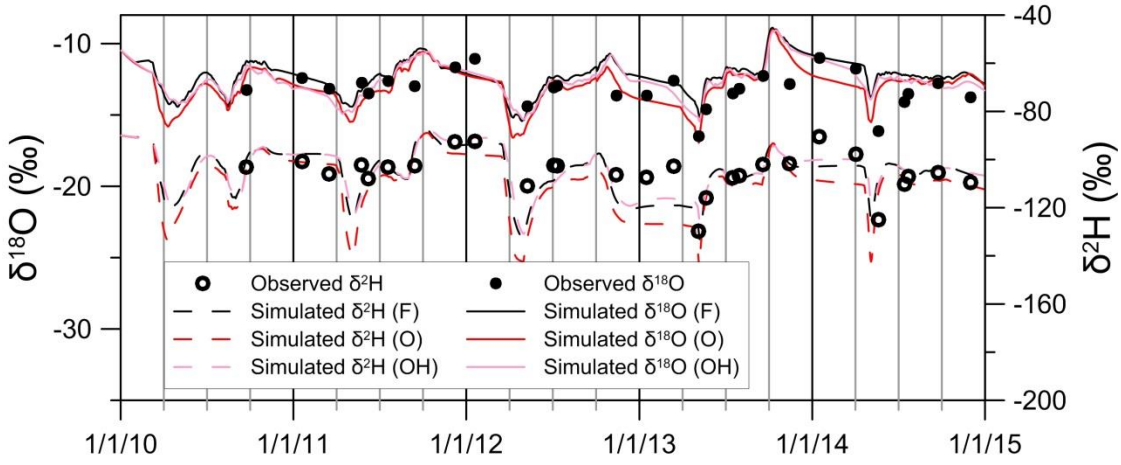

Figure B.2 Minago River below Hill Lake (R-MH-05UC702) calibrated isograph.

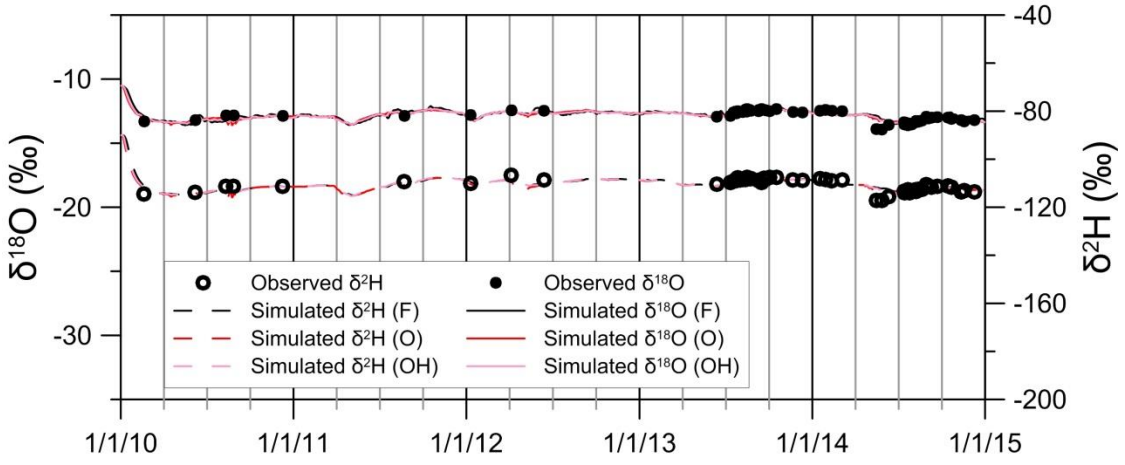

Figure B.3 Burntwood River below Miles Heart Bridge (R-MH-05TG702) calibrated isograph.

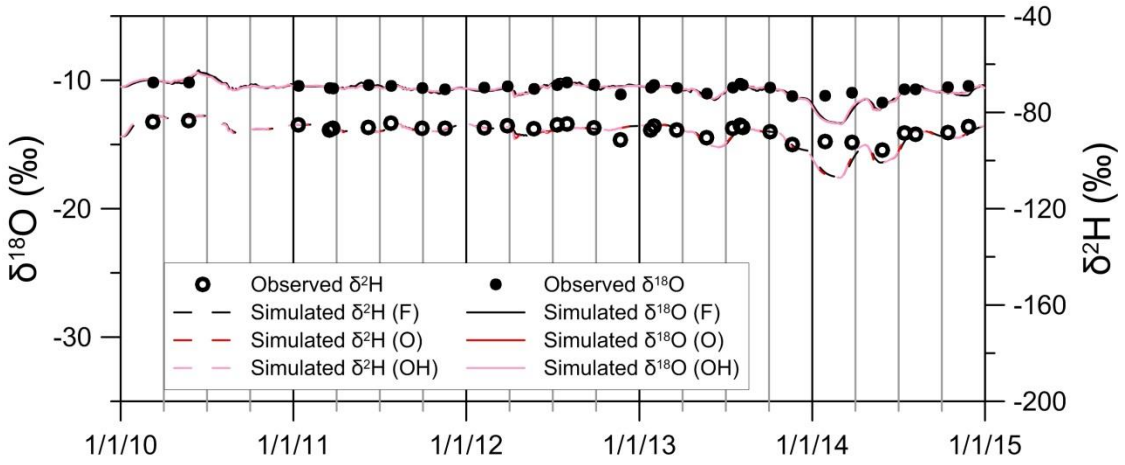

Figure B.4 Kelsey Generating Station (R-MH-05UE005 and R-MH-05UF792) calibrated isograph.

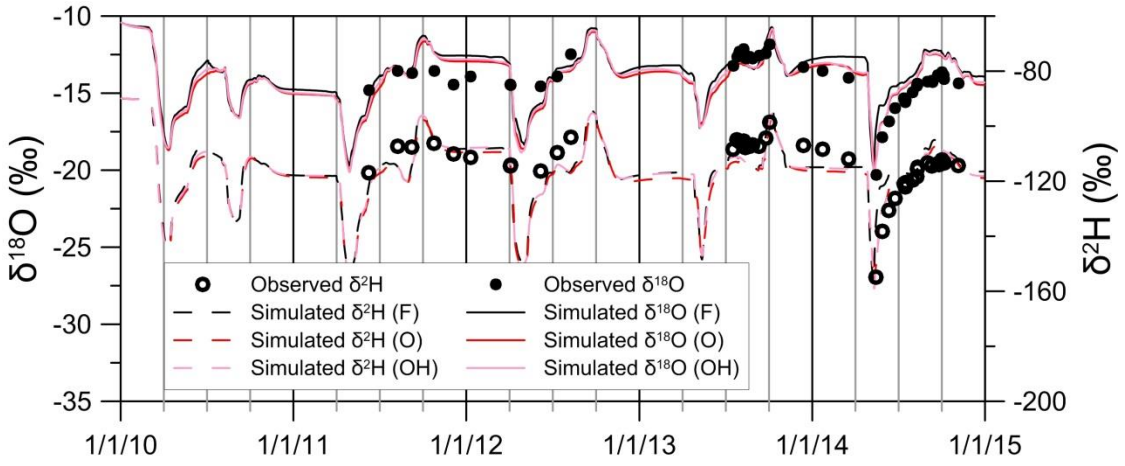

Figure B.5 Odei River near Thompson (R-MH-05TG003) calibrated isograph.

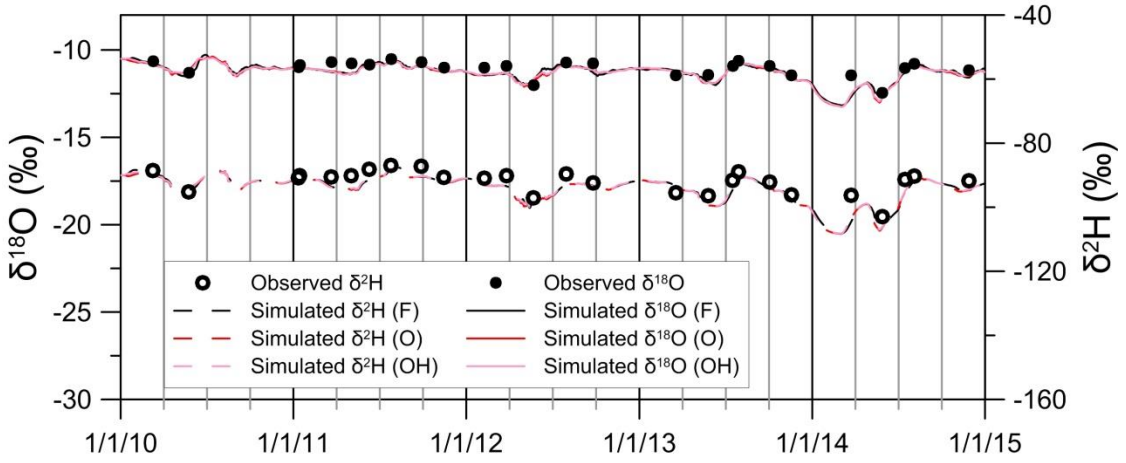

Figure B.6 Nelson River at Clarke Lake (R-MH-05UF766 and R-MH-05UF759) calibrated isograph.

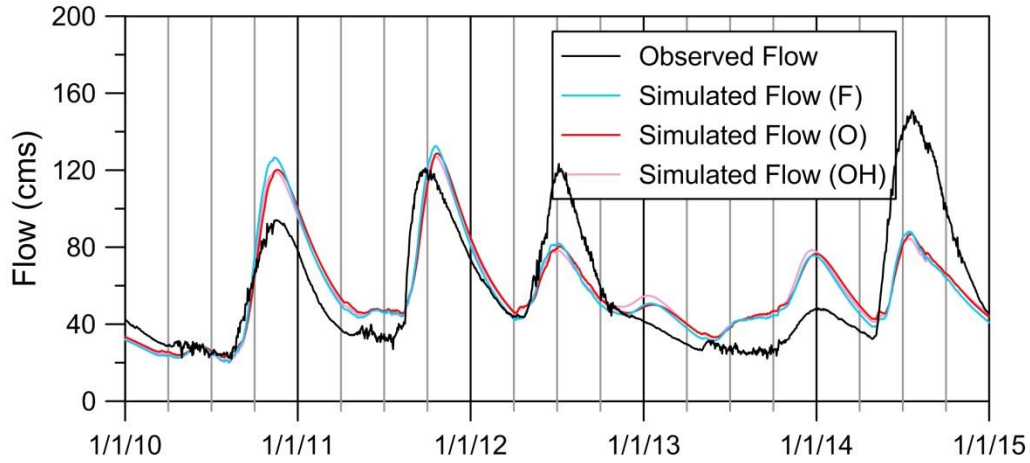

Figure B.7 Grass River above Standing Stone Falls (05TD001) hydrograph for the calibration period.

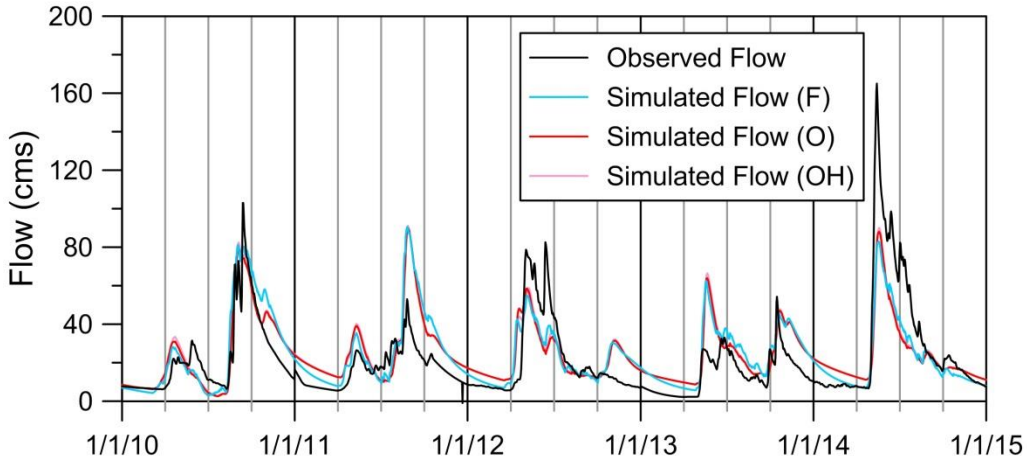

Figure B.8 Burntwood River above Leaf Rapids (05TE002) hydrograph for the calibration period.

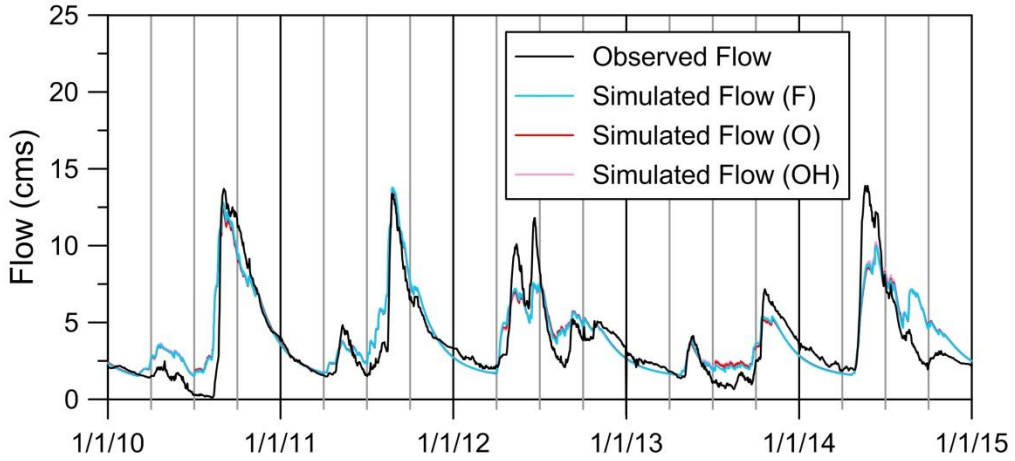

Figure B.9 Footprint River above Footprint Lake (05TF002) hydrograph for the calibration period.

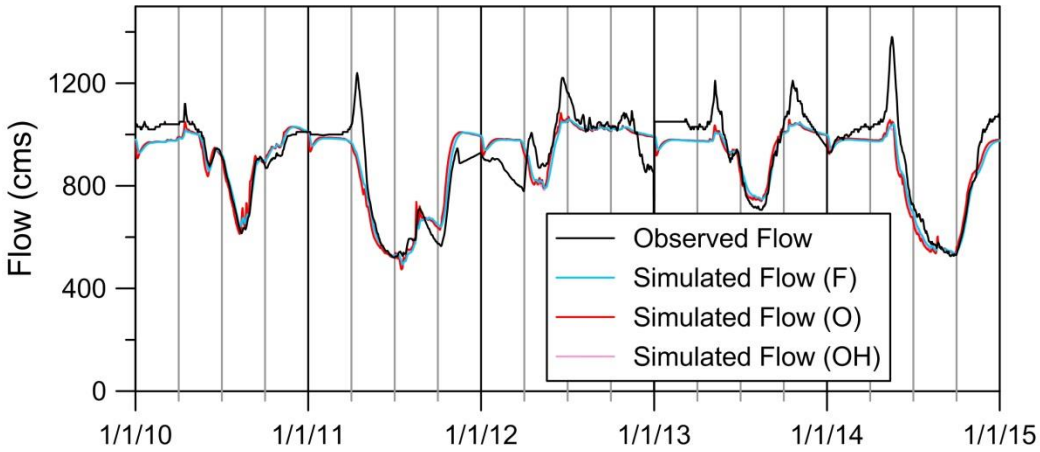

Figure B.10 Burntwood River near Thompson (05TG001) hydrograph for the calibration period.

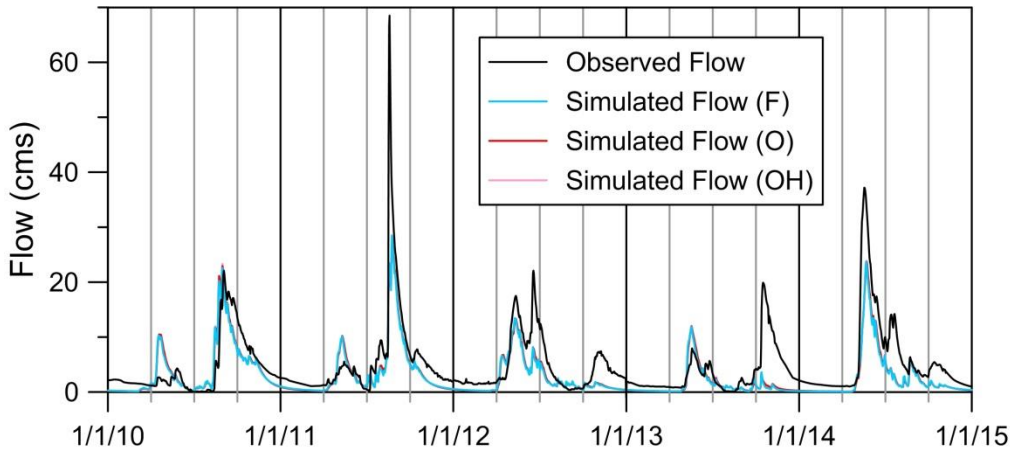

Figure B.11 Taylor River near Thompson (05TG002) hydrograph for the calibration period.

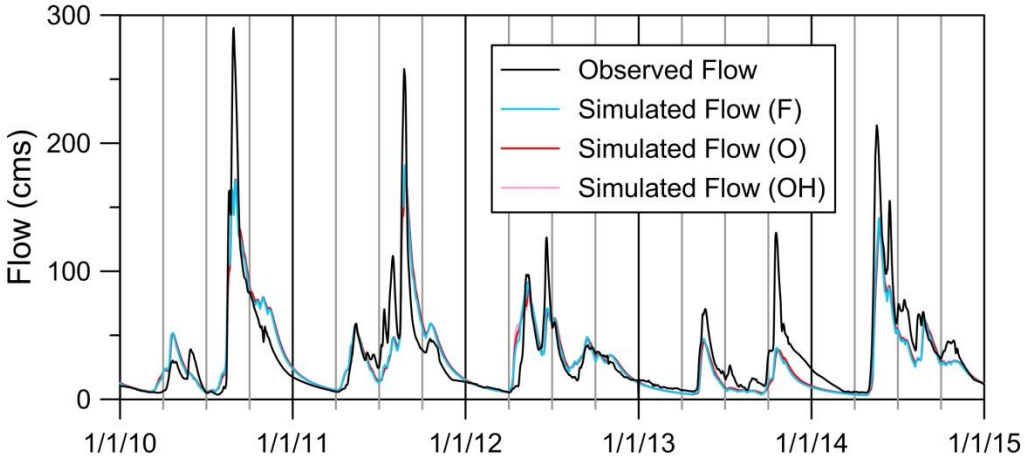

Figure B.12 Odei River near Thompson (05TG003) hydrograph for the calibration period.

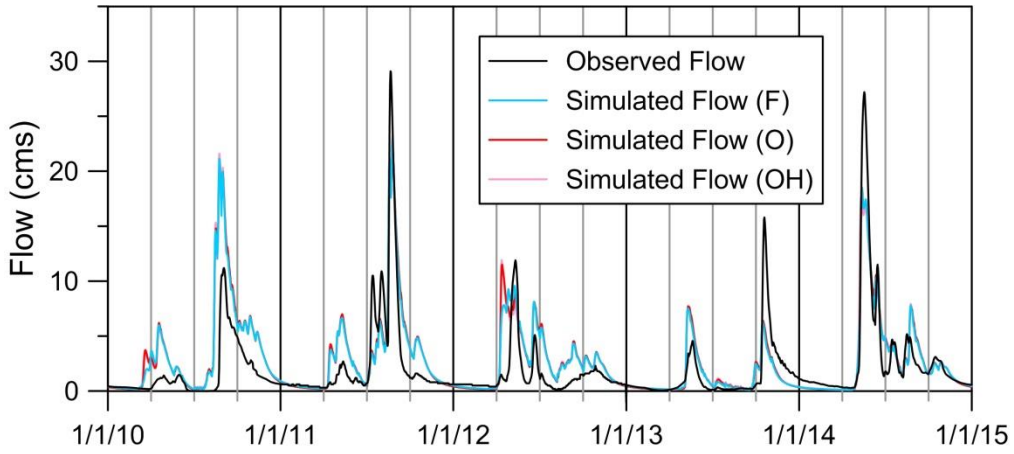

Figure B.13 Sapochi River near Nelson House (05TG006) hydrograph for the calibration period.

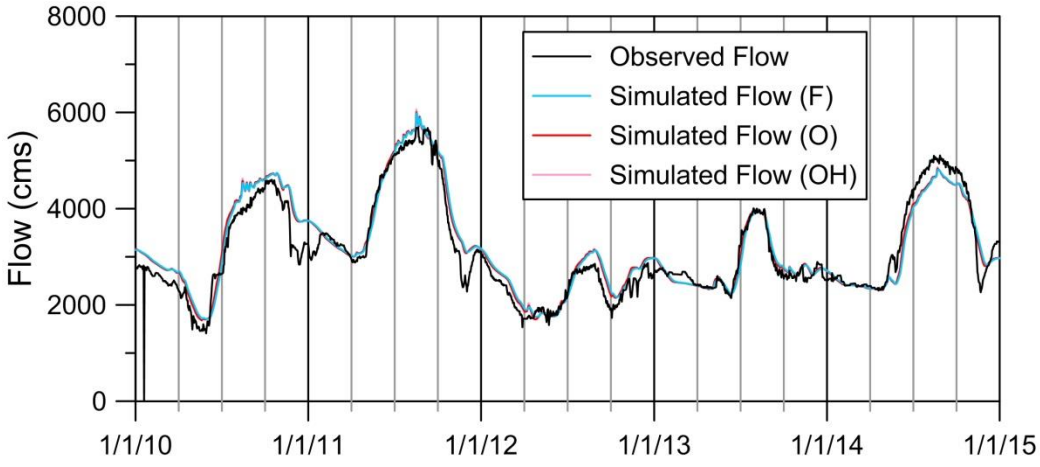

Figure B.14 Nelson River at Kelsey GS (05UE005) hydrograph for the calibration period.

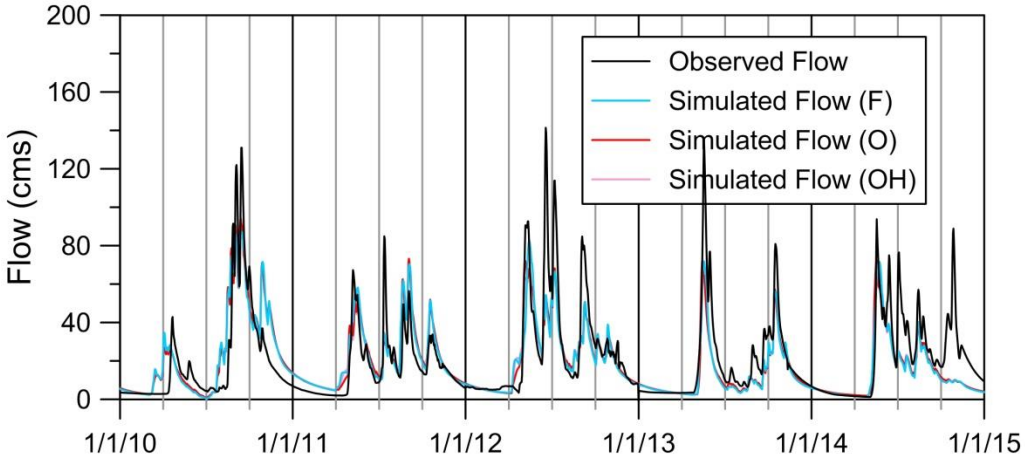

Figure B.15 Limestone River near Bird (05UG001) hydrograph for the calibration period.

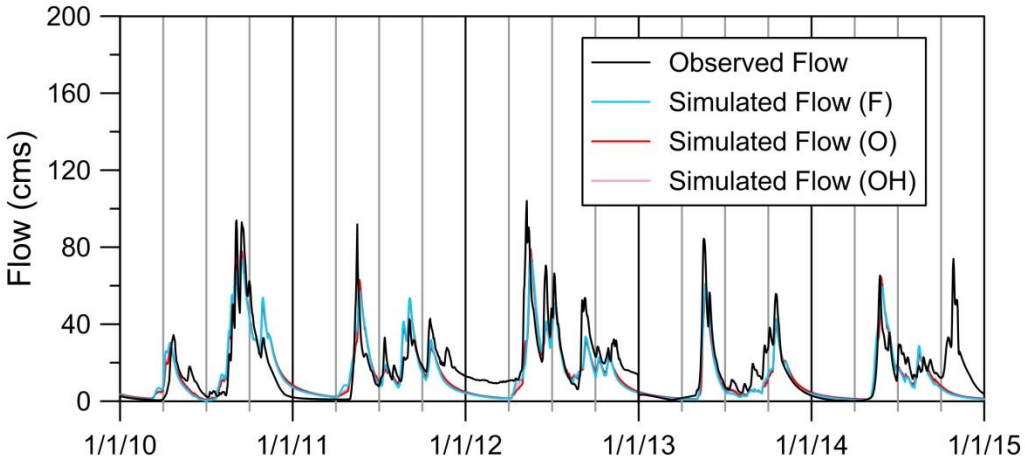

Figure B.16 Weir River above the mouth (05UH002) hydrograph for the calibration period.

Appendix C

All validation isographs and hydrographs are in this appendix. For isotope sampling location details, see Table 5.10, and for flow gauge information see Table 4.2.

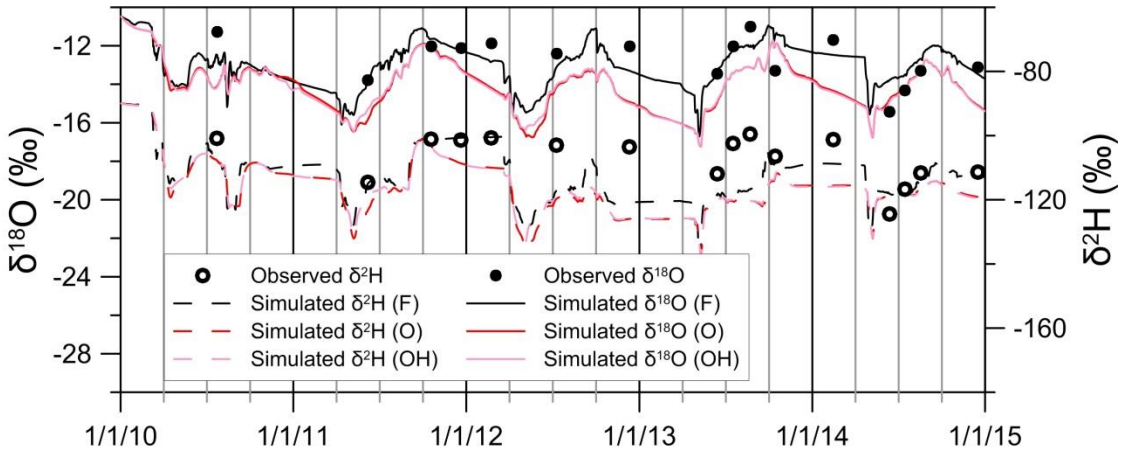

Figure C.1 Burntwood River above Leaf Rapids (R-MH-05TE703) validation isograph.

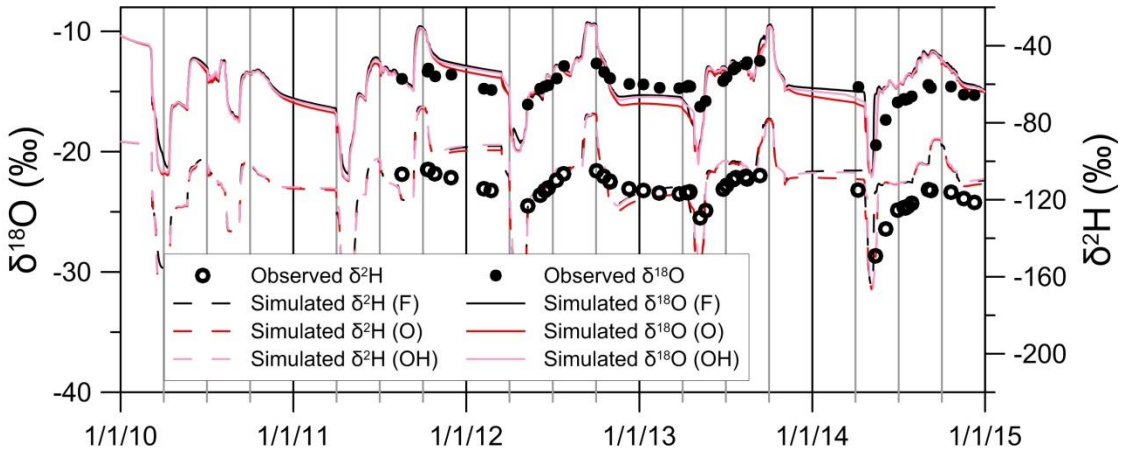

Figure C.2 Sapochi River (R-MH-05TG006) validation isograph.

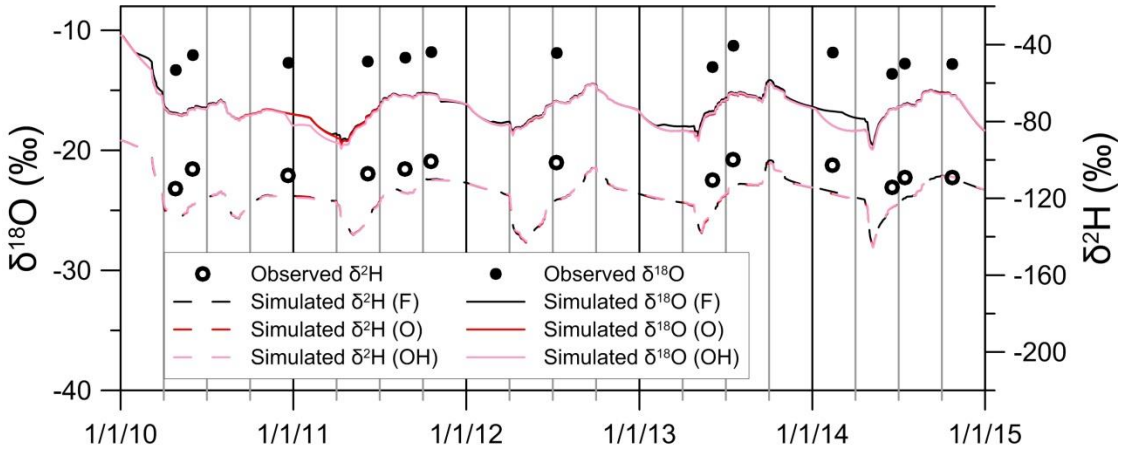

Figure C.3 Footprint River (R-MH-05TF782) validation isograph.

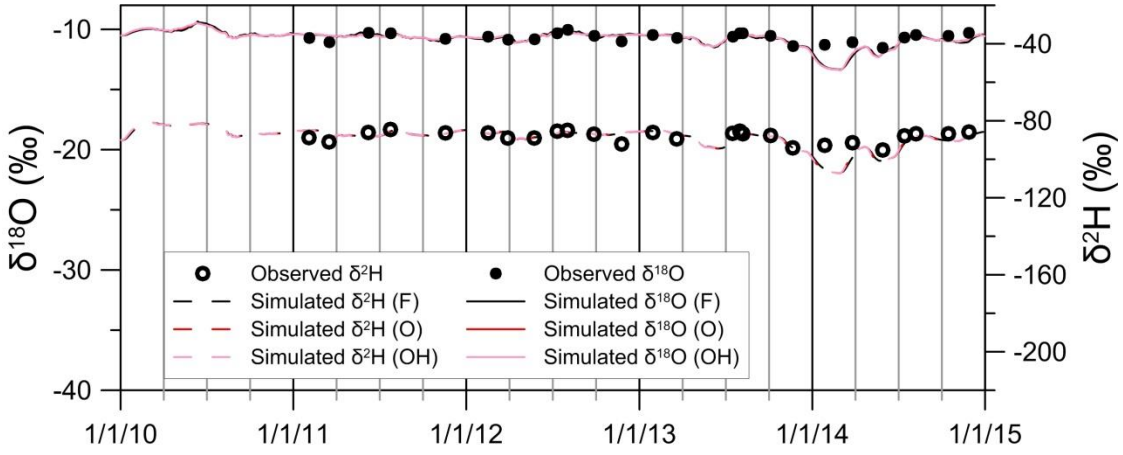

Figure C.4 Nelson at Clearwater Lake (R-MH-05UE703 and R-MH-05UE713) validation isograph.

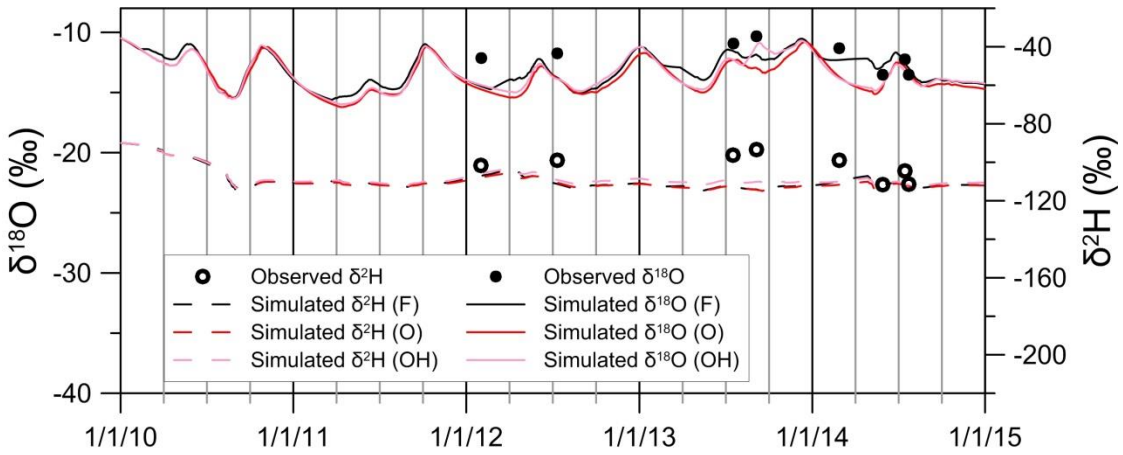

Figure C.5 Grass River below Standing Stone Falls (R-MH-05TD001) validation isograph.

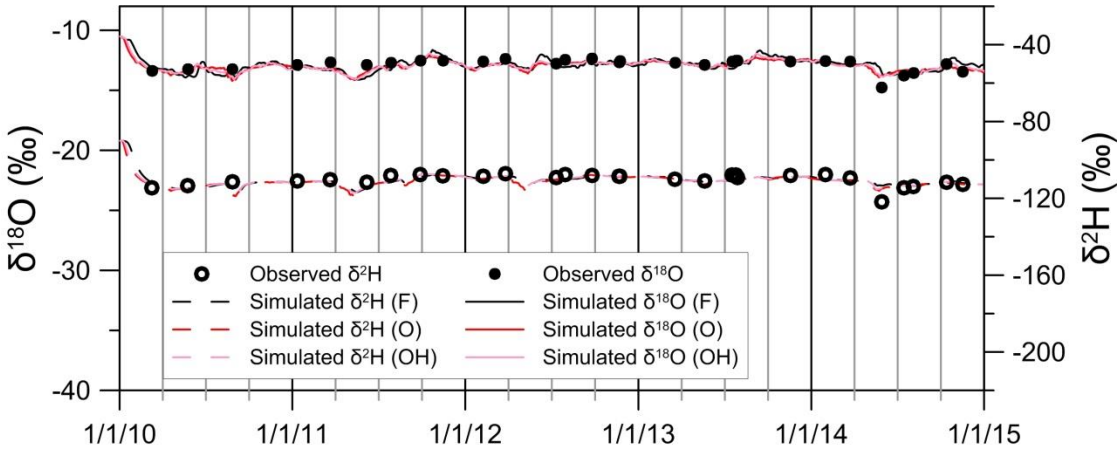

Figure C.6 Burntwood River above Split Lake (R-MH-05TG722) validation isograph.

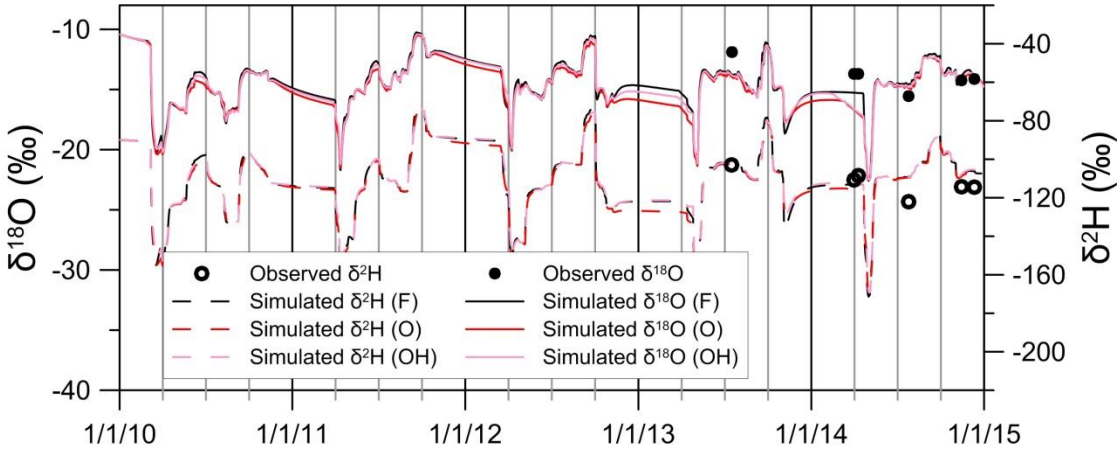

Figure C.7 Taylor River (R-MH-05TG002) validation isograph.

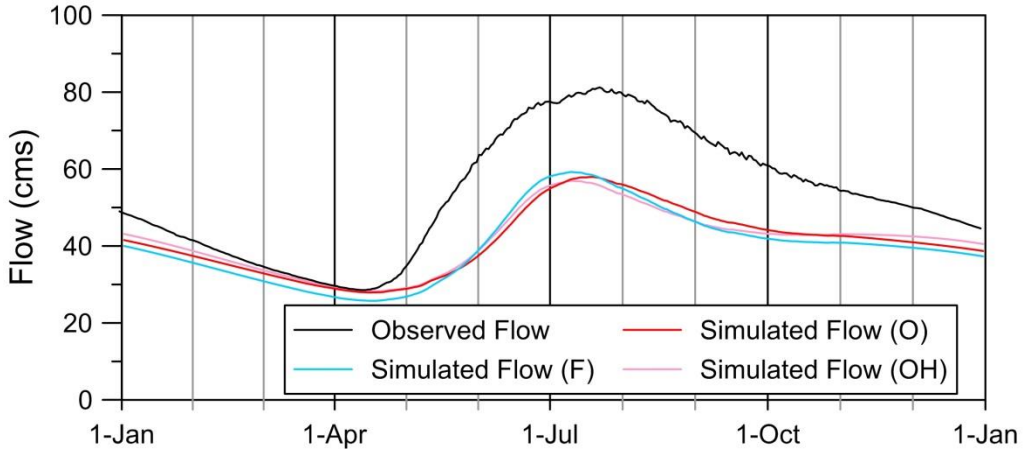

Figure C.8 Grass River above Standing Stone Falls (05TD001) average annual hydrograph for the validation period (1982-2009).

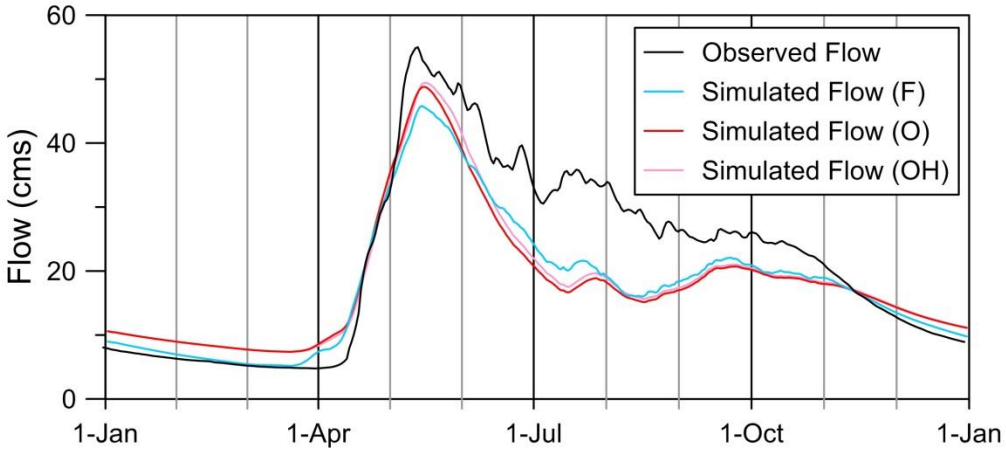

Figure C.9 Burntwood River above Leaf Rapids (05TE002) average annual hydrograph for the validation period (1982-2009).

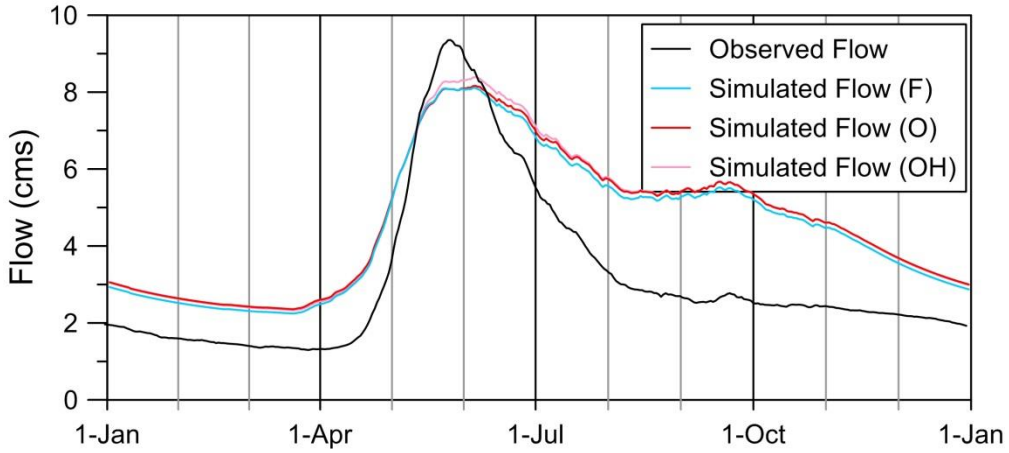

Figure C.10 Footprint River above Footprint Lake (05TF002) average annual hydrograph for the validation period (1982-2009).

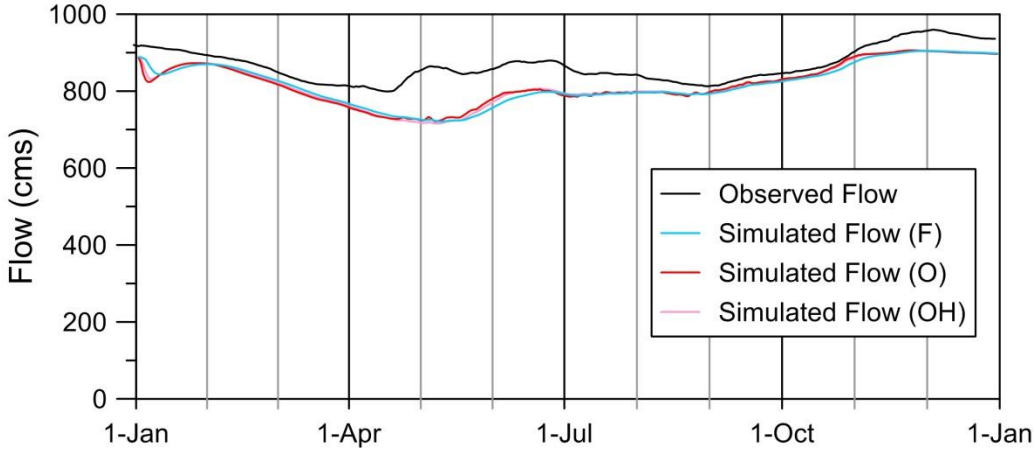

Figure C.11 Burntwood River near Thompson (05TG001) average annual hydrograph for the validation period (1982-2009).

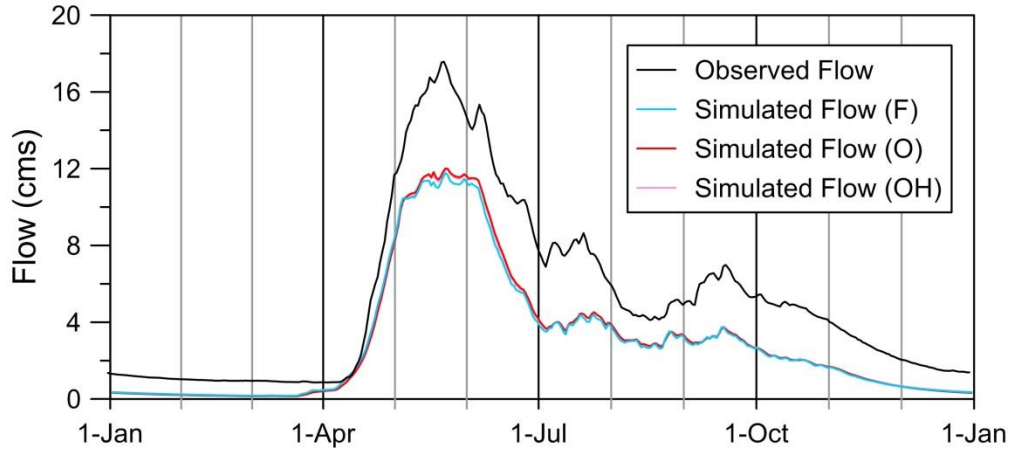

Figure C.12 Taylor River near Thompson (05TG002) average annual hydrograph for the validation period (1982-2009).

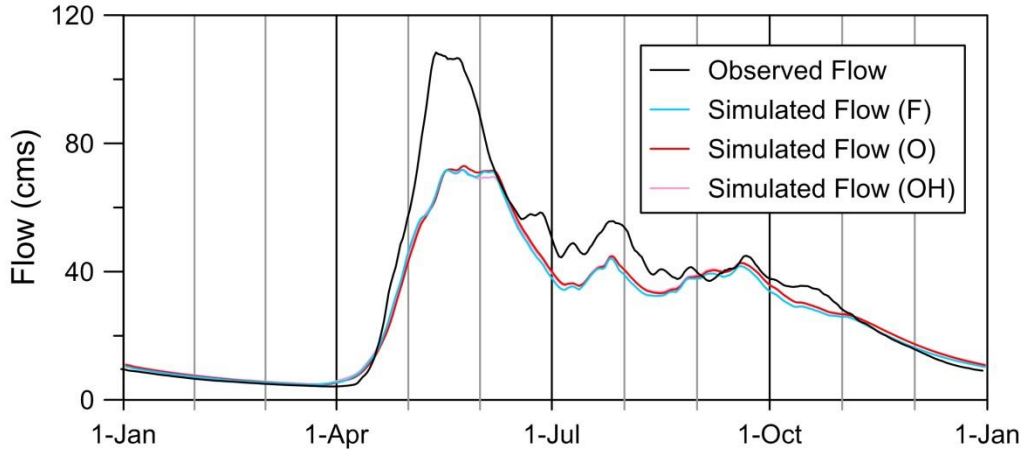

Figure C.13 Odei River near Thompson (05TG003) average annual hydrograph for the validation period (1982-2009).

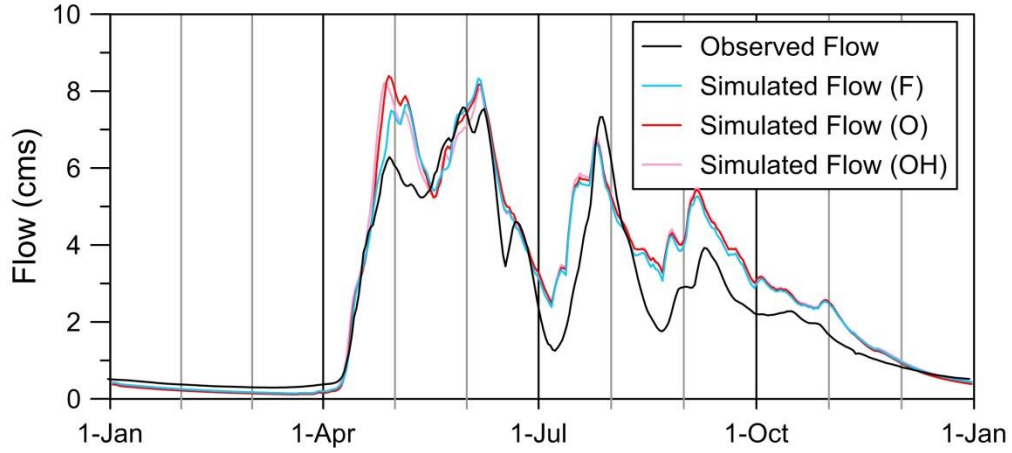

Figure C.14 Sapochi River near Nelson House (05TG006) average annual hydrograph for the validation period (1982-2009).

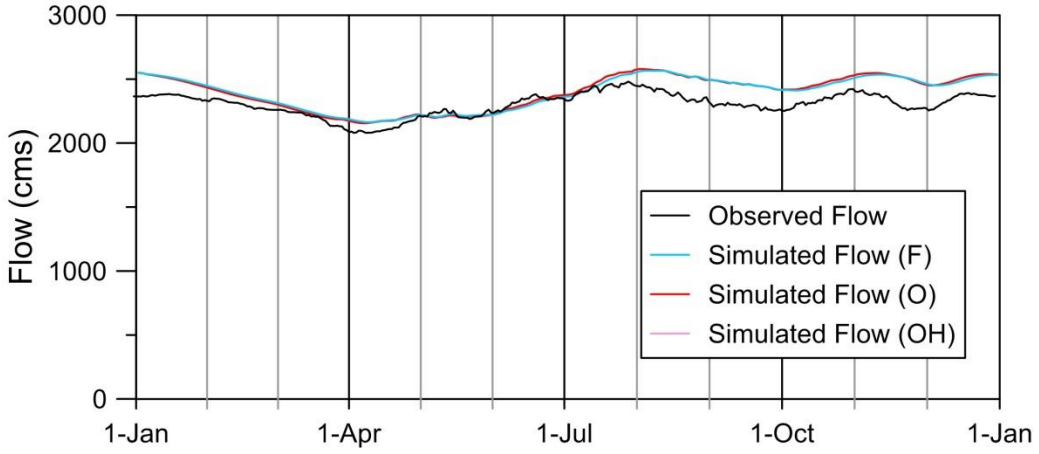

Figure C.15 Nelson River at Kelsey GS (05UE005) average annual hydrograph for the validation period (1982-2009).

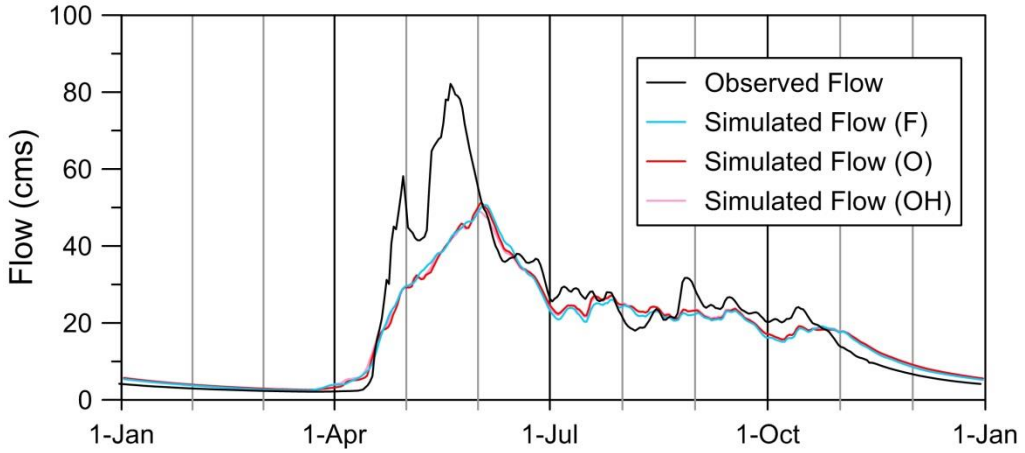

Figure C.16 Limestone River near Bird (05UG001) average annual hydrograph for the validation period (1982-2009).

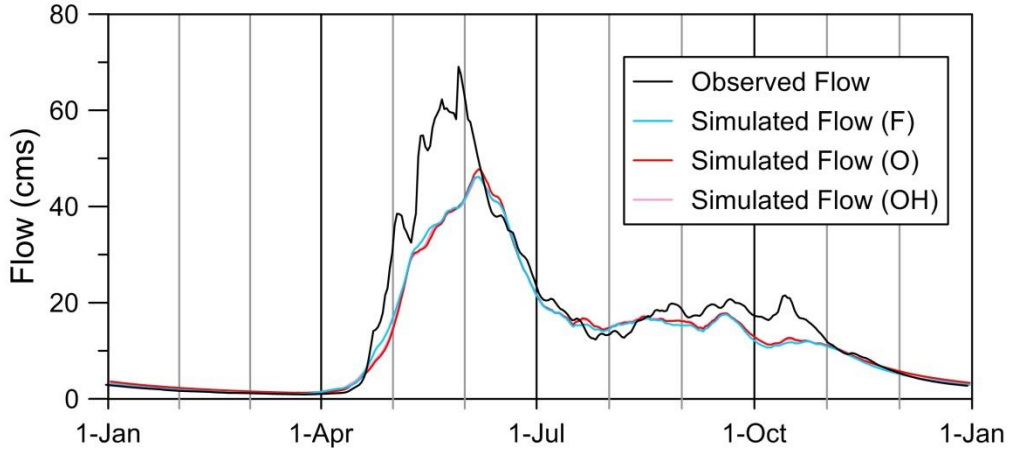

Figure C.17 Weir River above the mouth (05UH002) average annual hydrograph for the validation period (1982-2009).

Appendix D

This appendix contains isotope verification plots not included in Chapter 6.

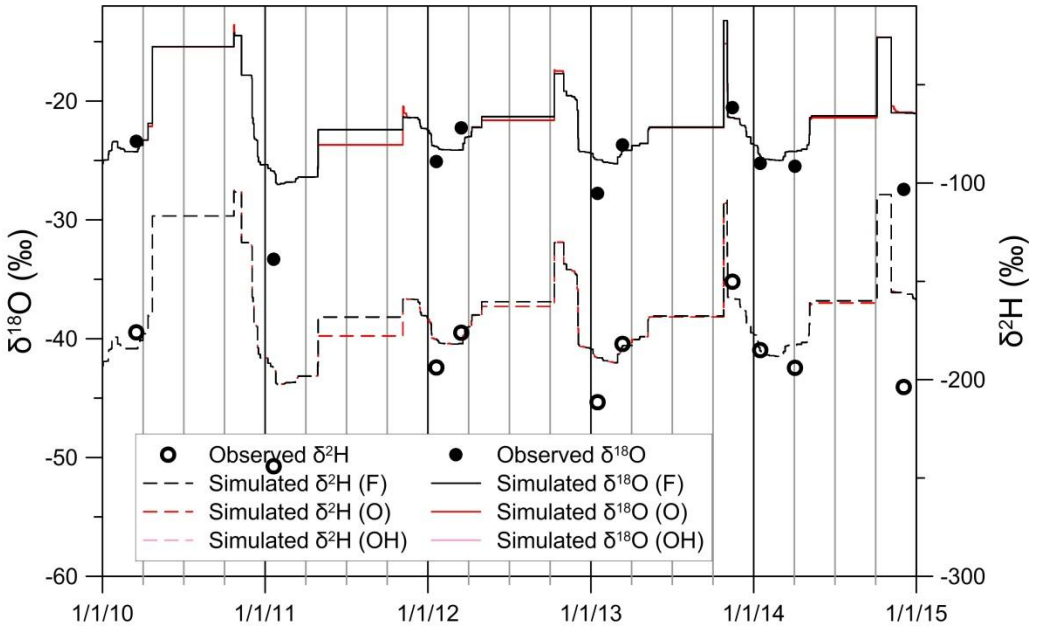

Figure D.1 Simulated and observed isotopic composition of the snowpack at Jenpeg.

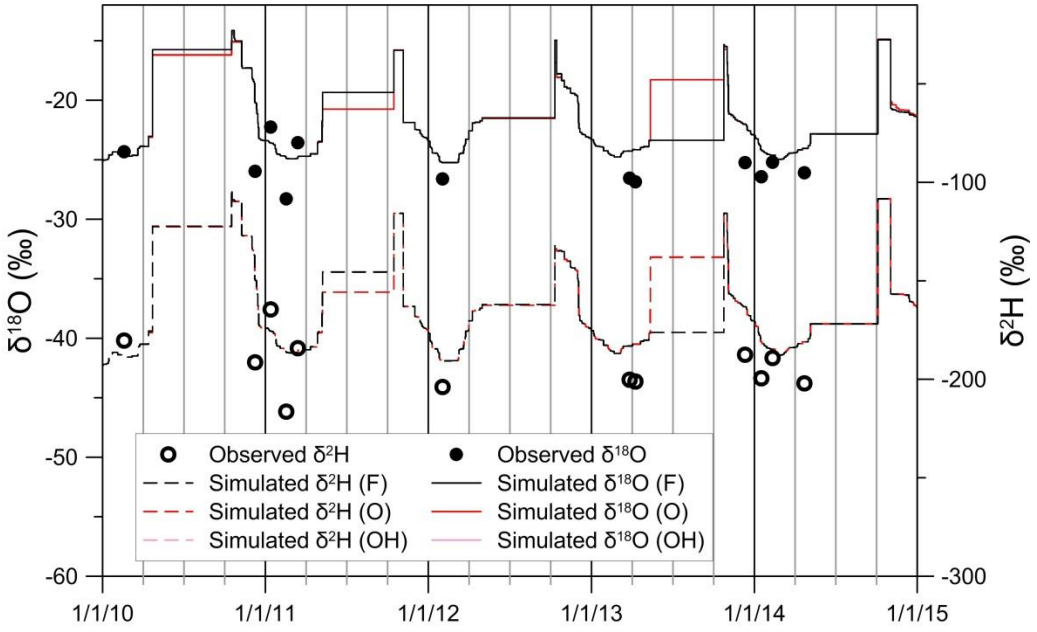

Figure D.2 Simulated and observed isotopic composition of the snowpack at Thompson.

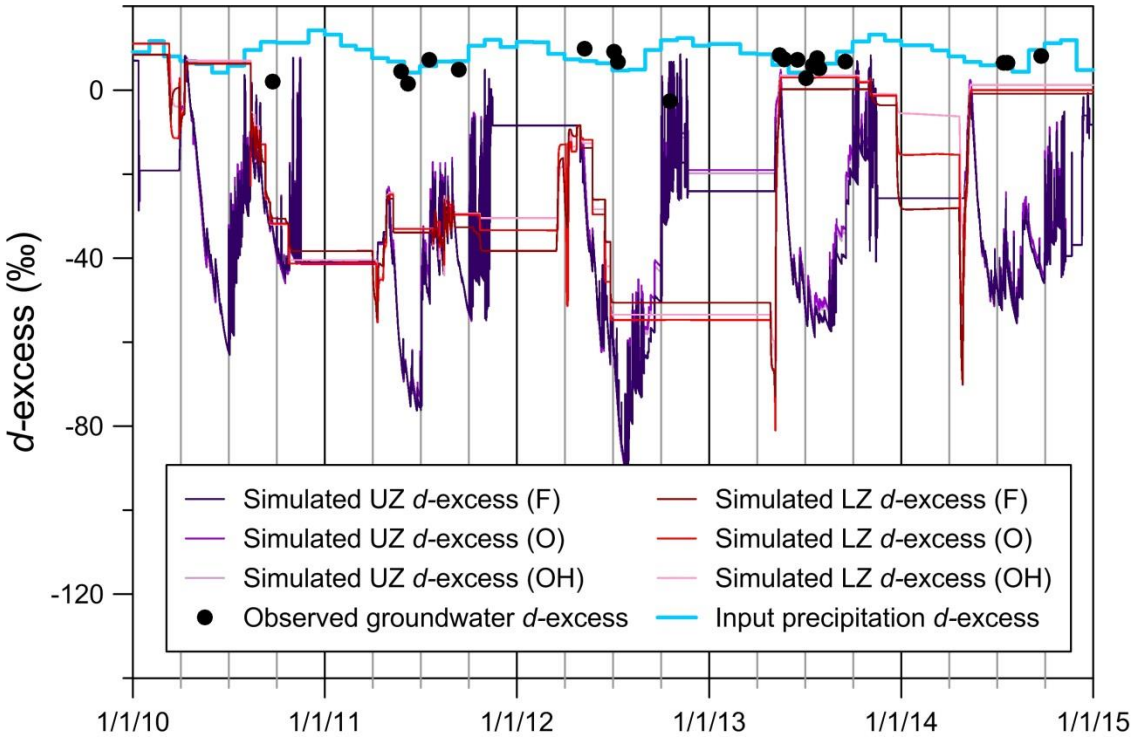

Figure D.3 Observed groundwater d-excess at Jenpeg and simulated upper and lower zone d-excess.

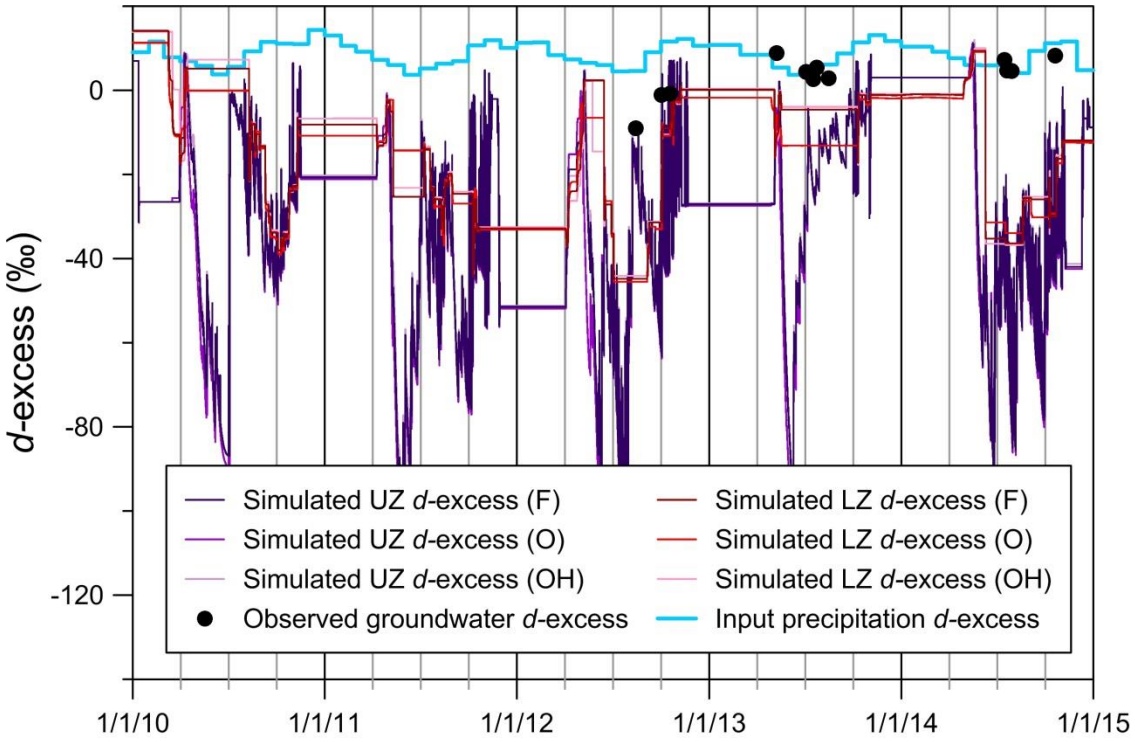

Figure D.4 Observed groundwater d-excess at Notigi and simulated upper and lower zone d-excess.

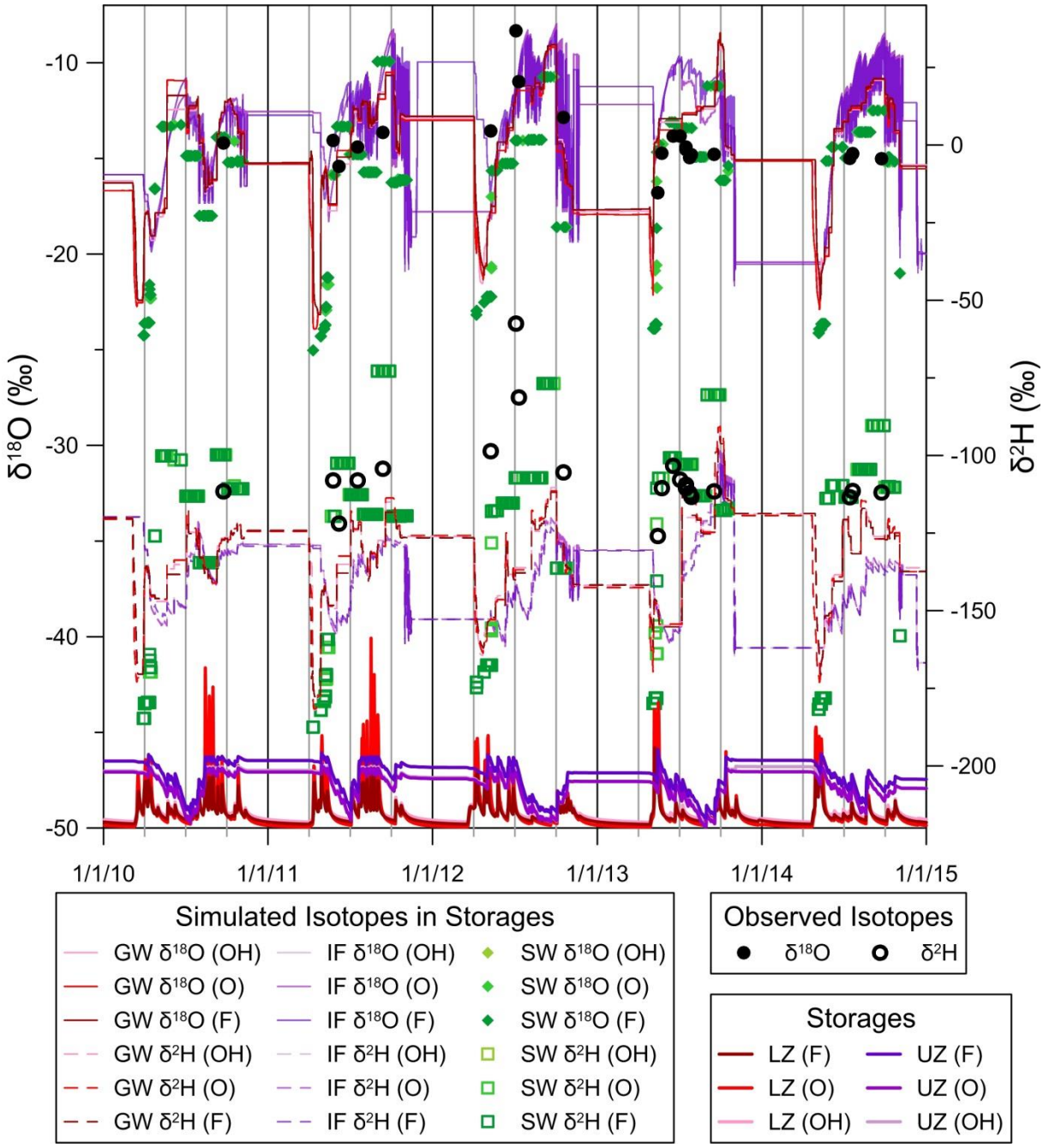

Figure D.5 Observed and simulated groundwater isotopes with simulated storage at Jenpeg.

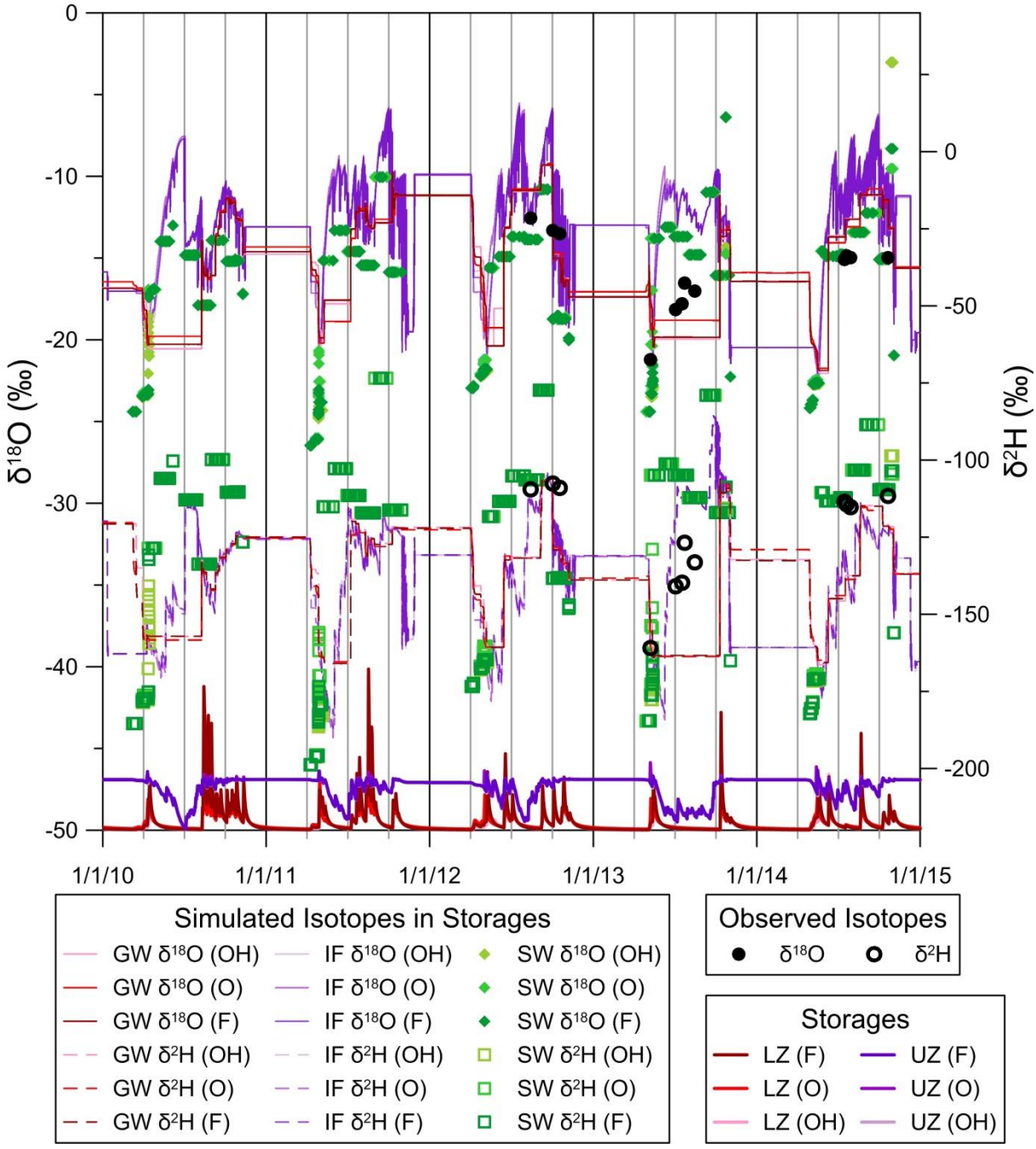

Figure D.6 Observed and simulated groundwater isotopes with simulated storage at Notigi.

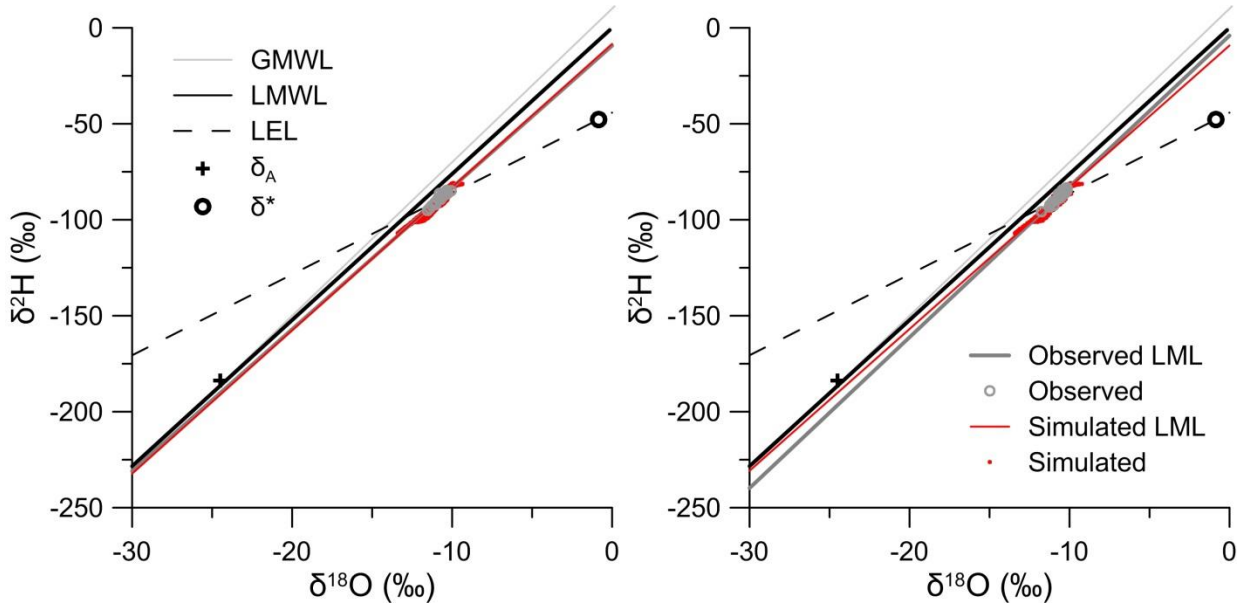

Figure D.7 Nelson at Clearwater Lake (R-MH-05UE703 and R-MH-05UE713) (left) and Kelsey Generating Station (R-MH-05UE005 and R-MH-05UF792) (right) isotope frameworks with all calibrations included in the simulated values (2010-2014).

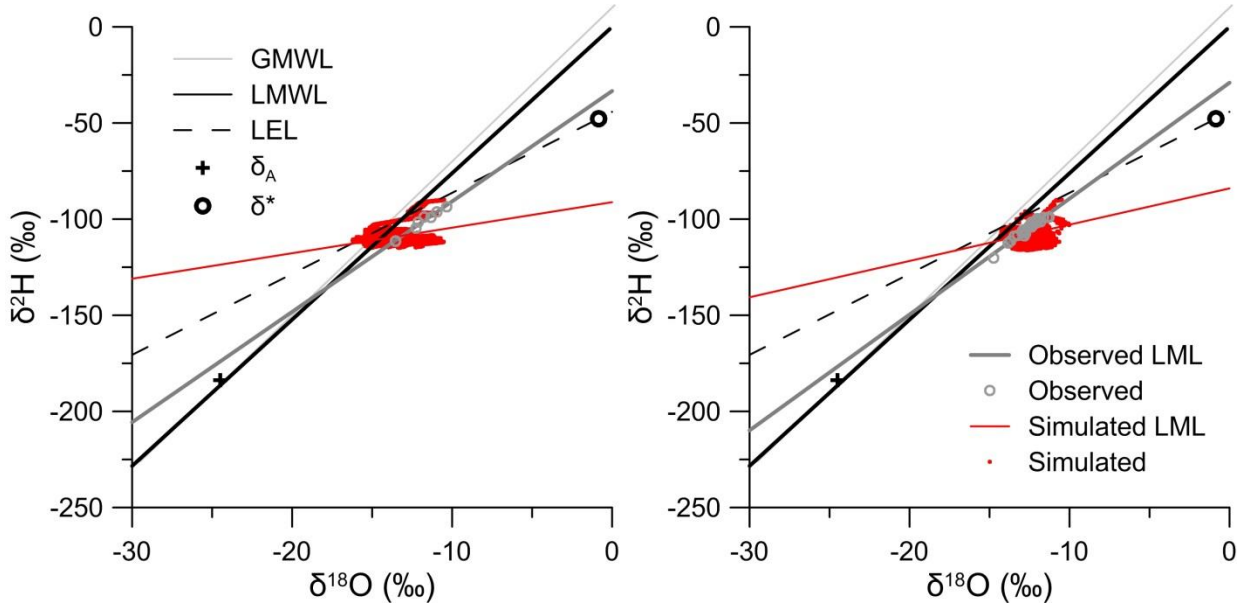

Figure D.8 Grass River below Standing Stone Falls (R-MH-05TD001) (left) and Setting Lake (R-MH-05TC701) (right) isotope frameworks with all calibrations included in the simulated values (2010-2014).

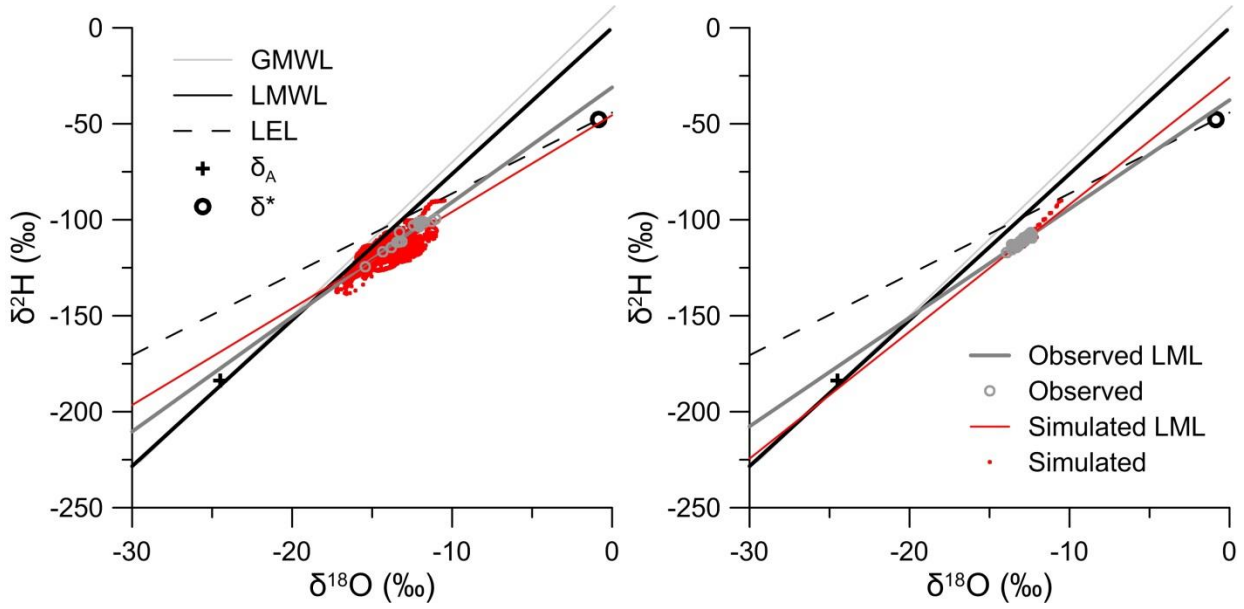

Figure D.9 Burntwood River above Leaf Rapids (R-MH-05TE703) (left) and Burntwood River below Miles Heart Bridge (R-MH-05TG702) (right) isotope frameworks with all calibrations included in the simulated values (2010-2014).

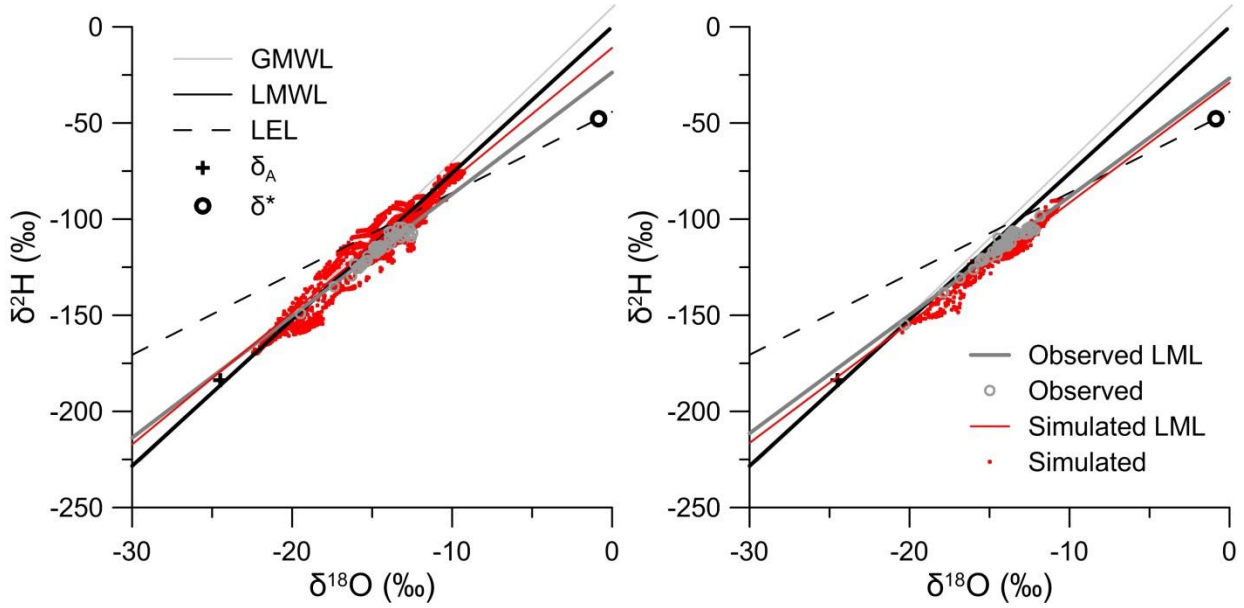

Figure D.10 Sapochi River (R-MH-05TG006) (left) and Odei River near Thompson (R-MH-05TG003) (right) isotope frameworks with all calibrations included in the simulated values (2010-2014).

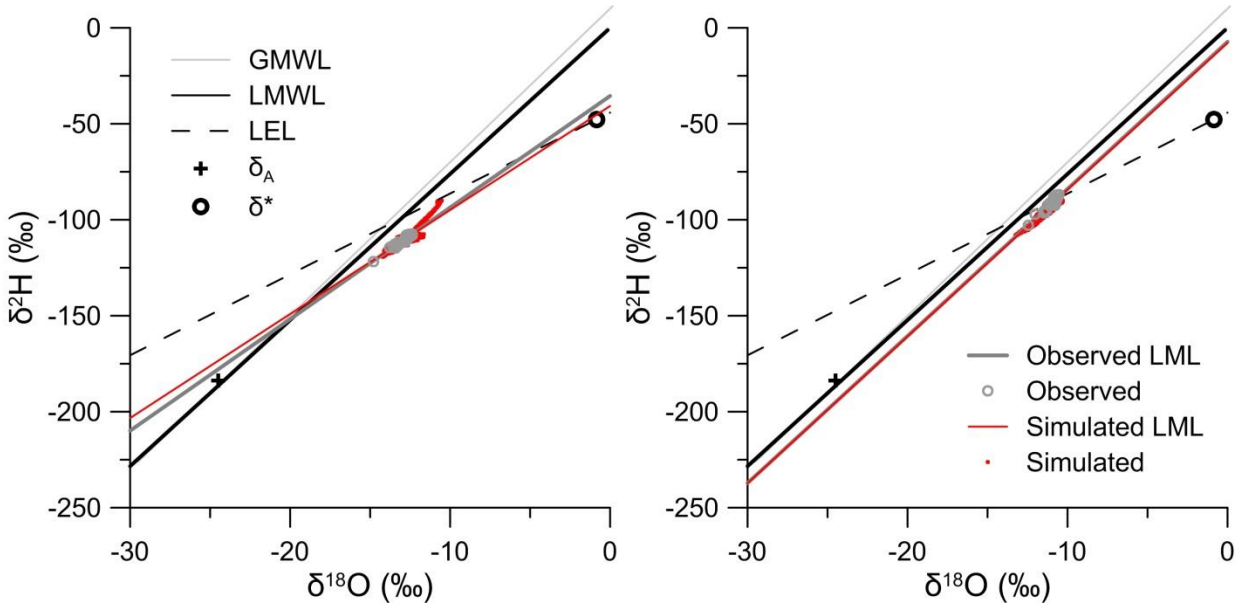

Figure D.11 Burntwood River above Split Lake (R-MH-05TG722) (left) and Nelson River at Clarke Lake (R-MH-05UF766 and R-MH-05UF759) (right) isotope frameworks with all calibrations included in the simulated values (2010-2014).

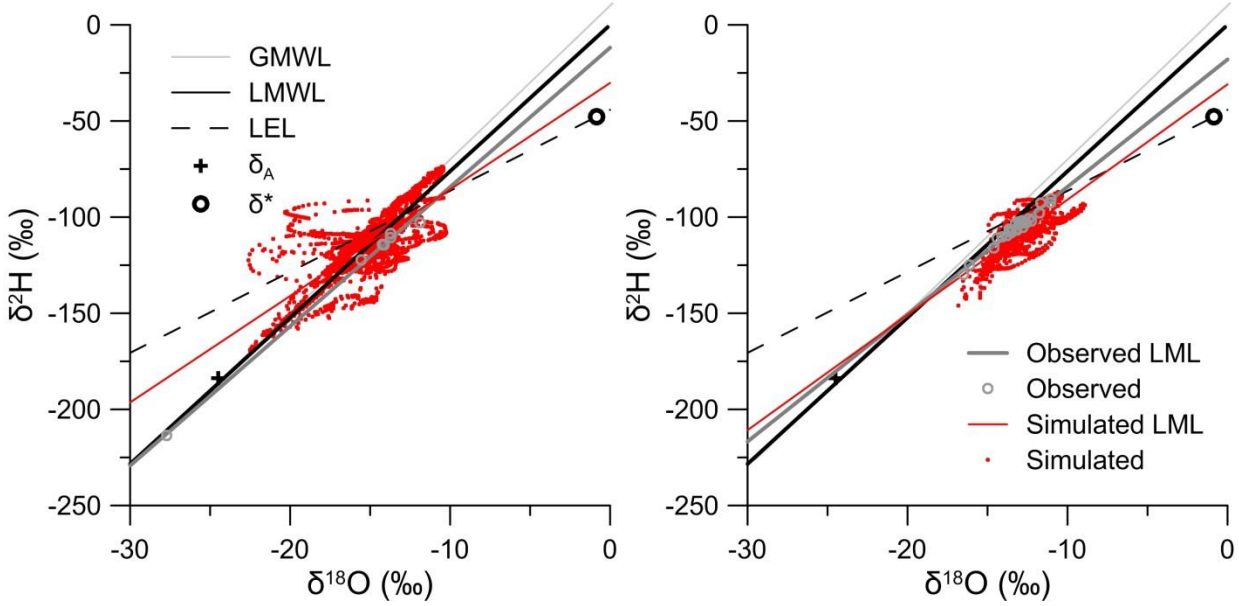

Figure D.12 Taylor River (R-MH-05TG002) (left) and Minago River below Hill Lake (R-MH-05UC702) (right) isotope frameworks with all calibrations included in the simulated values (2010-2014).

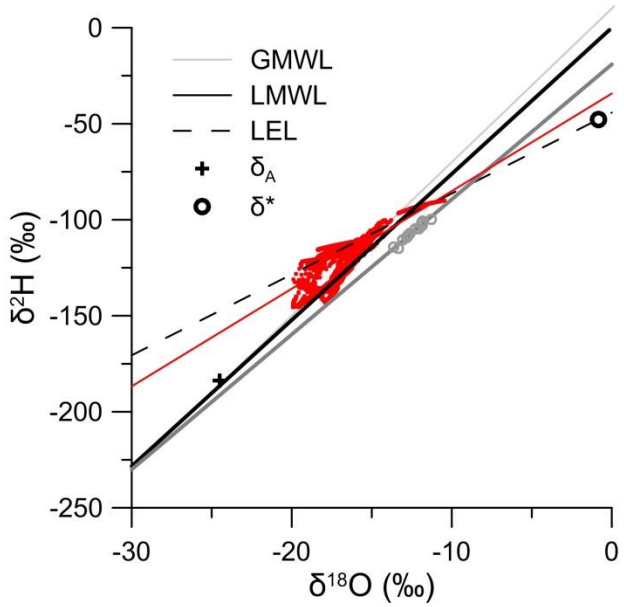

Figure D.13 Footprint River (R-MH-05TF782) isotope framework with all calibrations included in the simulated values (2010-2014).